ISSN 0368-0797
eISSN 2410-2091

МИСИС
УНИВЕРСИТЕТ НАУКИ И ТЕХНОЛОГИЙ

СибГИУ
Сибирский государственный индустриальный университет

ИЗВЕСТИЯ ВЫСШИХ УЧЕБНЫХ ЗАВЕДЕНИЙ ЧЕРНАЯ МЕТАЛЛУРГИЯ

IZVESTIYA. FERROUS METALLURGY

fermet.misis.ru

2025 Том Vol. 68 № No. 5

МИСИС УНИВЕРСИТЕТ
СибГИУ Сибирский государственный индустриальный университет

ISSN 0368-0797
eISSN 2410-2091

ИЗВЕСТИЯ ВЫСШИХ УЧЕБНЫХ ЗАВЕДЕНИЙ ЧЕРНАЯ МЕТАЛЛУРГИЯ

Научно-технический журнал

Издается с января 1958 г. Выпускается 6 раз в год

2025 Том Vol. 68 № No. 5

IZVESTIYA FERROUS METALLURGY

Scientific and Technical Journal

Published since January 1958. Issued 6 times a year

IZVESTIYA FERROUS METALLURGY

www.fermet.misis.ru

ISSN 0368-0797 *(Print)* ISSN 2410-2091 *(Online)*

Alternative title:

Izvestiya vuzov. Chernaya metallurgiya

Founders:

MISIS
UNIVERSITY OF SCIENCE AND TECHNOLOGY

SibSIU
Siberian State Industrial University

Publisher:

National University of Science and Technology "MISIS"

Editorial Office Address:

in Moscow
4 Leninskii Ave., Moscow 119049, Russian Federation
National University of Science and Technology "MISIS"
Tel.: +7 (495) 638-44-11 *E-mail*: ferrous@misis.ru

in Novokuznetsk
42 Kirova Str., Novokuznetsk, Kemerovo Region – Kuzbass
654007, Russian Federation
Siberian State Industrial University
Tel.: +7 (3843) 74-86-28 *E-mail*: redjizvz@sibsiu.ru

In accordance with paragraph 5 of the Rules for the formation of the Higher Attestation Comission list journal "Izvestiya. Ferrous metallurgy" is included in the list of leading peer-reviewed scientific journals, publication in which is taken into account in the defense of candidate and doctoral dissertations, as indexed in internatonal data bases.

Indexed: Scopus, Russian Science Citation Index (RSCI), Research Bible, Chemical Abstracts, OCLC and Google Scholar

Registered in Federal Service for Supervision in the Sphere of Mass Communications **PI number FS77-35456**.

ИЗВЕСТИЯ
ВЫСШИХ УЧЕБНЫХ ЗАВЕДЕНИЙ
ЧЕРНАЯ МЕТАЛЛУРГИЯ

www.fermet.misis.ru

ISSN 0368-0797 *(Print)* ISSN 2410-2091 *(Online)*

Варианты названия:

Известия вузов. Черная металлургия

Izvestiya. Ferrous Metallurgy

Учредители:

МИСИС
УНИВЕРСИТЕТ НАУКИ И ТЕХНОЛОГИЙ

СибГИУ
Сибирский государственный индустриальный университет

Издатель:

Национальный исследовательский технологический университет «МИСИС»

Адреса подразделений редакции:

в Москве
Россия, 119049, Москва, Ленинский просп., д. 4, стр. 1
Национальный исследовательский технологический университет «МИСИС»
Тел.: +7 (495) 638-44-11 *E-mail*: ferrous@misis.ru

в Новокузнецке
Россия, 654007, Новокузнецк,
Кемеровская обл. – Кузбасс, ул. Кирова, зд. 42
Сибирский государственный индустриальный университет
Тел.: +7 (3843) 74-86-28 *E-mail:* redjizvz@sibsiu.ru

В соответствии п. 5 Правил формирования перечня ВАК журнал «Известия вузов. Черная металлургия» входит в перечень ведущих рецензируемых научных журналов и изданий, публикация в которых учитывается при защитах кандидатских и докторских диссертаций как индексируемый в МБД.

Индексирование: Scopus, Russian Science Citation Index (RSCI), Research Bible, Chemical Abstracts, OCLC и Google Scholar

Зарегистрирован Федеральной службой по надзору в сфере связи и массовых коммуникаций **ПИ № ФС77-35456**.

Izvestiya. Ferrous Metallurgy.
2025;68(5)

Известия вузов. Черная металлургия.
2025;68(5)

CONTENTS / СОДЕРЖАНИЕ

METALLURGICAL TECHNOLOGIES

МЕТАЛЛУРГИЧЕСКИЕ ТЕХНОЛОГИИ

MATERIALS SCIENCE

МАТЕРИАЛОВЕДЕНИЕ

PHYSICO-CHEMICAL BASICS OF METALLURGICAL PROCESSES

ФИЗИКО-ХИМИЧЕСКИЕ ОСНОВЫ МЕТАЛЛУРГИЧЕСКИХ ПРОЦЕССОВ

CONTENTS *(Continuation)*

ECOLOGY AND RATIONAL USE OF NATURAL RESOURCES

СОДЕРЖАНИЕ *(продолжение)*

ЭКОЛОГИЯ И РАЦИОНАЛЬНОЕ ПРИРОДОПОЛЬЗОВАНИЕ

METALLURGICAL TECHNOLOGIES / МЕТАЛЛУРГИЧЕСКИЕ ТЕХНОЛОГИИ

UDC 669.053.2: 544.3
DOI 10.17073/0368-0797-2025-5-444-453

Original article
Оригинальная статья

Assessment of the technological possibility of joint processing of ilmenite and perovskite concentrates

S. N. Agafonov[1], L. Yu. Udoeva[1], A. S. Vusikhis[1], L. I. Leont'ev[1, 2, 3]

[1] **Vatolin Institute of Metallurgy of the Ural Branch of the Russian Academy of Sciences** (101 Amundsena Str., Yekaterinburg 620016, Russian Federation)
[2] **National University of Science and Technology "MISIS"** (4 Leninskii Ave., Moscow 119049, Russian Federation)
[3] **Presidium of the Russian Academy of Sciences (Department of Chemistry and Material Sciences)** (32a Leninskii Ave., Moscow 119991, Russian Federation)

agafonovs@ya.ru

Abstract. An urgent task facing the modern metallurgical industry is to increase the complexity of using mineral and technogenic raw materials by developing new technologies based on the principle of joint processing of raw materials from deposits that differ in the mineral composition of the ore component, for example, titanium-containing ores – ilmenite and perovskite. Joint processing of titanium-containing ores will improve the environmental and economic efficiency of processing domestic mineral raw materials, and will also create prerequisites for the development of titanium dioxide production in Russia. In order to scientifically substantiate the feasibility of joint processing of different types of titanium raw materials, the effect of temperature, reducing agent consumption and concentrate ratio on the phase formation process during carbothermic reduction of concentrate mixtures was established using thermodynamic modeling. The distribution of target metals by interaction products is considered, optimal parameters for the process of formation of rich titanium slags are proposed. The authors assessed the prospects for the associated extraction of rare and rare-earth metals. Thermodynamic analysis of the process of carbothermic reduction of mixtures, performed on model compositions of perovskite and ilmenite concentrates, showed that at low values of the perovskite concentrate / ilmenite concentrate (PC/IC) ratio, one can expect the formation of high-titanium slags with a TiO_2 content of more than 80 %. However, concentration of Nb extracted into the alloy and content of rare earth elements in the slag will decrease several times compared to their initial values in the perovskite concentrate. At a PC/IC ratio of 1, it is possible to accumulate up to 2.5 % Nb in the alloy with a TiO_2 content of up to 74 % in the slag. The advantage of joint processing of ilmenite and perovskite raw materials by the pyrometallurgical method is the ability to obtain rich titanium slags and selectively concentrate rare metals in the metallic phase, separating them from titanium, and rare earth metals in the slag within the framework of a single process flow sheet.

Keywords: titanium concentrates, ilmenite, perovskite, carbothermic reduction, thermodynamic modeling

Acknowledgements: The work was performed according to the State assignment of the Vatolin Institute of Metallurgy of the Ural Branch of RAS.

For citation: Agafonov S.N., Udoeva L.Yu., Vusikhis A.S., Leont'ev L.I. Assessment of the technological possibility of joint processing of ilmenite and perovskite concentrates. *Izvestiya. Ferrous Metallurgy*. 2025;68(5):444–453. *hhttps://doi.org/10.17073/0368-0797-2025-5-444-453*

Оценка технологической возможности совместной переработки ильменитовых и перовскитовых концентратов

С. Н. Агафонов[1], Л. Ю. Удоева[1], А. С. Вусихис[1], Л. И. Леонтьев[1, 2, 3]

[1] **Институт металлургии имени академика Н.А. Ватолина Уральского отделения РАН** (620016, Россия, Екатеринбург, ул. Амундсена, 101)
[2] **Национальный исследовательский технологический университет «МИСИС»** (Россия, 119049, Москва, Ленинский пр., 4)
[3] **Президиум РАН** (Россия, 119991, Москва, Ленинский пр., 32а)

agafonovs@ya.ru

Аннотация. Актуальной задачей, стоящей перед современной металлургической промышленностью, является повышение комплексности использования минерального и техногенного сырья путем разработки новых технологий, основанных на принципе совместной переработки сырья из месторождений, отличающихся минеральным составом рудной составляющей, например, титансодержащих руд – ильменитовых и перовскитовых. Совместная переработка титансодержащих руд позволит повысить экологическую и экономическую эффективность переработки отечественного минерального сырья, а также создаст предпосылки для развития производства диоксида титана

в России. С целью научного обоснования целесообразности совместной переработки разнотипного титанового сырья методом термодинамического моделирования установлено влияние температуры, расхода восстановителя и соотношения концентратов на процесс фазообразования при карботермическом восстановлении смесей концентратов. Рассмотрено распределение целевых металлов по продуктам взаимодействия, предложены оптимальные параметры процесса формирования богатых титановых шлаков. Оценены перспективы попутного извлечения редких и редкоземельных металлов. Термодинамический анализ процесса карботермического восстановления смесей, выполненный на модельных составах перовскитового концентрата (ПК) и ильменитового концентрата (ИК), показал, что при малых значениях соотношения ПК/ИК возможно образование высокотитанистых шлаков с содержанием TiO_2 более 80 %. Однако концентрация извлекаемого в сплав ниобия и содержание в шлаке редкоземельных элементов снизятся в разы по сравнению с их исходными значениями в перовскитовым концентрате. При соотношении ПК/ИК, равном 1, можно аккумулировать в сплаве до 2,5 % Nb при содержании в шлаке до 74 % TiO_2. Преимущество совместной переработки ильменитового и перовскитового сырья пирометаллургическим способом заключается в возможности в рамках одной технологической схемы получать богатые титановые шлаки и селективно концентрировать редкие металлы в металлической фазе, отделяя их от титана, и редкоземельные металлы в шлаке.

Ключевые слова: титановые концентраты, ильменит, перовскит, карботермическое восстановление, термодинамическое моделирование

Благодарности: Работа выполнена по Государственному заданию Института металлургии имени академика Н.А. Ватолина Уральского отделения РАН.

Для цитирования: Агафонов С.Н., Удоева Л.Ю., Вусихис А.С., Леонтьев Л.И. Оценка технологической возможности совместной переработки ильменитовых и перовскитовых концентратов. *Известия вузов. Черная металлургия*. 2025;68(5):444–453. https://doi.org/10.17073/0368-0797-2025-5-444-453

Introduction

Titanium is widely used in the paint and coatings, chemical, and other industries both as a metal and as a pigment-grade dioxide. The cessation of titanium raw material imports to the Russian Federation has resulted in a shortage of pigment titanium dioxide on the domestic market. At the same time, Russia possesses rich deposits of titanium ores [1] and their development is included in the near-term plans for the industry's growth. The main industrial type of titanium deposits in Russia is represented by zircon–rutile–ilmenite placers, which account for up to 60 % of titanium production. The second most significant are primary deposits of ilmenite and ilmenite–titanomagnetite ores. A large portion of titanium reserves is concentrated in perovskite–titanomagnetite ores. Processing of these ores remains problematic: on the one hand, perovskite ores are polymetallic, and the presence of rare and rare-earth metals makes them promising; on the other hand, no efficient technology for the comprehensive processing of such raw materials currently exists.

At present, in the Kola Peninsula, in addition to the extraction of ilmenite ores (Gremyaha–Vyrmes deposit), work has begun on the development of the Afrikanda perovskite–titanomagnetite deposit, whose ores contain, in addition to titanium-bearing minerals, niobium and rare-earth elements (REEs) [2 – 5].

The efficiency of subsequent TiO_2 production steps largely depends on the method used for ilmenite concentrate decomposition. According to published data, a variety of preparation techniques have been developed for this purpose. These methods are generally divided into pyrometallurgical and hydrochemical processes, both aimed at separating iron oxides from titanium dioxide.

Carbothermic reduction of ilmenite concentrates to produce high-titanium slags (75 – 85 % TiO_2) and hot metal is a well-established process. Numerous variations of this technology are typically related to the characteristics of the feedstock or to specific production objectives [6 – 8]. Smelting of the concentrate is performed in an electric arc furnace at temperatures up to 1600 °C, using carbonaceous reducing agents such as coke or anthracite. Flux-free operation yields slags with a residual FeO content of 10 – 12 %. The addition of lime or soda ash [9] increases the recovery of iron into the hot metal, lowering its residual concentration in the slag to 3 – 5 % FeO. In both cases, the process is conducted at 1600 – 1650 °C, and the titanium recovery to the slag remains nearly identical.

During beneficiation of Afrikanda ores, two main products are obtained – titanomagnetite and perovskite concentrates. The latter contains (wt. %): 48 – 50 TiO_2; 33 – 35 CaO; 2 – 4 REEs; 0.9 – 1.2 $(Nb, Ta)_2O_5$ [10]. Technologies developed at the Kola Science Center of the Russian Academy of Sciences for processing perovskite concentrate rely on hydrochemical decomposition methods employing nitric acid, sulfuric acid, or mixtures of these acids with hydrochloric acid [11 – 14].

The pyrometallurgical processing of perovskite concentrates has been investigated far less extensively, since hydrometallurgical decomposition methods are currently considered more practical. Nevertheless, acid-based technologies present serious environmental challenges, generating large volumes of aggressive wastes – acidic effluents, sludges, and off-gases – that require costly neutralization. These drawbacks diminish the overall cost-effectiveness of processing such complex titanium feedstocks. In contrast, the application of carbothermic reduction to titanium-bearing materials (ilmenite concentrate, rutile, titanium slag, etc.) [15; 16], including perovskite concentrate [17], may offer new opportunities for pyrometallurgical routes in titanium production.

High-titanium slags obtained by reduction smelting of ilmenite concentrates are known to be highly refrac-

tory and "short" [18; 19]. Their viscosity depends primarily on the FeO and TiO_2 contents and on the slag basicity (CaO/SiO_2) [20; 21]. To improve fusibility, calcium oxide is added to adjust the CaO/TiO_2 ratio toward the eutectic composition with a melting point of 1460 °C [22]. Building on existing ilmenite-processing technologies, the feasibility of using perovskite concentrate as a calcium-bearing fluxing additive has therefore been considered. Joint processing of ilmenite and perovskite concentrates offers clear advantages. Within a single integrated process flow sheet it enables the production of titanium-rich slags while simultaneously recovering rare and rare-earth metals.

To justify this approach, a thermodynamic analysis of the reactions between mixed concentrates and carbon was carried out to evaluate the feasibility of their joint carbothermic reduction.

Materials and methods

Samples of ilmenite concentrate (IC) and perovskite concentrate (PC) were used in this study. The chemical and phase compositions of the concentrates are presented in Table 1. *X*-ray diffraction, scanning electron microscopy, and energy-dispersive *X*-ray spectroscopy analyses revealed that titanium in the IC sample is concentrated in rutile (TiO_2) and in the product of ilmenite leucoxenization – pseudorutile ($Fe_2O_3 \cdot 3TiO_2$). In the PC sample, the main ore minerals are perovskite ($CaO \cdot TiO_2$), titanite ($CaTiSiO_5$), and ulvöspinel (Fe_2TiO_4). Rare metals, primarily niobium, are contained in loparite (5.0 %), ancylite (1.9 %), and thorite (26.5 %), while rare-earth elements (Ce, La, Nd) occur in perovskite (2.8 %) and loparite (22.8 % Ce).

To optimize process parameters and calculate the equilibrium composition of products and the main technological indicators, thermodynamic modeling was performed using the HSC Chemistry 6.12 software package (Outotec Oy) [23]. The model inputs were based on compositions of working materials close to those of the concentrate samples used in subsequent experimental studies. Since the program database contains no information on pseudorutile, it was substituted by ilmenite and rutile according to reaction (1), as reduction of pseudorutile proceeds through the sequential formation of ilmenite and then dititanate:

$$Fe_2Ti_3O_9 + C = 2FeTiO_3 + TiO_2 + CO(g); \quad (1)$$

$$FeTiO_3 + TiO_2 = FeTi_2O_5. \quad (2)$$

For simplification, and considering that the process is mainly influenced by the ore mineral components, the thermodynamic analysis was carried out using model compositions of PC and IC with elemental ratios corresponding to real titanium raw materials (wt. %):

– perovskite concentrate: 60 $CaO \cdot TiO_2$, 10 TiO_2, 10 SiO_2, 10 Fe_2TiO_4, 9 $CaCO_3$, 1 Nb_2O_5;

– ilmenite concentrate: 40 $FeO \cdot TiO_2$, 50 TiO_2, 8 Fe_2O_3, 2 SiO_2.

Results and discussion

An important factor in evaluating the efficiency of joint processing of titanium raw materials is determining the optimal PC/IC ratio in the charge for carbothermic reduction roasting.

Equilibrium in the chemically reacting PC–IC–carbon systems was analyzed for PC/IC ratios of 0.2, 0.5, 0.8, and 1.0 as a function of temperature (700 – 1700 °C) and carbon consumption. Calculations were performed for 100 kg of mixture plus carbon in an inert atmosphere containing 100 mol N_2.

Regardless of the component ratio, the metallic product – in which iron forms the base of the alloy – contains niobium and titanium carbides and iron silicides, whose amounts increase in proportion to carbon consumption (Fig. 1). As the PC/IC ratio increases, the niobium content in the alloy (as NbC) rises from 0.7 to 2.7 %, reflecting its higher initial concentration in the mixture. At 1500 °C, noticeable transfer of niobium into the alloy occurs when carbon consumption exceeds 4 kg per 100 kg of mixture, irrespective of the PC/IC ratio. Titanium appears in the alloy only at higher carbon contents: above 6 kg C for PC/IC = 0.2 – 0.4, above 5 kg C for PC/IC = 0.8, and above 4 kg C for PC/IC = 1.0.

With an increasing PC fraction, the $TiO_2/CaO \cdot TiO_2$ ratio in the slag also rises – from 4.5 at PC/IC = 0.2 to nearly equal proportions (1.1) at PC/IC = 1.0 (Fig. 2). According to the model, greater carbon consumption promotes the formation of lower titanium oxides, mainly through reduction of titanium from rutile (TiO_2) and ilmenite ($FeO \cdot TiO_2$), i.e., the mineral phases of the ilme-

Table 1. **Chemical composition of ilmenite and perovskite concentrates**

Таблица 1. **Химический состав ильменитового и перовскитового концентратов**

Concentrate	Ti	Fe	Al	Ca	Mg	Cr	Ce	Si	Nb
Ilmenite	41.43	18.90	1.53	0.13	0.22	0.60	–	0.90	–
Perovskite	20.78	7.23	0.71	16.79	1.67	–	0.49	5.25	0.81

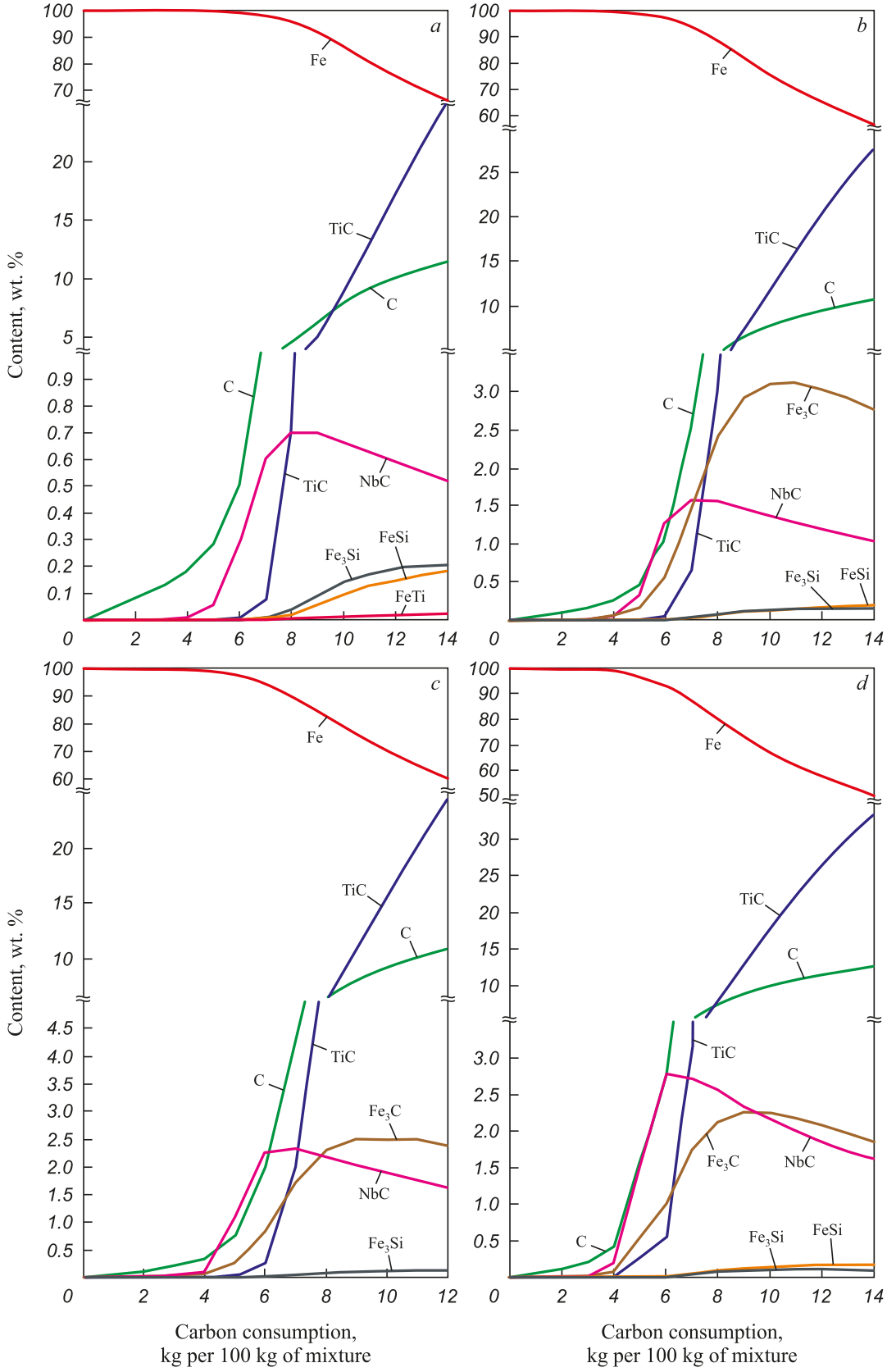

Fig. 1. Dependence of equilibrium composition of the slags from reduction of the model mixture of ore and concentrate with different PC/IC ratios on consumption of the reducing agent at a temperature of 1500 °C: *a* – 0.2; *b* – 0.5; *c* – 0.8; *d* – 1.0

Рис. 1. Зависимость равновесного состава шлаков восстановления модельной смеси руды и концентрата с различным соотношением ПК/ИК: *a* – 0,2; *b* – 0,5; *c* – 0,8; *d* – 1,0 от расхода восстановителя при температуре 1500 °С

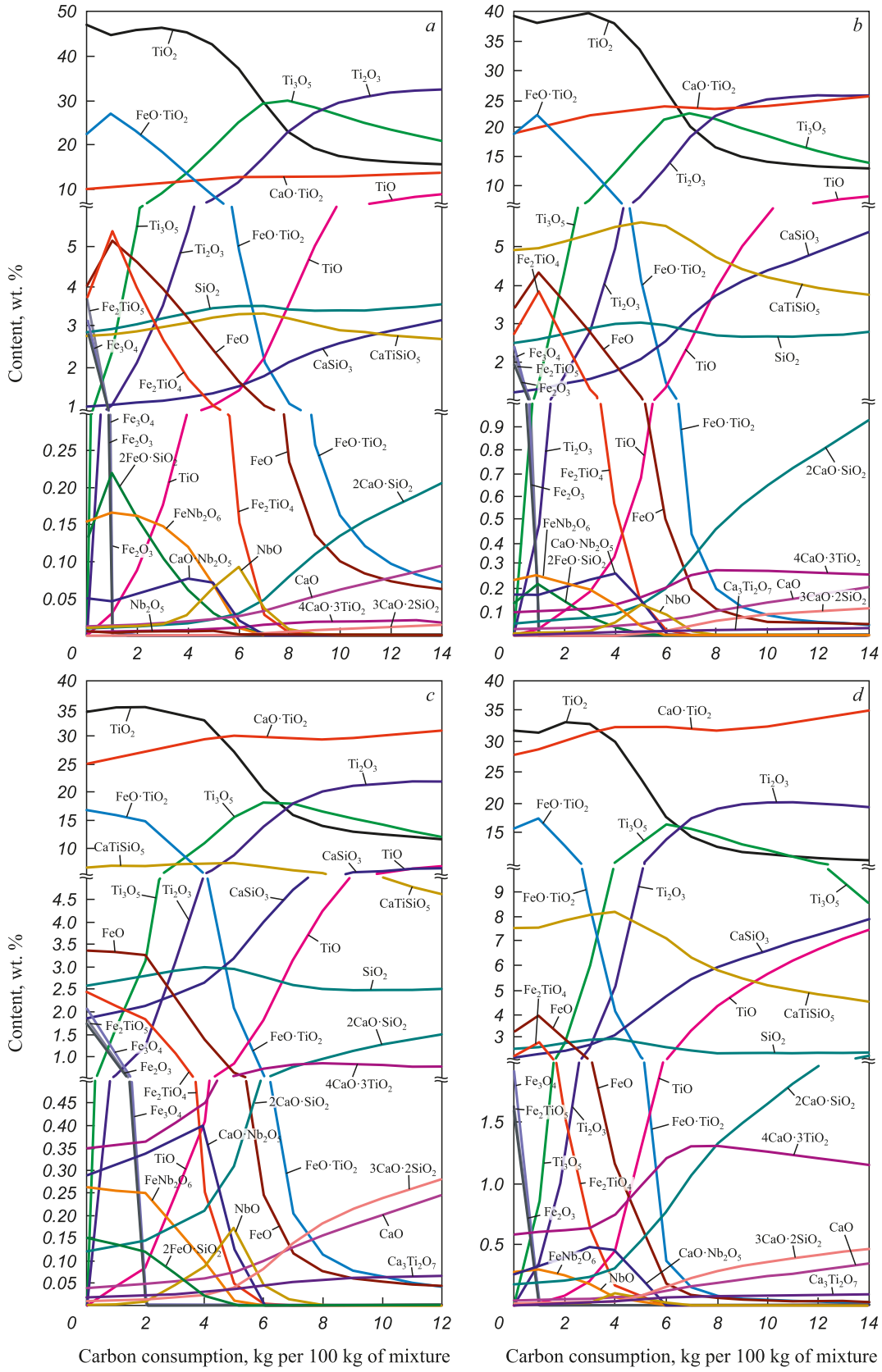

Fig. 2. Dependence of equilibrium composition of the alloys from reduction of the model mixture of ore and concentrate with different PC/IC ratios on consumption of the reducing agent at a temperature of 1500 °C:
a – 0.2; *b* – 0.5; *c* – 0.8; *d* – 1.0

Рис. 2. Зависимость равновесного состава сплавов восстановления модельной смеси руды и концентрата с различным соотношением ПК/ИК:
a – 0,2; *b* – 0,5; *c* – 0,8; *d* – 1,0 от расхода восстановителя при температуре 1500 °С

nite concentrate. The perovskite ($CaO·TiO_2$) content changes only slightly, increasing smoothly from 5 to 8 % over the entire range of carbon additions. At 1500 °C, titanium reduction from rutile and ilmenite starts at low carbon levels and reaches a maximum (for Ti_3O_5) at 6 – 8 kg C per 100 kg of concentrate mixture. With increasing PC fraction, the proportion of lower oxides (Ti_3O_5, Ti_2O_3, TiO) decreases, improving the technological properties of the slag.

Table 2 presents the equilibrium compositions of reduction products of IR and PC mixtures at 1500 °C. For each PC/IC ratio, carbon consumptions corresponding to the onset and maximum of niobium transfer into the alloy were selected. Before niobium recovery, the metallic phase corresponds to low- or medium-carbon steel (<0.25 or ≤0.55 % C). Complete niobium transfer to the metallic phase as carbide yields cast iron (hot-metal).

The effect of temperature on the equilibrium composition of carbothermic products was calculated for a PC/IC = 1.0 mixture at carbon consumption of 4 and 6 kg per 100 kg of charge, corresponding to the onset and maximum niobium recovery. Niobium appears in the alloy above 900 °C regardless of carbon level. In the temperature range above 1200 °C, where NbC formation is maximal, titanium also enters the alloy as carbide, reaching 0.5 % at 1500 °C. At higher temperatures, metallic niobium and iron silicides form.

The amount of titanium reduction products in the slag increases sharply with temperature. For Ti_3O_5 and Ti_2O_3, their contents rise by two orders of magnitude – from fractions of a percent to 10 and 15 % at 4 and 6 kg C, respectively. Monoxide TiO forms above 1000 °C; its growth with temperature is more sensitive to carbon level.

Up to 1100 °C, iron reduction from ilmenite leads to an increase in rutile, whose content then drops rapidly as TiO_2 is further reduced to lower titanium oxides.

Throughout the temperature range, the concentration of tetravalent titanium compounds bound with calcium – perovskite ($CaO·TiO_2$) and sphene ($CaTiSiO_5$) – changes only slightly, confirming the stability of Ti(IV) within calcium-bearing minerals. Therefore, introducing CaO flux additives into the carbothermic smelting charge is advisable. Such additions inhibit the formation of lower titanium oxides, preventing the development of high-melting slags with elevated fusion/crystallization temperatures. According to [18; 25], when processing high-titanium raw materials, easily fusible slags with crystallization temperatures of 1400 – 1450 °C and a TiO_2 content of approximately 60 % are obtained at a basicity (CaO/SiO_2) of 4.0. In the present calculations, for mixtures with a PC/IC ration equal to 0.2 – 1.0, the modeled slag basicity increases from 1.4 to 2.5 (Fig. 3), governed primarily by the initial CaO/SiO_2 ratio in the PC, since the IC contains ≤0.3 % CaO and ~2 % SiO_2. To condition the slag to the target CaO/SiO_2 = 4.0, CaO flux must be added to the charge; for PC/IC = 1, about 9.2 kg CaO per 100 kg of mixture is required (Fig. 3).

Thus, thermodynamic analysis of carbothermic reduction of the model mixtures using model PC and IC compositions showed that at low PC/IC ratios, the formation of high-titanium slags (>80 % TiO_2) can be expected. However, the niobium concentration in the alloy and the REE content in the slag decrease several-fold compared with their initial values in the perovskite concentrate. At a PC/IC ratio equal to 1, up to 2.5 % Nb can be accumulated in the alloy, with up to 74 % TiO_2 in the slag (Table 2). In this case, the REE concentration in the slag decreases by no more than 1.5 times.

To predict the product composition from reduction smelting of a PC–IC mixture, thermodynamic modeling of the process was performed over 700 – 1700 °C. The calculations used the complete chemical and mineralogical compositions of the titanium concentrate samples (Table 1) at a PC/IC ratio equal 1.

Temperature dependences of the equilibrium compositions of the reaction products were calculated for two levels of carbon consumption: 4 kg C per 100 kg of concentrate mixture, which prevents titanium transfer to the alloy in the form of carbide, and 6 kg C, which ensures maximum niobium recovery to the alloy. Flux additions were set at 10 kg CaO per 100 kg of concentrate mixture. The charge compositions for both variants are presented in Table 3. According to the calculations, at a low carbon consumption (4 kg per 100 kg of mixture), the alloy mainly consists of iron with small amounts of chromium (0.6 %) and carbon (0.5 %) (Table 4). At 1500 °C, the NbC content in the alloy reaches only hundredths of a percent. Titanium (IV) in the slag is present mainly as $CaO·TiO_2$ (up to 45 %), TiO_2 (up to 22 %),

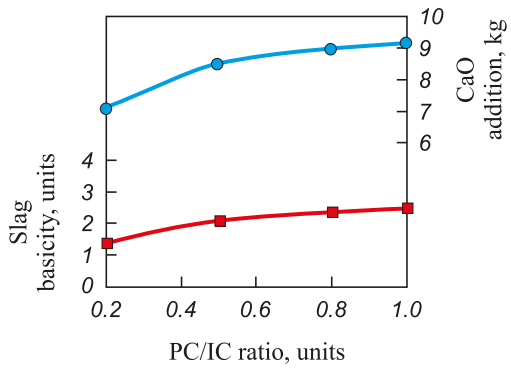

Fig. 3. Calculated dependence of basicity of the slags from carbothermic reduction of the model mixtures and the flux amount for its conditioning on PC/IC ratio

Рис. 3. Расчетная зависимость основности шлаков карботермического восстановления модельных смесей и количества флюса для его кондиционирования от соотношения ПК/ИК

Table 2. **Equilibrium compositions of the interaction products of mixtures of PC and IC with carbon**

Таблица 2. **Равновесные составы продуктов взаимодействия смесей ПК и ИК с углеродом**

PC/IC	Initial content in mixture, %						Carbon consumption, kg per 100 kg of mixture	Composition of reduction products										
								alloy, %					slag, %					
	TiO_2	FeO	Fe_2O_3	Nb_2O_5	CaO	SiO_2		yield	Fe	C	Nb	Ti	yield	CaO	SiO_2	TiO_2	FeO	Nb_2O_5
0.2	69.3	16.2	6.2	0.17	4.8	3.33	4.0	11.0	100.0	0	0	0	79.5	5.9	4.0	80.3	9.7	0.1
							8.0	16.9	96.0	2.8	0.6	0.6	66.6	6.5	4.0	89.0	0.5	0
0.5	64.6	15.0	5.3	0.33	10.0	4.67	5.0	12.7	99.6	0.1	0.3	0	75.4	12.1	5.7	78.8	3.0	0.4
							7.0	14.7	95.6	3.0	1.4	0	70.3	12.5	5.9	81.2	0.4	0
0.8	62.4	13.6	4.5	0.45	13.4	5.65	3.0	8.1	99.8	0.2	0	0	84.0	15.0	6.4	70.5	7.6	0.5
							6.0	13.0	95.5	2.3	2.0	0.2	73.4	15.9	6.9	76.7	0.5	0
1.0	61.2	12.9	4.1	0.50	15.2	6.10	4.0	10.3	99.4	0.4	0.2	0	83.5	17.5	7.1	71.7	3.0	0.7
							6.0	12.6	93.9	3.2	2.5	0.4	74.1	18.3	7.3	74.1	0.3	0

Table 3. **Composition of the charge of carbothermic reduction of mixtures of perovskite and ilmenite concentrates with a PC/IC ratio equal to 1**

Таблица 3. **Состав шихты карботермического восстановления смесей ПК и ИК при их соотношении, равном 1**

Charge composition	Content, %										
	Al	Ca	Ce	Fe	Mg	Nb	Si	Ta	Ti	C	Cr
Mixture of ore and concentrate	1.12	8.50	0.25	13.1	2.10	0.405	3.10	0.007	31.11	0.32	0.30
Charge *1* (100 kg of mixture, 10 kg CaO, 4 kg C)	0.98	7.50	0.22	11.5	1.84	0.360	2.72	0.006	27.29	9.04	0.26
Charge *2* (100 kg of mixture, 10 kg CaO, 6 kg C)	0.96	7.33	0.22	11.3	1.81	0.350	2.67	0.006	26.82	8.90	0.26

Table 4. **Calculated composition of the interaction products of a mixture of perovskite and ilmenite concentrate samples at 1500 °C**

Таблица 4. **Расчетный состав продуктов взаимодействия смеси проб ПК и ИК при 1500 °C**

Charge	Carbon consumption, kg	Alloy yield, %	Composition of alloy, %					Slag yield, %	Composition of slag, %							
			Fe	C	Nb	Cr	Ti		TiO_2	CaO	SiO_2	Nb_2O_5	CeO_2	Al_2O_3	MgO	FeO
1	4	12.1	98.9	0.5	0	0.6	0	89.3	59.2	25.8	7.8	0.7	0.35	2.3	1.6	2.2
2	6	14.9	90.3	4.3	2.7	2.0	0.7	85.6	62.4	24.3	8.9	0	0.41	2.3	1.7	0

and $CaTiSiO_5$ (10 %), as well as magnesium titanates $MgTiO_3$ and $MgTi_2O_5$ in amounts of 1.0 – 1.5 %. The remaining titanium occurs as suboxides: 2 % Ti_2O_3, 4 % Ti_3O_5, and 0.5 % TiO. The total titanium content in the slag, recalculated as TiO_2, is 59.2 %. Niobium from iron and calcium niobates is also reduced with increasing temperature, forming lower oxides NbO_2 and NbO. Cerium from CeO_2 is partially reduced to $Ce^{3+}AlO_3$, while remaining completely in the slag.

At carbon consumptions higher than the stoichiometric requirement for complete iron reduction (6 kg C), the alloy contains 3 % Nb in the form of carbide and 2.0 % Cr, with the recovery of both elements into the metallic phase approaching 100 % (Table 4). Tantalum also completely transfers to the alloy as carbide (0.06 % TaC), similarly to niobium. Titanium reduction to carbide starts at 1000 °C and reaches its maximum at 1500 – 1600 °C, corresponding to 0.7 % Ti. With further increase in carbon content, its concentration rises to 4.4 wt. %, exceeding that of niobium. By carbon content, the metallic product corresponds to cast iron (4.3 % C). An increase in carbon consumption to 6 kg does not significantly change the qualitative composition of the slag. Quantitatively, with increasing temperature, the proportions of niobium suboxides NbO and NbO_2 decrease sharply, amounting to less than 0.01 and 0.02 %, respectively, at 1500 °C, while the content of lower titanium oxides increases to about 10 %. The cerium concentration remains constant, both in the forms in which it occurs in the slag and in their relative proportions. It should be noted that for the selected mixture composition (PC/IC = 1), the cerium concentration in the slag (0.4 % CeO_2) is about 1.5 times lower than in the original perovskite concentrate (0.6 % CeO_2). Other components of the raw materials (Al, Mg, Si) originating from gangue minerals are present in the slag as simple or complex (binary and ternary) oxides, but their total content is small, limited to a few percent. According to the calculations, the introduced amount of flux (10 kg CaO) is insufficient to obtain slags with the desired basicity. At carbon consumptions of 4 and 6 kg, the CaO/SiO_2 ratios are 3.4 and 2.7, respectively. Thus, in the first case, the charge should contain 15 kg CaO, and in the second – 20 kg CaO. If the calcium deficiency is compensated by increasing the PC proportion in the mixture, the resulting titanium slag should have a higher content of rare and rare-earth metals.

Conclusions

The advantage of joint pyrometallurgical processing of ilmenite and perovskite raw materials lies in the possibility of producing titanium-rich slags and selectively concentrating rare metals in the metallic phase, separating them from titanium, while rare-earth elements remain concentrated in the slag. Moreover, this approach eliminates the need to beneficiate perovskite–titanomagnetite ore to obtain a concentrate by removing iron-bearing minerals and calcite.

According to the thermodynamic models obtained, the joint reduction of ilmenite and perovskite concentrates proceeds with the formation of an iron-based alloy and a high-titanium slag containing more than 70 % TiO_2. The composition of the smelting products depends on both temperature and carbon consumption. At 1500 °C and carbon inputs below the stoichiometric requirement for niobium transfer to the alloy, the metallic phase corresponds to low- or medium-carbon steel (≤0.55 % C). When niobium is completely transferred to the metallic phase in the form of carbide, the product corresponds to hot metal.

At low PC/IC ratios (<0.5), high-titanium slags with a TiO_2 content exceeding 80 % are expected to form. However, under these conditions, the niobium content in the alloy remains low, and the REE concentration in the slag decreases severalfold relative to their initial levels in the ore. Reduction of the concentrate mixture with a PC/IC ratio equal 1 at 1500 °C and 6 kg of carbon per 100 kg of mixture enables complete transfer of niobium to the alloy, which contains up to 3.0 % Nb, while producing a titanium-rich slag with 62 – 74 % TiO_2. In this case, the cerium concentration, as well as that of other REE, decreases by no more than 1.5 times.

References / Список литературы

1. Bykhovskii L.Z., Tigunov L.P. Titanium raw materials of Russia. *Rossiiskii chimicheskii zhurnal*. 2010;54(2):73–86. (In Russ.).

   Быховский Л.З., Тигунов Л.П. Титановое сырье России. *Российский химический журнал*. 2010;54(2):73–86.
2. Nikolaev A.I., Gerasimova L.G., Petrov V.B., Mayorov V.G. Perovskite concentrate - as a source for titanium and rare-metal products. *Kompleksnoe ispol'zovanie mineral'nogo syr'ya (KIMS)*. 2015;(2(293)):26–34. (In Russ.).

   Николаев А.И., Герасимова Л.Г., Петров В.Б., Майоров В.Г. Перовскитовый концентрат – перспективное нетрадиционное сырье для производства титановой и редкометалльной продукции. *Комплексное использование минерального сырья (КИМС)*. 2015;(2(293)):26–34.
3. Krasotkin I.S., Voitekhovskii Yu.L., Leskov A.L. Afrikanda: beginning of the story. In: *Proceedings of VIII All-Russian Fersman Scientific Session (April 18–19, 2011)*. 2011:23–30. (In Russ.).

   Красоткин И.С., Войтеховский Ю.Л., Лесков А.Л. Африканда: начало истории. В сб.: *Труды VIII Всероссийской Ферсмановской научной сессии, (18–19 апреля 2011 г.)*. 2011:23–30.
4. Sokolov S.V., Nechelyustov G.N., Bystrov I.G. Alkaline magmatism of the Earth and related deposits of strategic metals. School "Alkaline magmatism of the Earth". In: *Proceedings of the XXXIII Int. Conf. Vernadsky Institute of Geo-*

chemistry and Analytical Chemistry of the Russian Academy of Sciences. 2016:116–118. (In Russ.).

Соколов С.В., Нечелюстов Г.Н., Быстров И.Г. Щелочной магматизм земли и связанные с ним месторождения стратегических металлов. Школа «Щелочной магматизм Земли». В сб.: *Труды XXXIII Международной конференции Институт геохимии и аналитической химии им. В.И. Вернадского Российской Академии Наук*. 2016:116–118.

5. Gerasimova L.G., Artemenkov A.G., Nikolaev A.I., Shchukina E.S. Titanium-rare metal concentrates from raw materials of the Kola region and the possibility of their joint processing to obtain scarce products. *Arctic: Ecology and Economics*. 2024;14(2):217–225. (In Russ.). https://doi.org/10.25283/2223-4594-2024-2-217-225

Герасимова Л.Г., Артеменков А.Г., Николаев А.И., Щукина Е.С. Титано-редкометалльные концентраты из сырья Кольского региона и возможность их совместной переработки с получением дефицитной продукции. *Арктика: экология и экономика*. 2024;14(2):217–225. https://doi.org/10.25283/2223-4594-2024-2-217-225

6. Reznicenko V.A., Ustinov V.S., Karyazin I.A., A.N. Petrun'ko A.N. Electrometallurgy and Chemistry of Titanium. Moscow: Nauka; 1982:276. (In Russ.).

Резниченко В.А., Устинов В.С., Карязин И.А., Петрунько А.Н. Электрометаллургия и химия титана. Москва: Наука; 1982:276.

7. Ma N., Warner N.A. Smelting reduction of ilmenite by carbon in molten pig iron. *Canadian Metallurgical Quarterly*. 1999;38(3):165–173.

8. Smirnov K.I., Gamov P.A. Pyro-metallurgical processing of ilmenite concentrate with production of iron and titanium oxides. *Solid State Phenomena*. 2021;316:385–389. https://doi.org/10.4028/www.scientific.net/ssp.316.385

9. Gudim Yu.A., Meirzhan A., Roshchin V.E. Possibilities of pyrometallurgical enrichment of ilmenite concentrates. *Bulletin of the South Ural State University. Series: Metallurgy*. 2016;16(1):23–32. (In Russ.). http://dx.doi.org/10.14529/met160103

Гудим Ю.А., Мейржан А., Рощин В.Е. Возможности пирометаллургического обогащения ильменитовых концентратов. *Вестник Южно-Уральского государственного университета. Серия: Металлургия*. 2016;16(1):23–32. http://dx.doi.org/10.14529/met160103

10. Motov D.L. Technological solution to the perovskite problem. *Proceedings of VII All-Russian Fersman Scientific Session (May 2–5, 2010)*. 2010:187–192 (In Russ.).

Мотов Д.Л. Технологическое решение проблемы перовскита. В сб.: *Труды VII Всероссийской Ферсмановской научной сессии, (2–5 мая 2010 г.)*. 2010:187–192.

11. Goroshchenko Ya.G., Motov D.L., Belokoskov V.I., etc. On the issue and choice of a process flow sheet for obtaining titanium pigments from perovskite concentrate with concomitant extraction of rare metals. In: *Proceedings of the Conf. on Chemical Technology of Mineral Resources of the Kola Peninsula*. Leningrad: Academy of Sciences USSR; 1959;1:148–221. (In Russ.).

Горощенко Я.Г., Мотов Д.Л., Белокосков В.И. и др. К вопросу и выборе схемы технологического процесса для получения титановых пигментов из перовскитового концентрата с попутным извлечением редких металлов. *Сборник трудов по химической технологии минерального сырья Кольского полуострова*. Ленинград: Издательство АН СССР; 1959;1:148–221.

12. Kiselev Yu.G., Shchukina E.S. The solubility of the hydrated product obtained by perovskite nitric acid treatment in sulfuric acid. *Bulletin of the Kola Science Center of the Russian Academy of Sciences*. 2017;(2):81–86. (In Russ.).

Киселев Ю.Г., Щукина Е.С. Растворимость гидратного продукта, полученного при азотнокислотной обработке перовскита, в серной кислоте. *Вестник Кольского научного центра РАН*. 2017;(2):81–86.

13. Gerasimova L.G., Maslova M.V., Shchukina E.S. Preparation of titanium dioxide for heat-resistant sealants. *Theoretical Foundations of Chemical Engineering*. 2011;45(4):511–516. https://doi.org/10.1134/S0040579513050035

14. Gerasimova L.G., Mel'nik N.A., Nikolaev A.I., Petrov V.B., Shchukina E.S., Bychenya Yu.G. Hydrochloric acid technology of perovskite concentrate and its radiation assessment. *Ekologiya promyshlennogo proizvodstva*. 2015;89:54–58. (In Russ.).

Герасимова Л.Г., Мельник Н.А., Николаев А.И., Петров В.Б., Щукина Е.С., Быченя Ю.Г. Солянокислотная технология перовскитового концентрата и ее радиационная оценка. *Экология промышленного производства*. 2015;89:54–58.

15. Rezan S.A., Zhang G., Ostrovski O. Carbothermal reduction and nitridation of ilmenite concentrate. *ISIJ International*. 2012;52(3):363–368.

16. Xiao J., Jiang B., Huang K., Jiao S., Zhu H-m. Selective reduction of TiO_2–SiO_2 in the carbothermal reduction of titanium raw materials for preparation og titanium oxycarbide. In: *The Minerals, Metals &Materials Society: 7th Int. Symp. on High-Temperature Metallurgical Processing*. 2016:419–425. https://doi.org/10.1007/978-3-319-48093-0_52

17. Budin O.N., Kropachev A.N., Agafonov D.G., Cherepov V.V. Study into carbothermic method of titanium raw material decomposition in case of artificially synthesized perovskite. *Izvestiya. Non-Ferrous Metallurgy*. 2018;(5):23–30. (In Russ.). https://doi.org/10.17073/0021-3438-2018-5-23-30

Будин О.Н., Кропачев А.Н., Агафонов Д.Г., Черепов В.В. Изучение карботермического способа вскрытия титанового сырья на примере искусственно синтезированного перовскита. *Известия вузов. Цветная металлургия*. 2018;(5):23–30. https://doi.org/10.17073/0021-3438-2018-5-23-30

18. Vasyutinskii N.A. Titanium Slags. Moscow: Metallurgiya; 1972:208. (In Russ.).

Васютинский Н.А. Титановые шлаки. Москва: Металлургия; 1972:208.

19. Asanov A.V., Anoshkin I.V., Mal'kov A.V., Senin A.V., Roshchin A.V. Influence of chemical composition and temperature on the viscosity of high-titanium slags. *Bulletin of SUSU*. 2008;(9):7–9. (In Russ.).

Асанов А.В., Аношкин И.В., Мальков А.В., Сенин А.В., Рощин А.В. Влияние химического состава и температуры на вязкость высокотитанистых шлаков. *Вестник ЮУрГУ*. 2008;(9):7–9.

20. Jing J., Guo Y., Wang S., Chen F., Yang L., Yang J., Xu F., Yu L. Melting properties and phase composition transfor-

mation of Ti-bearing electric furnace slags in $CaO–SiO_2–MgO–Al_2O_3–50\%TiO_2$. *Metals and Materials International*. 2024;30:2045–2056.
https://doi.org/10.1007/s12540-024-01630-y

21. Yan Z.-m., Lv X.-w., Li Z.-s. Physicochemical properties and structure of titania-containing metallurgical slags: A review. *Journal of Iron and Steel Research International*. 2022;29:187–206.
https://doi.org/10.1007/s42243-021-00678-z

22. Daněk V., Nerád I. Phase diagram and structure of melts of the system $CaO–TiO_2–SiO_2$. *Chemical Papers*. 2002; 56(4):241–246.

23. Roine A. HSC Chemistry. Version 6.12 for Windows, Outotec Research Oy. Pori, Finland; 1974–2007.

24. Safonov A.V., Yakushevich N.F., Leboshkin V.N., Shadrin V.N., Gordin S.O. Carbothermic reduction of ilmenite concentrates in the solid phase. *Izvestiya. Ferrous Metallurgy*. 2004;47(2):19–22. (In Russ.).

Сафонов А.В., Якушевич Н.Ф., Лебошкин В.Н., Шадрин В.Н., Гордин С.О. Углетермическое восстановление ильменитовых концентратов в твердой фазе. *Известия вузов. Черная металлургия*. 2004;47(2):19–22.

25. Leont'ev L.I., Vatolin N.A., Shavrin S.V., Shumakov N.S. Pyrometallurgical Processing of Complex Ores. Moscow: Metallurgiya; 1997:432. (In Russ.).

Леонтьев Л.И., Ватолин Н.А., Шаврин С.В., Шумаков Н.С. Пирометаллургическая переработка комплексных руд. Москва: Металлургия; 1997:432.

Information about the Authors / Сведения об авторах

Sergei N. Agafonov, *Cand. Sci. (Eng.), Senior Researcher of the Laboratory of Rare Refractory Metals*, Vatolin Institute of Metallurgy of the Ural Branch of the Russian Academy of Sciences
ORCID: 0000-0001-6731-3595
E-mail: agafonovs@ya.ru

Lyudmila Yu. Udoeva, *Cand. Sci. (Eng.), Leading Researcher of the Laboratory of Rare Refractory Metals,* Vatolin Institute of Metallurgy of the Ural Branch of the Russian Academy of Sciences
ORCID: 0000-0002-8699-6587
E-mail: lyuud@yandex.ru

Aleksandr S. Vusikhis, *Cand. Sci. (Eng.), Senior Researcher of the Laboratory of Pyrometallurgy of Non-Ferrous Metals,* Vatolin Institute of Metallurgy of the Ural Branch of the Russian Academy of Sciences
ORCID: 0000-0002-6395-0834
E-mail: vas58@mail.ru

Leopol'd I. Leont'ev, *Academician, Adviser*, Presidium of the Russian Academy of Sciences; *Dr. Sci. (Eng.), Prof.*, National University of Science and Technology "MISIS"; *Chief Researcher,* Vatolin Institute of Metallurgy of the Ural Branch of the Russian Academy of Sciences
ORCID: 0000-0002-4343-914X
E-mail: leo@presidium.ras.ru

Сергей Николаевич Агафонов, *к.т.н., старший научный сотрудник лаборатории редких тугоплавких металлов*, Институт металлургии имени академика Н.А. Ватолина Уральского отделения РАН
ORCID: 0000-0001-6731-3595
E-mail: agafonovs@ya.ru

Людмила Юрьевна Удоева, *к.т.н., ведущий научный сотрудник лаборатории редких тугоплавких металлов*, Институт металлургии имени академика Н.А. Ватолина Уральского отделения РАН
ORCID: 0000-0002-8699-6587
E-mail: lyuud@yandex.ru

Александр Семенович Вусихис, *к.т.н., старший научный сотрудник лаборатории пирометаллургии цветных металлов*, Институт металлургии имени академика Н.А. Ватолина Уральского отделения РАН
ORCID: 0000-0002-6395-0834
E-mail: vas58@mail.ru

Леопольд Игоревич Леонтьев, *академик, советник*, Президиум РАН; *д.т.н., профессор*, Национальный исследовательский технологический университет «МИСИС»; *главный научный сотрудник*, Институт металлургии имени академика Н.А. Ватолина Уральского отделения РАН
ORCID: 0000-0002-4343-914X
E-mail: leo@presidium.ras.ru

Contribution of the Authors / Вклад авторов

S. N. Agafonov – calculations, conducting experiments.

L. Yu. Udoeva – setting the research task, calculations, writing the text, drawing conclusions.
A. S. Vusikhis – setting the research task, calculations, writing the text, drawing conclusions.
L. I. Leont'ev – scientific guidance, analysis of research results, editing the text.

С. Н. Агафонов – проведение расчетов, проведение экспериментов.
Л. Ю. Удоева – постановка задачи исследования, проведение расчетов, подготовка текста, формирование выводов.
А. С. Вусихис – постановка задачи исследования, проведение расчетов, подготовка текста, формирование выводов.
Л. И. Леонтьев – научное руководство, анализ результатов исследований, редактирование статьи.

Received 08.07.2025
Revised 10.07.2025
Accepted 28.08.2025

Поступила в редакцию 08.07.2025
После доработки 10.07.2025
Принята к публикации 28.08.2025

METALLURGICAL TECHNOLOGIES / МЕТАЛЛУРГИЧЕСКИЕ ТЕХНОЛОГИИ

UDC 621.365.2:662.612.11/321/322
DOI 10.17073/0368-0797-2025-5-454-460

Original article
Оригинальная статья

Comparative analysis of kinetic and diffusion modes of natural gas combustion in EAF burners

I. V. Glukhov[1, 2], G. V. Voronov[1], O. Yu. Sheshukov[1, 3], M. V. Kalganov[1, 2]

[1] **Ural Federal University named after the first President of Russia B.N. Yeltsin** (19 Mira Str., Yekaterinburg 620002, Russian Federation)
[2] **OJSC "Scientific Research Institute of Metallurgical Heat Engineering" (VNIIMT)** (16 Studencheskaya Str., Yekaterinburg 620137, Russian Federation)
[3] **Vatolin Institute of Metallurgy of the Ural Branch of the Russian Academy of Sciences** (101 Amundsena Str., Yekaterinburg 620016, Russian Federation)

ermia12@yandex.ru

Abstract. In modern electric arc furnaces (EAF), charge heating by natural gas (NG) combustion products with process oxygen is widely used to reduce the power consumption and intensify the thermal performance. In existing EAF burners, gas and oxygen are supplied separately through oxygen gas and refining burners, which ensures the diffusion combustion mode. The diffusion mode in conditions of EAF working space has a number of disadvantages, such as non-optimal distribution of temperature and concentration fields of combustion products, increased burn-off of iron-containing components of the charge. This paper presents the results of a computational study of the physico-chemical properties of combustion products along the torch length for the burners of VAI FUCHS, SMS DEMAG and NTPF Etalon Ltd. companies at oxygen concentration in the oxidizer of 95 wt. %. The results of computer modeling of temperature fields in the torches were analyzed in order to assess the risk of flame "slip" into the burner internal volume. The authors carried out a comparative study of the characteristics of torches in the burner devices with diffusion and kinetic combustion modes. Based on the data obtained, a transition from the diffusion mode of natural gas combustion to the kinetic mode is proposed, which can increase the energy efficiency of using burners, uniformity of temperature and concentration fields of combustion products, and reduce carbon monoxide of the iron-containing charge. The study was performed using computer modeling in ANSYS software package in CFX module. The obtained results can be useful for optimizing thermal processes in EAF working space, reducing power consumption and preventing emergency operation of burners.

Keywords: EAF, burner, natural gas, oxygen, torch, concentration, temperature field, mode, diffusion, kinetic

For citation: Glukhov I.V., Voronov G.V., Sheshukov O.Yu., Kalganov M.V. Comparative analysis of kinetic and diffusion modes of natural gas combustion in EAF burners. *Izvestiya. Ferrous Metallurgy*. 2025;68(5):454–460. https://doi.org/10.17073/0368-0797-2025-5-454-460

Сравнительный анализ кинетического и диффузионного режимов горения природного газа в горелках дуговой сталеплавильной печи

И. В. Глухов[1, 2], Г. В. Воронов[1], О. Ю. Шешуков[1, 3], М. В. Калганов[1, 2]

[1] **Уральский Федеральный университет имени первого Президента России Б.Н. Ельцина** (Россия, 620002, Екатеринбург, ул. Мира, 19)
[2] **ОАО «Научно-исследовательский институт металлургической теплотехники» (ВНИИМТ)** (Россия, 620137, Екатеринбург, ул. Студенческая, 16)
[3] **Институт металлургии имени академика Н.А. Ватолина Уральского отделения РАН** (620016, Россия, Екатеринбург, ул. Амундсена, 101)

ermia12@yandex.ru

Аннотация. В современных дуговых сталеплавильных печах (ДСП) для снижения расхода электроэнергии и интенсификации тепловой работы широко применяется нагрев шихты продуктами сгорания природного газа с технологическим кислородом. В существующих горелках, применяемых на ДСП, газ и кислород подаются раздельно через газокислородные и рафинирующие горелки, что обеспечивает диффузионный режим горения. Диффузионный режим в условиях использования в рабочем объеме ДСП имеет ряд недостатков, таких как неоптимальное распределение температурных и концентрационных полей продуктов сгорания, повышенный угар железосодержащих компонентов шихты. В данной работе представлены результаты расчетного исследования физико-химических свойств продуктов сгорания по длине факела для горелок фирм VAI FUCHS, SMS DEMAG и НТПФ «Эталон» при концентрации кислорода в окислителе 95 мас. %. Были проанализированы результаты компьютерного моделирования температурных полей факелов с целью оценки риска «проскока» пламени во внутренний объем горелки. Авторы провели сравнительное исследование характеристик факелов в горелочных устройствах с диффузионным и кинетическим режимами горения. На основании полученных данных предложен переход от диффузионного режима сжигания природного газа к кинетическому, что может повысить энергоэффективность использования горелок, равномерность температурных и концентрационных полей продуктов сгорания, а также снизить угар железосодержащей шихты. Исследование производилось с помощью компьютерного моделирования в пакете программ ANSYS в модуле CFX. Полученные результаты могут быть полезны для оптимизации тепловых процессов в рабочем объеме ДСП, снижения расхода электроэнергии и предотвращения аварийных режимов эксплуатации горелок.

Ключевые слова: дуговая сталеплавильная печь, горелка, природный газ, кислород, факел, концентрация, температурное поле, режим, диффузионный, кинетический

Для цитирования: Глухов И.В., Воронов Г.В., Шешуков О.Ю., Калганов М.В. Сравнительный анализ кинетического и диффузионного режимов горения природного газа в горелках дуговой сталеплавильной печи. *Известия вузов. Черная металлургия*. 2025;68(5):454–460. https://doi.org/10.17073/0368-0797-2025-5-454-460

Introduction

Diffusion combustion of natural gas with process oxygen examined under conditions where the gas mixture forms in the free volume of the furnace, outside the burner [1 – 3]. In the diffusion combustion mode, gas and oxidizer are supplied separately until they meet at the interface between the gas and oxidizer streams. Due to molecular diffusion, a mixture is formed that is characteristic of a laminar diffusion flame at low flow velocities, or a molar diffusion process promoting large-scale turbulence typical of a turbulent diffusion flame. The gas–oxidizer mixture is partially formed both before ignition and during combustion, which complicates analysis of this process. The temperature, composition of combustion products, and their physical and thermophysical properties in the combustion zone – separated by the flame front from the initial mixture – affect both the primary stage of mixing and the rate of chemical reactions.

Temperature in the diffusion flame zone corresponds to the combustion temperature of a stoichiometric premixed mixture, provided that the thermal diffusivity coefficient equals the mutual diffusion coefficient of the gas and oxidizer and that heat losses to the surroundings are negligible. The fundamental principles of diffusion combustion theory were developed and published in [4 – 6]. In operating fuel-fired furnaces, taking into account their design features, technological processes, and thermal conditions, it is advisable to implement the kinetic combustion mode of natural gas with oxygen, which involves preparing a well-mixed premixed gas–oxygen mixture [7 – 10]. In this case, the mixture-formation stage is effectively excluded from the sequence of physicochemical processes. Heating and melting of the initial materials occur primarily through heat and mass transfer from the combustion products, with no unburned hydrocarbons remaining in the gas phase [11 – 14].

Thus, the aim of this study is to carry out a comparative analysis of kinetic and diffusion combustion modes of natural gas with an oxygen–air mixture (OAM) in EAF burners, based on computer modeling of temperature fields and CO/H_2 concentrations.

Objectives:

To compare the torch characteristics of the VG burner (kinetic mode) and its analogues (VAI FUCHS, SMS DEMAG, and NTPF Etalon) during combustion of natural gas with oxygen and to evaluate the influence of combustion modes on:

– distribution of the temperature fields;

– the maximum concentrations of CO and H_2.

Materials and methods

A comparative study was carried out to analyze the torch characteristics during natural gas combustion with an oxygen–air mixture (OAM) in burners of various designs. The investigation included:

– diffusion burners used in modern electric arc furnaces (EAFs) manufactured by NTPF Etalon, SMS DEMAG, and VAI FUCHS;

– the VG burner, a promising design operating in the kinetic combustion mode, which ensures preliminary mixing of the components in the diffuser (Fig. 1).

Experimental studies of combustion require significant time and financial resources for developing test procedures and using specialized measuring equipment. In contrast, computer modeling makes it possible to optimize burner design without manufacturing intermediate prototypes and to quickly analyze how design parameters and operating modes affect torch formation and its characteristics. Computer modeling greatly shortens development time and provides a reliable basis for evaluating the efficiency of various design modifications and technical solutions [15 – 17].

Combustion modeling was performed in the ANSYS software package (CFX module) using the following models and settings:

– extended Coherent Flamelet Model (ECFM);

– Total Energy heat transfer model;

– k–ε turbulence model.

Boundary conditions for the burners were as follows:

– oxygen flow rate: 0.553 kg/s (95 wt. %);

– natural gas flow rate: 0.092 kg/s (the natural gas composition was normalized to an equivalent methane concentration of 100 wt. %).

The variation of temperature (T, K) and the maximum CO and H_2 concentrations in the cross-section of combustion products along the torch length were determined (Figs. 2 – 4).

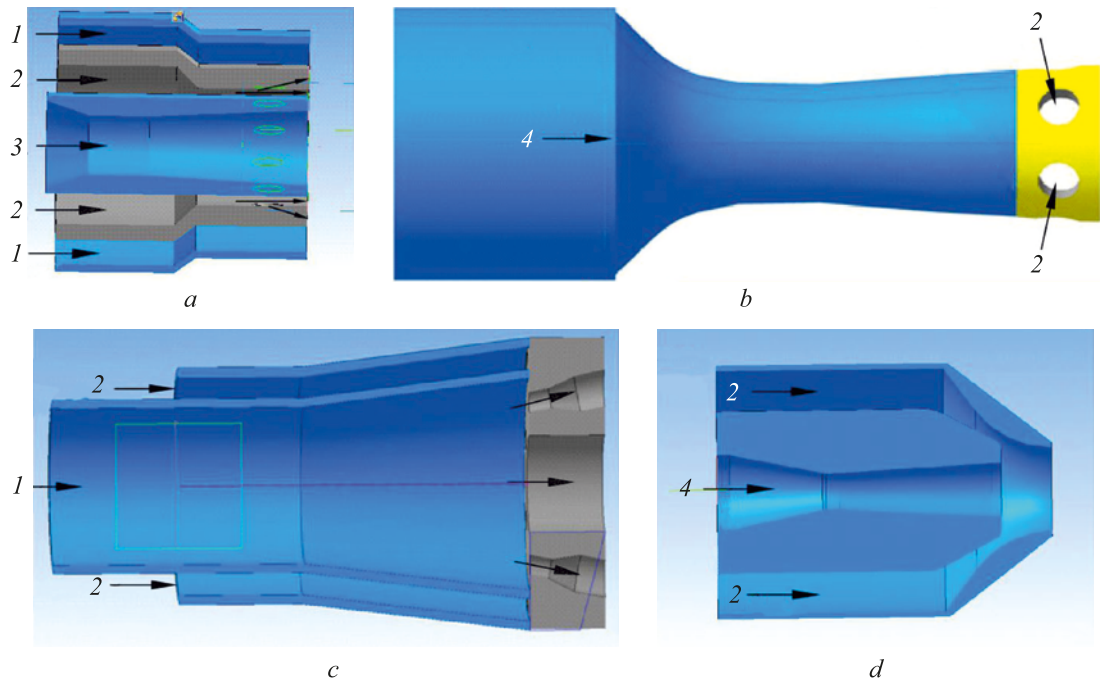

Fig. 1. Schemes of gas-oxygen burners designs:
a – VAI FUCHS; *b* – VG; *c* – NTPF Etalon; *d* – SMS DEMAG
1 – oxygen supply for combustion; *2* – natural gas supply;
3 – oxygen supply in refining mode; *4* – oxygen supply for combustion and refining mode

Рис. 1. Схемы конструкций газокислородных горелок:
a – фирмы VAI FUCHS; *b* – версии VG; *c* – фирмы НТПФ «Эталон»; *d* – фирмы SMS DEMAG
1 – подвод кислорода на горение; *2* – подвод природного газа;
3 – подвод кислорода в режиме фришевания; *4* – подвод кислорода на горение и в режиме фришевания

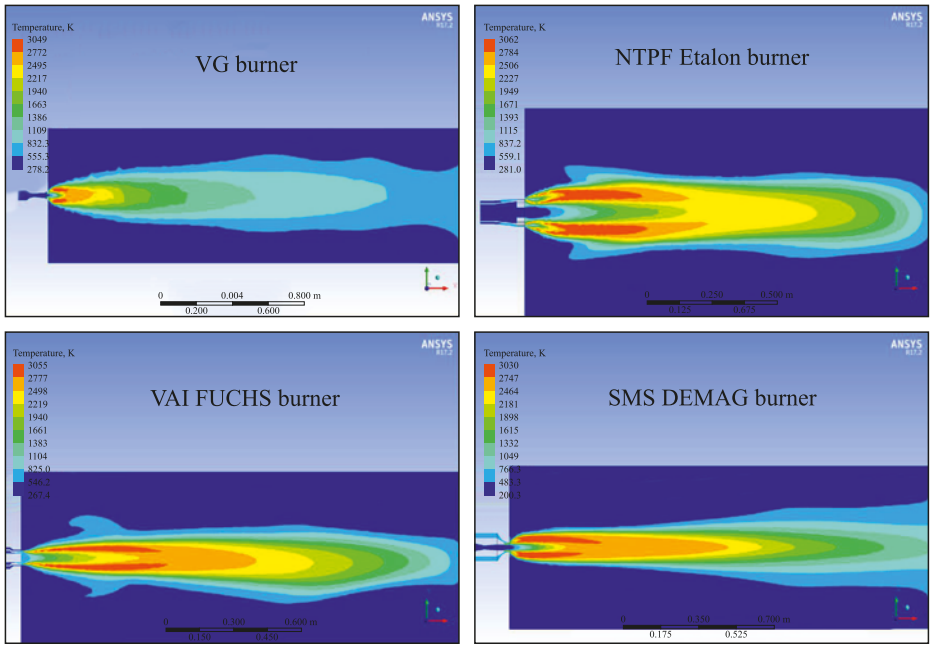

Fig. 2. Temperature fields of combustion products of the burner when burning natural gas with oxygen-air mixture, oxygen mass concentration – 95 %

Рис. 2. Температурные поля продуктов сгорания горелок при сжигании природного газа с КВС, массовая концентрация кислорода составляет 95 %

As a result, comparative performance characteristics were obtained for burners with kinetic and diffusion combustion modes: the VG burner (kinetic mode) and the diffusion burners of NTPF Etalon, VAI FUCHS, and SMS DEMAG, operating at equal natural gas and oxygen flow rates.

Based on the analysis of the results, zones of intensive combustion were identified, corresponding to regions of minimal CH_4 concentration and maximum temperature:

– for the NTPF Etalon burner – at a torch length of about 500 mm;

– for the VG burner – at a torch length of 100 – 200 mm;

– for the SMS DEMAG burner – at a torch length of about 500 mm;

– for the VAI FUCHS burner – at a torch length of over 1000 mm.

Afterburning regions can be diagnosed by elevated CO and H_2. The VG burner showed the lowest maxima –

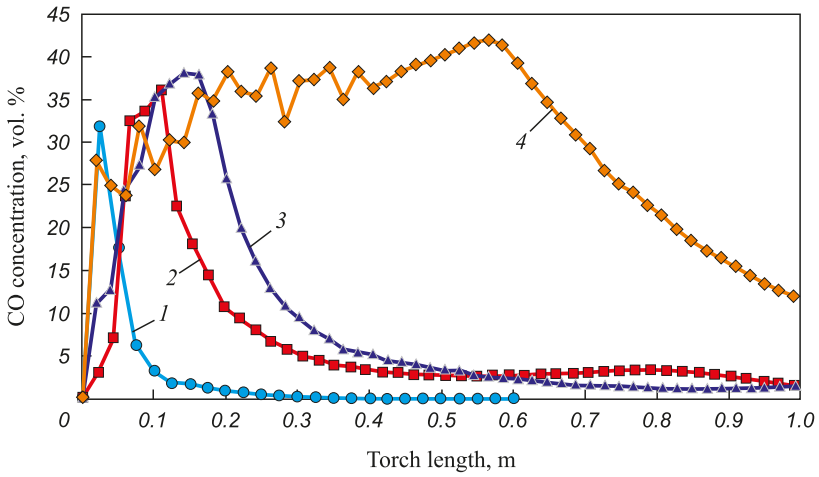

Fig. 3. Change in the maximum concentration of CO in cross-section of combustion products along the torch length of the burners: *1* – VG; *2* – SMS DEMAG; *3* – NTPF Etalon; *4* – VAI FUCHS

Рис. 3. Изменение максимальной концентрации оксида углерода в поперечном сечении продуктов сгорания по длине факела горелок: *1* – версии VG; *2* – фирмы SMS DEMAG; *3* – фирмы НТПФ «Эталон»; *4* – фирмы VAI FUCHS

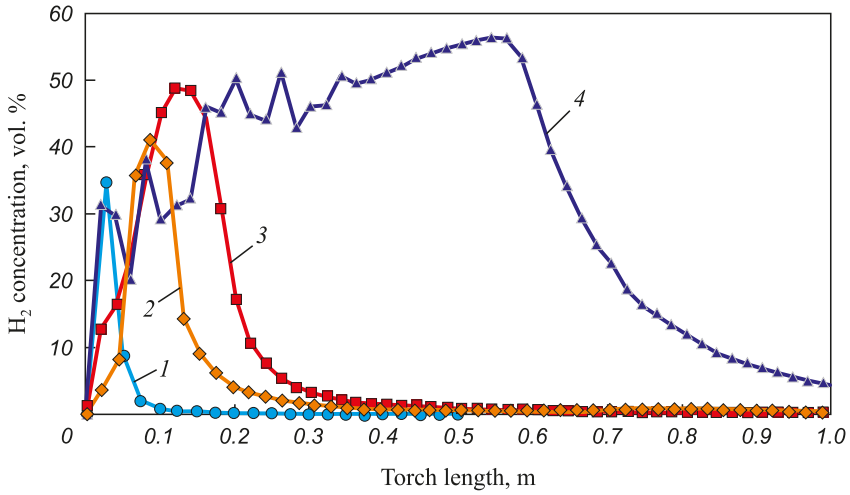

Fig. 4. Change in the maximum concentration of hydrogen in cross-section of combustion products along torch length of the burners: *1* – VG; *2* – SMS DEMAG; *3* – NTPF Etalon; *4* – VAI FUCHS

Рис. 4. Изменение максимальной концентрации водорода в поперечном сечении продуктов сгорания по длине факела горелок: *1* – версии VG; *2* – фирмы SMS DEMAG; *3* – фирмы НТПФ «Эталон»; *4* – фирмы VAI FUCHS

32 vol. % CO and 35 vol. % H_2 – whereas diffusion burners exhibited 36 – 42 vol. % CO and 41 – 56 vol. % H_2. These reductions (by 4 – 12 vol. % for CO and 6 – 14 vol. % for H_2) indicate more complete and uniform natural-gas combustion in the kinetic combustion mode than in diffusion systems.

The criterion for the absence of flame-slip risk was taken to be the absence of regions with temperatures above 800 °C inside the burner's internal cavity. No such high-temperature zones were detected for any of the burners examined. The maximum temperature of the combustion products in the torch ranged from 2757 to 2792 °C, while, at the same time, the gas-dynamic velocity in local flow regions varied widely – from 250 to 750 m/s (see Table). It should be noted that the temperature of the combustion products in the VG burner torch (2776 °C) corresponds to a gas-dynamic flow velocity 1.15 – 3.75 times higher than that of burners operating in the diffusion combustion mode [18; 19].

The optimal efficiency of the VG burner under EAF operating conditions can also be achieved by maintaining the proper vertical distance from the molten bath surface (bath level), the angle of inclination in the vertical plane, and the tangential direction of combustion product flow in the horizontal plane [15; 20]. This configuration enables the most efficient utilization of the thermal energy of the combustion products for rapid and uniform heating of the charge, which enhances the steelmaking intensity, reduces power consumption, and increases overall productivity.

CONCLUSIONS

This study shows that the VG burner, operating in the kinetic combustion mode, outperforms diffusion burners. It provides complete, rapid combustion of hydrocarbons in the premixed stream and prevents flame slip into the burner internal volume.

Performance indicators of the burners

Показатели работы горелок

Parameter	VG burner	NTPF Etalon burner	SMS DEMAG burner	VAI FUCHS burner
Maximum local velocity of combustion products, m/s	750	200	650	250
Length of the intensive combustion zone, mm	100	500	300	>1000
Maximum local temperature, K (°C)	3049 (2776)	3062 (2789)	3030 (2757)	3065 (2792)
Maximum local hydrogen (H_2) concentration in combustion products, vol. %	35	49	41	56
Maximum local carbon monoxide (CO) concentration in combustion products, vol. %	32	38	36	42

The results support the adoption of kinetic-type burners in modern steelmaking operations.

References / Список литературы

1. Belkovskii A.G., Kats Ya.L., Krasnyanskii M.V. Current state and development trends of steel production technology in EAF and their designs. *Ferrous Metallurgy. Bulletin of Scientific, Technical and Economic Information*. 2013;(3): 72–78. (In Russ.).

   Белковский А.Г., Кац Я.Л., Краснянский М.В. Современное состояние и тенденции развития технологии производства стали в ДСП и их конструкции. *Черная металлургия. Бюллетень научно-технической и экономической информации*. 2013;(3):72–78.
2. Ryabov A.B., Chumanov I.V., Shishimirov M.V. Modern Methods of Steel Smelting in Electric Arc Furnaces: Tutorial. Moscow: Teplotekhnik; 2007:192. (In Russ.).

   Рябов А.Б., Чуманов И.В., Шишимиров М.В. Современные способы выплавки стали в дуговых печах: Учебное пособие. Москва: Теплотехник; 2007:192.
3. Voronov G.V., Glukhov I.V. Thermal and physical properties of methane family hydrocarbon and oxygen combustion products in state-of-the-art arc steel furnace. *IOP Conference Series: Materials Science and Engineering*. 2020;969(1):012043. https://doi.org/10.1088/1757-899X/969/1/012043
4. Zel'dovich Ya.B. Theory of Combustion and Detonation of Gases. Moscow; Leningrad: USSR Academy of Sciences; 1944:71. (In Russ.).

   Зельдович Я.Б. Теория горения и детонации газов. Москва; Ленинград: Издательство АН СССР; 1944:71.
5. Shchetinkov E.S. Physics of Gas Combustion. Moscow: Nauka; 1965:739. (In Russ.).

   Щетинков Е.С. Физика горения газов. Москва: Наука; 1965:739.
6. Zel'dovich Ya.B., Barenblatt G.I., Librovich V.B., Makhviladze G.M. Mathematical Theory of Combustion and Explosion. Moscow: Nauka; 1980:479. (In Russ.).

   Зельдович Я.Б., Баренблат Г.И., Либрович В.Б., Махвиладзе Г.М. Математическая теория горения и взрыва. Москва: Наука; 1980:479.
7. Abel M., Hein M. The SIMETAL ultimate at Colakoglu, Turkey. *Iron and Steel Technology*. 2009;6(2):56–64.
8. Rathaba P.L., Craig I.K., Pistorius P.C. Influence of oxyfuel burner subsystem on the EAF process. *IFAC Proceedings Volumes*. 2004;37(15):215–220. https://doi.org/10.1016/S1474-6670(17)31026-1
9. Abel M., Knapp H., Moxon P., Cooke R. Oxygen-injection technology using Fuchs RCB burner in an EAF. *Millennium Steel*. 2004;(28):28–30.
10. Gottardi R., Miani S., Partyka A. Decarburization efficiency in EAF with hot metal charge. *Iron & Steel Technology*. 2012;(1):61–69.
11. Voronov G.V., Glukhov I.V. Natural gas burning with process oxygen in up-to-date arc steel furnace operating space. In: *Proceedings of the 7th Int. Conf. on Industrial Engineering (ICIE 2021)*. 2022;358–365. https://doi.org/10.1007/978-3-030-85233-7_43
12. Gottardi R., Engin B., Miani S. Single EAF and single billet caster for 320 t/h productivity. *SEAISI Quarterly Journal*. 2009;2:13–22.
13. Kopfle J. EAF metallics. In: *5th Steel Scrap Conf., November 9–10, Chicago, 2011*. 2011:271–282.
14. Kirschen M., Risonarta V., Pfeifer H. Energy efficiency and the influence of gas burners to the energy related carbon dioxide emissions of electric arc furnaces in steel industry. *Energy*. 2009;34(9):1065–1072. https://doi.org/10.1016/j.energy.2009.04.015
15. Sung Y., Lee S., Han K., Koo J., Lee S., Jang D., Oh C., Jang B. Improvement of energy efficiency and productivity in an electric arc furnace through the modification of sidewall injector systems. *Processes*. 2020;8(10):1202. https://doi.org/10.3390/pr8101202
16. Kovačič M., Stopar K., Vertnik R., Šarler B. Comprehensive electric arc furnace electric energy consumption modeling: A pilot study. *Energies*. 2019;12(11):2142. https://doi.org/10.3390/en12112142
17. Brhel J., Farmer C., Shver V. The JetBOxTM burner injector system for EAF steelmaking. *Millennium Steel*. 2006;87–97.
18. Voronov G.V., Glukhov I.V. Physicochemical properties of natural gas and oxygen combustion products at diffusion and kinetic burning. In: *Proceedings of the 7th Int. Conf. on Industrial Engineering (ICIE 2021)*. 2022;318–324. https://doi.org/10.1007/978-3-030-85233-7_38
19. Voronov G.V., Antropov M.V., Glukhov I.V. Gas dynamics in the working space of a modern electric-arc steelmaking furnace. *Refractories and Industrial Ceramics*. 2015;55(6): 498–500. https://doi.org/10.1007/s11148-015-9752-1
20. Vintovkin A.A., Ladygichev M.G., Gusovskii V.L., Kapinova T.V. Burner Devices of Industrial Furnaces and Combustion Chambers (Designs and Technical Characteristics): Reference Book. Moscow: Teplotekhnik; 2008:553. (In Russ.).

    Винтовкин А.А., Ладыгичев М.Г., Гусовский В.Л., Капинова Т.В. Горелочные устройства промышленных печей и топок (конструкции и технические характеристики): Справочник. Москва: Теплотехник; 2008:553.

Information about the Authors / Сведения об авторах

Il'ya V. Glukhov, *Cand. Sci. (Eng.), Assist. Prof. of the Chair "Thermal Physics and Informatics in Metallurgy"*, Ural Federal University named after the first President of Russia B.N. Yeltsin; *Chief Specialist of the Technology Bureau*, OJSC "Scientific Research Institute of Metallurgical Heat Engineering"
ORCID: 0000-0001-6506-1865
E-mail: ermia12@yandex.ru

Илья Васильевич Глухов, *к.т.н., доцент кафедры теплофизики и информатики в металлургии*, Уральский Федеральный университет имени первого Президента России Б. Н. Ельцина; *главный специалист технологического бюро*, ОАО «Научно-исследовательский институт металлургической теплотехники»
ORCID: 0000-0001-6506-1865
E-mail: ermia12@yandex.ru

***German V. Voronov*,** *Dr. Sci. (Eng.), Prof. of the Chair "Thermal Physics and Informatics in Metallurgy"*, Ural Federal University named after the first President of Russia B.N. Yeltsin

***Oleg Yu. Sheshukov*,** *Dr. Sci. (Eng.), Prof., Director of the Institute of New Materials and Technologies*, Ural Federal University named after the first President of Russia B.N. Yeltsin; *Chief Researcher of the Laboratory of Powder, Composite and Nano-Materials*, Vatolin Institute of Metallurgy of the Ural Branch of the Russian Academy of Sciences
ORCID: 0000-0002-2452-826X
E-mail: o.j.sheshukov@urfu.ru

***Mikhail V. Kalganov*,** *Cand. Sci. (Eng.), Assist. Prof. of the Chair "Thermophysics and Informatics in Metallurgy"*, Ural Federal University named after the first President of Russia B.N. Yeltsin; *Head of the TLC "Special Purpose Draft Devices"*, OJSC "Scientific Research Institute of Metallurgical Heat Engineering"
ORCID: 0009-0005-7176-2285
E-mail: m.v.kalganov@urfu.ru

***Герман Викторович Воронов*,** *д.т.н., профессор кафедры теплофизики и информатики в металлургии*, Уральский Федеральный университет имени первого Президента России Б. Н. Ельцина

***Олег Юрьевич Шешуков*,** *д.т.н., профессор, директор Института новых материалов и технологий*, Уральский федеральный университет имени первого Президента России Б.Н. Ельцина; *главный научный сотрудник лаборатории порошковых, композиционных и нано-материалов*, Институт металлургии имени академика Н.А. Ватолина Уральского отделения РАН
ORCID: 0000-0002-2452-826X
E-mail: o.j.sheshukov@urfu.ru

***Михаил Владимирович Калганов*,** *к.т.н., доцент кафедры теплофизики и информатики в металлургии*, Уральский Федеральный университет имени первого Президента России Б. Н. Ельцина; *руководитель ВТК «Тягодутьевые устройства специального назначения»*, ОАО «Научно-исследовательский институт металлургической теплотехники»
ORCID: 0009-0005-7176-2285
E-mail: m.v.kalganov@urfu.ru

Contribution of the Authors

I. V. Glukhov – setting the research task, performing computer modeling, writing the text.
G. V. Voronov – setting the research task.
O. Yu. Sheshukov – setting the research task, editing the text.

M. V. Kalganov – discussion of the results, editing the text.

Вклад авторов

И. В. Глухов – постановка задачи исследований, выполнение компьютерного моделирования, написание статьи.
Г. В. Воронов – постановка задачи исследований.
О. Ю. Шешуков – постановка задачи исследований, редактирование статьи.
М. В. Калганов – обсуждение результатов, редактирование статьи.

Received 21.04.2025
Revised 25.07.2025
Accepted 28.08.2025

Поступила в редакцию 21.04.2025
После доработки 25.07.2025
Принята к публикации 28.08.2025

UDC 622:788
DOI 10.17073/0368-0797-2025-5-461-467

Original article
Оригинальная статья

Carburization of pellets to a carbon content of more than 4.5 % during metallization in shaft furnaces

E. R. Sabirov[1, 2], A. Yu. Pokolenko[1], A. M. Bizhanov[3], I. S. Bersenev[1, 2], N. A. Spirin[2]

[1] **LLC "NPVP TOREKS"** (72 Starozhilov Str., Yekaterinburg 620902, Russian Federation)
[2] **Ural Federal University named after the first President of Russia B.N. Yeltsin** (19 Mira Str., Yekaterinburg 620002, Russian Federation)
[3] **National University of Science and Technology "MISIS"** (4 Leninskii Ave., Moscow 119049, Russian Federation)

e.sabirov@torex-npvp.ru

Abstract. Hot Briquetted Iron (HBI) or Direct Reduced Iron (Pellets) (DRI) is one of the most sought-after products in the steel industry because its use enables the environmentally friendly production of high grade steels. The purpose of this paper is to study the process of pellets carburization under the conditions of a shaft direct reduction (metallization) furnace in comparison with the carburization of pellets due to the preparation of an ore-carbon burden. Hot briquetted iron produced in the HYL-III process is different from Midrex briquettes in terms of carbon content. Difference in the amount of carbon is attributed to the processes of carburization and pyrolysis of natural gas in the shaft furnace workspace, as well as difference in composition of the gas phase and pressure in the workspace of the HYL and Midrex furnaces. As is known, the HYL-III process utilizes vapor conversion (higher H_2/CO ratio) at elevated gas pressures beneath the furnace top, in contrast to the Midrex process. An increase in the carbon monoxide (CO) content in the gas phase of the Midrex process (carbon dioxide conversion) results in intensification on the pellet surface that was reduced to metal. The findings of the study demonstrated that carburization of pellets to a greater than 4.5 % carbon content through the process of gas metallization (direct reduction) in shaft furnaces is indeed feasible. The Midrex process, which relies on the reducing agent, mostly carbon monoxide (CO), allows for the treatment of pellets with methane. In contrast, the HYL process, which utilizes hydrogen (H_2) mostly as the reducing agent, necessitates the addition of solid carbon, such as soot or coke breeze etc., to the burden for carburization. This finding suggests the potential for utilization of carbon-containing briquettes in metallization processes. Carbon, despite its presence in the form of a separate phase (soot), cannot be separated from the iron-containing components of pellets by magnetic separation or washing and does not pose any danger.

Keywords: HBI, direct reduced pellets, Midrex, HYL, shaft furnace, carbon, CO, soot, briquettes

For citation: Sabirov E.R., Pokolenko A.Yu., Bizhanov A.M., Bersenev I.S., Spirin N.A. Carburization of pellets to a carbon content of more than 4.5 % during metallization in shaft furnaces. *Izvestiya. Ferrous Metallurgy*. 2025;68(5):461–467.
https://doi.org/10.17073/0368-0797-2025-5-461-467

Исследование процесса науглероживания окатышей до содержания углерода более 4,5 % при металлизации в шахтных печах

Э. Р. Сабиров[1, 2], А. Ю. Поколенко[1], А. М. Бижанов[3], И. С. Берсенев[1, 2], Н. А. Спирин[2]

[1] **ООО «НПВП ТОРЭКС»** (Россия, 620902, Екатеринбург, ул. Старожилов, 72)
[2] **Уральский федеральный университет имени первого Президента России Б.Н. Ельцина** (Россия, 620002, Екатеринбург, ул. Мира, 19)
[3] **Национальный исследовательский технологический университет «МИСИС»** (Россия, 119049, Москва, Ленинский пр., 4)

e.sabirov@torex-npvp.ru

Аннотация. Горячебрикетированное железо (ГБЖ, HBI) или восстановленные окатыши (DRI) являются одним из наиболее востребованных продуктов металлургической отрасли, поскольку их использование позволяет обеспечить экологичное производство высококачественных сталей. Одним из важных параметров качества такой продукции служит содержание углерода. Цель данной работы состоит в исследовании процесса науглероживания окатышей в условиях шахтной печи металлизации в сопоставлении с науглероживанием окатышей за счет формирования рудо-углеродной шихты. Углерод в окатышах распределен между карбидами железа и отдельной фазой – сажей. Горячебрикетированное железо, полученное по технологии Хил-3, отличается по содержанию углерода от брикетов Мидрекс. Разница в количестве углерода объясняется протеканием процессов науглероживания и пиролиза природного газа в рабочем пространстве шахтной печи, а также отличием в составе газовой фазы и давления в рабочем пространстве в печах Хил и Мидрекс. Как известно, процесс Хил-3 использует паровую конверсию (соотношение H_2/CO выше) при более высоком давлении газа под колошником в сравнении с Мидрекс. Более высокое содержание CO в газовой фазе процесса Мидрекс (углекислотная конверсия) приводит к интенсификации процесса на восстановленной до металла поверхности окатыша. Результаты исследования показали, что науглероживание окатышей до содержания углерода более 4,5 % при использовании газовой металлизации в шахтных печах действительно возможно. При этом для процесса Мидрекс (восстановитель преимущественно CO) это возможно за счет обработки окатышей метаном, а для процесса Хил (восстановитель преимущественно H_2) для науглероживания необходимо добавлять в шихту твердый углерод (сажа, коксик и т. д.). Указанное открывает потенциальные возможности использования углеродсодержащих брикетов при металлизации. Углерод, несмотря на его нахождение в виде отдельной фазы (сажи), не может быть отделен от железосодержащих компонентов окатышей магнитной сепарацией или отмывкой и не представляет опасности.

Ключевые слова: ГБЖ, восстановленные окатыши, Мидрекс, Хил, шахтная печь, углерод, CO, сажа, брикеты

Для цитирования: Сабиров Э.Р., Поколенко А.Ю., Бижанов А.М., Берсенев И.С., Спирин Н.А. Исследование процесса науглероживания окатышей до содержания углерода более 4,5 % при металлизации в шахтных печах. *Известия вузов. Черная металлургия*. 2025;68(5): 461–467. https://doi.org/10.17073/0368-0797-2025-5-461-467

Introduction and problem statement

Hot Briquetted Iron (HBI) or direct reduced pellets (DRI) are among the most sought-after products in the steel industry, since their use enables the environmentally friendly production of high-grade steels [1 – 4]. This, in particular, explains the increasing production of direct reduced iron[1]. One of the important quality parameters of this product is the carbon content, which led to the development of the ACT Midrex technology[2]. According to the developer, this technology makes it possible to achieve a carbon content in metallized pellets of up to 4.5 wt. %. Assessing the conditions required to achieve this level and comparing them with the alternative approaches is an important objective, as it expands the tools available for improving the metallurgical properties of HBI. One of the factors determining the quality of the metallized product (including the carbon content) is the material composition of pellets [5]. This aspect is not analyzed in the present study (the raw material in all the samples is identical), and the investigation focuses solely on the kinetics of carburization. The basis for the study was the primary data reported in [5; 6], along with additional experiments. Table 1 shows the distribu-

[1] World Steel Association. World steel in figures 2024. Available at URL: https://worldsteel.org/data/world-steel-in-figures-2024/#direct-reduced-iron-production-2019-to-2023 (Accessed 13.05.2025).

[2] MIDREX Technologies Inc. Increasing carbon flexibility in MIDREX DRI products adjustable to 4–5 %: excellent temperature retention with MIDREX ACT. Available at URL: https://www.midrex.com/tech-article/increasing-carbon-flexibility-in-midrex-dri-products-adjustable-to-4-5-excellent-temperature-retention-with-midrex-act (Accessed 13.05.2025).

Table 1. **Average carbon content in HBI [6]**

Таблица 1. **Усредненное содержание углерода в ГБЖ [6]**

Carbon content, wt. %		
HYL-III No. 1	Midrex No. 2	Midrex No. 3
0.96	1.43	1.27

tion of carbon in HBI produced at Lebedinsky Mining and Processing Plant (Lebedinsky GOK) across three technological lines.

According to these data, HBI produced by the HYL-III process differs in carbon content from Midrex briquettes. The difference in carbon amount between the samples is attributed to the processes of carburization and natural gas pyrolysis in the shaft furnace workspace, as well as to differences in the gas phase composition and pressure in the furnace workspace of the HYL and Midrex processes [7 – 9]. It is well known, the HYL-III process employs vapor conversion (higher H_2/CO ratio) at higher gas pressures beneath the furnace top compared to Midrex. The higher CO content in the gas phase of the Midrex process (carbon dioxide conversion) intensifies the reaction on the metallic surface of the pellet [10]:

$$Fe + 6CO \rightarrow Fe_3C + 3CO_2. \quad (1)$$

Carbon in pellets is distributed between iron carbides and a separate phase – soot. The purpose of this study is to investigate the process of carburization of pellets (to a carbon content >4.5 %) in a shaft furnace, in comparison with carburization of pellets through the formation of an ore–carbon burden.

Investigation of gas-phase carburization of direct reduced pellets

To determine the conditions influencing the carburization of pellets, a research stand was prepared (Fig. 1). It consisted of gas cylinders (*1*), a vertical electric furnace containing a reaction crucible (*2*), a combustion chamber (*3*), gas supply (*4*) and exhaust systems (*5*) with filters, and a gas analyzer (*6*).

Methane was fed into the reaction crucible and heated as it passed between the walls of the outer and inner tubes, flowing downward. It then moved upward through the perforated bottom (ceramic beads) of the inner tube

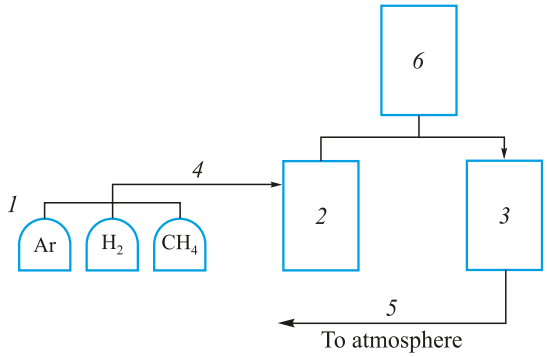

Fig. 1. Diagram of the research stand

Рис. 1. Блок-схема исследовательского стенда

Table 2. **Experimental conditions and formation rate of soot with pellets**

Таблица 2. **Условия опытов и скорость образования сажи с окатышами**

Experiment	Temperature, °C	Methane flow rate, L/min	Mass growth rate, g/h
1	1000	0.781	14.55
2	1100	0.781	16.39
3	1100	1.757	50.09

and was discharged from the crucible. It then entered a sealed vessel filled with water, which served both as a filter and as a cooler to cool the gas before its delivery to the analyzer. Downstream of the analyzer, the gas was routed to the combustion chamber. This chamber was used to neutralize explosive components formed during methane cracking, preventing their accumulation and potential ignition in the laboratory. The temperature and gas flow rate were kept constant during the isothermal holding stage. During the test, elapsed time, mass, temperature, inlet-gas flow rate, and outlet-gas composition were recorded and logged. Methane decomposition was monitored by changes in retort mass and by analyzing the chemical composition of the outlet gas. Methane (CH_4 – 99.99 %; balance CO, CO_2, N_2, H_2O, O_2, C_mH_n) was supplied from a cylinder, and argon (Ar – 99.993 %) was used as the inert gas.

Experiments were conducted to simulate the carburization zone of a shaft furnace using direct reduced pellets (degree of reduction 95 %). The tests were carried out at temperatures of 1000 and 1100 °C (Table 2). The methane flow rate was determined from the reaction zone volume, the gas tract capacity of the unit, and the need to maintain a stable regulation range. The data in Table 2 show that the presence of direct reduced pellets resulted in an increase in pellet mass due to soot deposition.

At a methane flow rate of 1.757 L/min, the maximum increase in pellet mass due to carbon deposition was 56.48 g/h, with most of the carbon depositing on the surface of the metallized pellets and within their pores. As a result, upon completion of the tests, the samples grew in size (from 12 to 20 – 22 mm), and their shape changed from spherical to angular (Fig. 2). Phase analysis revealed up to 5 wt. % total carbon and more than 2 wt. % carbon in the form of soot.

To determine the possibility of separating the soot carbon from the metal, the pellets were ground to a –100 μm fraction. When the dry fine material was separated by a magnet into magnetic and non-magnetic fractions, it was found that all of the material was magnetic. Washing the ground material in water also failed to separate the phases. Therefore, isolating carbon as a separate product by these methods proved impossible.

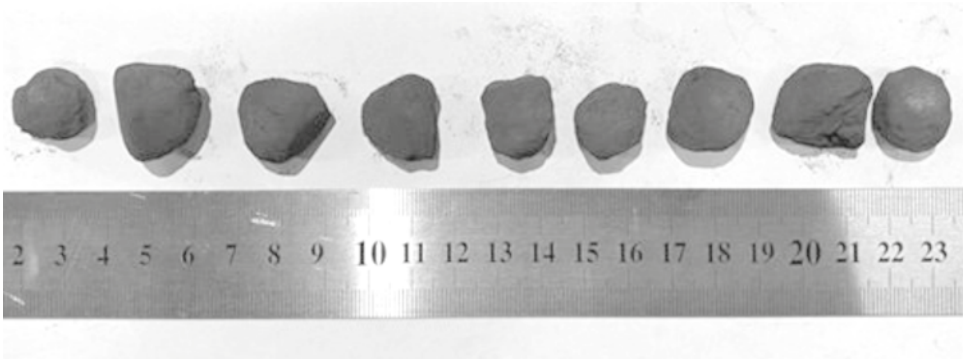

Fig. 2. View of pellets after reduction

Рис. 2. Вид окатышей после восстановления

Investigation of solid-carbon carburization of direct reduced pellets

Pellets and briquettes with an organic binder were prepared for the laboratory tests. The organic binder does not reduce the content of valuable components in the metallized product. It promotes the development of a microporous structure during reduction – heat treatment and ensures adequate strength of the products at intermediate production stages (green handling, drying). Limestone from the Lebedinsky GOK was used as the flux. The chemical composition of the components is given in Table 3. The soot contained 99.59 % carbon. The particle-size distribution of the components met the requirements for pellet production. The charge for briquettes and pellets consisted of 89.62 % concentrate, 5.35 % soot, 2.03 % limestone, and 3 % organic binder (dry basis).

A laboratory stand (Fig. 1) was used to carry out the reduction–heat treatment of ore–carbon samples. The heat treatment was carried out as follows. The samples were heated together with the furnace to 1000 °C in an inert atmosphere (argon remained in the retort after leak-tightness testing). During heating, iron oxides were reduced by the solid reductant (soot) present in the samples, as no air was supplied to the retort. The smoke generated during carbon reduction was vented to atmosphere. When the sample mass reached a constant value and smoke emission from the retort ceased, it was it was considered that the carbon had fully burned out. Hydrogen was then introduced into the reaction crucible and the reduction of the pellets continued to a degree of reduction >90 %. When constant mass was attained, the hydrogen supply to the retort was stopped and replaced with inert gas. The retort was removed from the furnace, and the inert gas continued to be supplied until the temperature fell to 60 °C. The retort was then disassembled and the sample taken out.

The experiments showed that the surfaces of the dried pellets tended to crumble during loading and transfer. Because the pellets were not coated with chalk or cement suspensions to suppress sintering, sintering occurred during reduction. For the reduced samples (Fig. 3), we determined compressive strength (minimum requirement ≥30 kg/pellet) and the chemical composition of the target components (Table 4). In addition, tests were performed on samples reduced solely by soot – i.e., without hydrogen supply to the retort – to assess the effect of carbon on oxygen removal from the iron-ore particles.

The data indicate that the compressive strength of pellets reduced solely by soot differed by no more than ~3 % (relative). Accordingly, carbon-containing briquettes can be used in metallization without compromising the strength of the reduced products, as also suggested in [11; 12]. The compressive strength of pellets reduced by soot was 1.5 – 2.0 times lower than that of pellets reduced by hydrogen. This is attributed to the presence of different phases in the samples characteristic of a metallization degree of ~45 %: Fe_3O_4, FeO, and Fe_{met}. In contrast, when the pellets had a homogeneous structure represented by metallic iron, their strength increased. This

Table 3. **Chemical composition of burden components**

Таблица 3. **Химический состав компонентов шихты**

Component	Chemical composition (dry basis), wt. %								
	Fe_{tot}	FeO	CaO	SiO_2	MgO	Al_2O_3	S	P	LOI
Concentrate	70.13	30.37	0.12	2.56	0.23	0.11	0.147	0.015	0
Limestone	0	0	52.21	2.18	0	1.70	0	0	44.81

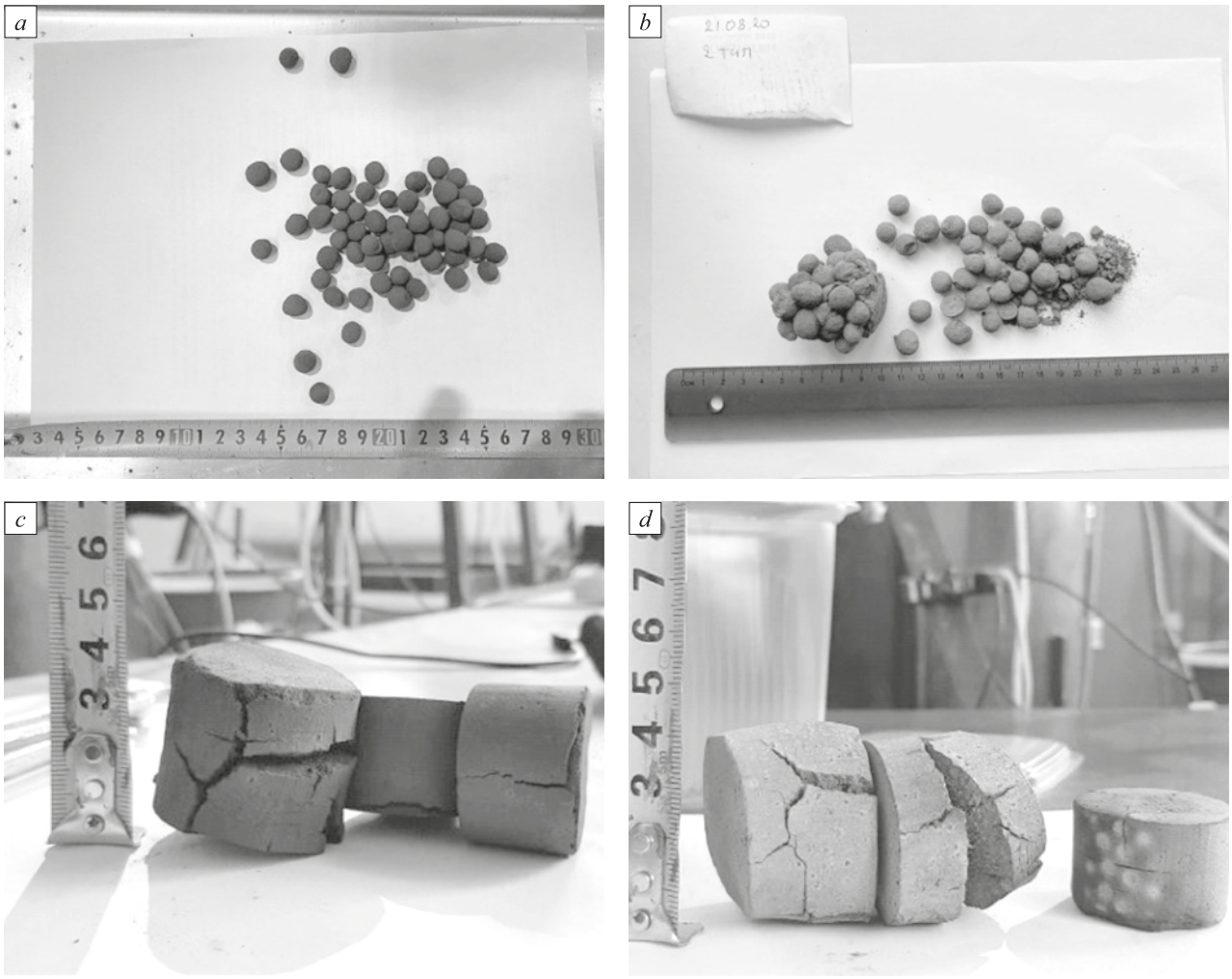

Fig. 3. Typical appearance of the reduced samples of pellets (*a*, *b*) and briquettes (*c*, *d*), reduced without hydrogen (*a*, *c*) and with hydrogen (*b*, *d*)

Рис. 3. Типичный вид восстановленных образцов окатышей (*a*, *b*) и брикетов (*c*, *d*), восстановленных без водорода (*a*, *c*) и с водородом (*b*, *d*)

Table 4. **Physico-chemical properties of the reduced samples**

Таблица 4. **Физико-химические показатели восстановленных образцов**

Sample			Compressive strength, kg/pellet (kg/briquette)	Fe_{tot}, %	Fe_{met}, %	C, %	S, %	SiO_2, %	Degree of metallization, %
Pellets	Binder *1*	without H_2	43.48	83.40	37.32	0.19	0.200	2.98	44.70
		with H_2	63.40	96.92	91.64	0.20	0.016	3.25	94.50
	Binder *2*	without H_2	42.60	79.52	34.31	0.41	0.200	2.87	43.15
		with H_2	88.31	98.48	92.19	0.19	0.024	3.24	93.61
Briquettes	Binder *1*	without H_2	148.84	77.26	28.70	0.54	0.230	2.77	37.15
		with H_2	261.21	91.82	87.48	0.34	0.072	3.21	95.27
	Binder *2*	without H_2	142.41	75.66	23.05	1.27	0.220	3.35	30.47
		with H_2	187.72	91.69	89.47	0.24	0.053	2.86	97.58

agrees with the results reported in [13; 14]. The compressive strength of briquettes likewise increased with metallization degree, mirroring the trend observed for pellets. Reduction of ore–carbon samples solely by soot (no H_2 feed) yielded a degree of reduction of ~45 – 50 %. At this stage, extensive reaction surfaces developed owing to burnout of the organic binder and carbon, as well as the magnetite → wüstite phase transition.

Conclusions

The experiments demonstrate that achieving >4.5 wt. % carbon in pellets by gas-phase metallization in shaft furnaces is feasible. In the Midrex process (reducing agent predominantly CO), this can be attained by methane treatment of pellets; in the HYL process (reducing agent predominantly H_2), carburization requires adding solid carbon (soot, coke breeze, etc.) to the burden. Although present as a separate phase (soot), carbon cannot be separated from the iron-bearing pellet components by magnetic separation or washing and poses no hazard. During reduction and carburization of pellets and briquettes, deformation occurred, accompanied by volumetric expansion and crack formation.

References / Список литературы

1. Petrov S.P. Ferrous Metallurgy in Asian Russia in the Second and Third Decades of the 21st Century. Novosibirsk: Institute of Economics and Industrial Organization of the Siberian Branch of RAS; 2023:240. (In Russ.).

   Петров С.П. Черная металлургия азиатской России во втором и третьем десятилетиях XXI века. Новосибирск: Институт экономики и организации промышленного производства Сибирского отделения РАН; 2023:240.
2. Budanov I.A. Macroeconomic prospects of steel metal production. *Stal'*. 2024;(6):47–53. (In Russ.).

   Буданов И.А. Макроэкономические перспективы производства металла. *Сталь*. 2024;(6):47–53.
3. Bilici S., Holtz G., Jülich A., etc. Global trade of green iron as a game changer for a near-zero global steel industry? A scenario-based assessment of regionalized impacts. *Energy and Climate Change*. 2024;5:100161. https://doi.org/10.1016/j.egycc.2024.100161
4. Anderson S.H. HBI improves eat energy efficiency and yield and downstream operating results: Educated use of DRI. Charlotte, NC, USA: MIDREX Technologies Inc.; 2001:1–11.
5. Bersenev I.S., Vokhmyakova I.S., Borodin A.V., etc. Prediction of the quality of hot briquetted iron (HBI) based on data on the material composition of pellets. *Steel in Translation*. 2022;52(7):673–676. https://doi.org/10.3103/S0967091222070038
6. Vokhmyakov I.S., Bersenev I.S., Borodin A.V., Sivkov O.G., Stepanova A.A., Kirienkov A.N. Mechanism of oxidation for hot briquetting iron (HBI). *Steel in Translation.* 2022;52(3):331–336. https://doi.org/10.3103/S0967091222030160
7. Kumar T.K.S., Alatalo J., Ahmed H., etc. Effect of temperature and gas mixtures on cementite formation during the carburization of hydrogen-reduced DRI. *Journal of Sustainable Metallurgy*. 2022;8:1450–1464. https://doi.org/10.1007/s40831-022-00601-0
8. Perrone A., Cavaliere P., Sadeghi B., Dijon L., Laska A., Koszelow D. Carburization behavior of high-grade pellets after direct reduction in pure hydrogen. *Journal of Sustainable Metallurgy*. 2024;10:1991–2008. https://doi.org/10.1007/s40831-024-00906-2
9. Dishwar R.K., Mandal A.K., Sinha O.P. Studies on reduction behaviour of highly fluxed iron ore pellets for application in steelmaking. *Materials Today: Proceedings*. 2021;46(3):1471–1475. https://doi.org/10.1016/j.matpr.2020.10.886
10. Bogdandy L., Engell H.-J. Die Reduktion der Eisenerze. Düsseldorf: Springer Verlag; 1967:539. (In Germ.).

    Богданди Л.А., Энгель Г.Ю. Восстановление железных руд. Москва: Металлургия; 1971;520.
11. Lohmeier L., Thaler C., Harris C., Wollenberg R., Schröder H.-W., Braeuer A.S. Use of bentonite and organic binders in the briquetting of particulate residues from the Midrex process for improving the thermal stability and reducibility of the briquettes. *Steel Research International.* 2021;92(12):2100210. https://doi.org/10.1002/srin.202100210
12. Mizutani M., Nishimura T., Orimoto T., Higuchi K., Nomura S., Saito K., Kasai E. Influence of reducing gas composition on disintegration behavior of iron ore agglomerates. *ISIJ International*. 2017;57(9):1499–1508. https://doi.org/10.2355/isijinternational.ISIJINT-2017-074
13. Dwarapudi S., Sekhar C., Paul I., Modi K., Pal A.R., Chakraborty U., Das B.K. Effect of fluxing agents on the quality and microstructure of hematite pellets. *International Journal of Metallurgical Engineering*. 2017;6(1):18–30.
14. Kurunov I.F., Bizhanov A.M., Wakeel A.K., Mishra B. Behavior of extrusion briquettes in Midrex reactors. Part 2. *Metallurgist*. 2016;60(3-4):243–247. https://doi.org/10.1007/s11015-016-0281-z

Information about the Authors / Сведения об авторах

Emil' R. Sabirov, *Senior Engineer*, LLC "NPVP TOREKS"; *Postgraduate,* Ural Federal University named after the first President of Russia B.N. Yeltsin
E-mail: e.sabirov@torex-npvp.ru

Aleksei Yu. Pokolenko, *Head of Advanced Technologies Group*, LLC "NPVP TOREKS"
E-mail: a.pokolenko@torex-npvp.ru

Aitber M. Bizhanov, *Cand. Sci. (Eng.), Leading Expert of the Chair of Functional Nanosystems and High-Temperature Materials*, National University of Science and Technology "MISIS"
ORCID: 0000-0002-0583-1984
E-mail: bizhanov@briket-brex.ru

Эмиль Рифатович Сабиров, *старший инженер,* ООО «НПВП ТОРЭКС»; *аспирант,* Уральский федеральный университет имени первого Президента России Б.Н. Ельцина
E-mail: e.sabirov@torex-npvp.ru

Алексей Юрьевич Поколенко, *руководитель группы перспективных технологий*, ООО «НПВП ТОРЭКС»
E-mail: a.pokolenko@torex-npvp.ru

Айтбер Махачевич Бижанов, *к.т.н., ведущий эксперт кафедры функциональных наносистем и высокотемпературных материалов*, Национальный исследовательский технологический университет «МИСИС»
ORCID: 0000-0002-0583-1984
E-mail: bizhanov@briket-brex.ru

***Ivan S. Bersenev*,** *Cand. Sci. (Eng.), Head of the Scientific and Analytical Department*, LLC "NPVP TOREKS"; *Assist. Prof. of the Chair of Metallurgy of Iron and Alloys*, Ural Federal University named after the first President of Russia B.N. Yeltsin
ORCID: 0009-0000-4270-6042
E-mail: i.bersenev@torex-npvp.ru

***Nikolai A. Spirin*,** *Dr. Sci. (Eng.), Prof., Head of the Chair "Thermal Physics and Informatics in Metallurgy"*, Ural Federal University named after the first President of Russia B.N. Yeltsin
ORCID: 0000-0001-9078-589X
E-mail: n.a.spirin@urfu.ru

***Иван Сергеевич Берсенев*,** *к.т.н., руководитель научно-аналитического отдела*, ООО «НПВП ТОРЭКС»; *доцент кафедры металлургии железа и сплавов*, Уральский федеральный университет имени первого Президента России Б.Н. Ельцина
ORCID: 0009-0000-4270-6042
E-mail: i.bersenev@torex-npvp.ru

***Николай Александрович Спирин*,** *д.т.н., профессор, заведующий кафедрой теплофизики и информатики в металлургии*, Уральский федеральный университет имени первого Президента России Б.Н. Ельцина
ORCID: 0000-0001-9078-589X
E-mail: n.a.spirin@urfu.ru

Contribution of the Authors

E. R. Sabirov – problem statement, literary review, experimental studies, analysis of results, drawing conclusions.

A. Yu. Pokolenko – experimental studies.
A. M. Bizhanov – experimental studies.
I. S. Bersenev – problem statement, literary review, analysis of results, drawing conclusions.
N. A. Spirin – problem statement, analysis of results, drawing conclusions.

Вклад авторов

Э. Р. Сабиров – постановка задачи, обзор литературных источников, экспериментальные исследования, анализ результатов и формулировка выводов.
А. Ю. Поколенко – экспериментальные исследования.
А. М. Бижанов – экспериментальные исследования.
И. С. Берсенев – постановка задачи, обзор литературных источников, анализ результатов и формулировка выводов.
Н. А. Спирин – постановка задачи, анализ результатов и формулировка выводов.

Received 12.05.2025
Revised 28.05.2025
Accepted 28.08.2025

Поступила в редакцию 12.05.2025
После доработки 28.05.2025
Принята к публикации 28.08.2025

MATERIALS SCIENCE / МАТЕРИАЛОВЕДЕНИЕ

UDC 669.04: 532.696
DOI 10.17073/0368-0797-2025-5-468-475

Original article
Оригинальная статья

Interaction of Al_2O_3-based ceramics with slag melt 45 % CaO – 40 % Al_2O_3 – 10 % SiO_2 – 5 % MgO

A. A. Aleksandrov[1] ✉, S. N. Anuchkin[1], A. G. Kanevskiy[1], S. B. Rumyantseva[1], K. V. Grigorovich[1, 2]

[1] **Baikov Institute of Metallurgy and Materials Science, Russian Academy of Sciences** (49 Leninskii Ave., Moscow 119334, Russian Federation)
[2] **National University of Science and Technology "MISIS"** (4 Leninskii Ave., Moscow 119049, Russian Federation)

✉ a.a.aleksandrov@gmail.com

Abstract. In steelmaking, the refractory material used as a lining is easily destroyed by slag, which not only decreases the service life of ceramics but also makes worse a production quality because of increase in the number of nonmetallic inclusions in metal. If the slag has good wettability, it tends to penetrate the refractory through pores and cracks. As a result, a boundary layer is formed, which has a structure and properties different from the initial material. The sessile drop method was used to study the interaction of Al_2O_3-based refractory ceramics with the liquid slag 45 % CaO – 40 % Al_2O_3 – 10 % SiO_2 – 5 % MgO. The substantial decrease in the wetting angle to 20° in the initial 5 min of experiment and the further small decrease to 13.5° in the next 115 min were observed. The microstructural examination and elemental mapping of the boundaries of cross sections of slag and ceramics were carried out. The slag consists of several phases, namely: $Ca_2(Mg_{0.25}Al_{0.75})(Si_{1.25}Al_{0.75}O_7)$; $CaAl_2O_4$, $CaAl_4O_7$ and $MgAl_2O_4$. As was found, the slag–ceramics boundary layer consisted of calcium aluminate ($CaAl_4O_7$) and, at the grain boundaries of aluminum oxide in the refractory material, hibonite ($CaAl_{12}O_{19}$) was formed. *X*-ray diffraction analysis of initial ceramics showed that it contained ~8 % $CaAl_4O_7$, and after interaction with the slag ~32 % $CaAl_{12}O_{19}$. At a depth of 4 mm, the presence of calcium aluminates both in the central and peripheral zones of ceramics was observed. This indicates the slag penetration into the ceramics and their chemical interaction.

Keywords: refractory ceramics, slag, aluminum oxide, slag–ceramics interaction, wetting angle, microstructure, *X*-ray diffraction analysis

Acknowledgements: The work was performed within the framework of the State assignment to no. 075-00319-25-00. The authors express their gratitude to A.B. Mikhailova, A.A. Rakitin, K.Yu. Demin and A.O. Morozov for their assistance.

For citation: Aleksandrov A.A., Anuchkin S.N., Kanevskiy A.G., Rumyantseva S.B., Grigorovich K.V. Interaction of Al_2O_3-based ceramics on with slag melt 45 % CaO – 40 % Al_2O_3 – 10 % SiO_2 – 5 % MgO. *Izvestiya. Ferrous Metallurgy*. 2025;68(5):468–475. https://doi.org/10.17073/0368-0797-2025-5-468-475

Взаимодействие керамики на основе Al_2O_3 со шлаковым расплавом 45 % CaO – 40 % Al_2O_3 – 10 % SiO_2 – 5 % MgO

А. А. Александров[1] ✉, С. Н. Анучкин[1], А. Г. Каневский[1], С. Б. Румянцева[1], К. В. Григорович[1, 2]

[1] **Институт металлургии и материаловедения им. А.А. Байкова РАН** (Россия, 119334, Москва, Ленинский пр. 49)
[2] **Национальный исследовательский технологический университет «МИСИС»** (Россия, 119049, Москва, Ленинский пр., 4)

✉ a.a.aleksandrov@gmail.com

Аннотация. При выплавке стали огнеупорный материал, используемый в качестве футеровки, легко разрушается за счет шлака, что не только уменьшает срок службы керамики, но и снижает качество продукции, увеличивая количество неметаллических включений в металле. Если шлак имеет хорошую смачиваемость, то он стремится проникнуть в огнеупор через поры и трещины. В результате образуется пограничный слой со структурой и свойствами, отличными от исходного огнеупора. В данной работе для исследования взаимодействия огнеупорного материала на базе Al_2O_3 с жидким шлаком 45 % CaO – 40 % Al_2O_3 – 10 % SiO_2 – 5 % MgO был использован метод лежащей капли. Показано существенное снижение значений краевого угла смачивания до 20° в первые 5 мин опыта и последующее незначительное уменьшение до 13,5° в течение 115 мин. Исследована микроструктура и выполнено элементное картирование границ поперечных

срезов шлака и керамики. Показано, что шлак состоит из нескольких фаз: $Ca_2(Mg_{0,25}Al_{0,75})(Si_{1,25}Al_{0,75}O_7)$, $CaAl_2O_4$, $CaAl_4O_7$ и $MgAl_2O_4$. Обнаружено, что пограничный слой шлак – керамика состоит из алюмината кальция ($CaAl_4O_7$), а на границах зерен оксида алюминия огнеупора происходит образование фазы ибонита ($CaAl_{12}O_{19}$). Рентгенофазовый анализ исходной керамики показал, что она содержит ~8 % $CaAl_4O_7$, а после взаимодействия со шлаком ~32 % $CaAl_{12}O_{19}$. Анализ керамики на глубине около 4 мм показал присутствие алюминатов кальция как в центральной, так и в краевых областях. Это указывает на проникновение шлака в керамику и его химическое взаимодействие с ней.

Ключевые слова: огнеупорная керамика, шлак, оксид алюминия, взаимодействие шлак – керамика, краевой угол смачивания, микроструктура, рентгенофазовый анализ

Благодарности: Работа выполнена по государственному заданию 075-00319-25-00. Авторы выражают благодарность Михайловой А.Б., Ракитину А.А., Демину К.Ю. и Морозову А.О. за помощь в работе.

Для цитирования: Александров А.А., Анучкин С.Н., Каневский А.Г., Румянцева С.Б., Григорович К.В. Взаимодействие керамики на основе Al_2O_3 со шлаковым расплавом 45 % CaO – 40 % Al_2O_3 – 10 % SiO_2 – 5 % MgO. *Известия вузов. Черная металлургия*. 2025;68(5):468–475. https://doi.org/10.17073/0368-0797-2025-5-468-475

Introduction

The increasing requirements for steel quality and the improvement of steel cleanliness through the removal of nonmetallic inclusions are among the main objectives of metallurgy. Nonmetallic inclusions are formed during steel deoxidation, erosion and corrosion of refractories, ingress of slag particles into the melt, and directly during metal solidification. In steelmaking, the refractory used as a lining is easily destroyed by slag, which not only decreases the service life of refractory ceramics but also reduces production quality by increasing the number of nonmetallic inclusions in the metal. Frequent replacement of refractories increases costs and decreases productivity, thus negating the advantages of introducing new methods for liquid steel treatment.

As noted in [1 – 3], the destruction of refractories is most often caused by chemical corrosion and slag penetration. Corrosion damage of refractory ceramics is mainly due to their chemical interaction with slags [4]. The corrosion behavior is strongly influenced by the wettability of refractories by slags [5; 6]. Good wettability indicates active interaction and means that the slag easily reacts with the refractory material, causing its chemical corrosion [6 – 9]. If the slag has good wettability, it tends to penetrate the refractory through pores and cracks [10]. As a result, a boundary layer is formed, with structure and properties different from those of the initial refractory.

Developing refractories resistant to slag attack remains a significant research focus in modern metallurgy [11 – 15]. Thermophysical properties, viscosity, surface tension, and wetting angle are the primary indicators of slag–refractory interaction and penetration. In recent decades, numerous studies of the interaction between refractories and various slags have employed the sessile drop method, in which a slag sample is placed on a refractory ceramic substrate [7 – 9; 16 – 18]. This method makes it possible to analyze the wettability of refractory ceramics by slag melts, to study surface tension and wetting angle as functions of temperature, gas phase, and contact time between the drop and the substrate, and to examine the chemical interaction between the refractory and the slag.

An important aspect of metallurgical production is purging of the melt with inert gases at various stages of steel treatment. During ladle treatment, purging plugs interact both with liquid metal [19] and, after the melt has been poured out of the ladle, with slag. This service environment leads to wear of the plugs; therefore, to study changes in the composition of the plug ceramics, it is necessary to investigate their interaction not only with liquid steel but also with slag. As a rule, a typical ladle slag used in the processing of low-carbon steels (pipe steels, automotive sheet steels, etc.) has the composition: 45 % CaO, 40 % Al_2O_3, 10 % SiO_2, 5 % MgO, with basicity $CaO/SiO_2 = 4.5$. The purpose of this study is to investigate the interaction of slag in the $CaO–Al_2O_3–SiO_2–MgO$ system with Al_2O_3-based ceramics, and to analyze changes in the microstructure and macrostructure of the ceramics and the slag as functions of temperature and interaction time.

Materials and methods

The materials investigated were the refractory used to manufacture ladle purging plugs (95.81 % Al_2O_3, 2.22 % MgO, 1.35 % CaO, 0.33 % Na_2O, 0.06 % SiO_2, 0.02 % Fe_2O_3) and a ladle slag (45 % CaO, 40 % Al_2O_3, 10 % SiO_2, 5 % MgO). The slag of this composition was prepared from pre-annealed pure oxides. The oxide powders were first mixed in a vibratory cup mill (IV-1). The obtained mixture was then melted in an Al_2O_3 crucible placed inside an outer graphite crucible, using an induction furnace powered by a high-frequency generator CEIA Power Cube 180/50 (50 kHz, 180 kVA). After melting, the resulting slag was crushed and pressed into pellets 6 mm in diameter, 6 mm in height, and weighing approximately 0.3 g.

The experiments were conducted in a vacuum resistance furnace equipped with a graphite heater, housing a seamless molybdenum tube. A ceramic substrate (40×30×6 mm) was placed on a stand at the tube center,

and a slag pellet was positioned on the substrate surface. An optical system provided magnified imaging, which was recorded with a digital camera for subsequent processing. A detailed description and schematic of the setup are given in [20]. The experiments were performed as follows. The system was evacuated to 5 Pa, after which the slag sample was heated to 1273 K. The test was then carried out in an atmosphere of high-purity Ar. After the slag melted and the temperature reached 1783 – 1793 K, the sample was held isothermally for 2 h. Changes in the slag pellet profile were recorded with a digital camera as functions of holding time and temperature. Upon completion of the experiments, cross sections of the slag and ceramics at the contact area were prepared, and the interaction zone was examined using a scanning electron microscope (SEM) equipped with an electron probe microanalyzer JEOL JXA-iSP100. For *X*-ray diffraction (XRD) analysis, a Tongda TD-3700 diffractometer with a vertical goniometer and a high-speed Mythen detector was used. The phase composition of the samples was determined with the QualX software package using the PDF2 ICDD database, while the quantitative phase composition was refined in the MAUD software package by the Rietveld method.

Results and discussion

The interaction of slag (45 % CaO, 40 % Al_2O_3, 10 % SiO_2, 5 % MgO) with aluminum oxide-based refractory ceramics was studied. Fig. 1 shows the change in the slag sample profile depending on temperature and holding time. From the recorded images of the slag drop profile, the wetting angle (Fig. 2) was calculated as the mean value between the right and left contact angles. Notably, the starting point of measurement corresponded to the onset of slag tablet melting (Fig. 1, *a*), whereas the formation of a completely liquid slag drop (Fig. 1, *d*) occurred only after 220 s. Analysis of the wetting angle revealed a sharp decrease during the first 5 min of the test and a short plateau lasting 1.5 – 3.0 min (31.0 – 29.5°), probably associated with the melting process. After complete formation of the drop, the wetting angle (θ) decreased from 28 to 20° within 1.5 min (up to 5 min of the test), followed by a gradual decrease to 13.5° over 115 min. Fig. 2 shows the variation in the wetting angle with temperature and holding time. During the test, partial penetration of slag into the ceramics was observed (Figs. 1, *e* – *f*). These findings demonstrate good wettability of the refractory ceramics by the slag, which can subsequently lead to erosion and chemical corrosion, ultimately reducing the service life of the refractory [5; 21; 22]. Therefore, the microstructure of the slag and ceramics after the test was examined in more detail.

Fig. 1 shows a cross section of the ceramic substrate after the experiment, indicating the zones of slag and ceramics where the analyses were performed. Using a scanning electron microscope JEOL JXA-iSP100, the slag–ceramics interaction zones (zones *1* and *2* in

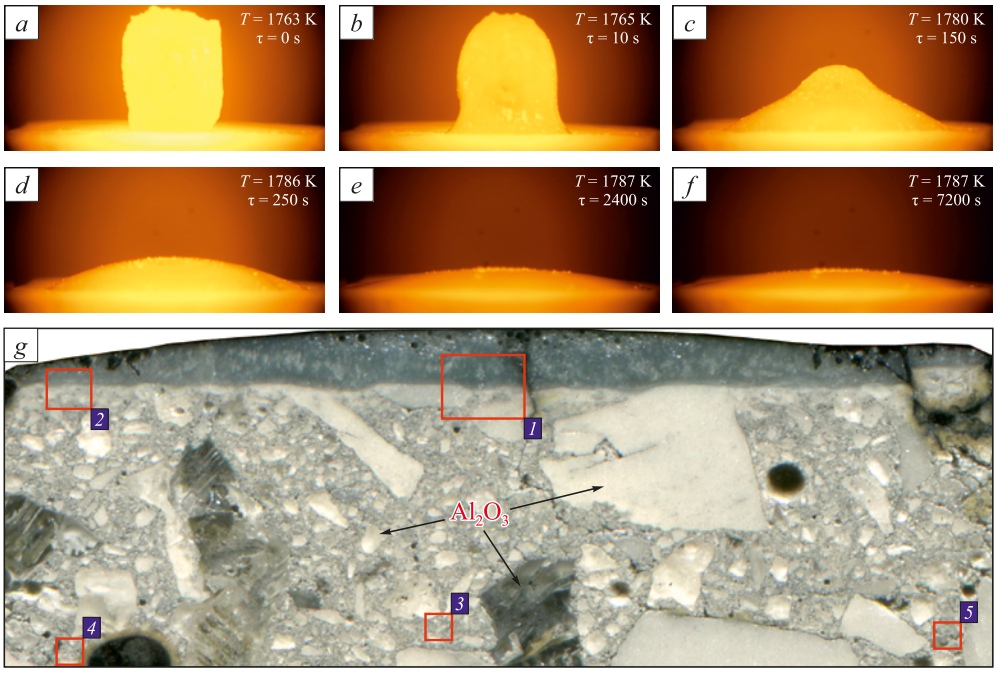

Fig. 1. Slag sample profile depending on holding time and temperature (*a* – *f*);
cross section of ceramic substrate after experiment with indication of slag and ceramics zones (*1* – *5*) (*g*)

Рис. 1. Изменение профиля образца шлака в зависимости от времени выдержки и температуры (*a* – *f*)
и поперечный срез керамической подложки после эксперимента с указанием исследуемых участков шлака и керамики (*1* – *5*) (*g*)

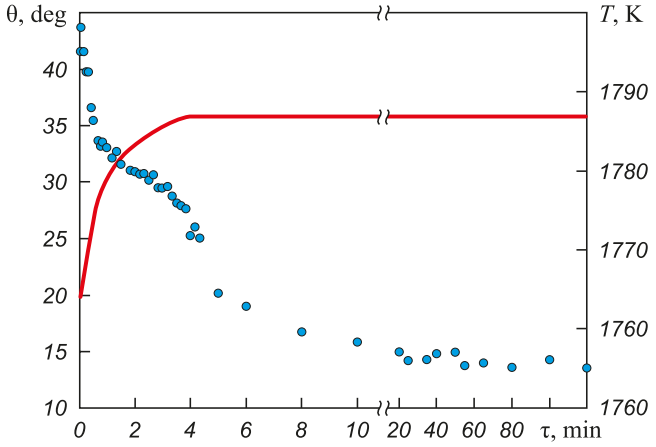

Fig. 2. Wetting angle depending on temperature and holding time:
● – θ, deg; — – *T*, K

Рис. 2. Изменение краевого угла смачивания
в зависимости от температуры и времени выдержки:
● – θ, град; — – *T*, K

Fig. 1) and various zones of the ceramics (zones *3 – 5* in Fig. 1) were examined.

Fig. 3 presents the microstructure and elemental mapping of the slag–ceramics boundary layer (zone *1* in Fig. 1). The slag consists of several structural zones: light-gray, gray, and dark-gray. In the light-gray zone, the presence of calcium, silicon, aluminum, and magnesium was observed (spectrum 1–1 in Fig. 3). The elemental compositions of the spectra are given in the Table. The gray zone contains aluminum and calcium (spectrum 1–2 in Fig. 3), whereas the dark-gray zone is rich in magnesium and aluminum (spectrum 1–3 in Fig. 3). XRD analysis of the initial slag (Fig. 4, *a*) and the slag after interaction with ceramics (Fig. 4, *b*) showed that it consists of four phases: $Ca_2(Mg_{0.25}Al_{0.75})(Si_{1.25}Al_{0.75}O_7)$, $CaAl_2O_4$, $CaAl_4O_7$, and $MgAl_2O_4$. Based on the elemental analysis, it can be assumed that the light-gray zone corresponds to $Ca_2(Mg_{0.25}Al_{0.75})(Si_{1.25}Al_{0.75}O_7)$, the dark-gray zone to $MgAl_2O_4$, and the gray zone to calcium aluminates [23]. The quantitative phase ratio changed only slightly before and after the experiment: approximately 62 and 57 % for $Ca_2(Mg_{0.25}Al_{0.75})(Si_{1.25}Al_{0.75}O_7)$, 16 and 15 % for $CaAl_2O_4$, 10 and 14 % for $CaAl_4O_7$, and 14 and 14 % for $MgAl_2O_4$, respectively.

Elemental analysis and mapping of the ceramics interaction zone (Fig. 3) revealed possible diffusion of magnesium and calcium from the slag into the ceramics (spectra 1–4 and 1–5 in Fig. 3). The boundary layer consists of calcium aluminate (spectrum 1–6 in Fig. 3), which, according to the phase diagram [23], corresponds to $CaAl_4O_7$. At the grain boundaries of aluminum oxide (spectrum 1–7 in Fig. 3), a phase containing calcium and aluminum (spectrum 1–8 in Fig. 3) was detected, corresponding to hibonite ($CaAl_{12}O_{19}$). Small aluminum oxide grains were found to have completely transformed into hibonite (spectrum 1–9 in Fig. 3. XRD analysis of the initial ceramics (Fig. 4, *c*) showed that it contained approximately 82 % Al_2O_3, 10 % $MgAl_2O_4$, and 8 % $CaAl_4O_7$. After interaction with the slag (Fig. 4, *d*), the ceramics consisted of about 56 % Al_2O_3, 12 % $MgAl_2O_4$, and 32 % $CaAl_{12}O_{19}$. These results indicate penetration of slag into the ceramics and its chemical interaction with the material, accompanied by the formation of calcium aluminates.

Fig. 5 shows the microstructures of the slag–ceramics interaction zone (zone *2* in Fig. 1) and various zones of the ceramics (zones *3 – 5* in Fig. 1). Elemental

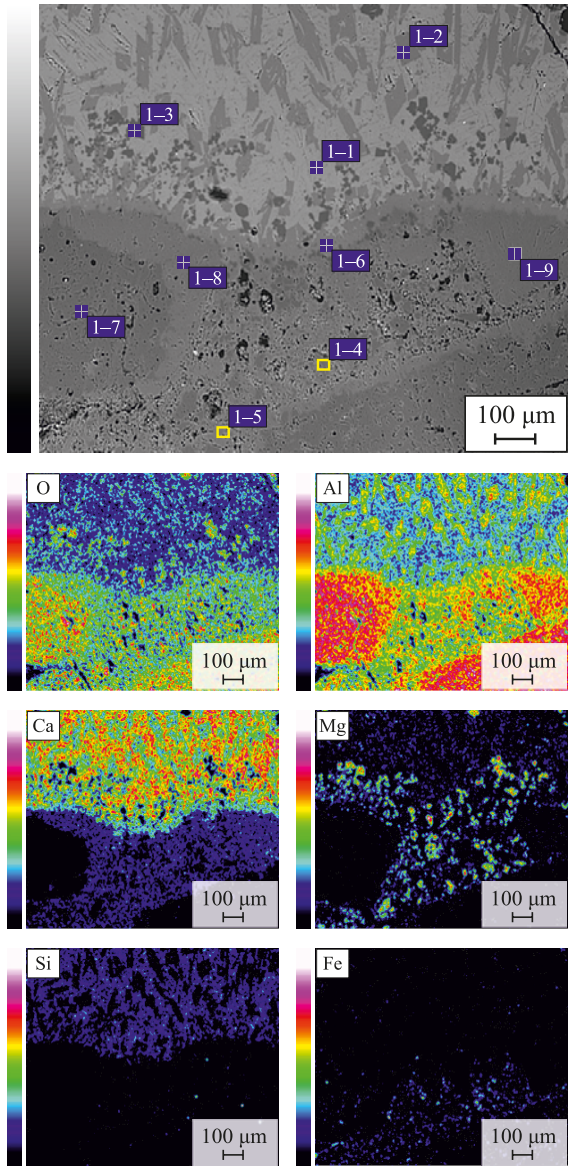

Fig. 3. Microstructure (backscattered electron mode) and elemental mapping of the boundary of slag–ceramics cross section (zone *1*, Fig. 1). Elemental analysis of spectra is given in Table

Рис. 3. Микроструктура (режим обратно отраженных электронов) и элементное картирование границы поперечного среза шлак – керамика (участок *1* на рис. 1).
Элементный анализ спектров представлен в таблице

Elemental composition of the slag and ceramics represented in Figs. 4 and 5

Элементный состав шлака и керамики, представленных на рис. 3 и 5

Figure	Spectrum	Elemental composition, wt. %					
		O	Mg	Al	Si	Ca	Na
3	1–1	41.24	2.23	22.03	8.33	26.17	–
	1–2	43.29	0.49	39.86	0.82	15.54	–
	1–3	45.89	17.28	36.83	–	–	–
	1–4	47.74	13.21	38.28	–	0.77	–
	1–5	48.97	0.38	45.20	0.63	4.82	–
	1–6	44.11	0.61	39.58	0.80	14.9	–
	1–7	50.15	–	49.85	–	–	–
	1–8	47.32	0.41	45.66	0.84	5.77	–
	1–9	46.15	0.43	46.24	0.83	6.35	–
5	2–1	39.98	2.59	21.59	8.55	27.29	–
	2–2	43.14	0.77	40.57	–	15.52	–
	2–3	44.36	17.69	37.82	–	0.13	–
	2–4	43.84	0.31	40.84	–	15.01	–
	2–5	46.17	0.44	46.33	0.82	6.24	–
	2–6	46.14	0.38	46.84	0.55	6.09	–
	2–7	48.13	–	51.87	–	–	–
	3–1	47.23	11.92	40.85	–	–	–
	3–2	49.49	1.73	43.61	–	4.66	0.51
	3–3	48.66	1.95	44.45	–	4.94	–
	4–1	44.11	2.01	46.77	–	7.11	–
	4–2	50.12	1.89	43.87	–	4.12	–
	4–3	45.07	–	41.22	–	13.71	–
	5–1	46.83	10.62	42.55	–	–	–
	5–2	47.36	–	52.64	–	–	–
	5–3	43.40	–	40.90	–	15.70	–
	5–4	46.20	1.89	45.78	0.50	5.63	–

analysis of the slag–ceramics interaction zone (Fig. 5, *a*) demonstrates that (1) the slag phase also consists of three structural zones (spectra 2–1 to 2–3 in Fig. 5, *a*); (2) the interfacial zone is composed of calcium aluminate (spectrum 2–4 in Fig. 5, *a*); and (3) as in the central interaction zone, complete transformation of small aluminum oxide grains into hibonite ($CaAl_{12}O_{19}$) (spectrum 2–5 in Fig. 5, *a*) and its formation along the boundaries of larger grains were observed (spectra 2–6 and 2–7 in Fig. 5, *a*).

Elemental analysis of the central zone of the ceramics at a depth of about 4 mm (Fig. 5, *b*) revealed both the alumomagnesium component of the ceramics (spectrum 3–1 in Fig. 5, *b*) and an increased calcium content (spectra 3–2 and 3–3 in Fig. 5, *b*). This confirms slag penetration into the ceramic substrate during the experi-

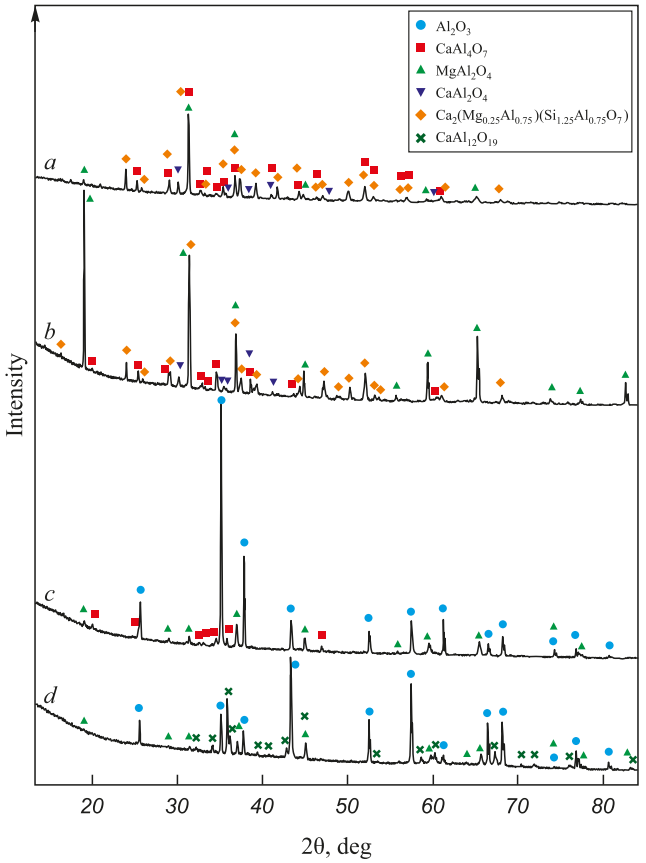

Fig. 4. XRD spectra of the initial slag (*a*), slag after its interaction with ceramics (*b*), those of the initial ceramics (*c*), and after its interaction with slag (*d*)

Рис. 4. Дифракционные спектры исходного шлака (*a*), шлака после взаимодействия с керамикой (*b*), исходной керамики (*c*) и керамики после взаимодействия со шлаком (*d*)

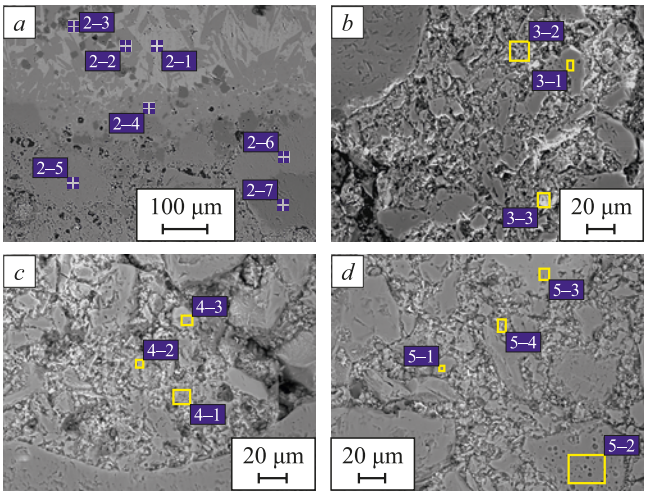

Fig. 5. Microstructure (backscattered electron mode) of the various zones shown in Fig. 1: *a* – zone *2*; *b* – zone *3*; *c* – zone *4*; *d* – zone *5*. Elemental analysis of spectra is given in Table

Рис. 5. Микроструктура (режим обратно отраженных электронов) различных областей на рис. 1: *a* – участок *2*; *b* – участок *3*; *c* – участок *4*; *d* – участок *5*. Элементный анализ спектров представлен в таблице

ment. Figs. 5, *c* and *d* show the edge zones of the ceramics at a depth of approximately 4 mm. These zones contain the alumomagnesium component (spectrum 5–1 in Fig. 5, *d*) and aluminum oxide grains (spectrum 5–2 in Fig. 5, *d*), as well as areas with elevated calcium content (spectra 4–1 to 4–3, 5–3, and 5–4 in Figs. 5, *c*, *d*), corresponding in composition to phases close to calcium aluminates $CaAl_4O_7$ and $CaAl_{12}O_{19}$.

Thus, it can be concluded that during the experiment, chemical interaction of the slag with the ceramics occurred, resulting in the formation of hibonite ($CaAl_{12}O_{19}$) within both small and large aluminum oxide grains, accompanied by noticeable slag penetration into the ceramic substrate.

Conclusions

The interaction of aluminum oxide-based refractory ceramics, used in the manufacture of purging plugs, with ladle slag of composition 45 % CaO, 40 % Al_2O_3, 10 % SiO_2, and 5 % MgO was investigated. A substantial decrease in the wetting angle (θ) to 20° was observed during the first 5 min of the test, followed by a slight further decrease to 13.5° over 115 min. This indicates good wettability of aluminum oxide-based refractory ceramics by the slag.

Microstructural examination and elemental mapping of the cross-sectional slag–ceramics boundary layer revealed that the slag consists of several structural zones: light-gray, gray, and dark-gray. According to XRD analysis, the light-gray zone corresponds to the compound $Ca_2(Mg_{0.25}Al_{0.75})(Si_{1.25}Al_{0.75}O_7)$, the dark-gray region to $MgAl_2O_4$, and the gray region to calcium aluminates. Only minor changes in the phase ratios were observed before and after the experiment.

Analysis of the interaction zone showed possible diffusion of magnesium and calcium from the slag into the ceramics. The slag–ceramics boundary layer was found to consist of calcium aluminate ($CaAl_4O_7$). At the grain boundaries of aluminum oxide, the formation of a phase corresponding to hibonite ($CaAl_{12}O_{19}$) was observed. Small aluminum oxide grains were completely transformed into hibonite. XRD analysis of the initial ceramics showed that it contained approximately 8 % $CaAl_4O_7$, while the ceramics after interaction with slag contained about 32 % $CaAl_{12}O_{19}$. This confirms slag penetration into the ceramics and its chemical interaction with the material accompanied by the formation of calcium aluminates.

Elemental analysis of the ceramics at a depth of about 4 mm revealed the presence of calcium aluminates (close in composition to $CaAl_4O_7$ and $CaAl_{12}O_{19}$) in both the central and peripheral zones. This indicates slag penetration into the ceramic substrate during the experiment.

References / Список литературы

1. Han J.S., Kang J.G., Shin J.H., Chung Y., Park J.H. Influence of CaF_2 in calcium aluminate-based slag on the degradation of magnesia refractory. *Ceramics International*. 2018;44(11):13197–13204. https://doi.org/10.1016/j.ceramint.2018.04.145
2. Ren X.M., Ma B.Y., Li S.M., Li H.X., Liu G.Q., Yang W.G., Qian F., Zhao S.X., Yu J.K. Comparison study of slag corrosion resistance of MgO–$MgAl_2O_4$, MgO–CaO and MgO–C refractories under electromagnetic field. *Journal of Iron Steel Research International*. 2021;28(1):38–45. https://doi.org/10.1007/s42243-020-00421-0
3. Yan Z., Deng Z., Zhu M. Penetration behavior of CaO–SiO_2–FeO_x–MgO–($CaCl_2$) slags in MgO refractory. *Metallurgical and Materials Transactions B*. 2023;54(3):1582–1592. https://doi.org/10.1007/s11663-023-02787-4
4. Park J.H., Suk M.O., Jung I.H., Guo M., Blanpain B. Interfacial reaction between refractory materials and metallurgical slags containing fluoride. *Steel Research International*. 2010;81(10):860–868. https://doi.org/10.1002/srin.201000157
5. Wang Y.-x., Li Y.-g., Gao Y.-b., Huang Zh., Zhang H.-j. High-temperature wetting behavior between slag and refractory. *Journal of Iron Steel Research International*. 2024; 31:1304–1319. https://doi.org/10.1007/s42243-024-01252-z
6. Gehre P., Aneziris C.G., Berek H., Parr C., Reinmöller M. Corrosion of magnesium aluminate spinel-rich refractories by sulphur-containing slag. *Journal of the European Ceramic Society*. 2015;35(5):1613–1620. https://doi.org/10.1016/j.jeurceramsoc.2014.11.031
7. Park J., Lee K., Pak J.J., Chung Y. Initial wetting and spreading phenomena of a CaO–SiO_2 liquid slag on MgO substrates. *ISIJ International*. 2014;54(9):2059–2063. https://doi.org/10.2355/isijinternational.54.2059
8. Yu B., Lv X., Xiang S., Bai C., Yin J. Wetting behavior of calcium ferrite melts on sintered MgO. *ISIJ International*. 2015;55(8):1558–1564. https://doi.org/10.2355/isijinternational.ISIJINT-2014-830
9. Park J., Jeon J., Lee K., Park J.H., Chung Y. Initial wetting and spreading rates between SiC and CaO–SiO_2–MnO slag. *Metallurgical and Materials Transactions B*. 2016; 47(3):1832–1838. https://doi.org/10.1007/s11663-016-0606-0
10. Huang F., Liu C., Maruoka N., Kitamura S.Y. Dissolution behaviour of MgO based refractories in CaO–Al_2O_3–SiO_2 slag. *Ironmaking & Steelmaking*. 2015;42(7):553–560. https://doi.org/10.1179/1743281215Y.0000000003
11. Zou Y., Huang A., Wang R., Fu L., Gu H., Li G. Slag corrosion-resistance mechanism of lightweight magnesia-based refractories under a static magnetic field. *Corrosion Science*. 2020;167:108517. https://doi.org/10.1016/j.corsci.2020.108517
12. Fu L., Huang A., Lian P., Gu H. Isolation or corrosion of microporous alumina in contact with various CaO–Al_2O_3–SiO_2 slags. *Corrosion Science*. 2017;120:211–218. https://doi.org/10.1016/j.corsci.2017.01.018
13. Ren X., Ma B., Li S., Li H., Liu G., Zhao S., Yang W., Qian F., Yu J. Slag corrosion characteristics of MgO-based

refractories under vacuum electromagnetic field. *Journal of the Australian Ceramic Society*. 2019;55:913–920. https://doi.org/10.1007/s41779-019-00323-9

14. Ma B., Yin Y., Zhu Q., Zhai Y., Li Y., Li G., Yu J. Slag corrosion and penetration behaviors of $MgAl_2O_4$ and Al_2O_3 based refractories. *Refractories and Industrial Ceramics*. 2016; 56(5):494–501. https://doi.org/10.1007/s11148-016-9876-y

15. Vázquez B.A., Pena P., De Aza A.H., Sainz M.A., Caballero A. Corrosion mechanism of polycrystalline corundum and calcium hexaluminate by calcium silicate slags. *Journal of the European Ceramic Society*. 2009;29(8):1347–1360. https://doi.org/10.1016/j.jeurceramsoc.2008.08.031

16. Song J., Liu Y., Lv X., You Z. Corrosion behavior of Al_2O_3 substrate by SiO_2–MgO–FeO–CaO–Al_2O_3 slag. *Journal of Materials Research and Technology*. 2020;9(1):314–321. https://doi.org/10.1016/j.jmrt.2019.10.060

17. Shen P., Zhang L., Wang Y., Sridhar S., Wang Q. Wettability between molten slag and dolomitic refractory. *Ceramics International*. 2016;42(14):16040–16048. https://doi.org/10.1016/j.ceramint.2016.07.113

18. Wang C., Xie C., Xu J., Wan K. Wettability and spreading kinetics between some refractory materials and molten calcium aluminate slag. *Steel Research International*. 2025;(6):2400895. https://doi.org/10.1002/srin.202400895

19. Shvarts K., Kraus O. Study of penetration of liquid metal into purge plugs. *Ogneupory i tekhnicheskaya keramika*. 2013;(4-5):52–56. (In Russ.).

Шварц К., Краус О. Изучение проникновения жидкого металла в продувочные пробки. *Огнеупоры и техническая керамика*. 2013;(4-5):52–56.

20. Ahuchkin S.N., Burtsev V.T., Zagumennikov M.V., Sidorov V.V., Rigin V.E. Study of the surface properties of nickel-based melts by the constrained drop method: I. Surface tension. *Russian Metallurgy (Metally)*. 2010;(1):13–17. https://doi.org/10.1134/S0036029510010039

Анучкин С.Н., Бурцев В.Т., Загуменников М.В., Сидоров В.В., Ригин В.Е. Исследование поверхностных свойств расплавов на основе никеля методом большой капли. I. Поверхностное натяжение. *Металлы*. 2010;(1):15–20.

21. Yang M., Yan Z., Li Z., Lv X., Bai C. Modelling the dissolutive wetting of slag-oxide system at high temperatures. *Metallurgical and Materials Transactions B*. 2025;56(2): 1573–1587. https://doi.org/10.1007/s11663-024-03429-z

22. Monaghan B.J., Abdeyazdan H., Dogan N., Rhamdhani M.A., Longbottom R.J., Chapman M.W. Effect of slag composition on wettability of oxide inclusions. *ISIJ International*. 2015;55(9):1834–1840. https://doi.org/10.2355/isijinternational.ISIJINT-2015-168

23. Slag Atlas: Handbook. Düsseldorf: Verlag Stahleisen GmbH; 1995:634.

Information about the Authors / Сведения об авторах

Aleksandr A. Aleksandrov, *Cand. Sci. (Eng.), Senior Researcher, Head of the A.M. Samarin Laboratory of Physical Chemistry of Metal Melts*, Baikov Institute of Metallurgy and Materials Science, Russian Academy of Sciences
ORCID: 0000-0002-5028-7623
E-mail: a.a.aleksandrov@gmail.com

Sergei N. Anuchkin, *Cand. Sci. (Eng.), Senior Researcher of the A.M. Samarin Laboratory of Physical Chemistry of Metal Melts*, Baikov Institute of Metallurgy and Materials Science, Russian Academy of Sciences
ORCID: 0000-0002-2650-0818
E-mail: AnuchkinSN@yandex.ru

Akim G. Kanevskiy, *Cand. Sci. (Eng.), Senior Researcher of the A.M. Samarin Laboratory of Physical Chemistry of Metal Melts*, Baikov Institute of Metallurgy and Materials Science, Russian Academy of Sciences
ORCID: 0000-0002-9280-9442
E-mail: akanev48@gmail.com

Sof'ya B. Rumyantseva, *Cand. Sci. (Eng.), Research Associate of the Laboratory of Materials Diagnostics*, Baikov Institute of Metallurgy and Materials Science, Russian Academy of Sciences
ORCID: 0000-0003-4508-2524
E-mail: sbvarlamova@gmail.com

Konstantin V. Grigorovich, *Academician, Dr. Sci. (Eng.), Head of the Laboratory of Materials Diagnostics*, Baikov Institute of Metallurgy and Materials Science, Russian Academy of Sciences; *Prof. of the Chair of Metallurgy of Steel, New Production Technologies and Metal Protection*, National University of Science and Technology "MISIS"
ORCID: 0000-0002-5669-4262
E-mail: grigorov@imet.ac.ru

Александр Александрович Александров, *к.т.н., старший научный сотрудник, заведующий лабораторией физикохимии металлических расплавов им. академика А.М. Самарина*, Институт металлургии и материаловедения им. А.А. Байкова РАН
ORCID: 0000-0002-5028-7623
E-mail: a.a.aleksandrov@gmail.com

Сергей Николаевич Анучкин, *к.т.н., старший научный сотрудник лаборатории физикохимии металлических расплавов им. академика А.М. Самарина*, Институт металлургии и материаловедения им. А.А. Байкова РАН
ORCID: 0000-0002-2650-0818
E-mail: AnuchkinSN@yandex.ru

Аким Горациевич Каневский, *к.т.н., старший научный сотрудник лаборатории физикохимии металлических расплавов им. академика А.М. Самарина*, Институт металлургии и материаловедения им. А.А. Байкова РАН
ORCID: 0000-0002-9280-9442
E-mail: akanev48@gmail.com

Софья Борисовна Румянцева, *к.т.н, научный сотрудник лаборатории диагностики материалов*, Институт металлургии и материаловедения им. А.А. Байкова РАН
ORCID: 0000-0003-4508-2524
E-mail: sbvarlamova@gmail.com

Константин Всеволодович Григорович, *академик РАН, д.т.н., заведующий лабораторией диагностики материалов*, Институт металлургии и материаловедения им. А.А. Байкова РАН; *профессор кафедры металлургии стали, новых производственных технологий и защиты металлов*, Национальный исследовательский технологический университет «МИСИС»
ORCID: 0000-0002-5669-4262
E-mail: grigorov@imet.ac.ru

Contribution of the Authors

A. A. Aleksandrov – planning and carrying out the experiments, sampling of ceramics and slag, experimental data processing, writing the text.
S. N. Anuchkin – planning and carrying out the experiments, experimental data processing, writing the text.

A. G. Kanevskiy – analysis of the published data on slag-refractory interaction, carrying out the experiments, discussion of experimental results.
S. B. Rumyantseva – examination of the slag-refractory interaction zone using a JEOL JXA-iSP100 scanning electron microscope (SEM), discussion of experimental results.
K. V. Grigorovich – problem formulation, scientific guidance.

Вклад авторов

А. А. Александров – планирование и проведение экспериментов, отбор проб керамики и шлака, обработка полученных экспериментальных данных, подготовка текста статьи.
С. Н. Анучкин – планирование и проведение экспериментов, обработка полученных экспериментальных данных, подготовка текста статьи.
А. Г. Каневский – анализ литературных источников по взаимодействию в системе шлак–огнеупор, проведение экспериментов, обсуждение результатов.
С. Б. Румянцева – исследование зоны взаимодействия шлак–огнеупор на сканирующем электронном микроскопе (СЭМ) JEOL JXA-iSP100, обсуждение результатов.
К. В. Григорович – постановка задачи, общее руководство исследованием.

Received 29.04.2025
Revised 11.05.2025
Accepted 14.06.2025

Поступила в редакцию 29.04.2025
После доработки 11.05.2025
Принята к публикации 14.06.2025

MATERIALS SCIENCE / МАТЕРИАЛОВЕДЕНИЕ

UDC 669.15-198
DOI 10.17073/0368-0797-2025-5-476-481

Original article
Оригинальная статья

Correlation between the structure and properties of ferroalloys

I. N. Kel' ✉, **V. I. Zhuchkov, O. V. Zayakin**

Vatolin Institute of Metallurgy of the Ural Branch of the Russian Academy of Sciences (101 Amundsena Str., Yekaterinburg 620016, Russian Federation)

✉ dunnington@mail.ru

Abstract. The paper reviews the studies on relationship between the structure, phase composition, and properties of ferroalloys, as well as their impact on the quality of treated metals. The requirements for ferroalloys include not only chemical composition but also a range of properties: optimal melting temperature, oxidation resistance, density, and time of dissolution in the treated melt. The structure and phase composition of the alloys are also crucial, as they affect friability, element segregation within the ingot, crushability, and formation of fine fractions. The study presents research findings aimed at addressing the issue of spontaneous disintegration of ferrosilicon caused by the eutectoid transformation of leboite and presence of impurities. Methods to prevent ferroalloy disintegration are proposed, including rapid cooling, reducing impurity content, and stabilizing the structure through additives such as boron. The structural features of other alloys, such as silicocalcium, are also examined, where improved crushability is achieved by slowing crystallization and modifying phase composition. Approaches to modeling the phase composition of ferroalloys are discussed, including thermodynamic-diagram methods and polygonal phase diagram analysis. The results of studies on rapid cooling of modifiers demonstrate enhanced efficiency due to the fine-grained structure and uniform distribution of active elements. It was established that the structure of ferroalloys influences the primary crystallization of cast iron, determining graphite morphology and matrix structure. The impact of phase composition and non-metallic inclusions (oxides, sulfides) in ferroalloys on steel properties is also demonstrated. Based on the review, the necessity of considering the structural and phase characteristics of ferroalloys is highlighted, as this can improve metallurgical product quality, reduce material consumption, and minimize adverse effects.

Keywords: structure, phase composition, ferroalloy, inclusions, modifiers, physicochemical properties

Acknowledgements: The work was performed according to the state assignment for the Vatolin Institute of Metallurgy of the Ural Branch of RAS.

For citation: Kel' I.N., Zhuchkov V.I., Zayakin O.V. Correlation between the structure and properties of ferroalloys. *Izvestiya. Ferrous Metallurgy*. 2025;68(5):476–481. https://doi.org/10.17073/0368-0797-2025-5-476-481

Корреляция структуры и характеристик ферросплавов

И. Н. Кель ✉, **В. И. Жучков, О. В. Заякин**

Институт металлургии имени академика Н.А. Ватолина Уральского отделения РАН (Россия, 620016, Екатеринбург, ул. Амундсена, 101)

✉ dunnington@mail.ru

Аннотация. В статье представлен обзор исследований взаимосвязи структуры и фазового состава со свойствами ферросплавов, а также их влияния на качество обрабатываемых металлов. Требования, предъявляемые к ферросплавам, включают в себя не только химический состав, но и ряд свойств: рациональную температуру плавления, устойчивость к окислению, плотность и время растворения в обрабатываемом расплаве. Структура и фазовый состав сплавов также имеют решающее значение, поскольку они влияют на рассыпаемость, ликвацию элементов в объеме слитка, способность к дроблению и образованию мелких фракций. В работе приведены результаты исследований, направленных на решение проблемы самопроизвольного рассыпания ферросилиция, вызванного эвтектоидным превращением лебоита и наличием примесей. Предложены методы борьбы с дезинтеграцией ферросплава путем быстрого охлаждения, снижения доли примесей и стабилизации структуры с помощью таких добавок, как бор. В статье рассмотрены структурные особенности других сплавов, например, силикокальция, где улучшение дробимости достигается за счет замедления кристаллизации и изменения фазового состава. Обсуждаются подходы к моделированию фазового состава ферросплавов, включая термодинамически-диаграммный метод и анализ полигональных диаграмм состояния. Результаты исследований по быстрому охлаждению модификаторов демонстрируют повышенную эффективность за счет мелкодисперсной структуры и равномерного распределения активных элементов. Установлено, что структура ферросплавов влияет на первичную кристаллизацию чугуна, определяя морфологию графита и матрицы. Показано влияние фазового состава и типа неметаллических включений (оксиды, сульфиды) ферросплавов на свойства стали. На основе проведенного обзора

подчеркивается необходимость учета структурно-фазовых характеристик ферросплавов, что позволит повысить качество металлургической продукции, снизить расход материалов и минимизировать негативные эффекты.

Ключевые слова: структура, фазовый состав, ферросплав, включения, модификаторы, физико-химические свойства

Благодарности: Исследование выполнено по государственному заданию Института металлургии имени академика Н.А. Ватолина Уральского отделения РАН.

Для цитирования: Кель И.Н., Жучков В.И., Заякин О.В. Корреляция структуры и характеристик ферросплавов. *Известия вузов. Черная металлургия*. 2025;68(5):476–481. https://doi.org/10.17073/0368-0797-2025-5-476-481

A key objective of metallurgy is the development of new types of metal products capable of maintaining their operational characteristics under extreme environmental conditions. Consequently, the development of metals with improved properties and the emergence of advanced smelting technologies have stimulated interest and deeper studies of the physicochemical characteristics of ferroalloys that affect these properties.

This has created a need to produce ferroalloys with a low melting temperature and oxidation susceptibility, optimal density, minimal dissolution time, and minimal cooling of liquid steel upon their addition. The quality of ferroalloys depends not only on their chemical composition, impurity content, and gas saturation, but also on friability, element segregation within the ingot, magnetic properties, crushability, and the tendency to form fine fractions.

Given these requirements, the Institute of Metallurgy of the Ural Branch of the Russian Academy of Sciences (IMET UB RAS) proposed an approach to developing new compositions of complex ferroalloys that more effectively improve the service characteristics of the treated metal, achieve higher assimilation by steel, dissolve more rapidly, and introduce less contamination [1]. The most extensively studied parameters include the melting temperature, density, oxidation resistance of ferroalloys, the thermal effect during interaction with steel, dissolution time in liquid steel, and thermophysical characteristics. At the same time, the relationship between the structure and phase composition of ferroalloys and their properties has been largely overlooked.

Reference books and monographs [2 – 4] provide data on the phase composition of various industrial grades of ferroalloys. For each alloy, these data can vary significantly, as they depend on the casting method and ingot crystallization rate.

The structure and phase composition of a ferroalloy affect not only the alloy's own properties (melting temperature, hardness, strength, etc.) but also the characteristics of the treated metal (cast iron or steel), particularly during modification.

Researchers turned their attention to the structure of ferroalloys after frequent occurrences of spontaneous disintegration of ferrosilicon were reported [1; 5; 6]. Its structural components are intermetallic phases (silicides): Fe_2Si (β-phase), Fe_5Si_3 (η-phase), and $FeSi_2$ (ξ-phase, leboite), which has two allotropic modifications – high- and low-temperature. During cooling of the alloy after crystallization, the initial stages of the eutectoid transformation occur in metastable leboite, leading to the formation of Guinier–Preston zones, while the resulting elastic stresses cause cracking of structural components. This process is also associated with the presence of unstable excess phases in the ingot when exposed to a humid atmosphere.

It has been observed that even at standard phosphorus levels (0.03 – 0.04 %), ferrosilicon with 49 – 51 % Si is prone to disintegration. In 75 % ferrosilicon (FeSi75), the excess-phases formation – primarily promoted by calcium, aluminum, and phosphorus – triggers ingot disintegration and the release of phosphine (PH_3) and arsine (AsH_3). Within these excess phases, silicon and iron help stabilize the structure, reducing the ingots' susceptibility to disintegration in the presence of atmospheric moisture. Trace arsenic present in the melt tends to become enriched in Ca–Al–P–bearing phases.

According to [1; 5], ferrosilicon disintegration is associated with several factors: the eutectoid transformation of leboite; silicon segregation accompanied by the formation of silicon-enriched melt; and elevated concentrations of impurity elements (Al, Ca, Ti, As, P, S, C), which tend to form phosphides that readily react with atmospheric moisture.

Electron microscopy of disintegrating ferrosilicon samples revealed aluminum enrichment along crack paths, with pronounced segregation, including as aluminum phosphide (AlP). In FeSi65 ingots, this results in structural regions prone to disintegration. In addition to a significant amount of aluminum phosphide, titanium phosphides and magnesium arsenides were also identified in the disintegrating alloys; these compounds may likewise act as crack initiators.

Structural analysis indicates that FeSi65 disintegration is primarily caused by (i) reduced silicon content (<65 %), (ii) elevated aluminum content (>1 %), including as phosphides, and (iii) segregation driven by casting and crystallization conditions. These factors favor the formation of structurally unstable leboite and the enrichment of impurity phosphides in localized regions of the ingot, leading to FeSi65 disintegration in the presence of atmospheric moisture.

According to [5], effective mitigation measures include promoting rapid crystallization to suppress silicon and component segregation, lowering the contents of phosphorus, calcium, and aluminum, and stabilizing the ferrosilicon by introducing alloying additions such as boron into the melt.

A case was reported in [7] where a new, efficient alloy (AMS) containing 60 – 65 wt. % Mn, 25 – 30 wt. % Si, and 5 – 8 wt. % Al failed to be adopted in practice due to disintegration. Although its production showed high technical and economic efficiency, and its use as a steel deoxidizer improved steel quality while significantly reducing ferroalloy consumption, the alloy underwent substantial disintegration during storage in air, accompanied by the release of explosive gases containing PH_3. Structural examination established that the disintegration was driven by the interaction of phosphides and carbides with atmospheric moisture. The authors of [7] further note additional causes of AMS disintegration: the reaction of aluminum carbide with water, forming aluminum hydroxide and metallic aluminum; and polymorphic transformations in the $Mn_4Si_2Al_3$ phase and in the solid solution of silicon with Mn and Al, which initiate microcrack growth and ultimately lead to alloy failure.

Another unfavorable characteristic of ferroalloys is poor crushability, which accelerates wear of crushing equipment and complicates casting.

The effect of structure and phase composition on the crushability of the calcium–silicon alloy (grade SK15, containing 15 wt. % Ca, 20 wt. % Fe, 1 wt. % Al, 0.2 wt. % C, balance Si) was investigated in [8]. The principal phases are $FeSi_2$ and CaSi, and their ratio depends directly on the calcium content (10 – 30 wt. %). It was found that impurity elements in silicocalcium form a series of discrete secondary phases as fine precipitates – such as $CaAl_2Si_2$, $Ba(Si,Al)_4$, and Ca_2MgSi_3. The presence of numerous small, rounded $FeSi_2$-type crystals in the SK15 alloy leads to structural refinement, which decreases its crushability. To improve crushability, it was proposed to slow the crystallization rate to obtain a coarse-grained structure and to reduce the iron content. Additions of chromium, manganese, nickel, and copper lead to the formation of the corresponding disilicides and modify the $CaSi_2$ phases, thereby affecting the properties of silicocalcium and, in particular, improving its fire and explosion safety.

Approaches to modeling the phase composition of ferroalloys have been developed. Akberdin et al. [9] introduced a thermodynamic–diagram approach that constructs ternary and quaternary phase diagrams from the geometric regularities of phase equilibria and, from these diagrams, derives mathematical relations to predict the most probable phase assemblages.

Another approach, proposed by B.F. Belov et al. [10], is the prediction of the phase composition of ferroalloys using structural–chemical analysis of the condensed phases of a polygonal phase diagram (PPD). This method is based on geometrically subdividing the concentration triangle using field lines (edge–edge) or radial lines (vertex–edge). The intersection points of these lines represent the reaction products, i.e., the phases of the ternary system.

Systematic research into how the structure and phase composition of ferroalloys affect the properties of treated metals dates to the late 20th century. Brodova et al. [11 – 13] showed that the structure of master alloys – specifically the size and defect density of Al_3Zr intermetallic crystals – governs the efficiency of zirconium alloying and modification of aluminum alloys.

Ryabchikov and colleagues [14 – 16] investigated the production and application of quenched microcrystalline silicon ferroalloys containing alkaline-earth metals and magnesium, and assessed their effect on cast-iron properties.

In [14], they compared two magnesium-containing modifiers (48 wt. % Si, 5 – 6 wt. % Mg, 2 wt. % Ca, 6 wt. % REM, balance Fe) used for cast-iron treatment: one rapidly cooled between two rotating copper rolls and the other cast into ingots.

The rapidly cooled (chip-type) modifier exhibited a structure markedly different from that of the ingot. Its structural components were 10 – 100 times smaller, and the chemically active elements were distributed more uniformly throughout the volume. When used in cast iron treatment, the rapidly cooled modifier reduced the white layer depth from 7 to 4 mm. Moreover, the modifier consumption decreased by 25 – 30 % while maintaining the same modification efficiency. The rapidly cooled modifiers were also easily crushed, provided a higher yield of usable fractions, and exhibited less tendency to overgrinding compared with the conventional modifier.

A comparative morphological assessment presented in [14] showed that both types of modifiers contained the same primary phases: $FeSi_2$, free silicon, magnesium-containing phases (Mg_2Si, $CaMgSi_x$), and a small amount (<0.1 %) of *X*-ray amorphous SiMgO (according to *X*-ray and electron probe microanalysis). No differences in phase composition between chip-type and ingot-type modifiers were detected by *X*-ray diffraction. Metallographic analysis, however, did not reveal clear boundaries between magnesium-containing phases. Differences in phase fractions were observed: $FeSi_2$ fraction in ingots was, on average, about 4 % higher than in chips; free silicon was about 7 % higher in ingots; conversely, the magnesium–silicon phase content was higher in chips by an average of 12.7 %. Consequently, the phase containing the elements responsible for the modification effect occupied a larger area fraction in chip-type modifiers than in ingot-type ones. In addition, the modifiers differed in the thick-

ness of $FeSi_2$ lamellae. In ingots, $FeSi_2$ lamellae were about five times thicker than those of the Mg_2Si phase, whereas in chip-type modifiers the characteristic lamellar thicknesses were comparable. According to the authors, this promotes a more uniform distribution of modifying elements throughout the cross-section, faster dissolution kinetics, and higher recovery (uptake) during modification with chip-type modifiers.

Further research on the effect of ferroalloy microstructure on the properties of treated metals was conducted by A.G. Panov, D.A. Boldyrev, E.S. Zakirov, and others [17 – 19].

According to [17; 19], the effect of modifier structure on cast iron properties is attributed to primary crystallization processes that alter the morphology and quantity of graphite, as well as the matrix structure of the treated metal.

Structural fragments of FeSi and α-$FeSi_2$ transferred from the modifier into the cast-iron melt interact with melt components exhibiting short-range order similar to that of cementite. As a result, chemical bonds between Fe, Si, and C atoms are rearranged, forming new carbon-depleted Fe – C – Si structures. Upon subsequent cooling, these structures act as precursors and nucleation sites for ferrite and austenite. Consequently, in cast irons treated with coarse-crystalline modifiers, the primary crystallization of graphite, austenite, and ferrite proceeds more actively, whereas in those treated with fine-crystalline modifiers, these processes are suppressed and cementite and ledeburite crystallize instead.

Magnesium–silicon phases (Mg_2Si) inherited from the modifier participate in the formation of disordered regions within the cast-iron melt. Their size affects both the rate of magnesium removal and the elimination of non-metallic inclusions from the melt. This, in turn, influences the amount and morphology of graphite. Refinement of magnesium-containing phases enhances both spheroidizing and graphitizing effects.

In addition to the structure and phase composition of ferroalloys, their non-metallic inclusions (oxides, sulfides, and others) also influence the quality of the treated metal [20 – 25].

Studies [20 – 22] have shown that ferrosilicon contains a certain amount of SiO_2, which, during alloying, transfers into the steel and contributes to its contamination.

The authors of [24] investigated non-metallic inclusions in ferrotitanium and their behavior during steel alloying. This ferroalloy contains large, irregular inclusions primarily composed of CaO and SiO_2, which, upon entering the treated metal, transform into spherical inclusions containing TiO_2, Al_2O_3, and CaO.

In [25], the effect of ferroniobium inclusions on the early stages of its dissolution during steel microalloying was examined. The study identified a mechanism for the formation of Al – O and Al – Ti – Nb – O inclusions in steel. According to the authors, Ti – O inclusions transform into heterogeneous inclusions consisting of a Ti – O core surrounded by an outer Nb – Ti – O shell.

Conclusions

The review underscores the need to account for the structure and phase composition of ferroalloys, as well as the potential to modify both the alloys and the treated metal by transforming the ferroalloy's structural and phase characteristics.

Accordingly, further research should focus on the effects of the cooling rate and time–temperature parameters on the phase-structure evolution in ferroalloys, and broaden the range of alloys investigated.

References / Список литературы

1. Zhuchkov V.I., Zayakin O.V., Mikhailova L.Yu. Physical Chemistry and Technology in Metallurgy. Yekaterinburg: Al'fa-Print; 2021:272. (In Russ.).
Жучков В.И., Заякин О.В., Михайлова Л.Ю. Физическая химия и технология в металлургии. Екатеринбург: ООО Универсальная типография «Альфа-Принт»; 2021:272.
2. Gasik L.N., Ignatiev V.S., Gasik M.I. Structure and Quality of Industrial Ferroalloys and Master Alloys. Kiev: Tekhnika; 1975:52 p. (In Russ.).
Гасик Л.Н., Игнатьев В.С., Гасик М.И. Структура и качество промышленных ферросплавов и лигатур. Киев: Техника; 1975:52.
3. Vertii I.G., Rozhdestvenskaya T.A., Mikhailov G.G., Vasiliev V.I. Ferroalloys, Slags, Refractories: Microstructure Atlas. Chelyabinsk: Metall; 1994:112. (In Russ.).
Вертий И.Г., Рождественская Т.А., Михайлов Г.Г., Васильев В.И. Ферросплавы, шлаки, огнеупоры. Атлас микроструктур. Челябинск: Металл; 1994:112.
4. Iskhakov A.D., Voronin B.V. Ferroalloys, Modifiers, Master Alloys: Reference Book. Vol. 1. Chelyabinsk: Tsitsero; 2009:259. (In Russ.).
Исхаков А.Д., Воронин Б.В. Ферросплавы, модификаторы, лигатуры: Справочник. Т. 1. Челябинск: Цицеро; 2009:259.
5. Zakharov R.G., Petrova S.A., Zhdanov A.V., Zhuchkov V.I. Effect of the structure of ferrosilicon on its desintegration. *Russian Metallurgy (Metally)*. 2014;2014(1):3–16. https://doi.org/10.1134/S0036029514010145
Захаров Р.Г., Петрова С.А., Жданов А.В., Жучков В.И. Изучение влияния структуры ферросилиция на его рассыпаемость. *Металлы*. 2014;(1):8–13.
6. Zhuchkov V.I., Gasik M.I., Sheshukov O.Yu. Structure and physicochemical characteristics of ferroalloys. *Electrometallurgiya*. 2006;(6):39–44. (In Russ.).
Жучков В.И., Гасик М.И., Шешуков О.Ю. Структура и физико-химические характеристики ферросплавов. *Электрометаллургия*. 2006;(6):39–44.

7. Gasik M.I., Lyakishev N.P., Emlin B.I. Theory and Technology of Ferroalloy Production. Moscow: Metallurgiya; 1988:784. (In Russ.).

Гасик М.И., Лякишев Н.П., Емлин Б.И. Теория и технология производства ферросплавов. Москва: Металлургия; 1988:784.

8. Povolotskii V.D., Komisarova T.A., Chuvashin I.I. Structure and phase composition of silicocalcium. In: Improving the Efficiency and Quality of Ferroalloys (Collection of Sci. Papers). Moscow: Metallurgiya; 1986:96–100. (In Russ.).

Поволоцкий В.Д., Комисарова Т.А., Чувашин И.И. Структура и фазовый состав силикокальция: Сборник научных трудов «Повышение эффективности и качества ферросплавов». Москва: Металлургия; 1986:96–100.

9. Khurmetbek Zh., Dzhaksembaev D.M., Akberdin A.A. Mathematical model of phase composition diagram of the Fe–Ti–Al system. *Vestnik of D. Serikbayev East Kazakhstan State Technical University*. 2016;(4):118–122. (In Russ.).

Хурметбек Ж., Джексембаев Д.М., Акбердин А.А. Математическая модель диаграммы фазового состава системы Fe–Ti–Al. *Вестник Восточно-Казахстанского государственного технического университета им. Д. Серикбаева*. 2016;(4):118–122.

10. Belov B.F., Babanin A.Ya., Bakin I.V., etc. Classification of alloys in the iron-silicon-carbon system. *Stal'*. 2019;(6): 16–19. (In Russ.).

Белов Б.Ф., Бабанин А.Я., Бакин И.В. и др. Классификация сплавов системы железо – кремний – углерод. *Сталь*. 2019;(6):16–19.

11. Brodova I.G., Polents I.V., Popel' P.S. The role of master alloy structure in zirconium modification of aluminum alloys. *Fizika metallov i metallovedenie*. 1993;76(5): 123–131. (In Russ.).

Бродова И.Г., Поленц И.В., Попель П.С. Роль структуры лигатурных сплавов при модифицировании алюминиевых сплавов цирконием. *Физика металлов и металловедение*. 1993;76(5):123–131.

12. Brodova I.G., Bashlikov D.V., Polents I.V. Influence of heat time melt treatment on the structure and the properties of rapidly solidified aluminum alloys with transition metals. *Materials Science Forum*. 1998;269–272:589–594. https://doi.org/10.4028/www.scientific.net/MSF.269-272.589

13. Brodova I.G., Polents I.V., Bashlikov D.V., Popel P.S., Chikova O.A. The forming mechanism of ultradispersed phases in rapidly solidified aluminium alloys. *Nanostructured Materials*. 1995;6(1–4):477–479. https://doi.org/10.1016/0965-9773(95)00100-X

14. Ryabchikov I.V., Solov'ev N.M. Silicon ferroalloys with fine-crystalline structure. In: *Steel and Ferroalloy Production: Theory and Practice.* Chelyabinsk: NIIM; 1998: 175–182. (In Russ.).

Рябчиков И.В., Соловьев Н.М. Кремнистые ферросплавы с мелкокристаллической структурой. *Научные труды «Производство стали и ферросплавов. Теория и практика»*. НИИМ: Челябинск; 1998:175–182.

15. Ryabchikov I.V., Panov A.G., Kornienko A.E. On the quality characteristics of modifiers. *Stal'*. 2007;(6):18–23. (In Russ.).

Рябчиков И.В., Панов А.Г., Корниенко А.Э. О качественных характеристиках модификаторов. *Сталь*. 2007; (6):18–23.

16. Vyaznikova E.A., Smirnova V.G., Sheshukov O.Yu., Zhuchkov V.I., Zayakin O.V., Ryabchikov I.V. Influence of cooling rate on the structure and phase composition of magnesium-containing modifiers. *Stal'*. 2008;(8):66. (In Russ.).

Вязникова Е.А., Смирнова В.Г., Шешуков О.Ю., Жучков В.И., Заякин О.В., Рябчиков И.В. Влияние скорости охлаждения на структуру и фазовый состав магний-содержащих модификаторов. *Сталь*. 2008;(8):66.

17. Panov A.G. Effect of the microstructure of cast Fe–Mg–Ni master alloys on crystallization and microstructure of modified high-strength cast iron. *Izvestiya. Ferrous Metallurgy*. 2010;53(11):55–60. (In Russ.).

Панов А.Г. Влияние микроструктуры литых Fe–Mg–Ni лигатур на кристаллизацию и микроструктуру модифицированного высокопрочного чугуна. *Известия вузов. Черная металлургия*. 2010;53(11):55–60.

18. Boldyrev D.A., Popova L.I., Davydov S.V. Phase electron microscopy and X-ray microanalysis of the structure of CGI modifiers. *Stal'*. 2018;(4):42–45. (In Russ.).

Болдырев Д.А., Попова Л.И., Давыдов С.В. Фазовый электронно-микроскопический анализ и рентгеноспектральный микроанализ структуры ЧВГ-модификаторов. *Сталь*. 2018;(4):42–45.

19. Zakirov E.S. Improving the stability of structure and properties of critical machine parts made of cast iron with spheroidal and vermicular graphite: Extended Abstract of Cand. Sci. Diss. Kazan; 2023:24 p. (In Russ.).

Закиров Э.С. Повышение стабильности структуры и свойств ответственных деталей машиностроения из чугуна с шаровидными и вермикулярным графитом: Автореферат диссертации… кандидата технических наук. Казань; 2023:24.

20. Wang Y., Karasev A., Park J.H., Jönsson P.G. Non-metallic inclusions in different ferroalloys and their effect on the steel quality: A review. *Metallurgical and Materials Transactions B*. 2021;52:2892–2925. https://doi.org/10.1007/s11663-021-02259-7

21. Michelic S.K., Bernhard C. Significance of nonmetallic inclusions for the clogging phenomenon in continuous casting of steel – A review. *Steel Research International*. 2022;93(7):2200086. https://doi.org/10.1002/srin.202200086

22. Pindar S., Pande M.M. Investigation of inclusion characteristics in ferrosilicon killed high silicon steels. *Steel Research International*. 2024;95(9):2400331. https://doi.org/10.1002/srin.202400331

23. Wang J., Song Sh., Ke X., Nyembwe A., Xue Zh. Characterization of LC/HC-FeMn alloys and their melting mechanism in the molten iron. *Journal of Materials Research and Technology*. 2023;27:7740–7747. http://dx.doi.org/10.1016/j.jmrt.2023.11.211

24. Kellner H.E.O., Karasev A.V., Memarpour A., Jönsson P.G. Evolution of non-metallic inclusions from FeTi70R alloys during alloying of Fe–40Ni–20Cr steels. *Steel Research International*. 2016;87(11):1461–1468. https://doi.org/10.1002/srin.201500428

25. Wang Y., Karasev A., Park J.H., Jönsson P.G. Interfacial reactions and inclusion formations at an early stage of FeNb alloy additions to molten iron. *ISIJ International*. 2021;61(1):209–218. https://doi.org/10.2355/isijinternational.ISIJINT-2020-353

Information about the Authors / Сведения об авторах

Il'ya N. Kel', *Cand. Sci. (Eng.), Senior Researcher of the Laboratory of Steel and Ferroalloys*, Vatolin Institute of Metallurgy of the Ural Branch of the Russian Academy of Sciences
ORCID: 0000-0001-6411-6932
E-mail: dunnington@mail.ru

Vladimir I. Zhuchkov, *Dr. Sci. (Eng.), Prof., Chief Researcher of the Laboratory of Steel and Ferroalloys*, Vatolin Institute of Metallurgy of the Ural Branch of the Russian Academy of Sciences
ORCID: 0000-0002-8621-7467
E-mail: ntm2000@mail.ru

Oleg V. Zayakin, *Corresponding Member of RAS, Dr. Sci. (Eng.), Chief Researcher, Head of the Laboratory of Steel and Ferroalloys*, Vatolin Institute of Metallurgy of the Ural Branch of the Russian Academy of Sciences
ORCID: 0009-0009-9831-1993
E-mail: zferro@mail.ru

Илья Николаевич Кель, *к.т.н., старший научный сотрудник лаборатории стали и ферросплавов*, Институт металлургии имени академика Н.А. Ватолина Уральского отделения РАН
ORCID: 0000-0001-6411-6932
E-mail: dunnington@mail.ru

Владимир Иванович Жучков, *д.т.н., профессор, главный научный сотрудник лаборатории стали и ферросплавов*, Институт металлургии имени академика Н.А. Ватолина Уральского отделения РАН
ORCID: 0000-0002-8621-7467
E-mail: ntm2000@mail.ru

Олег Вадимович Заякин, *член-корреспондент РАН, д.т.н., главный научный сотрудник, заведующий лабораторией стали и ферросплавов*, Институт металлургии имени академика Н.А. Ватолина Уральского отделения РАН
ORCID: 0009-0009-9831-1993
E-mail: zferro@mail.ru

Contribution of the Authors / Вклад авторов

I. N. Kel' – search and generalization of literary data, writing the text.

V. I. Zhuchkov – discussion and analysis of the obtained data, editing the text.
O. V. Zayakin – analysis of the obtained data, editing the text.

И. Н. Кель – поиск и обобщение литературных данных, написание текста.
В. И. Жучков – обсуждение и анализ полученных данных, редактирование текста.
О. В. Заякин – анализ данных, редактирование текста.

Received 15.05.2025
Revised 16.06.2025
Accepted 17.06.2025

Поступила в редакцию 15.05.2025
После доработки 16.06.2025
Принята к публикации 17.06.2025

MATERIALS SCIENCE / МАТЕРИАЛОВЕДЕНИЕ

UDC 620.186:621.791.722
DOI 10.17073/0368-0797-2025-5-482-487

Original article
Оригинальная статья

Dependence of structure and properties of VT23 alloy on laser deposition parameters

D. E. Safarova, K. O. Bazaleeva, Yu. Yu. Ponkratova, A. V. Alekseev

Peoples' Friendship University of Russia named after Patrice Lumumba (6 Miklukho-Maklaya Str., Moscow 117198, Russian Federation)

safarova_de@pfur.ru

Abstract. The study analyzes the effect of laser power and velocity on the structural phase state and properties of complex-alloyed titanium alloy VT23 (Ti–Al–V–Mo–Cr–Fe) obtained by direct laser deposition. VT23 titanium alloy has a unique combination of strength, corrosion resistance, and biocompatibility, which makes it in demand in the aerospace and medical industries. However, traditional manufacturing methods (casting, stamping) often fail to provide the required accuracy and quality of complex parts. In this work, *X*-ray phase analysis and optical metallography revealed that the deposited samples consist of α- and β-phases (~20 % β-phase) with a typical "basket weave" structure. In macrostructure of the obtained samples, thermal bands and interlayer boundaries were recorded, the formation of which is associated with the peculiarities of crystallization process during direct laser deposition. The results of optical metallography showed that microstructure of the deposited material combines large columnar crystals in the overlap areas of two adjacent layers, as well as small equiaxed grains. Despite this distribution of structural components, the microhardness (~488 $HV_{0.2}$) remains homogeneous throughout the deposited samples in both the laser scanning and sample deposition directions. The results confirm that direct laser deposition can be used to produce VT23 titanium alloy parts with a controlled microstructure. Optimization of the process parameters of direct laser deposition minimizes the probability of defect formation and provides stable mechanical properties, which opens prospects for application of the technology in the production of critical parts.

Keywords: additive technologies, direct laser deposition, titanium alloys, complex alloys, microstructure, phase composition, mechanical properties

Acknowledgements: The work was performed within the framework of the research project No. 202514-0-000 of the Scientific Project Grant Support System of the Peoples' Friendship University of Russia named after Patrice Lumumba.

For citation: Safarova D.E., Bazaleeva K.O., Ponkratova Yu.Yu., Alekseev A.V. Dependence of structure and properties of VT23 alloy on laser deposition parameters. *Izvestiya. Ferrous Metallurgy*. 2025;68(5):482–487. https://doi.org/10.17073/0368-0797-2025-5-482-487

Зависимость структуры и свойств сплава ВТ23 от параметров лазерного выращивания

Д. Э. Сафарова, К. О. Базалеева, Ю. Ю. Понкратова, А. В. Алексеев

Российский университет дружбы народов им. Патриса Лумумбы (Россия, 117198, Москва, ул. Миклухо-Маклая, 6)

safarova_de@pfur.ru

Аннотация. В данном исследовании проведен анализ влияния мощности лазера и скорости его перемещения на структурно-фазовое состояние и свойства сложнолегированного титанового сплава ВТ23, полученного методом прямого лазерного выращивания. Титановый сплав ВТ23 обладает уникальным сочетанием прочности, коррозионной стойкости и биосовместимости, что делает его востребованным в аэрокосмической и медицинской отраслях. Однако традиционные методы производства (литье, штамповка) часто не обеспечивают необходимой точности и качества сложных деталей. В данной работе методами рентгенофазового анализа и оптической металлографии установлено, что выращенные образцы состоят из α- и β-фаз (~20 % β-фазы) с характерной структурой «корзиночного плетения». В макроструктуре полученных образцов зафиксированы полосы термического воздействия и межслоевые границы, образование которых связано с особенностями процесса кристаллизации при прямом лазерном выращивании. Результаты оптической металлографии показали, что микроструктура выращенного материала сочетает в себе крупные столбчатые кристаллы в местах перекрытия двух соседних слоев, а также мелкие равноосные зерна. Несмотря на такое распределение структурных составляющих микротвердость (~488 $HV_{0,2}$) остается однородной по всему объему напечатанных образцов как в направлении сканирования лазера, так и в направлении выращивания образца. Результаты подтверждают, что прямое лазерное выращивание позволяет получать заготовки из титанового сплава ВТ23 с контролируемой микроструктурой. Оптимизация параметров процесса прямого лазерного выращивания минимизирует вероятность образования дефектов и обеспечивает стабильные механические свойства, что открывает перспективы для применения технологии в производстве ответственных деталей.

Ключевые слова: аддитивные технологии, прямое лазерное выращивание, титановые сплавы, сложные сплавы, микроструктура, фазовый состав, механические свойства

Благодарности: Работа выполнена в рамках проекта НИР № 202514-0-000 Системы грантовой поддержки научных проектов РУДН.

Для цитирования: Сафарова Д.Э., Базалеева К.О., Понкратова Ю.Ю., Алексеев А.В. Зависимость структуры и свойств сплава ВТ23 от параметров лазерного выращивания. *Известия вузов. Черная металлургия*. 2025;68(5):482–487.
https://doi.org/10.17073/0368-0797-2025-5-482-487

Introduction

Titanium alloys are widely known for their exceptional combination of high strength-to-weight ratio, excellent corrosion resistance, and biocompatibility, which makes them indispensable in aerospace, biomedical, and high-performance engineering applications [1 – 6]. Among these alloys, VT23 (Ti–Al–V–Mo–Cr–Fe) is particularly valued for its superior thermal stability, creep resistance, and weldability – properties that are critically important for aerospace components such as airframe structures, engine parts, and rocket housings [2 – 3]. Moreover, its biocompatibility and mechanical compatibility with human bone have promoted its use in medical implants, including orthopedic and dental prostheses [4 – 6]. However, traditional manufacturing methods such as casting and stamping often face challenges associated with the high reactivity, low thermal conductivity, and significant deformation resistance of titanium alloys, which complicate the production of complex geometries free of defects [4].

Additive manufacturing (AM) has emerged as a transformative approach to overcoming these limitations, with direct laser deposition (DLD) – one of the most promising directed energy deposition (DED) technologies – attracting particular attention. DLD offers unprecedented advantages such as near-net-shape fabrication, minimal material waste, and the ability to produce complex geometries that are difficult or even impossible to achieve by conventional means. Unlike powder bed fusion technologies such as selective laser melting (SLM), DLD enables the fabrication of large-scale parts, in-situ alloying, and hybrid manufacturing (e.g., repair or coating of existing components). However, the unique thermal cycles and rapid solidification inherent to DLD can lead to microstructural heterogeneity, residual stresses, and anisotropic mechanical properties that must be carefully managed to ensure optimal performance [4 – 10].

A critical issue in DLD of titanium alloys is the formation of large columnar grains and strong crystallographic textures along the build direction, which can adversely affect ductility and fatigue strength [4 – 15]. Furthermore, improper selection of process parameters may result in process-induced defects such as porosity, unmelted particles, and thermal cracking. Recent studies on similar titanium alloys (e.g., Ti–6Al–4V and TA15) produced by DLD have shown that laser power, scanning velocity, hatch spacing, and layer thickness have a pronounce [4 – 7; 9 – 10]. For instance, excessive energy input may cause porosity formation, while insufficient energy leads to lack of fusion. In addition, high cooling rates typical of DLD often promote the formation of acicular α′-martensite, which increases strength but reduces ductility compared with conventional α + β microstructures [4 – 7].

Considering these issues, the main objective of the present study is to systematically investigate the effect of direct laser deposition process parameters – including laser power, scanning velocity, and hatch spacing – on the microstructural evolution, phase composition, and mechanical properties of the VT23 alloy. By correlating the process–structure–property relationship, this study aims to establish optimized DLD parameters that minimize defects while achieving a balanced combination of strength and ductility.

Materials and methods

In this work, VT23 titanium alloy samples were fabricated by direct laser deposition (DLD). The chemical composition of the alloy is presented in the Table.

Wall samples measuring 50×90×90 mm were fabricated by DLD method on a VT1-0 titanium alloy substrate. Deposition parameters were as follows: laser power of 1000 and 1100 W; scanning velocity of 1 m/min; and overlap between adjacent tracks equal to 0.7 of the track width.

Favorable process parameters were first screened on single tracks and then on monolayers.

The quality of a single track was evaluated according to the following criteria:

– track shape factor f ($f = h/L$, where h is the bead height above the substrate; L is the single track width, Fig. 1, *a*)) should be within the range [0.20; 0.33];

Chemical composition of VT23 powder

Химический состав порошка ВТ23

Mass fraction, wt. %									
Ti	Al	V	Mo	Cr	Fe	O	H	N	C
Base	4.8	4.5	2.6	1.2	0.4	0.12	0.004	0.018	0.03

– penetration coefficient d should be within the range [0.1; 0.4]

$$d = \frac{S_p}{S_p + S_h},$$

where S_p and S_h are the bead areas below and above the substrate surface, respectively;

– track width L should be within 1.7 – 3.0 mm for a laser spot diameter of 1.8 mm;

– base angle of the bead θ should be less than 90° [11 – 17].

Another important quality criterion was the absence of cracks.

The parameters of the monolayers had to satisfy the following conditions:

– height variation of the monolayer (h_2/h_1) did not exceed 30 % of its maximum height;

– penetration depth was less than two-thirds of the layer height (Fig. 1, *b*) [12; 17].

To study the structure, two sections were examined – along the deposition direction (*XZ*), and – along the laser scanning direction (*XY*) (Fig. 2).

Metallographic studies were performed on microsections prepared using standard procedures: grinding on abrasive paper and polishing with diamond suspensions (down to 1 μm). Etching to reveal structural features was carried out in a solution containing 3 mL HF, 15 mL HNO_3, and 82 mL H_2O.

Structural examinations were conducted using an Olympus GX-51 inverted optical microscope at magnifications ranging from 50 to 500×.

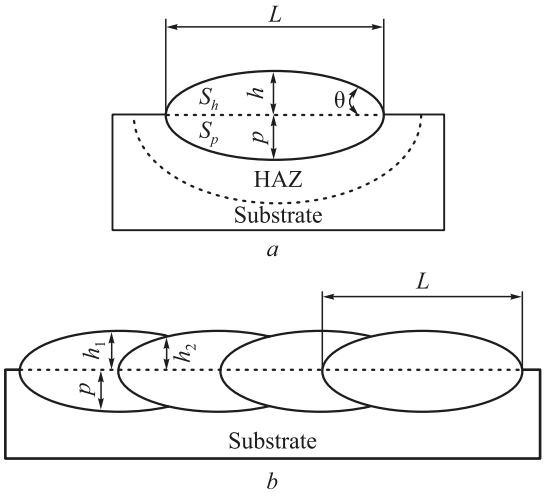

Fig. 1. Scheme of shapes:
a – single track; *b* – monolayer

Рис. 1. Схема форм:
a – единичный трек; *b* – монослой

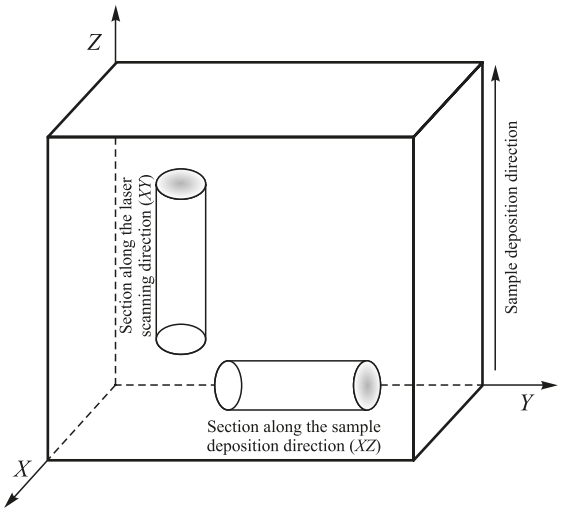

Fig. 2. Sample cutting scheme

Рис. 2. Схема вырезки образцов

For the analysis of the phase composition, samples were prepared for *X*-ray diffraction analysis. The preparation included grinding and electrolytic polishing using a Struers LectroPol-5 unit in A2 electrolyte (78 mL $HClO_4$, 90 mL distilled water, 730 mL C_2H_6O, 100 mL $C_6H_{14}O_2$) for 15 min at 10 V.

X-ray diffraction patterns were obtained on a Bruker D8 Advance diffractometer with Bragg–Brentano focusing geometry, using CuK_α radiation over a 2θ range of 30–100° with a step size Δ2θ = 0.07° and an exposure time of 2 s per point. The tube voltage and current were 40 kV and 35 mA, respectively. A semiconductor multichannel detector and the following slit system were used: a 2 mm divergence slit on the tube, and Soller slits (2.5 mm plate spacing) on both the tube and detector sides. During data acquisition, the samples were rotated at 60 rpm. The diffraction spectra were processed using Diffrac.Eva and Diffrac.Topas software packages.

Microhardness of the material was measured using a Pruftechnik KB50 SR microhardness tester by the recovered-imprint method under a 200 g (1.9 N) load.

Results and discussion

X-ray diffraction analysis revealed that the deposited material consists of the characteristic α- and β-phases, with HCP and BCC lattices, respectively (Fig. 3). Since the diffraction peaks of α′-martensite coincide with those of the α-phase, its presence in the structure cannot be unambiguously confirmed from the diffraction pattern. The amount of β-phase was found to be approximately 20 %.

Optical metallography of the bulk samples revealed no macroscopic defects. After direct laser deposition, the α-phase appears as regions of basket-weave mor-

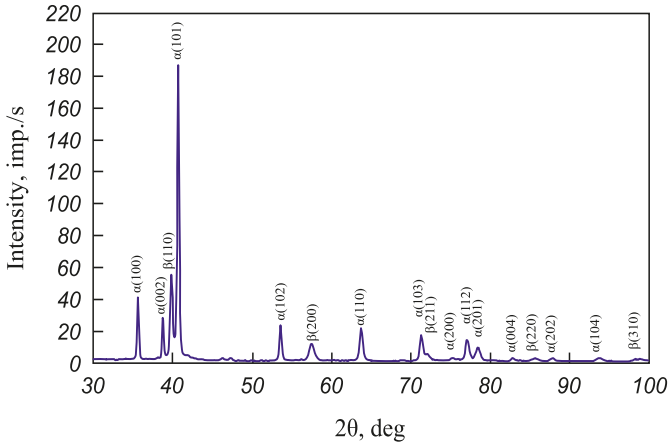

Fig. 3. *X*-ray pattern of VT23 alloy obtained by direct laser deposition

Рис. 3. Дифрактограмма сплава ВТ23, полученного прямым лазерным выращиванием

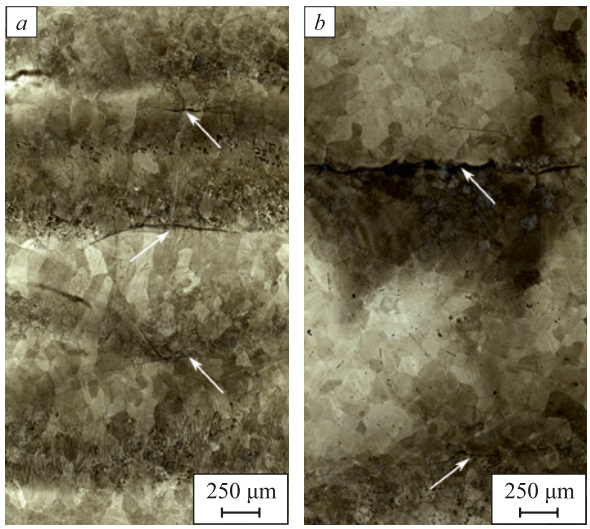

Fig. 4. Microstructure of VT23 alloy after direct laser deposition: *a* – laser scanning direction; *b* – sample deposition direction

Рис. 4. Микроструктура сплава ВТ23 после прямого лазерного выращивания: *a* – направление сканирования лазера; *b* – направление роста образца

phology and as a network along the boundaries of primary β-grains – features typical of this alloy both in the quenched state and after deposition [1 – 3; 8; 18 – 20]. In the scanning plane, large (~100 μm) equiaxed regions of primary β were observed.

Fig. 4 shows two types of bands distinguished by their etching contrast. According to the literature, the wide dark regions correspond to thermal-affected bands, while the narrow lines indicated by arrows are interlayer bands [18 – 20]. The thermally affected bands form in overlap zones of adjacent layers, where repeated thermal exposure during successive passes induces reheating and recrystallization, producing the observed etching contrast. The interlayer bands are regularly spaced and trace the boundaries of individual melt pools.

As noted in [19], the formation of interlayer bands depends on the degree of alloying and the rate of diffusion processes in titanium alloys.

The grain morphology of the obtained material also deserves attention. During deposition, non-uniform nucleation occurs on partially melted powder particles within the melt pool, resulting in the formation of fine equiaxed grains. Subsequently, epitaxial growth develops: grains grow from the bottom of the melt pool, inheriting the structure of the underlying layer, which produces large columnar grains. The final grain morphology is therefore determined by the competition between these two mechanisms [20].

Structural examinations revealed heterogeneity in the size of structural constituents, as the material consists of a combination of large columnar and small equiaxed grains. This heterogeneity might suggest a non-uniform distribution of microhardness throughout the volume. However, the measurements showed that the microhardness of the deposited material is homogeneous throughout the deposited samples.

Additionally, the microhardness of the VT23 titanium alloy produced by direct laser deposition varied slightly with build direction and averaged 485 ± 5 $HV_{0.2}$ along the laser scanning direction (*XY*) and 490 ± 20 $HV_{0.2}$ along the sample deposition direction (*XZ*).

Conclusions

The direct laser deposition (DLD) technology enables the fabrication of defect-free VT23 titanium alloy samples.

X-ray diffraction analysis confirmed that the deposited alloy consists of α- and β-phases; however, differentiation between the α- and α′-phases is difficult due to the similarity of their crystal lattices.

The structure of the obtained alloy exhibits regions of different etching contrast, which most likely indicates recrystallization during deposition. The microstructure is represented by a basket-weave arrangement composed of randomly oriented α-phase plates.

The average microhardness of the material does not vary from the substrate to the top surface and remains at approximately 488 ± 10 $HV_{0.2}$ both along the laser scanning direction and along the sample deposition direction.

References / Список литературы

1. Belov S.P., Brun M.Ya., Glazunov S.G., Kolachev B.A. Metallurgy of Titanium and Its Alloys. Moscow: Metallurgiya; 1992:352 p. (In Russ.).

Белов С.П., Брун М.Я., Глазунов С.Г., Колачев Б.А. Металловедение титана и его сплавов. Москва: Металлургия; 1992:352.

2. Khorev A.I. Complex Alloying and Thermomechanical Processing of Titanium Alloys. Moscow: Mashinostroenie; 1979:228. (In Russ.).

Хорев А.И. Комплексное легирование и термомеханическая обработка титановых сплавов. Москва: Машиностроение; 1979:228.

3. Khorev A.I. Theory of alloying and heat treatment of high and ultra-high strength (α+β)-titanium alloys. *Vestnik mashinostroeniya*. 2010;(7):32–39. (In Russ.).

Хорев А.И. Теория легирования и термической обработки конструкционных (α+β)-титановых сплавов высокой и сверхвысокой прочности. *Вестник машиностроения*. 2010;(7):32–39.

4. Jiang J., Liang C., Chen Y., Wang Y., Cui H., Xu J., Zhang D.Z. The influence of process parameters on the density, microstructure, and mechanical properties of TA15 titanium alloy fabricated by selective laser melting. *Metals*. 2025;15(3):233. https://doi.org/10.3390/met15030233

5. Fang Y., Dai G., Guo Y., Sun Z., Liu H., Yuan Q. Effect of laser oscillation on the microstructure and mechanical properties of laser melting deposition titanium alloys. *Acta Metallurgica Sinica*. 2022;59(1):136–146. https://doi.org/10.11900/0412.1961.2021.00600

6. Liu Z., He B., Lyu T., Zou Y. A review on additive manufacturing of titanium alloys for aerospace applications: Directed energy deposition and beyond Ti-6Al-4V. *JOM*. 2021;73:1804–1818. https://doi.org/10.1007/s11837-021-04670-6

7. Zhu Y., Tian X., Li J., Wang H. Microstructure evolution and layer bands of laser melting deposition Ti–6.5 Al–3.5 Mo–1.5 Zr–0.3 Si titanium alloy. *Journal of Alloys and Compounds*. 2014;616:468–474. https://doi.org/10.1016/j.jallcom.2014.07.161

8. Gladkovskii S.V., Veselova V.E., Patselov A.M., Khotinov V.A. The influence of deformation stability of β-phase in titanium alloy BT23 on the phase composition, microstructure, and mechanical properties after tension and impact test. *Vestnik Permskogo natsional'nogo issledovatel'skogo politekhnicheskogo universiteta. Mashinostroenie, materialovedenie*. 2019;21(4):26–33. (In Russ.). https://doi.org/10.15593/2224-9877/2019.4.03

Гладковский С.В., Веселова В.Е., Пацелов А.М., Хотинов В.А. Влияние деформационной стабильности β-фазы в титановом сплаве ВТ23 на фазовый состав, структуру и механические свойства при растяжении и ударном изгибе. *Вестник Пермского национального исследовательского политехнического университета. Машиностроение, материаловедение*. 2019;21(4):26–33. https://doi.org/10.15593/2224-9877/2019.4.03

9. Dang L., He X., Tang D., Wu B., Li Y. A fatigue life posterior analysis approach for laser-directed energy deposition Ti-6Al-4V alloy based on pore-induced failures by kernel ridge. *Engineering Fracture Mechanics*. 2023;289:109433. https://doi.org/10.1016/j.engfracmech.2023.109433

10. Ravi G.A., Qiu C., Attallah M.M. Microstructural control in a Ti-based alloy by changing laser processing mode and power during direct laser deposition. *Materials Letters*. 2016;179:104–108. https://doi.org/10.1016/j.matlet.2016.05.038

11. OST 1-90013–81. Industry Standard. Titanium Alloys. Grades. Moscow: VIAM; 1981:7. (In Russ.).

ОСТ 1-90013–81. Отраслевой стандарт. Титановые сплавы. Марки. Срок введения с 01.07.1981. Москва: ВИАМ; 1981:7.

12. Grigor'yants A.G., Misyurov A.I., Tret'yakov R.S. Analysis of the influence of coaxial laser cladding parameters on bead formation. *Tekhnologiya mashinostroeniya*. 2011;(11):19–21. (In Russ.).

Григорьянц А.Г., Мисюров А.И., Третьяков Р.С. Анализ влияния параметров коаксиальной лазерной наплавки на формирование валиков. *Технология машиностроения*. 2011;(11):19–21.

13. Gibson I., Rosen D., Stucker B., Khorasani M. Additive Manufacturing Technologies. Cham, Switzerland: Springer; 2021;675. https://doi.org/10.1007/978-3-030-56127-7

14. Lewandowski J.J., Seifi M. Metal additive manufacturing: A review of mechanical properties. *Annual Review of Materials Research*. 2016;46:151–186. https://doi.org/10.1146/annurev-matsci-070115-032024

15. De Oliveira U., Ocelik V., De Hosson J.T.M. Analysis of coaxial laser cladding processing conditions. *Surface and Coatings Technology*. 2005;197(2–3):127–136. https://doi.org/10.1016/j.surfcoat.2004.06.029

16. Harooni A., Nasiri A.M., Gerlich A.P., Khajepour A., Khalifa A., King J.M. Processing window development for laser cladding of zirconium on zirconium alloy. *Journal of Materials Processing Technology*. 2016;230:263–271. https://doi.org/10.1016/j.jmatprotec.2015.11.028

17. Bazaleeva K.O., Tsvetkova E.V., Safarova D.E., Ponkratova Yu.Yu., Lugovoi M.E., Alekseev A.V., Baskov F.A. The influence of technological parameters of the laser engineered net shaping process on the quality of the formed object from titanium alloy VT23. *Obrabotka metallov: tekhnologiya, oborudovanie, instrumenty*. 2024;26(2):186–198. (In Russ.). https://doi.org/10.17212/1994-6309-2024-26.2-186-198

Базалеева К.О., Цветкова Е.В., Сафарова Д.Э., Понкратова Ю.Ю., Луговой М.Е., Алексеев А.В., Басков Ф.А. Влияние технологических параметров процесса прямого лазерного выращивания на качество формируемого объекта из титанового сплава ВТ23. *Обработка металлов: технология, оборудование, инструменты*. 2024;26(2):186–198. https://doi.org/10.17212/1994-6309-2024-26.2-186-198

18. Shvetsov O.V., Kondrat'ev S.Yu. Effect of quenching and aging modes on the performance properties of the VT23 alloy. *Global'naya energiya*. 2018;24(2):119–133. (In Russ.). https://doi.org/10.18721/JEST.240210

Швецов О.В., Кондратьев С.Ю. Влияние режимов закалки и старения на эксплуатационные свойства сплава ВТ23. *Глобальная энергия*. 2018;24(2):119–133. https://doi.org/10.18721/JEST.240210

19. He B., Li J., Cheng X., Wang H.M. Brittle fracture behavior of a laser additive manufactured near-β titanium alloy after low temperature aging. *Materials Science and Engineering: A*. 2017;699:229–238. https://doi.org/10.1016/j.msea.2017.05.050

20. Wang T., Zhu Y.Y., Zhang S.Q., Tang H.B., Wang H.M. Grain morphology evolution behavior of titanium alloy components during laser melting deposition additive manufacturing. *Journal of Alloys and Compounds*. 2015;632:505–513. https://doi.org/10.1016/j.jallcom.2015.01.256

Information about the Authors / Сведения об авторах

Daria E. Safarova, *Junior Researcher, Postgraduate of the Chair of Engineering Technology*, Peoples' Friendship University of Russia named after Patrice Lumumba
ORCID: 0000-0002-2811-8292
E-mail: safarova_de@pfur.ru

Kseniya O. Bazaleeva, *Cand. Sci. (Phys.-Math.), Deputy Director of Additive and Edge Technologies Centre*, Peoples' Friendship University of Russia named after Patrice Lumumba
ORCID: 0000-0002-6205-3154
E-mail: bazaleeva-ko@rudn.ru

Yuliya Yu. Ponkratova, *Research Associate*, Peoples' Friendship University of Russia named after Patrice Lumumba
ORCID: 0009-0000-1094-3529
E-mail: ponkratova_yuyu@rudn.ru

Andrei V. Alekseev, *Engineer-Technologist of Additive and Edge Technologies Centre,* Peoples' Friendship University of Russia named after Patrice Lumumba
ORCID: 0009-0008-7394-6370
E-mail: alexeev-anvs@rudn.ru

Дарья Эйнуллаевна Сафарова, *младший научный сотрудник, аспирант кафедры машиностроительных технологий*, Российский университет дружбы народов им. Патриса Лумумбы
ORCID: 0000-0002-2811-8292
E-mail: safarova_de@pfur.ru

Ксения Олеговна Базалеева, *к.ф.-м.н., заместитель директора центра аддитивных и порубежных технологий*, Российский университет дружбы народов им. Патриса Лумумбы
ORCID: 0000-0002-6205-3154
E-mail: bazaleeva-ko@rudn.ru

Юлия Юрьевна Понкратова, *научный сотрудник*, Российский университет дружбы народов им. Патриса Лумумбы
ORCID: 0009-0000-1094-3529
E-mail: ponkratova_yuyu@rudn.ru

Андрей Васильевич Алексеев, *инженер-технолог центра аддитивных и порубежных технологий*, Российский университет дружбы народов им. Патриса Лумумбы
ORCID: 0009-0008-7394-6370
E-mail: alexeev-anvs@rudn.ru

Contribution of the Authors / Вклад авторов

D. E. Safarova – problem statement, analysis of research results, formulation of conclusions.
K. O. Bazaleeva – study of phase composition, analysis of research results.
Yu. Yu. Ponkratova – complex metallographic study.

A. V. Alekseev – formation of research samples.

Д. Э. Сафарова – постановка задачи, анализ результатов исследований, формулировка выводов.
К. О. Базалеева – исследование фазового состава, анализ результатов исследований.
Ю. Ю. Понкратова – комплексное металлографическое исследование.
А. В. Алексеев – формирование исследовательских образцов.

Received 11.04.2025
Revised 27.04.2025
Accepted 28.08.2025

Поступила в редакцию 11.04.2025
После доработки 27.04.2025
Принята к публикации 28.08.2025

ФИЗИКО-ХИМИЧЕСКИЕ ОСНОВЫ МЕТАЛЛУРГИЧЕСКИХ ПРОЦЕССОВ / **PHYSICO-CHEMICAL BASICS OF METALLURGICAL PROCESSES**

УДК 669.187.28.539.55
DOI 10.17073/0368-0797-2025-5-488-494

Оригинальная статья
Original article

Features of application of boron-containing slags in stainless steel smelting

A. A. Babenko, R. R. Shartdinov, D. A. Lobanov,
A. N. Smetannikov, A. G. Upolovnikova, V. S. Gulyakov

Vatolin Institute of Metallurgy of the Ural Branch of the Russian Academy of Sciences (101 Amundsena Str., Yekaterinburg 620016, Russian Federation)

rr.shartdinov@gmail.com

Abstract. Traditionally, for stainless steel smelting in the process of argon-oxygen decarburization, fluorspar is used to liquefy the slag and ensure the normal course of the refining and reduction of chromium oxide. Fluospar is characterized by high volatility at high temperatures of the steel-making process, while the resulting compounds are toxic and hazardous to the environment. For this reason, the paper considers the replacement of fluorspar with boron oxide, which is also capable of forming low-melting eutectics with the main components of slag, at the final stage of steel processing during the argon-oxygen decarburization process – during the desulfurization period. It was found that, despite an increase in the degree of slag polymerization as a result of the introduction of boron oxide to 6 %, due to its ability to form low-melting compounds, an increase in its content has a beneficial effect on the fluidity of slags of the studied $CaO–SiO_2–B_2O_3$–2 % Cr_2O_3–3 % Al_2O_3–8 % MgO system at a basicity of CaO/SiO_2 of 1.0 and 2.5. The content of 6 % B_2O_3 in slag with a high basicity of 2.5 makes it possible to achieve viscosity values of 0.3 Pa·s, which are favorable for sulfur removal. In this case, the equilibrium sulfur content in the metal can reach 0.003 % according to the thermodynamic modeling. As a result of the experimental studies, the minimum sulfur content was 0.006 %, which is close to the equilibrium concentration. During the treatment of steel samples with slags, direct steel microalloying with boron in the amount of 0.002 – 0.003 % occurred. A small amount of boron transferred to steel during direct microalloying, according to literary data, has a beneficial effect on the ductility and corrosion resistance of the metal product.

Keywords: argon-oxygen decarburization, desulfurization period, viscosity, crystallization onset temperature, slag, structure, stainless steel

Acknowledgements: The work was carried out according to the state assignment for Vatolin Institute of Metallurgy, UB RAS using the equipment of the Collaborative Usage Center “Composition of Compounds” of the Institute of High Temperature Electrochemistry of UB RAS.

For citation: Babenko A.A., Shartdinov R.R., Lobanov D.A., Smetannikov A.N., Upolovnikova A.G., Gulyakov V.S. Features of application of boron-containing slags in stainless steel smelting. *Izvestiya. Ferrous Metallurgy*. 2025;68(5):488–494. https://doi.org/10.17073/0368-0797-2025-5-488-494

Особенности применения борсодержащих шлаков при выплавке нержавеющей стали

А. А. Бабенко, Р. Р. Шартдинов, Д. А. Лобанов,
А. Н. Сметанников, А. Г. Уполовникова, В. С. Гуляков

Институт металлургии имени академика Н.А. Ватолина Уральского отделения РАН (Россия, 620016, Екатеринбург, ул. Амундсена, 101)

rr.shartdinov@gmail.com

Аннотация. Традиционно для выплавки нержавеющей стали в процессе аргонокислородного рафинирования для разжижения шлака и обеспечения нормального течения процессов рафинирования и восстановления оксида хрома применяется плавиковый шпат, отличающийся высокой летучестью при высоких температурах сталеплавильного передела. Образующиеся при этом соединения ядовиты и опасны для окружающей среды. По этой причине в работе рассмотрена замена плавикового шпата оксидом бора, который также способен образовывать легкоплавкие эвтектики с основными компонентами шлака в момент заключительного этапа обработки стали в ходе процесса аргонокислородного рафинирования – в период десульфурации. Установлено, что несмотря на рост степени полимери-

зации шлака в результате ввода до 6 % B_2O_3, за счет способности оксида бора образовывать легкоплавкие соединения рост его содержания благоприятно сказывается на жидкоподвижности шлаков изучаемой системы $CaO–SiO_2–B_2O_3$–2 % Cr_2O_3–3 % Al_2O_3–8 % MgO при основности (CaO/SiO_2) 1,0 и 2,5. Содержание 6 % B_2O_3 в шлаке высокой основности 2,5 позволяет достичь благоприятных для удаления серы значений вязкости 0,3 Па·с. В данном случае равновесное содержание серы в металле может достигать 0,003 % согласно термодинамическому моделированию. В результате экспериментальных исследований минимальное содержание серы составило 0,006 %, что приближается к равновесной концентрации. В ходе обработки образцов стали шлаками происходило прямое микролегирование стали бором в количестве 0,002 – 0,003 %. Небольшое количество бора, перешедшего в сталь в процессе прямого микролегирования, согласно литературным данным благоприятно сказывается на пластичности и коррозионной стойкости металлопродукта.

Ключевые слова: аргонокислородное рафинирование, период десульфурации, вязкость, температура начала кристаллизации, структура, шлак, нержавеющая сталь

Благодарности: Работа выполнена по Государственному заданию ИМЕТ УрО РАН с использованием оборудования ЦКП «Состав вещества» ИВТЭ УрО РАН.

Для цитирования: Бабенко А.А., Шартдинов Р.Р., Лобанов Д.А., Сметанников А.Н., Уполовникова А.Г., Гуляков В.С. Особенности применения борсодержащих шлаков при выплавке нержавеющей стали. *Известия вузов. Черная металлургия*. 2025;68(5):488–494. https://doi.org/10.17073/0368-0797-2025-5-488-494

Introduction

At present, the argon–oxygen decarburization (AOD) process [1; 2] is widely used in the smelting of low-carbon stainless steels. The process proceeds in two stages: the oxidation and reduction periods. During the first stage, carbon is oxidized; during the second, chromium, which has been oxidized in the first period, is reduced. When deep desulfurization is required at the end of the reduction period, most of the existing slag is skimmed, and a new highly basic slag with a low chromium oxide content is introduced [1]. The desulfurization reaction is limited by mass transfer in the slag; therefore, the slag is traditionally liquefied with environmentally hazardous fluorspar [1; 3; 4]. As a replacement for fluorspar, boron oxide can be used, as it is also capable of forming low-melting eutectics with calcium oxide [5 – 7].

In this work, four slags of the $CaO–SiO_2–B_2O_3$–2 % Cr_2O_3–3 % Al_2O_3–8 % MgO system, close in composition to slags of the desulfurization period, were prepared. Experimental studies of the viscosity, crystallization onset temperature, and structure of these slags were performed, as well as thermodynamic modeling and experimental investigation of the desulfurization of metal under slags of this oxide system.

Materials and methods

The physicochemical characteristics of four slags were investigated in this work. Their compositions are presented in Table 1. The basicity of the slags (B_{slag} = CaO/SiO_2) was 1.0 and 2.5, and the boron oxide content was 0 and 6 wt. % B_2O_3.

Synthetic slags were melted in molybdenum crucibles from analytically pure grade oxides that had been pre-calcined for 2 – 3 h at 800 °C (B_2O_3 at 105 °C) and thoroughly mixed. The obtained homogenized slag samples were crushed to produce powder.

The viscosity of the slags was measured by the electro-vibrational viscometry method [8] in a resistance furnace during gradual cooling of the melt contained in molybdenum crucibles under an argon atmosphere. Temperature was monitored with a tungsten–rhenium thermocouple W–5%Re/W–20%Re (WR5/20). The crystallization onset temperature (hereinafter, the crystallization temperature, was determined from the break (kink) in the viscosity polytherm plotted as ln η vs 1/*T* [9].

Thermodynamic modeling of the phase composition and equilibrium sulfur content was performed using the HSC Chemistry 6.12 software package [10]. The chemical compositions of the four slag samples are presented in Table 1. The metal contained (wt. %): 16.5 Cr, 0.02 C, 0.6 Si, 0.03 S, 1.6 Mn, 8.4 Ni, and 0.006 Al. The results of the calculated equilibrium sulfur concentration in the metal ($[S]_{calc}$) at 1600 °C are summarized in Table 1. The phases were conventionally grouped by melting point into low-, medium-, and high-temperature categories, as presented in Table 2.

Experimentally, the desulfurization process and the reduction behavior of boron were studied by holding steel under pre-melted slags *1 – 4* (Table 1) in magnesia crucibles for 10 – 60 min at 1600 °C in an Ar atmosphere. Each experimental charge (sample) consisted of 80 g of metal and 16 g of slag.

Table 1. **Composition of experimental slags and results of modeling metal desulfurization with them at 1600 °C**

Таблица 1. **Состав экспериментальных шлаков и результаты моделирования десульфурации металла под ними при 1600 °C**

Slag No.	Slag composition, wt. %						B_{slag}
	CaO	SiO_2	Al_2O_3	Cr_2O_3	MgO	B_2O_3	
1	43.50	43.50	3.00	2.00	8.00	0	1.0
2	62.14	24.86	3.00	2.00	8.00	0	2.5
3	57.86	23.14	3.00	2.00	8.00	6.00	2.5
4	40.50	40.50	3.00	2.00	8.00	6.00	1.0

Table 2. **Phase composition of the studied slags at 1600 °C**

Таблица 2. **Фазовый состав исследуемых шлаков при 1600 °C**

Phases	Melting point, °C	Slag No.			
		1	*2*	*3*	*4*
Low-temperature phases, %					
CB	1130	0	0	0.1	3.7
2CB	1280	0	0	5.2	8.4
CM2S	1391	8.4	0.01	0.1	10.9
Total		8.4	0.01	5.4	23.0
Medium-temperature phases, %					
2CM2S	1454	5.1	0.2	0.6	4.2
3CB	1460	0	0	12.6	0.9
3C2S	1460	20.8	5.5	8.1	11.5
CMS	1503	8.6	4.0	6.8	7.9
CS	1540	21.5	2.2	3.6	20.9
CA2S	1553	2.6	0.0001	0.002	4.1
MS	1557	3.6	0.1	0.2	5.1
3CM2S	1575	3.7	4.5	6.8	1.9
2CAS	1593	1.4	0.9	1.6	1.0
CA	1600	0.5	3.6	3.1	0.3
Total		67.8	21.0	43.4	57.8
High-temperature phases, %					
S	1710	3.6	0.01	0.04	5.5
A	2040	0.8	0.2	0.4	1.0
2CS	2130	15.6	56.3	39.8	9.6
CCr	2170	0.5	0.003	0.01	0.6
Cr	2435	0.5	0.0001	0.001	0.9
C	2570	0.3	15.5	5.3	0.2
M	2852	1.0	6.4	5.3	1.1
Total		22.3	78.4	50.8	18.9

N o t e . CB – $CaO{\cdot}B_2O_3$; 2CB – $2CaO{\cdot}B_2O_3$; 3CB – $3CaO{\cdot}B_2O_3$; CS – $CaO{\cdot}SiO_2$; 2CS – $2CaO{\cdot}SiO_2$; 3C2S – $3CaO{\cdot}2SiO_2$; C – CaO; CMS – $CaO{\cdot}MgO{\cdot}SiO_2$; M – MgO; A – Al_2O_3; CA – $CaO{\cdot}Al_2O_3$; S – SiO_2; MS – $MgO{\cdot}SiO_2$; CM2S – $CaO{\cdot}MgO{\cdot}2SiO_2$

The structure of the experimental slag samples was examined by Raman spectroscopy using a U 1000 Raman micro-spectrometer with an excitation laser wavelength of 532 nm.

Results and discussion

The results of viscosity measurements for the four studied slags, presented in Fig. 1, confirmed the high efficiency of boron oxide as a flux. The addition of 6 wt. % B_2O_3 markedly reduced both the viscosity and the crystallization onset temperature (t_{cr}) at low and high basicity.

To clarify the mechanism of boron oxide action and the processes occurring in the slag upon its addition, the phase composition and structural features of the slags were examined using thermodynamic modeling and Raman spectroscopy.

The results showed that the presence of boron oxide promotes the formation of a considerable amount of low-melting compounds, primarily various calcium borates, accompanied by a pronounced decrease in the content of free CaO (Table 2).

To assess the influence of boron oxide on slag structure, Raman spectra were recorded for the slags, and their deconvolution was performed using the Gaussian method [11] in the silicate range of 800 – 1200 cm^{-1}. This approach made it possible to express the degree of slag polymerization through the average number of bridging oxygen (BO) (Fig. 2, Table 3):

$$BO = 0 \cdot Q^0_{Si} + 1 \cdot Q^1_{Si} + 2 \cdot Q^2_{Si} + 3 \cdot Q^3_{Si} + 4 \cdot Q^4_{Si},$$

where Q^n_{Si} denotes $[SiO_4]$ tetrahedra with n bridging oxygen (O^0).

In Fig. 2, peaks corresponding to $[SiO_4]$ tetrahedra with up to three (O^0) appear in the wavenumber range 850 – 1060 cm^{-1} [12; 13], peaks of $[CrO_4]$ groups occur at 873 cm^{-1} [14], and those of Q^3_{Al} ($[AlO_4]$) at 780 cm^{-1} [15]. Three-dimensional $[BO_4]$ tetrahedra are located in the range of 900 – 920 cm^{-1} [16; 17] and overlap with the $[SiO_4]$ peaks.

When boron oxide is introduced into low-basicity slags (B = 1.0), the degree of polymerization increases from 0.73 to 1.28 due to an increase in the fractions Q^1_{Si}, Q^2_{Si} and species and the formation of Q^3_{Si} species at the expense of Q^0_{Si} species (Table 3). Boron oxide acts as a network former and complicates the slag structure. Additional polymerization is also indicated by the appea-

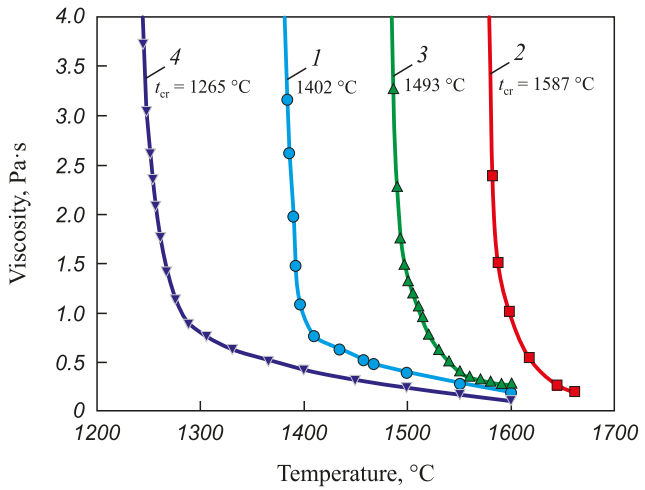

Fig. 1. Viscosity-temperature dependence of slags *1 – 4*

Рис. 1. Температурная зависимость вязкости шлаков *1 – 4*

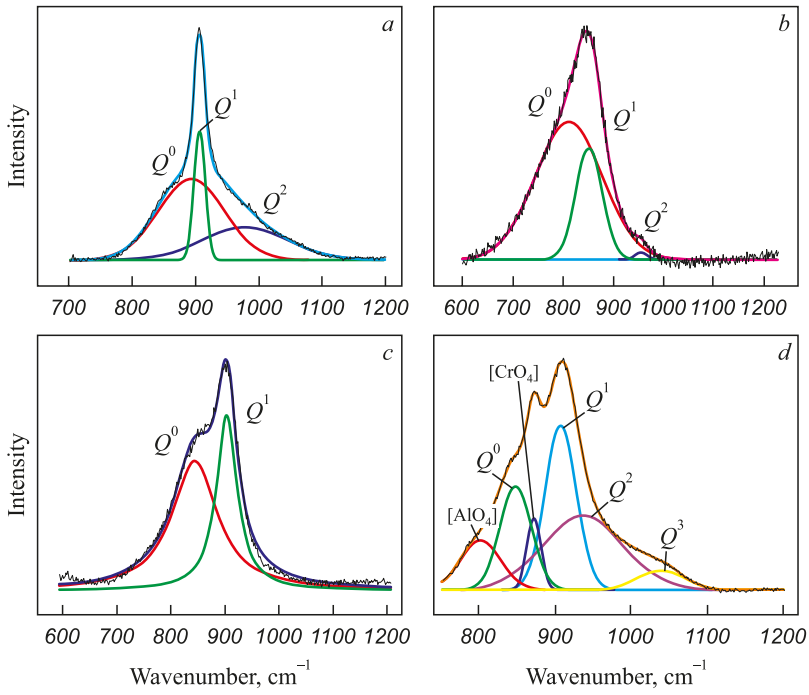

Fig. 2. Deconvoluted spectra of slag samples *1 – 4*

Рис. 2. Деконволированные спектры образцов шлака *1 – 4*

rance of [CrO_4] and Q^3_{Al} peaks in spectrum *4*, which are absent in spectrum *1*.

An increase in basicity to 2.5 – and, consequently, in the CaO content of the slag, which acts as a donor of free oxygen ions (O^{2-}), inevitably breaks down the previously formed silicate structures, so the degree of polymerization (BO) decreases markedly to 0.26 (slag *2*) and 0.38 (slag *3*) for 0 and 6 wt. % B_2O_3, respectively. Under high basicity and an increased concentration of (O^{2-}) boron oxide polymerizes the slag to a much lesser extent, primarily through an increase in the fraction of Q^1_{Si} species.

The high basicity of slags *2* and *3* (B_{slag} = 2.5) also leads to higher viscosity, despite their simpler structure compared to slags of lower basicity (BO decreases from 0.73 to 0.26 and from 1.28 to 0.38 for slags without and with 6 wt. % B_2O_3, respectively). The viscosity of slag *3* (with 6 wt. % B_2O_3), although having a relatively simple structure (BO = 0.38), sharply increases to 1.3 Pa·s at 1500 °C, together with its crystallization onset temperature of 1493 °C. This can be explained by the much smaller fraction of low-melting phases (5.4 %) and the increased proportion of high-melting ones (up to 50.8 %), represented mainly by $2CaO·SiO_2$ with a melting point of 2130 °C. The highly basic slag *2*, which does not contain boron oxide, is the most viscous and refractory in the system. Its crystallization onset temperature is 1587 °C, and its viscosity, despite a relatively simple structure (BO = 0.26), reaches 0.75 Pa·s at 1600 °C. This behavior is associated with the highest content of high-melting compounds (78.4 %), mainly $2CaO·SiO_2$ and free CaO.

Table 3. **Decovolution results and polymerization degree BO**

Таблица 3. **Результаты дековолюции и степень полимеризации BO**

Slag No.	Fraction of silicate structural elements in slags				BO
	Q^0_{Si}	Q^1_{Si}	Q^2_{Si}	Q^3_{Si}	
1	0.56	0.15	0.29	0	0.73
2	0.75	0.24	0.01	0	0.26
3	0.62	0.38	0	0	0.38
4	0.22	0.30	0.38	0.06	1.28

Despite the high degree of polymerization (BO = 1.28), slag *4* (B_{slag} = 1.0, 6 wt. % B_2O_3) shows low viscosity due to its highest content of low-melting phases (23 %). The viscosity ranges from 0.40 to 0.25 Pa·s within 1400 – 1500 °C, and its crystallization onset temperature is 1265 °C.

Slag *1* with the same basicity but without boron oxide has a much simpler structure (BO = 0.73), but its viscosity is higher – 0.9 – 0.4 Pa·s in the 1400 – 1500 °C range – and its crystallization onset temperature rises to 1402 °C. This can be attributed to the reduction in the fraction of low-melting phases to 8.4 %. In the absence of calcium borates, the low-melting phases are represented exclusively by $CaO·MgO·2SiO_2$ with a melting point of 1391 °C.

From the above results, it can be concluded that the effect of the balance between the phase composition and structure of the slags on their viscosity is clearly pronounced.

It is well established that higher basicity enhances desulfurization. However, the effectiveness of desulfurization is governed not only by the chemical activity of the oxide system but also by diffusion within the slag, which is limited by viscosity. Therefore, previous experiments involving holding the metal beneath a slag cover were carried out to confirm the influence of the kinetic factor [18]. Experiments involving the treatment of metal with boron-containing slags of basicity 1.0 and 2.5, with a maximum boron oxide content of 6 wt. %, showed rather high desulfurization efficiency (Table 4). According to thermodynamic modeling performed using the HSC Chemistry software package, the equilibrium sulfur content, $[S]_{calc}$, can reach 0.002 – 0.003 %. The experimentally obtained sulfur contents, $[S]_{exp}$, after holding the metal under the studied slags were close to equilibrium and amounted to 0.006 and 0.017 % for slags *3* and *4*, respectively. The role of viscosity becomes evident when comparing the highly basic slags. In slag 3, the relatively low viscosity enabled the experimental sulfur level to approach the equilibrium value after 60 min of holding. This effect was not observed with the much more viscous slag *2*, confirming diffusion-controlled nature of the process under those conditions.

A moderate reduction of boron by silicon (present in the metal at 0.3 wt. %) was also observed. The boron content in the metal, $[B]_{exp}$, after the holding period was 0.002 – 0.003 % (Table 4). According to the literature, such a boron level in austenitic stainless steel improves both corrosion resistance and ductility [19; 20].

Table 4. **Sulfur and boron content in metal depending on time of slag treatment at 1600 °C (initial sulfur content in metal – 0.03 %)**

Таблица 4. **Содержание серы и бора в металле в зависимости от времени выдержки под шлаком при 1600 °С (исходное содержание серы в металле 0,03 %)**

Slag No.	Holding time, min	$[S]_{exp}$, %	$[S]_{calc}$, %	$[B]_{exp}$, %	Viscosity, Pa·s
1	10	0.015	0.011	–	0.20
	20	0.015			
	30	0.014			
2	10	0.015	0.002	–	0.75
	30	0.010			
	60	0.011			
3	10	0.015	0.003	~0.002	0.30
	20	0.013			
	40	0.008			
	60	0.006			
4	10	0.016	0.014	~0.003	0.20
	20	0.017			
	30	0.017			

Conclusions

It was established that the addition of up to 6 wt. % B_2O_3 to the slag, although increasing the degree of structural polymerization (BO) from 0.73 to 1.28 at low basicity and from 0.26 to 0.38 at high basicity, ensures sufficiently high melt fluidity within the studied basicity range. This effect results from the tendency of boron oxide to form low-melting eutectics with the main slag components. The resulting highly basic slags, with a viscosity of about 0.3 Pa·s, a basicity of 2.5, and a B_2O_3 content of 6 wt. %, enable deep desulfurization of the metal, providing an equilibrium sulfur content of approximately 0.003 % according to thermodynamic modeling. Under desulfurization temperatures, these slags remain in the homogeneous liquid region and exhibit a crystallization onset temperature well below 1600 °C. Holding the metal beneath a slag cover reduced the sulfur content to about 0.006 %. During this treatment, 0.002 – 0.003 % boron was taken up by the steel. Published data indicate that this direct-microalloying level enhances both ductility and corrosion resistance.

References / Список литературы

1. Tokovoi O.K. Argon-Oxygen Decarburization of Stainless Steel: Monograph. Chelyabinsk: SUSU; 2015:250. (In Russ.).
Токовой О.К. Аргонокислородное рафинирование нержавеющей стали: Монография. Челябинск: Издательский центр ЮУрГУ; 2015:250.
2. Jalkanen H., Holappa L. Converter steelmaking. In: *Treatise on Process Metallurgy*. Vol. 3. Oxford: Elsevier; 2013:223–270. https://doi.org/10.1016/B978-0-08-096988-6.00014-6
3. Dyudkin D.A., Kisilenko V.V. Steel Production, in 3 vols. Vol. 3. Secondary Metallurgy. Moscow: Teplotekhnik; 2010: 544. (In Russ.).
Дюдкин Д.А., Кисиленко В.В. Производство стали: в 3-х томах. Т. 3: Внепечная металлургия стали. Москва: Теплотехник; 2010:544.
4. Visuri V.V., Mattila R., Kupari P., Fabritius T. A comparative study on refractory wear associated with fluxes for AOD slags. In: *Proceedings of the 7th Int. Congress on Science and Technology of Steelmaking, June 13–15, 2018, Venice, Italy*. 2018:13–15.
5. Wang H.-m., Li G.-r., Li B., Zhang X.-j., Yan Y.-q. Effect of B_2O_3 on melting temperature of CaO-based ladle refining slag. *ISIJ International*. 2010;17(10):18–22. https://doi.org/10.1016/S1006-706X(10)60177-X
6. Babenko A.A., Smirnov L.A., Upolovnikova A.G., Smetannikov A.N., Sychev A.V. Theoretical bases and technology of steel exhaustive metal desulfurization and direct microalloying with boron beneath basic boron-containing slags. *Metallurgist*. 2020;63(11-12):1259–1265. https://doi.org/10.1007/s11015-020-00937-6

Бабенко А.А., Смирнов Л.А., Уполовникова А.Г., Сметанников А.Н., Сычев А.В. Теоретические основы и технология глубокой десульфурации металла и прямого микролегирования стали бором под основными борсодержащими шлаками. *Металлург*. 2019;79(12):23–28.

7. Li Q., Yang Sh., Zhang Y., An Zh., Guo Zh.Ch. Effects of MgO, Na_2O, and B_2O_3 on the viscosity and structure of Cr_2O_3-bearing CaO–SiO_2–Al_2O_3 slags. *ISIJ International*. 2017;57(4):689–696. https://doi.org/10.2355/ISIJINTERNATIONAL.ISIJINT-2016-569
8. Shtengel'meier S.V., Prusov V.A., Bogechov V.A. Improvement of the technique of measuring viscosity using a vibration viscometer. *Zavodskaya laboratoriya*. 1985;(9):56–57. (In Russ.).

   Штенгельмейер С.В., Прусов В.А., Богечов В.А. Усовершенствование методики измерения вязкости вибрационным вискозиметром. *Заводская лаборатория*. 1985;(9):56–57.
9. Voskoboinikov V.G., Dunaev N.E., Mikhalevich A.G., Kukhtin T.I., Shtengel'meier S.V. Properties of Blast Furnace Slags: Reference Book. Moscow: Metallurgiya; 1975:180. (In Russ.).

   Воскобойников В.Г., Дунаев Н.Е., Михалевич А.Г., Кухтин Т.И., Штенгельмейер С.В. Свойства доменных шлаков: Справочник. Москва: Металлургия; 1975:180.
10. Roine A. Outokumpu HSC Chemistry for Windows. Chemical Reactions and Equilibrium Software with Extensive Thermochemical Database. Pori: Outokumpu research OY; 2002:269.
11. Mysen B.O., Virgo D., Scarfe C.M. Relations between the anionic structure and viscosity of silicate melts – a Raman spectroscopic study. *American Mineralogist*. 1980;65(7-8):690–710.
12. McMillan P. Structural studies of silicate glasses and melts – applications and limitations of Raman spectroscopy. *American Mineralogist*. 1984;69(7-8):622–644.
13. Matson D.W., Sharma S.K., Philpotts J.A. The structure of high-silica alkali-silicate glasses. A Raman spectroscopic investigation. *Journal of Non-Crystalline Solids*. 1983;58(2-3):323–352. https://doi.org/10.1016/0022-3093(83)90032-7
14. Weckhuysen B.M., Wachs I.F. Raman spectroscopy of supported chromium oxide catalysts. Determination of chromium–oxygen bond distances and bond orders. *Journal of the Chemical Society, Faraday Transactions*. 1996;92(11):1969–1973. https://doi.org/10.1039/FT9969201969
15. Kim T.S., Park J.H. Structure-viscosity relationship of low-silica calcium aluminosilicate melts. *ISIJ International*. 2014;54(9):2031–2038. https://doi.org/10.2355/isijinternational.54.2031
16. Cochain B., Neuville D.R., Henderson G.S., McCammon C.A., Pinet O., Richet P. Effects of the iron content and redox state on the structure of sodium borosilicate glasses: A Raman, Mössbauer and Boron K-Edge XANES spectroscopy study. *Journal of the American Ceramic Society*. 2012;95(3):962–971. https://doi.org/10.1111/j.1551-2916.2011.05020.x
17. Kim Y., Morita K. Relationship between molten oxide structure and thermal conductivity in the CaO–SiO_2–B_2O_3 system. *ISIJ International*. 2014;54(9):2077–2083. https://doi.org/10.2355/isijinternational.54.2077
18. Babenko A.A., Shartdinov R.R., Lobanov D.A., Smetannikov A.N., Upolovnikova A.G. Physicochemical properties of the CaO–SiO_2–B_2O_3–2%Cr_2O_3–3%Al_2O_3–8%MgO slag system. *Ferrous Metallurgy. Bulletin of Scientific, Technical and Economic Information*. 2023;79(9):736–744. (In Russ.). https://doi.org/10.32339/0135-5910-2023-9-736-744

   Бабенко А.А., Шартдинов Р.Р., Лобанов Д.А., Сметанников А.Н., Уполовникова А.Г. Физико-химические свойства шлаков системы CaO–SiO_2–B_2O_3–2%Cr_2O_3–3%Al_2O_3–8%MgO. *Черная металлургия. Бюллетень научно-технической и экономической информации*. 2023;79(9):736–744. https://doi.org/10.32339/0135-5910-2023-9-736-744
19. Cetin M. Effect of boron added corrosion behavior of cast 304 stainless steel. *Protection of Metals and Physical Chemistry of Surfaces*. 2019;55:1217–1225. https://doi.org/10.1134/S2070205119060054
20. Moshkevich E.I., Travinin V.I., Kissina L.B., Sidorov K.V. Improving the Technological Plasticity of Steel Kh18N9T. 2nd ed. Moscow: TsIINChM; 1964:10. (In Russ.).

    Мошкевич Е.И., Травинин В.И., Киссина Л.Б., Сидоров К.В. Улучшение технологической пластичности стали Х18Н9Т. 2-е изд. Москва: ЦИИНЧМ; 1964:10.

Information about the Authors / Сведения об авторах

Anatolii A. Babenko, *Dr. Sci. (Eng.), Prof., Chief Researcher of the Laboratory of Steel and Ferroalloys,* Vatolin Institute of Metallurgy of the Ural Branch of the Russian Academy of Sciences
ORCID: 0000-0003-0734-6162
E-mail: babenko251@gmail.com

Ruslan R. Shartdinov, *Cand. Sci. (Eng.), Research Associate of the Laboratory of Steel and Ferroalloys,* Vatolin Institute of Metallurgy of the Ural Branch of the Russian Academy of Sciences
ORCID: 0000-0003-0852-1161
E-mail: rr.shartdinov@gmail.com

Daniil A. Lobanov, *Cand. Sci. (Eng.), Senior Researcher of the Laboratory of Problems of Man-Made Formations,* Vatolin Institute of Metallurgy of the Ural Branch of the Russian Academy of Sciences
ORCID: 0009-0007-5659-1208
E-mail: summerdanny@yandex.ru

Анатолий Алексеевич Бабенко, *д.т.н., профессор, главный научный сотрудник лаборатории стали и ферросплавов,* Институт металлургии имени академика Н.А. Ватолина Уральского отделения РАН
ORCID: 0000-0003-0734-6162
E-mail: babenko251@gmail.com

Руслан Рафикович Шартдинов, *к.т.н., научный сотрудник лаборатории стали и ферросплавов,* Институт металлургии имени академика Н.А. Ватолина Уральского отделения РАН
ORCID: 0000-0003-0852-1161
E-mail: rr.shartdinov@gmail.com

Даниил Андреевич Лобанов, *к.т.н., старший научный сотрудник лаборатории проблем техногенных образований,* Институт металлургии имени академика Н.А. Ватолина Уральского отделения РАН
ORCID: 0009-0007-5659-1208
E-mail: summerdanny@yandex.ru

Artem N. Smetannikov, *Junior Researcher of the Laboratory of Steel and Ferroalloys*, Vatolin Institute of Metallurgy of the Ural Branch of the Russian Academy of Sciences
ORCID: 0000-0001-9206-0905
E-mail: artem.smetannikov.89@mail.ru

Alena G. Upolovnikova, *Cand. Sci. (Eng.), Senior Researcher of the Laboratory of Steel and Ferroalloys*, Vatolin Institute of Metallurgy of the Ural Branch of the Russian Academy of Sciences
ORCID: 0000-0002-6698-5565
E-mail: upol.ru@mail.ru

Vladimir S. Gulyakov, *Cand. Sci. (Eng.), Senior Researcher of the Laboratory of Steel and Ferroalloys*, Vatolin Institute of Metallurgy of the Ural Branch of the Russian Academy of Sciences
ORCID: 0009-0009-3030-0171
E-mail: gvs49@mail.ru

Артем Николаевич Сметанников, *младший научный сотрудник лаборатории стали и ферросплавов*, Институт металлургии имени академика Н.А. Ватолина Уральского отделения РАН
ORCID: 0000-0001-9206-0905
E-mail: artem.smetannikov.89@mail.ru

Алена Геннадьевна Уполовникова, *к.т.н., старший научный сотрудник лаборатории стали и ферросплавов*, Институт металлургии имени академика Н.А. Ватолина Уральского отделения РАН
ORCID: 0000-0002-6698-5565
E-mail: upol.ru@mail.ru

Владимир Сергеевич Гуляков, *к.т.н., старший научный сотрудник лаборатории стали и ферросплавов*, Институт металлургии имени академика Н.А. Ватолина Уральского отделения РАН
ORCID: 0009-0009-3030-0171
E-mail: gvs49@mail.ru

Contribution of the Authors

A. A. Babenko – scientific guidance, analysis of results, writing and editing the article.
R. R. Shartdinov – conducting an experiment, processing and analysis of results, writing and editing the article.
D. A. Lobanov – conducting an experiment, analysis of results.
A. N. Smetannikov – conducting an experiment, analysis of results.

A. G. Upolovnikova – modeling, processing and analysis of results, editing the article.
V. S. Gulyakov – analysis of results, editing the article.

Вклад авторов

А. А. Бабенко – научное руководство, анализ результатов, написание и редактирование статьи.
Р. Р. Шартдинов – проведение эксперимента, обработка и анализ результатов, написание и редактирование статьи.
Д. А. Лобанов – проведение эксперимента, анализ результатов.
А. Н. Сметанников – проведение эксперимента, анализ результатов.
А. Г. Уполовникова – моделирование, анализ результатов, редактирование статьи.
В. С. Гуляков – анализ результатов, редактирование статьи.

Received 26.05.2025
Revised 10.06.2025
Accepted 16.06.2025

Поступила в редакцию 26.05.2025
После доработки 10.06.2025
Принята к публикации 16.06.2025

PHYSICO-CHEMICAL BASICS OF METALLURGICAL PROCESSES / ФИЗИКО-ХИМИЧЕСКИЕ ОСНОВЫ МЕТАЛЛУРГИЧЕСКИХ ПРОЦЕССОВ

UDC 669.046.582.2
DOI 10.17073/0368-0797-2025-5-495-505

Original article
Оригинальная статья

Boron distribution between metal and slag during melting of metalized siderite concentrate in electric furnace

A. S. Vusikhis[1], S. N. Tyushnyakov[1], K. V. Pikulin[1], S. N. Agafonov[1] ✉, L. I. Leont'ev[1, 2, 3]

[1] **Vatolin Institute of Metallurgy of the Ural Branch of the Russian Academy of Sciences** (101 Amundsena Str., Yekaterinburg 620016, Russian Federation)
[2] **National University of Science and Technology "MISIS"** (4 Leninskii Ave., Moscow 119049, Russian Federation)
[3] **Presidium of the Russian Academy of Sciences (Department of Chemistry and Material Sciences)** (32a Leninskii Ave., Moscow 119991, Russian Federation)

✉ AgafonovS@yandex.ru

Abstract. The Ural metallurgical enterprises compensate for the deficit of iron ore raw materials by supplying materials from Central Russia, the Kola Peninsula and Kazakhstan. Carbonate iron ores (siderites) of the Bakalskoye deposit are poor ores and, despite large reserves (about 1 billion tons), are not in great demand among metallurgists due to their low quality (low iron content and high magnesium content). The prospects for developing the Bakalskoye deposit depend on the availability of new technologies for processing siderites. There is a technology for processing poor iron ores using the coke-free metallurgy method, including reducing roasting in a rotary kiln, grinding and magnetic separation to obtain a highly metallized product suitable for steelmaking. Laboratory studies and industrial tests confirmed its suitability for processing siderites. A modernized technology for processing siderites is proposed, in which the operations of grinding and magnetic separation are excluded, and the product of reducing roasting in a rotary kiln is loaded hot into an electric furnace for separating melting. The process is carried out in the presence of colemanite containing boric anhydride to obtain liquid slag. During melting, part of the boron passes into the metal melt. By means of thermodynamic modeling, an assessment of the distribution of boron between the metal and slag as a result of separating melting is carried out. With a content of 5 and 10 % of colemanite in the charge, depending on the proportion of carbon, up to 60 % of boron passes into the metal. Such metal can be used as a ligature for obtaining boron-containing steel or cast iron. When bubbling the metal melt with oxygen, boron content can be reduced to 0.0001 %.

Keywords: siderites, metallization, separation melting, colemanite, boron, distribution

Acknowledgements: The work was supported by the Russian Science Foundation, grant No. 25-29-00363, https://rscf.ru/project/25-29-00363/.

For citation: Vusikhis A.S., Tyushnyakov S.N., Pikulin K.V., Agafonov S.N., Leont'ev L.I. Boron distribution between metal and slag during melting of metalized siderite concentrate in electric furnace. *Izvestiya. Ferrous Metallurgy*. 2025;68(5):495–505.
https://doi.org/10.17073/0368-0797-2025-5-495-505

Распределение бора между металлом и шлаком в процессе плавки металлизованного сидеритового концентрата в электропечи

А. С. Вусихис[1], С. Н. Тюшняков[1], К. В. Пикулин[1], С. Н. Агафонов[1] ✉, Л. И. Леонтьев[1, 2, 3]

[1] **Институт металлургии имени академика Н.А. Ватолина Уральского отделения РАН** (620016, Россия, Екатеринбург, ул. Амундсена, 101)
[2] **Национальный исследовательский технологический университет «МИСИС»** (Россия, 119049, Москва, Ленинский пр., 4)
[3] **Президиум РАН** (Россия, 119991, Москва, Ленинский пр., 32а)

✉ AgafonovS@yandex.ru

Аннотация. Металлургические предприятия Урала компенсируют дефицит железорудного сырья поставкой материалов из Центральной России, Кольского полуострова и Казахстана. Карбонатные железные руды (сидериты) Бакальского месторождения относятся к бедным рудам и, несмотря на большие запасы (около 1 млрд т), не пользуются широким спросом у металлургов ввиду низкого качества (низкое содержание железа и высокое – магния). Перспективы освоения Бакальского месторождения зависят от наличия новых технологий переработки сидеритов. Существует технология переработки бедных железных руд методом бескоксовой металлургии, включающая восстановительный обжиг во вращающейся печи, измельчение и магнитную сепарацию с получением высокометаллизованного продукта, пригодного для сталеплавильного производства. Лабораторные исследования и промышленные испытания подтвердили ее пригодность для переработки сидеритов. Предложена модернизированная технология переработки сидеритов, в которой операции измельчения и магнитной сепарации исключены, а продукт восстановительного обжига во вращающейся печи в горячем виде загружается в электропечь для проведения разделительной плавки. Процесс осуществляют в присутствии колеманита, содержащего борный ангидрид, для получения жидкого шлака. В ходе плавки часть бора переходит в металлический расплав. Посредством термодинамического моделирования проведена оценка распределения бора между металлом и шлаком в результате разделительной плавки. Показано, что при содержании в шихте 5 и 10 % колеманита в зависимости от доли углерода в металл переходит до 60 % бора. Такой металл может быть использован в качестве лигатуры для получения борсодержащей стали или чугуна. При барботаже металлического расплава кислородом содержание бора может быть снижено до 0,0001 %.

Ключевые слова: сидериты, металлизация, разделительная плавка, колеманит, бор, распределение

Благодарности: Исследование выполнено за счет гранта Российского научного фонда № 25-29-00363, https://rscf.ru/project/25-29-00363/.

Для цитирования: Вусихис А.С., Тюшняков С.Н., Пикулин К.В., Агафонов С.Н., Леонтьев Л.И. Распределение бора между металлом и шлаком в процессе плавки металлизованного сидеритового концентрата в электропечи. *Известия вузов. Черная металлургия*. 2025;68(5):495–505. https://doi.org/10.17073/0368-0797-2025-5-495-505

Introduction

The reserves of carbonate iron (siderite) ores at the Bakalskoye deposit located near the town of Bakal in the Chelyabinsk Region are estimated at about 1 billion tons [1; 2]. However, the Ural metallurgical enterprises compensate for the deficit of iron ore raw materials by supplying materials from Central Russia (Mikhailovsky Mining and Processing Plant, Lebedinsky Mining and Processing Plant), the Kola Peninsula (Kostomuksha Mining and Processing Plant), and Kazakhstan (Sokolov–Sarbai Mining and Processing Plant) [3; 4]. Bakal siderites are classified as poor iron ores, containing less than 35 % iron and a large proportion of magnesium oxide. The low quality of the ore limits its demand; therefore, the production of siderite ore is much lower than the potential allowed by the mining and geological conditions. For example, in 2006, ore production amounted to 1.7 million tons, or less than 3 % of the total output in the Ural Federal District [5]. The only industrially implemented method for processing Bakal siderites is blast-furnace melting [1; 2]. Existing beneficiation methods [6; 7] make it possible to increase the iron content in the obtained concentrate. However, the entire amount of magnesium oxide remains in the concentrate, which restricts its use in blast-furnace smelting to the role of a charge additive and only in quantities ensuring that the magnesium oxide content in the final slag does not exceed 20 %. Therefore, the prospects for developing the Bakalskoye deposit depend on the availability of new technologies for processing siderites.

To expand the range of siderite applications and increase their processing efficiency, a pyrometallurgical beneficiation technology has been developed [2; 8; 9]. It includes reducing roasting of siderites in a rotary kiln using a solid reducing agent, followed by magnetic separation to obtain a highly metallized product. The resulting concentrate contains less than 5 % of gangue and, when briquetted, can serve as a feed material for an electric-arc furnace.

A process was proposed to reduce costs by eliminating grinding, magnetic separation, drying, and briquetting, in which hot metallized lump concentrate is fed directly

from the rotary kiln to the electric furnace instead of using briquettes [10]. Comparative analysis of the two melting routes showed that the specific power consumption for melting metallized briquettes loaded into the furnace at 25 °C amounts to 773 kW·h per ton of metal, whereas melting hot metallized lump concentrate at 1000 °C requires 725 kW·h per ton of metal [11].

It is well known that the addition of boric anhydride to slag lowers its melting temperature [12; 13]. Since the gangue in the metallized concentrate contains a large amount of magnesium oxide, boron oxide in the form of calcined colemanite is added to the charge to produce a liquid, free-flowing slag with a low melting temperature. This provides a slag viscosity of less than 0.4 Pa·s at 1600 °C and a melting temperature of 1300 – 1500 °C, depending on the colemanite content in the charge and the SiO_2/MgO ratio in the slag [14].

When boron oxide is present in the steelmaking slag, boron can pass into the metal [15]. this study uses thermodynamic modeling to evaluate how boron partitions between metal and slag during separation melting of metallized siderite concentrate in the presence of colemanite.

Materials and methods

Metallurgical processes occur at high temperatures and proceed at high rates; therefore, it can be assumed with sufficient confidence that during the melting of siderites the system reaches a state close to equilibrium. Consequently, to evaluate boron distribution between the metal and slag, the thermodynamic modeling (TDM) method was applied. This method is widely used to calculate multicomponent and multiphase systems when solving both theoretical and applied problems related to improving metallurgical technologies. Modeling of equilibrium states in the Fe – Ca – Si – Mg – Al – Mn – C – O system was performed using the IVTANTHERMO software package. Numerical values of the total enthalpy of the resulting equilibrium compositions were obtained using HSC Chemistry 6.12.

In siderite ores of the Bakal ore field, subjected to preliminary gravitational or *X*-ray radiometric beneficiation [16] for shale removal, the contents of most components differ only slightly. The main difference lies in the SiO_2/MgO ratio [17; 18]. Therefore, a concentrate of the following composition (wt. %) was taken as the initial material for the study: 33.08 Fe_{tot}; 38.94 FeO; 2.27 Fe_2O_3; 1.41 CaO; 0.66 SiO_2; 11.22 MgO; 0.38 Al_2O_3; 0.85 Mn. The SiO_2/MgO ratio was adjusted by adding quartz. The final compositions of the model concentrates are presented in Table 1.

The masses (m_c) and compositions of the metallized siderite concentrates (MSC) with a metallization degree of φ = 95 %, obtained from 1 kg of initial concentrate, are given in Table 2.

As a fluxing additive used to liquefy the slag, calcined colemanite [19] with the following composition (wt. %) was employed: 8 SiO_2; 34 CaO; 4 MgO; and 54 B_2O_3. In practice, the solid reducing agent (coke breeze) with a particle size of 3 – 5 mm is separated from MSC lumps sized 10 – 60 mm by screening. However, some portion of the reducing agent may enter the electric furnace

Table 1. **Compositions of the initial model concentrates used in thermodynamic modeling method as part of the working fluid**

Таблица 1. **Составы исходных модельных концентратов, используемых ТДМ в составе рабочего тела**

SiO_2/MgO ratio	Content, wt. %								
	Fe_{tot}	FeO	Fe_2O_3	CaO	SiO_2	MgO	Al_2O_3	MnO	LOI
0.75	31.34	38.30	2.23	1.39	8.28	11.04	0.37	1.08	37.31
1.00	30.50	37.28	2.17	1.35	10.74	10.74	0.36	1.05	36.31
1.25	29.70	36.30	2.12	1.31	13.07	10.46	0.35	1.02	35.36

Table 2. **Masses and compositions of MSCs with a metallization degree of 95 %**

Таблица 2. **Массы и составы МСК при степени металлизации 95 %**

SiO_2/MgO ratio	m_c, kg	Content, wt. %							
		Fe_{tot}	Fe_{met}	FeO	CaO	SiO_2	MgO	Al_2O_3	MnO
0.75	539.43	58.10	55.19	3.73	2.57	15.35	20.46	0.69	2.00
1.00	551.79	55.27	52.51	3.55	2.45	19.46	19.46	0.66	1.90
1.25	563.51	52.71	50.07	3.39	2.33	23.20	18.56	0.63	1.82

together with the concentrate; therefore, it was assumed in the calculations that the electric-furnace charge contains carbon.

Thus, the model systems used for calculating phase equilibria consisted of MSC (Table 2), colemanite, and carbon, taken in amounts of 0, 5, and 10 wt. % and 0, 2, 4, and 6 wt. %, respectively, relative to the mass of metallized concentrate. The modeling was carried out at a temperature of 1600 °C, pressure of 0.1 MPa, and under the assumption that the oxide and metallic phases behave as ideal solutions.

Results and discussion

Equilibrium calculations for the MSC–carbon system show that in the presence of carbon, the amounts of iron, manganese, and silicon oxides in the oxide phase decrease (Fig. 1), and these elements pass into the metal together with residual carbon (Fig. 2).

At a temperature of 1600 °C, corresponding to the melting temperature, the iron-based metal exists in a liquid state. To estimate the crystallization onset temperature of the slags obtained from equilibrium calculations, two methods were applied.

The first method was based on the results reported in [14], which analyzed the effect of the SiO_2/MgO ratio and the amount of colemanite in the charge on the transition temperature of slags from their high-temperature stability region to the low-temperature region, close to the liquidus temperature. The dependence is described by the following empirical equation:

$$T = 1801.7 - 199.5x - 28.6x^2 - 7.19y + 0.03y^2 - 4.0xy,$$

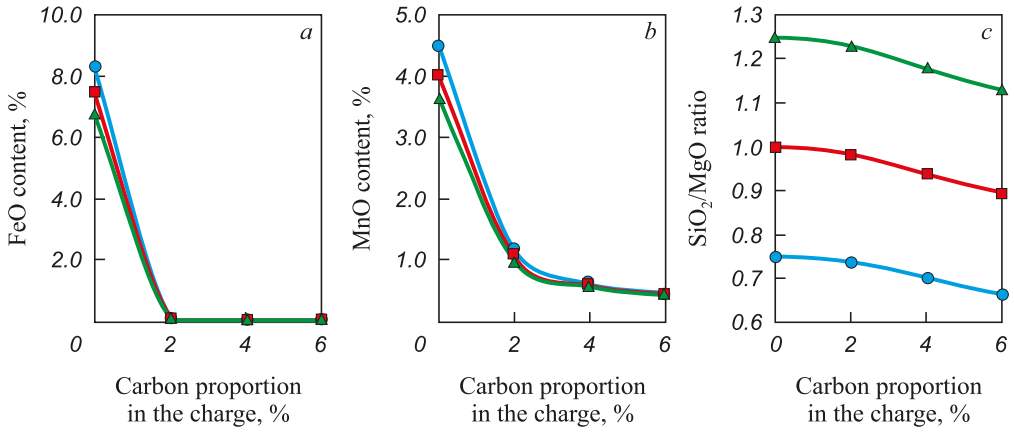

Fig. 1. Dependence of content of FeO (*a*), MnO (*b*), SiO_2/MgO ratio (*c*) in the oxide phase on carbon proportion in the charge: ● – 0.75; ■ – 1.00; ▲ – 1.25

Рис. 1. Зависимость содержания в оксидной фазе FeO (*a*), MnO (*b*), соотношения SiO_2/MgO (*c*) от доли углерода в шихте: ● – 0,75; ■ – 1,00; ▲ – 1,25

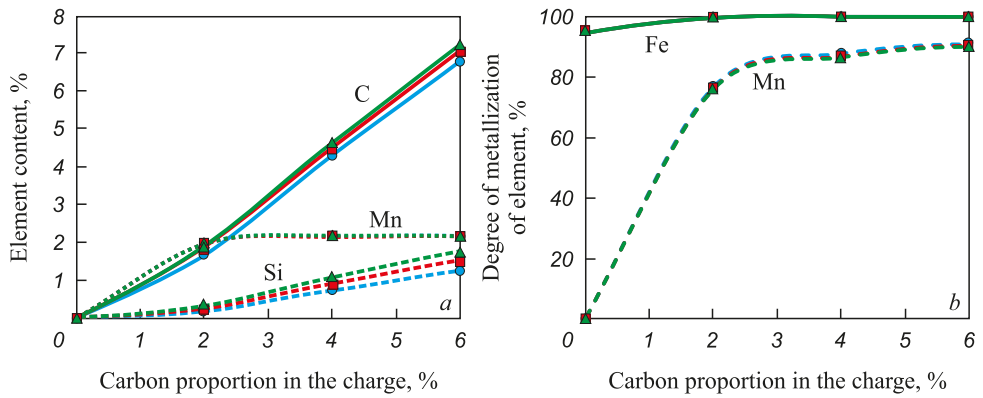

Fig. 2. Dependence of content of carbon, manganese and silicon in the metal (*a*) and metallization degree of iron and manganese (*b*) on carbon proportion in the charge: ● – 0.75; ■ – 1.00; ▲ – 1.25

Рис. 2. Зависимость содержания углерода, марганца и кремния в металле (*a*) и степени металлизации железа и марганца (*b*) от доли углерода в шихте: ● – 0,75; ■ – 1,00; ▲ – 1,25

where x is the SiO_2/MgO ratio (units); y is the colemanite content (wt. %).

It was established that in the absence of colemanite in the charge, the transition temperature decreases from 1640 to 1510 °C as the SiO_2/MgO ratio increases from 0.75 to 1.25.

A similar result was obtained using the second method described in [20], according to which the temperatures of the beginning (t_s) and end (t_l) of melting (solidus and liquidus, respectively) were determined from inflection points on the total entropy and enthalpy curves characterizing the system state. This approach was used as the basis for liquidus temperature calculations of the slag systems considered in this study.

The slags used as input were those whose compositions were determined from the equilibrium calculations in the MSC–carbon system. The results showed that in slags without carbon and with SiO_2/MgO = 0.75 – 1.25, t_l lies in the range of 1450 – 1600 °C (Fig. 3). In slags formed as a result of the interaction between MSC and carbon, a decrease in FeO content – caused by an increase in the carbon proportion – does not lead to a further increase in t_l (Fig. 4).

Thus, the calculated crystallization onset temperatures of oxide phases formed during the interaction of MSC with carbon indicated that at 1600 °C, corresponding to the electric furnace temperature, these phases remain heterogeneous. This confirms the need for a flux additive based on boric anhydride to liquefy the slag, for which colemanite was chosen.

Equilibrium calculations for the MSC–colemanite–carbon system showed the following. The addition of carbon increases the manganese and silicon content in

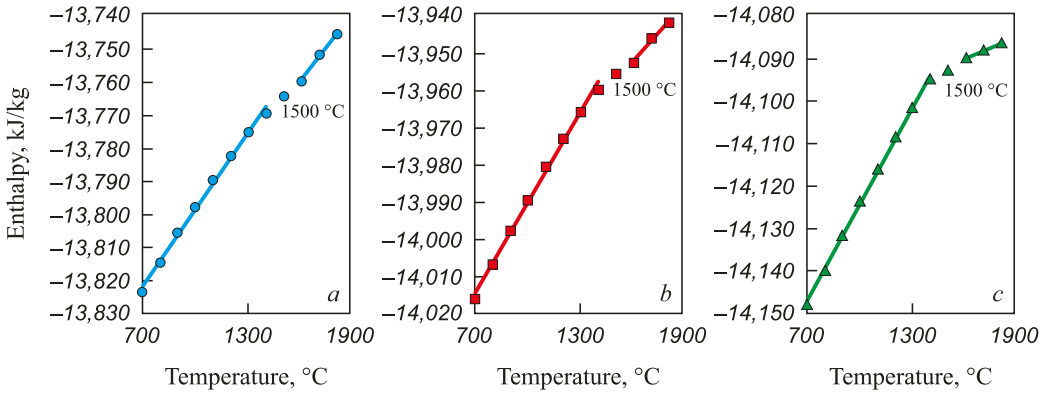

Fig. 3. Dependence of the system total enthalpy on temperature for slag systems not containing colemanite and carbon, with a change in SiO_2/MgO ratio:
a – 0.75; *b* – 1.00; *c* – 1.25

Рис. 3. Зависимость полной энтальпии системы от температуры для шлаковых систем, не содержащих в своем составе колеманит и углерод, при изменении соотношения SiO_2/MgO:
a – 0,75; *b* – 1,00; *c* – 1,25

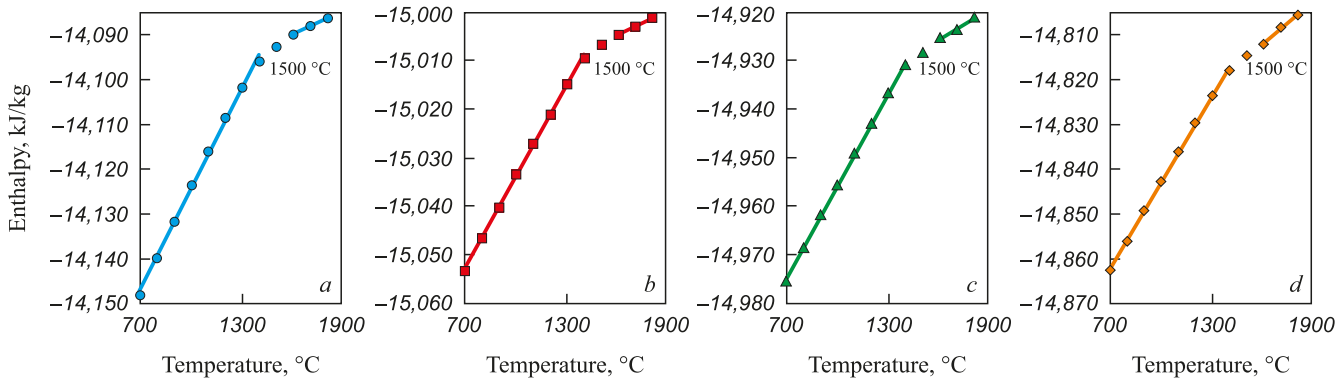

Fig. 4. Dependence of the system total enthalpy on temperature for slag systems calculated at SiO_2/MgO = 1.25 and not containing colemanite, with a change in carbon proportion, %:
a – 0; *b* – 2; *c* – 4; *d* – 6

Рис. 4. Зависимость полной энтальпии системы от температуры для шлаковых систем, рассчитанных при соотношении SiO_2/MgO = 1,25 и не содержащих в своем составе колеманит, при изменении доли углерода, %:
a – 0; *b* – 2; *c* – 4; *d* – 6

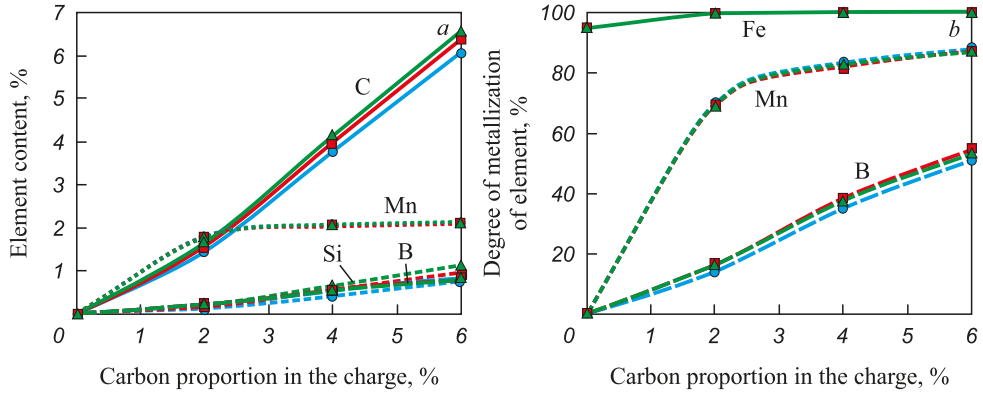

Fig. 5. Dependence of content of carbon, manganese, boron and silicon in the metal (*a*) and metallization degree of iron, manganese and boron (*b*) on carbon proportion in the charge with addition of 5 % of colemanite to the metallized siderite concentrates (MSC):
● – 0.75; ■ – 1.00; ▲ – 1.25

Рис. 5. Зависимость содержания углерода, марганца, бора и кремния в металле (*a*) и степени металлизации железа, марганца и бора (*b*) от доли углерода в шихте при добавке к МСК 5 % колеманита:
● – 0,75; ■ – 1,00; ▲ – 1,25

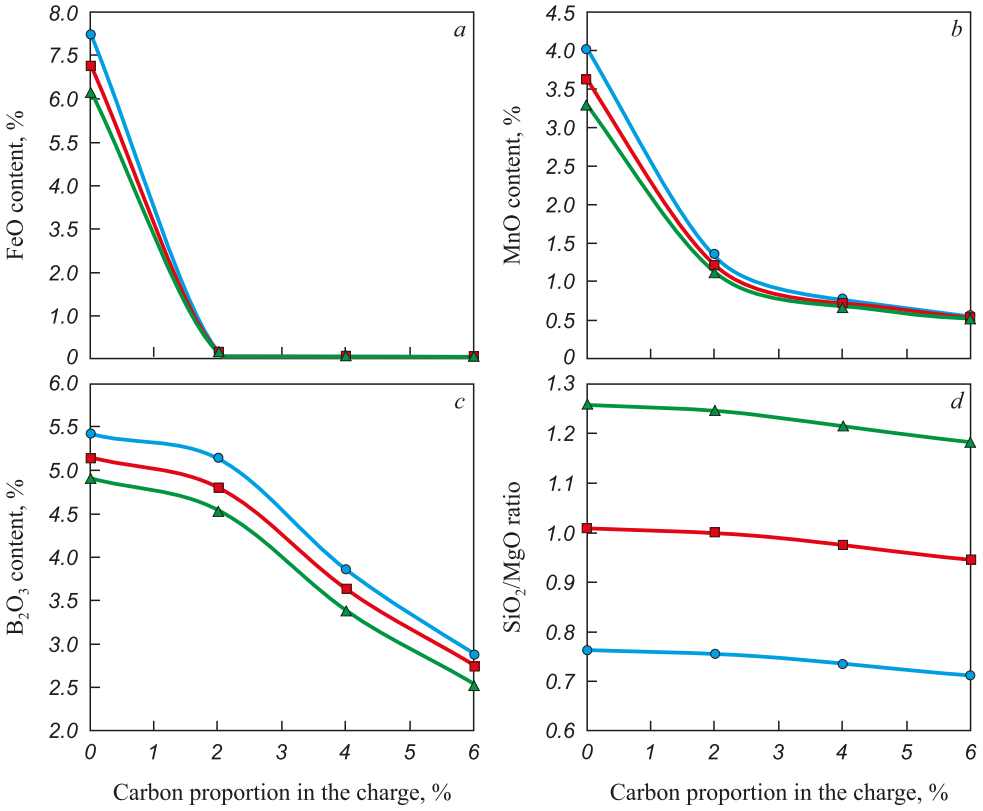

Fig. 6. Dependence of content in the oxide phase of FeO (*a*), MnO (*b*), B_2O_3 (*c*), and ratio SiO_2/MgO (*d*) on carbon proportion in the charge with addition of 5 % of colemanite to MSC:
● – 0.75; ■ – 1.00; ▲ – 1.25

Рис. 6. Зависимость содержания в оксидной фазе FeO (*a*), MnO (*b*), B_2O_3 (*c*) и соотношения SiO_2/MgO (*d*) от доли углерода в шихте при добавке к МСК 5 % колеманита:
● – 0,75; ■ – 1,00; ▲ – 1,25

the metal and decreases the amount of iron, manganese, and silicon oxides in the slag phase, similar to the MSC–carbon system (Figs. 5 – 8). In addition, boron passes into the metal, accompanied by a decrease in boron oxide content in the slag.

In the absence of carbon, the oxide phase compositions are close to those of the slags investigated in [14], where, as the SiO_2/MgO ratio increased from 0.75 to 1.25, t_l decreased from 1520 to 1370 °C, and the viscosity of all slags was below 0.3 Pa·s.

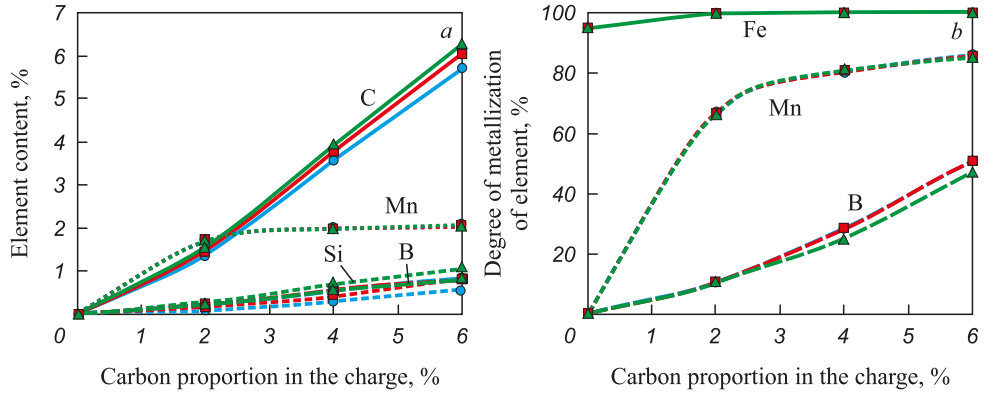

Fig. 7. Dependence of content of carbon, manganese, boron and silicon in the metal (*a*) and metallization degree of iron, manganese and boron (*b*) on carbon proportion in the charge with addition of 10 % of colemanite to MSC:
● – 0.75; ■ – 1.00; ▲ – 1.25

Рис. 7. Зависимость содержания углерода, марганца, бора и кремния в металле (*a*) и степени металлизации железа, марганца и бора (*b*) от доли углерода в шихте при добавке к МСК 10 % колеманита:
● – 0,75; ■ – 1,00; ▲ – 1,25

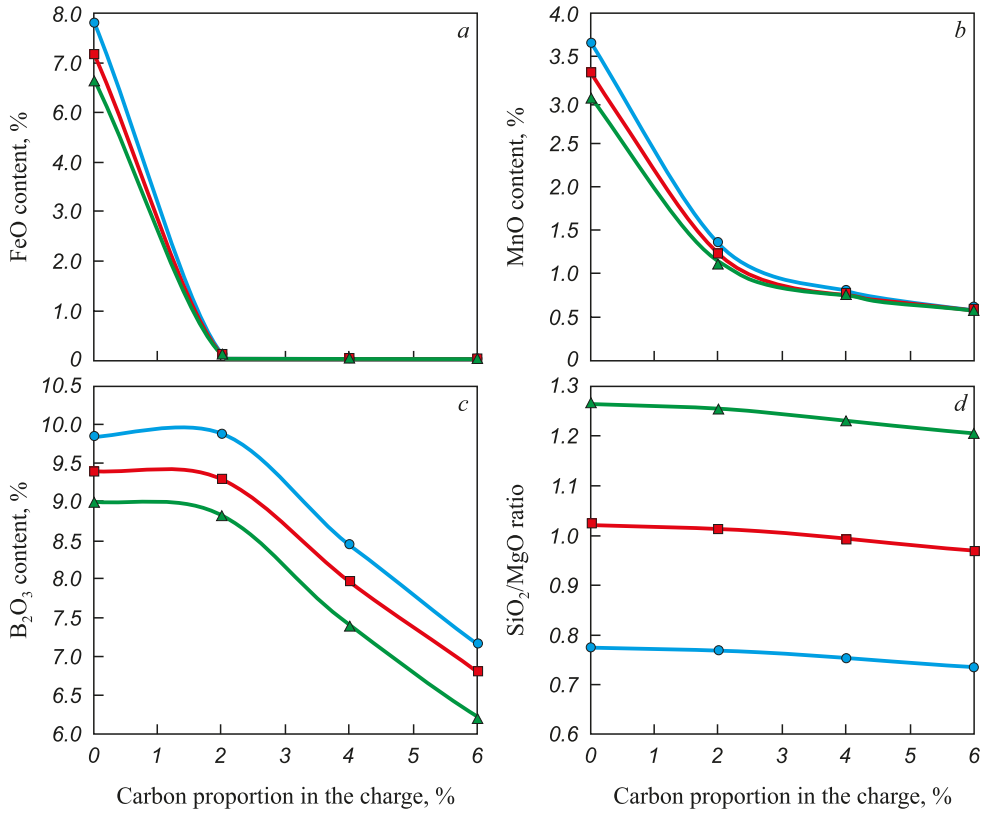

Fig. 8. Dependence of content in the oxide phase of FeO (*a*), MnO (*b*), B_2O_3 (*c*), and the ratio SiO_2/MgO (*d*) on carbon proportion in the charge with addition of 10 % of colemanite to MSC:
● – 0.75; ■ – 1.00; ▲ – 1.25

Рис. 8. Зависимость содержания в оксидной фазе FeO (*a*), MnO (*b*), B_2O_3 (*c*) и соотношения SiO_2/MgO (*d*) от доли углерода в шихте при добавке к МСК 10 % колеманита:
● – 0,75; ■ – 1,00; ▲ – 1,25

Evaluation of phase transition temperatures in the MSC–colemanite–carbon systems (Fig. 9) indicates a decrease in the liquidus temperature from 1500 to 1400 °C when 5 – 10 wt. % colemanite is added to the charge. This suggests that separation melting of metallized siderite concentrate in the presence of colemanite is feasible even when carbon is present in the charge. According to theoretical calculations, the slag in this case will have a sufficiently low melting temperature, allowing it to be removed from the furnace after

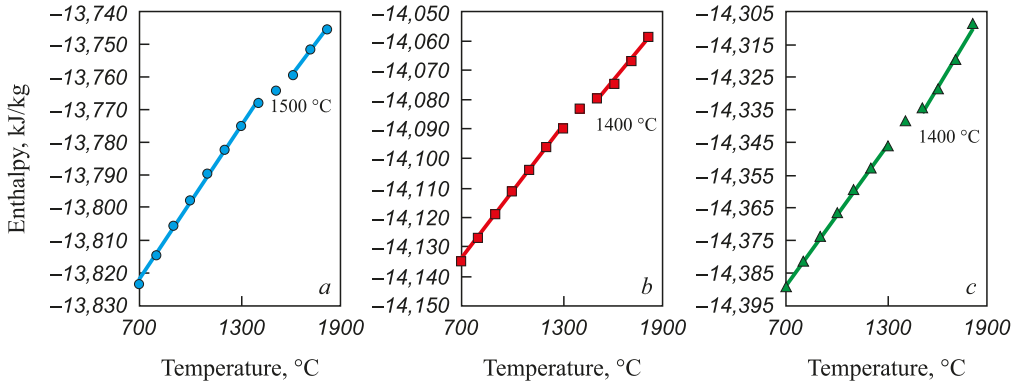

Fig. 9. Dependence of the system total enthalpy on temperature for slag systems calculated at $SiO_2/MgO = 0.75$ and not containing colemanite, with a change in carbon proportion, %:
a – 0; *b* – 5; *c* – 10

Рис. 9. Зависимость полной энтальпии системы от температуры для шлаковых систем, рассчитанных при соотношении $SiO_2/MgO = 0,75$ и не содержащих в своем составе углерод, при изменении соотношения колеманита, %:
a – 0; *b* – 5; *c* – 10

separation melting from the metal at 1600 °C. Depending on the carbon content in the charge, the metal will contain manganese, silicon, and boron.

Small additions of boron are known to improve the quality of cast iron [21; 22], steel [23 – 25], and surfacing materials [26]. They significantly refine the grain structure. Strengthening of grain boundaries by borides enhances high-temperature strength, as well as increased hardness and wear resistance, and sharply improves hardenability compared to similar steels without boron. Microadditions of boron (about 0.01 % in cast irons and 0.001 – 0.003 % in steels) can replace alloying elements such as nickel, chromium, molybdenum, and manganese in amounts 300 – 400 times greater than that of boron, while maintaining metal quality.

In the proposed technology, the amount of boron transferred to the metal is significantly higher than that required for producing quality cast iron or steel. Therefore, the resulting metal can be used as a master alloy, or its boron content should be substantially reduced, for example, by bubbling oxidation with oxygen.

To assess the feasibility of bubbling oxidation, additional thermodynamic modeling was performed using the methodology previously applied for modeling bubbling reduction of metals from oxide melts [27 – 29]. The initial model system consisted of metal with the following composition (%): 96.1 Fe; 1.7 C; 0.20 Si; 1.80 Mn; and 0.26 B (1 kg). The gas phase was oxygen, supplied in an amount of 7.3 dm^3 per kilogram of metal. Modeling was carried out at 1600 °C and 1 atm, assuming the melt to be an ideal solution.

The calculations were performed in the following sequence:

– input of initial data on the amount of metal melt and oxygen;

– equilibrium calculation of the system using thermodynamic modeling methods;

– recording equilibrium compositions and the amounts of components in the oxide and metallic melts, as well as in the gas phase;

– performing the next cycle, in which the composition of the metallic melt obtained in the previous step was taken as the initial state, while the slag was considered removed from the system and not accounted for; the gas composition and amount remained unchanged;

– repeating the cycles until the amount of oxidized components in the melt decreased to the specified level.

Fig. 10 shows the change in metal composition depending on oxygen consumption.

As a result of bubbling oxidation of the metal, the iron content increases to 99.86 %, the manganese content decreases to 0.13 %, silicon is completely oxidized, and boron content drops to 0.000002 %. From 1 kg of the ini-

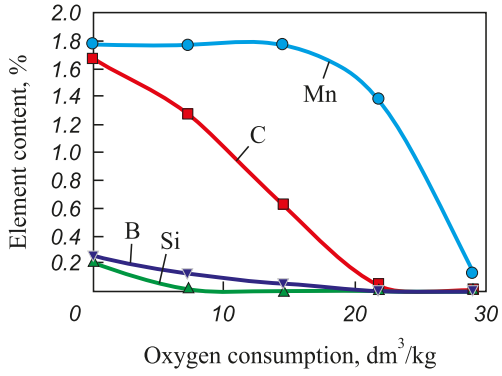

Fig. 10. Dependence of the components content in the metal on oxygen consumption

Рис. 10. Зависимость содержания компонентов в металле от расхода кислорода

tial metal, 940 g of final metal and 201 g of slag are formed, with the slag composition (wt. %) as follows: 46.7 FeO; 6.7 SiO_2; 34.3 MnO; 12.4 B_2O_3. This slag can be used together with colemanite as an additional source of boron.

Conclusions

Thermodynamic modeling of the separation melting of metallized siderite concentrate with colemanite in the presence of carbon made it possible to describe the distribution of boron between the metal and slag depending on the proportions of colemanite and carbon in the system. It is shown that adding 5 – 10 % colemanite to the charge reduces the slag melting temperature to 1400 °C, enabling efficient extraction of both metal and slag from the furnace at 1600 °C. With an increase in carbon content in the charge up to 6 %, a linear dependence of the degree of boron transfer to the metal was observed, reaching 60 %. The resulting boron-containing metal can be used as a master alloy for microalloying cast irons and steels, or as a semi-finished metal product suitable for secondary (ladle) treatment after preliminary oxygen bubbling. The slag produced during bubbling can be reused as an additional boron-bearing component of the charge. The results of the calculations can serve as a basis for planning and conducting experimental studies on the processes of separation melting of metallized siderite concentrates.

References / Список литературы

1. Krasnoborov V.A., Yaroshevskii S.L., Denisov A.A., Rudin V.S., Biryuchev V.I., Polushkin M.F. Efficiency and Prospects of Using Siderite Ores in Blast Furnace Melting. Donetsk: Novyi Mir; 1996:74. (In Russ.).

   Красноборов В.А., Ярошевский С.Л., Денисов А.А., Рудин В.С., Бирючев В.И., Полушкин М.Ф. Эффективность и перспективы применения сидеритовых руд в доменной плавке. Донецк: Новый мир; 1996:74.
2. Yur'ev B.P., Melamud S.G., Spirin N.A., Shatsillo V.V. Technological and Thermal Engineering Principles of Preparation of Siderite Ores for Metallurgical Processing. Yekaterinburg: Den' RA; 2016:428. (In Russ.).

   Юрьев Б.П., Меламуд С.Г., Спирин Н.А., Шацилло В.В. Технологические и теплотехнические основы подготовки сидеритовых руд к металлургическим переделам: Монография. Екатеринбург: ООО АМК «День РА»; 2016:428.
3. Volkov Yu.V., Sokolov I.V., Smirnov A.A. Strategy for development of raw material resources of the Urals. *Gornaya promyshlennost'*. 2006;(4):57–62. (In Russ.).

   Волков Ю.В., Соколов И.В., Смирнов А.А. Стратегия освоения сырьевых ресурсов Урала. *Горная промышленность*. 2006;(4):57–62.
4. Volkov Yu.V., Slavikovskii O.V., Sokolov I.V., Smirnov A.A. Prospects for development of raw material base of mining and metallurgical enterprises of the Urals. *GIAB*. 2007;(5):286–290. (In Russ.).

   Волков Ю.В., Славиковский О.В., Соколов И.В., Смирнов А.А. Перспективы развития сырьевой базы горно-металлургических предприятий Урала. *ГИАБ*. 2007;(5):286–290.
5. Pakhomov V.P., Dushin A.V. Assessment of mineral resource security of the Urals Federal District. *Ehkologiya regiona*. 2008;(3):129–143. (In Russ.).

   Пахомов В.П., Душин А.В. Оценка минерально-сырьевой безопасности УРФО. *Экология региона*. 2008;(3):129–143.
6. Zhunev A.G., Fedorenko N.V., Chervotkin V.V. Oxidative roasting of siderite ores in shaft furnaces. In: *Pelletizing of Iron Ores and Concentrates: Proceedings of the Institute "Uralmekhanobr"*. Sverdlovsk; 1976(3):28–38. (In Russ.).

   Жунев А.Г., Федоренко Н.В, Червоткин В.В. Окислительный обжиг сидеритовых руд в шахтных печах. В сб.: *Окускование железных руд и концентратов. Труды института «Уралмеханобр»*. 1976;(3):28–38.
7. Blank M.E., Chervotkin V.V., Konchakovskii V.R. Development and study of a two-stage method of iron ore raw materials metallization in a three-zone shaft furnace. In: *Theory and Practice of Direct Iron Production*. Moscow: Nauka; 1986:207–211. (In Russ.).

   Бланк М.Э., Червоткин В.В., Кончаковский В.Р. Разработка и исследование двухстадийного способа металлизации железорудного сырья в трехзонной шахтной печи. В сб.: *Теория и практика прямого получения железа*. Москва: Наука; 1986:207–211.
8. Melamud S.G., Shatsillo V.V., Dudchuk I.A., Mushketov A.A., Bratygin E.V., Yur'ev B.P. Enrichment of reduced siderite ore to produce concentrate for electrosteel smelting. *Steel in Translation*. 2011;41(6):492–498. https://doi.org/10.3103/S0967091211060076

   Меламуд С.Г., Шацилло В.В., Дудчук И.А., Мушкетов А.А., Братыгин Е.В., Юрьев Б.П. Разработка технологии обогащения металлизованной сидеритовой руды с получением концентрата для выплавки электростали. *Сталь*. 2011;(6):4–9.
9. Vusikhis A.S., Sheshukov O.Yu., Leont'ev L.I. Method of metallization of magnesium-containing carbonate iron ore materials. Patent RF no. 2489494. *Byulleten' izobretenii.* 2013;(22). (In Russ.).

   Вусихис А.С., Шешуков О.Ю., Леонтьев Л.И. Способ металлизации магнийсодержащих карбонатных железорудных материалов. Патент РФ 2489494. Бюл. 2013;(22).
10. Vusikhis A.S., Leont'ev L.I. Method for processing magnesium-containing carbonate iron ore materials. Patent RF no. 2820696. *Byulleten' izobretenii*. 2024;(16). (In Russ.).

    Вусихис А.С., Леонтьев Л.И. Способ переработки магнийсодержащих карбонатных железорудных материалов. Патент РФ 2820696. Бюл. 2024;(16).
11. Vusikhis A.S., Leon'yev L.I., Chesnokov Yu.A. Evaluating the efficiency of metallized siderite concentrate electric melting. *Izvestiya. Ferrous Metallurgy*. 2023;66(6):653–658. https://doi.org/10.17073/0368-0797-2023-6-653-658

    Вусихис А.С., Леонтьев Л.И., Чесноков Ю.А. Оценка эффективности электроплавки металлизованного сидеритового концентрата. *Известия вузов. Черная металлургия*. 2023;66(6):653–658. https://doi.org/10.17073/0368-0797-2023-6-653-658

12. Hongming W., Tingwing Z., Hua Z., Li G., Yan Y., Wang J. Effect of B_2O_3 on melting temperature, visocity and desulfurization capacity of CaO-based refining flus. *ISIJ International*. 2011;51(5):702–708. https://doi.org/10.2355/isijinternational.51.702

13. Ren Sh., Zhang J., Wu L., Liu W., Bai Y., Xing X., Su B., Kong D. Influence of B_2O_3 on viscosity of high Ti-bearing blast furnace slag. *ISIJ International*. 2012;52(6):984–991. https://doi.org/10.2355/isijinternational.52.984

14. Vusikhis A.S., Leont'ev L.I., Mikheenkov M.A. Effect of boric anhydride on viscosity of slags used in electric melting of metallized siderite concentrate. *Izvestiya. Ferrous Metallurgy*. 2023;66(5):597–603. https://doi.org/10.17073/0368-0797-2023-5-597-603

Вусихис А.С., Леонтьев Л.И., Михеенков М.А. Влияние борного ангидрида на вязкость шлаков электроплавки металлизованного сидеритового концентрата. *Известия вузов. Черная металлургия*. 2023;66(5):612–618. https://doi.org/10.17073/0368-0797-2023-5-597-603

15. Zhuchkov V.I., Salina V.A., Sychev A.V. The study of the process of metal-thermal reduction of boron from the slag of the system $CaO–SiO_2–MgO–Al_2O_3–B_2O_3$. *Materials Science Forum*. 2019;946:423–429. http://doi.org/10.4028/www.scientific.net/MSF.946.423

16. Zagainov S.A., Yur'ev B.P. Dressing Processes and Devices for Their Implementation. Yekaterinburg: UrFU; 2012:110. (In Russ.).

Загайнов С.А., Юрьев Б.П. Обогатительные процессы и устройства для их реализации. Екатеринбург: УрФУ; 2012:110.

17. Timeskov V.A. Mineralogy of Carbonate Ores and Host Carbonate Rocks of the Bakal Iron Ore Deposit in the Southern Urals. Kazan: Kazan University; 1963:214. (In Russ.).

Тимесков В.А. Минералогия карбонатных руд и вмещающих их карбонатных пород Бакальского железорудного месторождения на Южном Урале. Казань: Казанский университет; 1963:214.

18. Vusikhis A.S., Leont'ev L.I. Use of Siderite Ores in Production of Iron and Steel. Moscow; Vologda: Infra-Engineering; 2022:116. (In Russ.).

Вусихис А.С., Леонтьев Л.И. Применение сидеритовых руд при производстве чугуна и стали. Москва; Вологда: Инфра-Инженерия; 2022:116.

19. Öztürk Ç., Akpınar S., Tığ M. Effect of calcined colemanite addition on properties of porcelain tile. *Journal of the Australian Ceramic Society*. 2022;58:321–331. https://doi.org/10.1007/s41779-021-00674-2

20. Marshuk L.A., Vusikhis A.S., Leont'ev L.I. Study of physicochemical characteristics of oxide systems $CaO–SiO_2–Al_2O_3–MgO$ by thermodynamic modeling. In: *Proceedings of the VI Congress with Int. Participation "Technogen-2023", July 11–14, 2023*. Yekaterinburg; 2023:361–363. (In Russ.).

Маршук Л.А., Вусихис А.С., Леонтьев Л.И. Исследование физико-химических характеристик оксидных систем $CaO–SiO_2–Al_2O_3–MgO$ методом термодинамического моделирования. *Труды VI Конгресса с международным участием «Техноген-2023», 11–14 июля 2023*. Екатеринбург; 2023:361–363.

21. Kolokol'tsev V.M., Petrochenko E.V., Molochkova O.S. Influence of boron modification and cooling conditions during solidification on structural and phase state of heat- and wear-resistant white cast iron. *Izvestiya. Ferrous Metallurgy*. 2019;62(11):887–893. (In Russ.). https://doi.org/10.17073/0368-0797-2019-11-887-893

Колокольцев В.М., Петроченко Е.В., Молочкова О.С. Влияние бора и температурных режимов охлаждения металла в литейной форме на структурно-фазовое состояние жароизносостойких белых чугунов. *Известия вузов. Черная металлургия*. 2019;62(11):887–893. https://doi.org/10.17073/0368-0797-2019-11-887-893

22. Gimaletdinov R.Kh., Gulakov A.A., Tukhvatulin I.Kh. Influence of chemical composition on the properties of the working layer of centrifugally cast indefinite rolling rolls. *Bulletin of Magnitogorsk State Technical University named after G.I. Nosov*. 2016;14(3):78–89. (In Russ.).

Гималетдинов Р.Х., Гулаков А.А., Тухватулин И.Х. Влияние химического состава на свойства рабочего слоя центробежно-литых индефинитных прокатных валков. *Вестник Магнитогорского государственного технического университета им. Г.И. Носова*. 2016;14(3):78–89.

23. Kel' I.N., Zhuchkov V.I., Sychev A.V. Application of boron-containing materials in ferrous metallurgy. *Ferrous Metallurgy. Bulletin of Scientific, Technical and Economic Information*. 2018;(5):48–53. (In Russ.).

Кель И.Н., Жучков В.И., Сычев А.В. Применение борсодержащих материалов в черной металлургии. *Черная металлургия. Бюллетень научно-технической и экономической информации*. 2018;(5):48–53.

24. Nazyuta L.Yu., Tsurkan M.L., Tikhonyuk L.S., Tarasenko O.S., Khavalits Yu.V. Influence of boron on technological properties of medium-carbon structural steels of ordinary assortment. *Visn. priazov. state. technical. un-tu*. 2018;(37):22–28. (In Russ.).

Назюта Л.Ю., Цуркан М.Л., Тихонюк Л.С., Тарасенко О.С., Хавалиц Ю.В. Влияние бора на технологические свойства среднеуглеродистых конструкционных сталей рядового сортамента. *Вісник приазовського державного технічного університету*. 2018;(37):22–28.

25. Baradyntseva E.P., Glazunova N.A., Rogovtsova O.V. Effect of boron microalloying on hardenability of steels. *Lit'e i metallurgiya*. 2016;(3(84)):70–74. (In Russ.).

Барадынцева Е.П., Глазунова Н.А., Роговцова О.В. Влияние микролегирования бором на прокаливаемость сталей. *Литье и металлургия*. 2016;(3(84)):70–74.

26. Lyamin A.V., Madrakhimov D.U. Influence of boron on phase state and properties of surfacing materials. *Molodoi uchenyi*. 2021;(4(346)):24–26. (In Russ.).

Лямин А.В., Мадрахимов Д.У. Влияние наличия бора на фазовое состояние и на свойства наплавочных материалов. *Молодой ученый*. 2021;(4(346)):24–26.

27. Vusikhis A.S., Leont'ev L.I., Selivanov E.N., Chentsov V.P. Modeling the process of gas reduction of metals from a multicomponent oxide melt in bubbling layer. *Butlerovskie soobshcheniya*. 2018;55(7):58–63. (In Russ.).

Вусихис А.С., Леонтьев Л.И., Селиванов Е.Н., Ченцов В.П. Моделирование процесса газового восстановления металлов из многокомпонентного оксидного расплава в барботируемом слое. *Бутлеровские сообщения*. 2018;55(7):58–63.

28. Vusikhis A.S., Dmitriev A.N., Kudinov D.Z., Leontiev L.I. The study of liquid and gas phases interaction during

the reduction of metal oxides from the melts by gas reductant in bubbled layer. In: *The Third Int. Conf. on Mathematical Modeling and Computer Simulation of Materials Technologies (MMT-2004), Ariel, Israel*. 2004;1:72–77.

29. Dmitriev A., Leontiev L., Vusikhis A., Kudinov D. Liquid and gas interaction during reduction in bubbled layer. In: *Proceeding of the European Metallurgical Conference (EMC-2005). Dresden, Germany*. 2005;3:1349–1358.

Information about the Authors / Сведения об авторах

Aleksandr S. Vusikhis, *Cand. Sci. (Eng.), Senior Researcher of the Laboratory of Pyrometallurgy of Non-Ferrous Metals*, Vatolin Institute of Metallurgy of the Ural Branch of the Russian Academy of Sciences
ORCID: 0000-0002-6395-0834
E-mail: vas58@mail.ru

Александр Семенович Вусихис, *к.т.н., старший научный сотрудник лаборатории пирометаллургии цветных металлов*, Институт металлургии имени академика Н.А. Ватолина Уральского отделения РАН
ORCID: 0000-0002-6395-0834
E-mail: vas58@mail.ru

Stanislav N. Tyushnyakov, *Cand. Sci. (Eng.), Senior Researcher of the Laboratory of Pyrometallurgy of Non-Ferrous Metals*, Vatolin Institute of Metallurgy of the Ural Branch of the Russian Academy of Sciences
ORCID: 0000-0002-0864-0462
E-mail: tyushnyakov.sn@gmail.com

Станислав Николаевич Тюшняков, *к.т.н., старший научный сотрудник лаборатории пирометаллургии цветных металлов*, Институт металлургии имени академика Н.А. Ватолина Уральского отделения РАН
ORCID: 0000-0002-0864-0462
E-mail: tyushnyakov.sn@gmail.com

Kirill V. Pikulin, *Cand. Sci. (Eng.), Senior Researcher of the Laboratory of Rare Refractory Metals*, Vatolin Institute of Metallurgy of the Ural Branch of the Russian Academy of Sciences
ORCID: 0000-0002-5843-0041
E-mail: pikulin.imet@gmail.com

Кирилл Владимирович Пикулин, *к.т.н., старший научный сотрудник лаборатории редких тугоплавких металлов*, Институт металлургии имени академика Н.А. Ватолина Уральского отделения РАН
ORCID: 0000-0002-5843-0041
E-mail: pikulin.imet@gmail.com

Sergei N. Agafonov, *Cand. Sci. (Eng.), Senior Researcher of the Laboratory of Rare Refractory Metals*, Vatolin Institute of Metallurgy of the Ural Branch of the Russian Academy of Sciences
ORCID: 0000-0001-6731-3595
E-mail: agafonovs@ya.ru

Сергей Николаевич Агафонов, *к.т.н., старший научный сотрудник лаборатории редких тугоплавких металлов*, Институт металлургии имени академика Н.А. Ватолина Уральского отделения РАН
ORCID: 0000-0001-6731-3595
E-mail: agafonovs@ya.ru

Leopol'd I. Leont'ev, *Academician, Adviser*, Presidium of the Russian Academy of Sciences; *Dr. Sci. (Eng.), Prof.*, National University of Science and Technology "MISIS"; *Chief Researcher*, Vatolin Institute of Metallurgy of the Ural Branch of the Russian Academy of Sciences
ORCID: 0000-0002-4343-914X
E-mail: leo@presidium.ras.ru

Леопольд Игоревич Леонтьев, *академик, советник*, Президиум РАН; *д.т.н., профессор*, Национальный исследовательский технологический университет «МИСИС»; *главный научный сотрудник*, Институт металлургии имени академика Н.А. Ватолина Уральского отделения РАН
ORCID: 0000-0002-4343-914X
E-mail: leo@presidium.ras.ru

Contribution of the Authors / Вклад авторов

A. S. Vusikhis – setting the research task, performing calculations, writing the text, formation of conclusions.
S. N. Tyushnyakov – performing calculations, analysis of results.

K. V. Pikulin – performing calculations, analysis of results.

S. N. Agafonov – performing calculations, conducting experiments.

L. I. Leont'ev – scientific guidance, analysis of results, editing the article.

А. С. Вусихис – постановка задачи исследования, проведение расчетов, подготовка текста, формирование выводов.
С. Н. Тюшняков – проведение расчетов, анализ результатов исследований.
К. В. Пикулин – проведение расчетов, анализ результатов исследований.
С. Н. Агафонов – проведение расчетов, проведение экспериментов.
Л. И. Леонтьев – научное руководство, анализ результатов исследований, редактирование статьи.

Received 11.06.2025
Revised 16.06.2025
Accepted 25.06.2025

Поступила в редакцию 11.06.2025
После доработки 16.06.2025
Принята к публикации 25.06.2025

PHYSICO-CHEMICAL BASICS OF METALLURGICAL PROCESSES / **ФИЗИКО-ХИМИЧЕСКИЕ ОСНОВЫ МЕТАЛЛУРГИЧЕСКИХ ПРОЦЕССОВ**

ГВС 669.141.31:669.112.21
DOI 10.17073/0368-0797-2025-5-506-516

Original article
Оригинальная статья

Formation of iron-carbon melts and technological aspects of carburization

A. G. Gudov[1] ✉, S. P. Burmasov[1], L. A. Smirnov[2]

[1] **Ural Federal University named after the first President of Russia B.N. Yeltsin** (19 Mira Str., Yekaterinburg 620002, Russian Federation)
[2] **JSC "Ural Institute of Metals"** (14 Gagarina Str., Yekaterinburg 620062, Russian Federation)

✉ a.g.gudov@urfu.ru

Abstract. Based on the results of viscometric studies of the patterns of precision iron-carbon melts formation, the need to take into account the structural state of the initial iron melt and the carbon material when developing the optimal carburization technology is substantiated. Considering the kinematic viscosity value and stability of the values of this structure-sensitive property as indicators of the non-equilibrium degree of the iron-carbon melt structural state, it is shown that the optimal solution should be considered to be the carburization of liquid iron with a predominantly fcc-like short-range order structure, which can be facilitated by introducing carbon into the charge composition, forced heating and melting with the formation of a melt with significant overheating above the liquidus temperature. Using the data of *X*-ray structural analysis, it was experimentally established that when using carbon materials subjected to graphitization for carburization, it is advisable to reduce the proportion of the amorphous phase, increase the size of crystallites and the graphitization degree, and improve the structural homogeneity. The experimentally determined difference in the nature of melt formation during carburization of pure iron and in the case of simultaneous deoxidation and carburization of highly oxidized metal is associated with the process of deactivation of the carbon material surface by oxygen, the development degree of which depends on reactivity of the carbon material and decreases with an increase in the degree of its graphitization and a decrease in the defectiveness of the crystal structure. During the simultaneous deoxidation and carburization of highly oxidized iron, a significant role of the deoxidizer type was established, which is associated with the different partial influence of the materials used on structural state of the iron melt and with the different neutralization degree of the effect of oxygen on deactivation of the surface of carburizer particles.

Keywords: iron-carbon melt, structural state, carburization, structure of carbon material, type of deoxidizer

Acknowledgements: The authors express their gratitude to Murzin A.V. for valuable comments during the discussion of the work.

For citation: Gudov A.G., Burmasov S.P., Smirnov L.A. Formation of iron-carbon melts and technological aspects of carburization. *Izvestiya. Ferrous Metallurgy*. 2025;68(5):506–516. https://doi.org/10.17073/0368-0797-2025-5-506-516

Исследование формирования железоуглеродистых расплавов и технологические аспекты науглероживания

А. Г. Гудов[1] ✉, С. П. Бурмасов[1], Л. А. Смирнов[2]

[1] **Уральский федеральный университет имени первого Президента России Б.Н. Ельцина** (Россия, 620002, Екатеринбург, ул. Мира, 19)
[2] **АО Уральский институт металлов** (Россия, 620062, Екатеринбург, ул. Гагарина, 14)

✉ a.g.gudov@urfu.ru

Аннотация. На основе результатов вискозиметрических исследований закономерностей формирования прецизионных железоуглеродистых расплавов обоснована необходимость учета структурного состояния исходного железного расплава и углеродного материала при разработке оптимальной технологии науглероживания. Рассматривая величину кинематической вязкости и стабильность значений этого структурно-чувствительного свойства как показатели степени неравновесности структурного состояния железоуглеродистого расплава, авторы показывают, что оптимальным решением следует считать науглероживание жидкого железа с преимущественно ГЦК-подобной структурой ближнего порядка. Этому может способствовать ввод углерода в состав шихты, форсированный нагрев и плавление с формированием расплава при значительном перегреве над температурой ликвидус. С привлечением данных рентгеноструктурного анализа

экспериментально установлено, что при использовании для науглероживания углеродных материалов, подвергнутых графитации, целесообразно снижение доли аморфной фазы, увеличение размера кристаллитов и степени графитации, повышение структурной однородности. Экспериментально установленное различие характеров формирования расплава при науглероживании чистого железа и в случае одновременного раскисления и науглероживания высокоокисленного металла связано с процессом дезактивации поверхности углеродного материала кислородом, степень развития которого зависит от реакционной способности углеродного материала и снижается при увеличении степени его графитации и уменьшении дефектности кристаллической структуры. При одновременном раскислении и науглероживании высокоокисленного железа установлена значительная роль типа раскислителя, что связано с разным парциальным влиянием используемых материалов на структурное состояние расплава железа и с разной степенью нейтрализации влияния кислорода на процесс дезактивации поверхности частиц науглероживателя.

Ключевые слова: железоуглеродистый расплав, структурное состояние, науглероживание, структура углеродного материала, тип раскислителя

Благодарности: Авторы выражают благодарность Мурзину А.В. за ценные замечания при обсуждении работы.

Для цитирования: Гудов А.Г., Бурмасов С.П., Смирнов Л.А. Исследование формирования железоуглеродистых расплавов и технологические аспекты науглероживания. *Известия вузов. Черная металлургия*. 2025;68(5):506–516.
https://doi.org/10.17073/0368-0797-2025-5-506-516

Introduction

Carburization has become an integral element in steel production using modern high-intensity technologies. This increases the relevance of studying the patterns of iron–carbon melt formation, since the establishment of an equilibrium structural state of the melt prior to crystallization is a prerequisite for achieving the maximum level of service properties of the metal [1 – 4]. Different degrees of completion of the relaxation process of the non-equilibrium structural state of the melt caused by carburization lead to an increase in the heterogeneity of the metal and the instability of its properties [5; 6]. Insufficient attention to this factor may explain why the use of modern technological schemes for steel production, despite their enhanced ability to refine the metal from undesirable impurities, does not guarantee the stability of high service properties of steel products [7].

Modern methods for assessing the degree of non-equilibrium of the structural state of iron melts are based on the study of structure-sensitive properties of melts, in particular on viscometric studies. In most cases, a higher degree of equilibrium of the melt's structural state at a fixed composition corresponds to higher kinematic viscosity values and greater stability of this structure-sensitive property [1 – 4].

As shown in the authors' previous studies [8], iron melts can exist within a spectrum of similar structural states, and the stability of one of these states increases when a solution with carbon is formed. To further elucidate the regularities of iron carburization, the authors continued viscometric studies on the formation of precision iron–carbon melts. The experiments were carried out in a vacuum high-temperature viscometer under an atmosphere of ultra-pure helium (>99.9999 %), using the torsional oscillation method of a crucible containing the metal to determine the kinematic viscosity of the melt. This method minimizes the perturbing influence on the structural state of the melt. The results obtained at this stage make it possible to identify a number of factors that must be considered when developing the parameters of the optimal carburization technology for iron.

Influence of structural state of the initial iron melt

Fig. 1 presents the results of a viscometric study of the formation of a pure iron melt at 1873 K obtained through a multistage hydrogen refining process of carbonyl iron. Two heating modes up to 1873 K were used:

– mode *1*: isothermal holding for 900 s at 1473 K (within the thermodynamic stability region of γ-Fe), followed by forced heating to 1873 K within 120 s;

– mode *2*: holding for 1200 s near the melting point (within the thermodynamic stability region of δ-Fe), nearly equilibrium slow melting for 8400 s with minimal

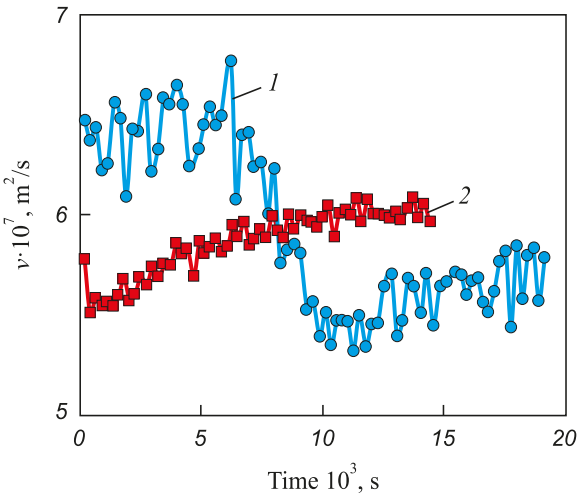

Fig. 1. Results of the viscometric study of dynamics of pure iron melt formation in the case of different heating and melting modes:
1 – mode *1*; *2* – mode *2* (crucible material – BeO)

Рис. 1. Результаты исследования методом вискозиметрии динамики формирования расплава чистого железа в случае разных режимов нагрева и плавления:
1 – режим *1*; *2* – режим *2* (материал тигля – BeO)

overheating above the melting temperature, and subsequent heating to 1873 K at an average rate of 2 K/min.

The obtained data indicate a significant influence of the heating and melting mode on the structural state of the resulting iron melt. According to the authors, the difference in the structural states of the melt may be associated with the "inheritance" of different short-range order structures from the initial solid metal. In the first case, the increased kinematic viscosity values after melting can be attributed to a more densely packed structure with a predominantly FCC-like atomic coordination. In the second case, a BCC-like configuration of atomic micro-groupings is inherited. It is worth noting that, under the thermodynamic conditions implemented for pure iron melts, the structural state with a predominantly FCC-like atomic coordination is relatively unstable. During isothermal holding at 1873 K, a transition occurs to a structural state with predominantly BCC-like atomic coordination. The pronounced high-frequency oscillations of kinematic viscosity observed in the case of forced heating may be attributed to significant micro-inhomogeneity of the forming structural state of the melt, caused by partial transformation of γ-Fe to δ-Fe as a result of the overlap of two phase transitions and the coexistence of FCC- and BCC-like atomic groupings.

The implementation of carburization under the above heating and melting modes can therefore be associated with the formation of a carbon solution in different structural states of the initial iron melt. As shown in Fig. 2, *a*, the formation of an iron–carbon melt under the first heating and melting mode leads to the development of a structural state with a markedly higher kinematic viscosity, which, according to currently accepted views, corresponds to a more equilibrium structural state of the melt. This is further supported by an analysis of the stability of the realized structural states of the iron–carbon melt: for the state with lower kinematic viscosity, there is a clear tendency to transform into a state with higher viscosity, both under isothermal holding at 1873 K and during subsequent cooling from 1873 K to crystallization (Fig. 2, *b*).

The above results suggest that, during carburization of iron, the optimal process should be considered the carburization of liquid iron possessing a predominantly FCC-like short-range order structure. However, it is also possible that the instability and non-equilibrium character of the initial structural state – enhanced by the strongly non-equilibrium melting mode – play a substantial, if not decisive, role in this process.

Influence of the carbon material structure

From the standpoint of differences in carburizer quality, current research mainly focuses on its chemical composition – primarily the carbon content (or ash content) and nitrogen concentration. According to the authors, attention should also be paid to the structure of the carbon material itself. It is the structure, above all, that may determine the influence of the carbon material type on the nature of melt-formation behavior and the resulting structural state after iron carburization (Fig. 3).

Based on *X*-ray diffraction (XRD) analysis (Table 1), comparing carbon materials subjected to graphitization (graphites of different grades, e.g., GMZ and GII-A,

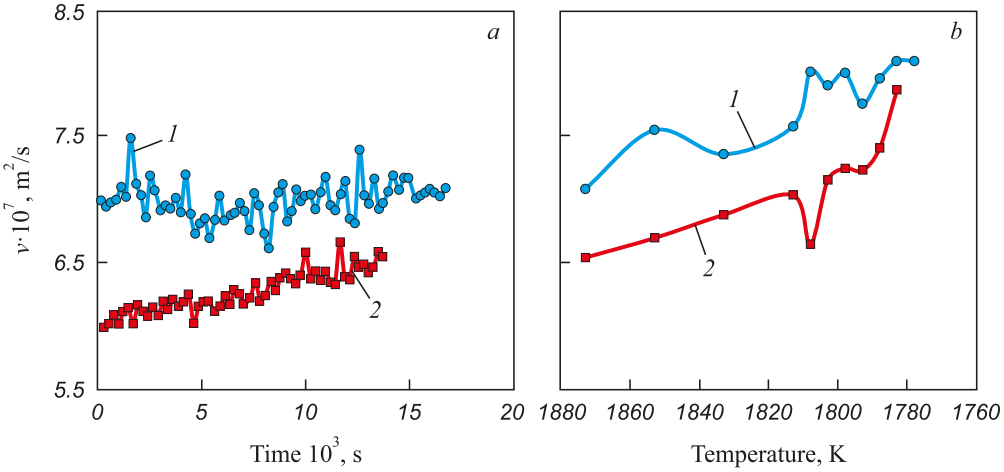

Fig. 2. Results of the viscometric study of dynamics of the Fe – 0.1 % C melt formation in the case of different heating and melting modes:
1 – mode *1*; *2* – mode *2* (crucible material – BeO, carburizer – diamond powder);
a – isothermal holding at 1873 K; *b* – subsequent stepwise cooling to crystallization with isothermal holding at each temperature for 600 s

Рис. 2. Результаты исследования методом вискозиметрии динамики формирования расплава Fe – 0,1 % C в случае разных режимов нагрева и плавления:
1 – режим *1*; *2* – режим *2* (материал тигля – BeO, науглероживатель – алмазный порошок);
a – изотермическая выдержка при 1873 K; *b* – последующее ступенчатое охлаждение до кристаллизации с изотермической выдержкой при каждой температуре 600 с

and electrode scrap), the data indicate that a decrease in the kinematic viscosity of the resulting iron–carbon melt – and, in line with current understanding, a corresponding increase in the degree of structural non-equilibrium – is associated with a higher amorphous-phase fraction (likely due to a non-graphitizing binder or its partial graphitization), a smaller crystallite (coherent domain) size, and a lower degree of graphitization (three-dimensional ordering within crystallites) [9].

The results shown in Fig. 4, obtained from carburization tests in which the same pure converter iron was carburized using graphite of GII-A grade supplied by three different manufacturers, also indicate that it is not the graphite type itself but its structure that plays the decisive role. Along with confirming the previously described effect of the graphite structural parameters (Table 2) on the viscosity level of the iron–carbon melt, these data demonstrate a substantial influence of the initial graphite structural heterogeneity on both the relaxation time of the melt's structural-state non-equilibrium after graphite addition and the amplitude of the high-frequency oscillatory component of kinematic viscosity changes, which can be associated with the degree of micro-inhomogeneity of the melt. The maximum structural heterogeneity of graphite – characterized by a combination of a relatively low-defect crystalline phase and a large amorphous phase fraction (Fig. 4, *b*) – leads to the greatest micro-inhomogeneity and instability of the structural state of the iron–carbon melt. Reducing the graphite heterogeneity, either by increasing the defectiveness of the crystalline phase (Fig. 4, *a*) or by decreasing the amorphous phase fraction (Fig. 4, *c*), reduces both the amplitude of the high-frequency component and the stabilization time of kinematic viscosity values, although at different levels of this structure-sensitive property, corresponding to different degrees of non-equilibrium structural state of the melt. The behavior of the subsequent polytherms indicates a higher degree of structural non-equilibrium, characterized by lower kinematic viscosity values.

The mechanism of carbon transfer from the carburizer into liquid iron is one of the key aspects of the physicochemical nature of the carburization process. According to A.A. Vertman and A.M. Samarin [10], based on the relatively low activation energy of graphite dissolution and the specific features of its crystal structure, the dissolution of graphite in liquid iron proceeds in at least two stages: (1) detachment of flat graphite layers from the surface of the solid particle and (2) dissolution of these detached layers.

Table 1. **Results of *X*-ray structural analysis of carbon materials**

Таблица 1. **Результаты рентгеноструктурного исследования углеродсодержащих материалов**

Type of carbon material	Phase No.	Compound (mineralogical name)	Space group	Quantity, %	Coherent scattering region, nm	Lattice parameters, nm	Degree of graphitization
GII-A graphite	*1*	Graphite-2H	$P6_3/mmc$	47.13	29	$a = 0.2459$; $c = 0.6789$	0.53
	2	Graphite-3R	$R\text{-}3m$	25.72	21	$a = 0.2456$; $c = 1.0300$	0.08
	3	Аморфная фаза	–	27.15	–	–	–
GMZ graphite	*1*	Graphite	$P6_3/mmc$	100.00	87	$a = 0.2460$; $c = 0.6731$	0.87
Anthracite	*1*	Graphite-2H	$P6_3/mmc$	16.36	2.04	$a = 0.2200$; $c = 0.6952$	–
	2	Graphite-3R	$R\text{-}3m$	83.64	1.62	$a = 0.2474$; $c = 1.2035$	–
Glassy carbon	*1*	Graphite-2H	$P6_3/mmc$	60.53	1.45	$a = 0.2127$; $c = 0.7471$	–
	2	Graphite-3R	$R\text{-}3m$	39.47	3.24	$a = 0.2438$; $c = 1.0310$	0.04
Electrode scrap	*1*	Graphite-2H	$P6_3/mmc$	18.00	2000	$a = 0.2463$; $c = 0.6714$	0.97
	2	Graphite-2H	$P6_3/mmc$	82.00	2000	$a = 0.2438$; $c = 0.6757$	0.72
Diamond powder	*1*	Diamond	$Fd3m$	97.72	1260	$a = 0.3567$	–
	2	Diamond-n	$R3$	2.28	45	$a = 0.3610$	–

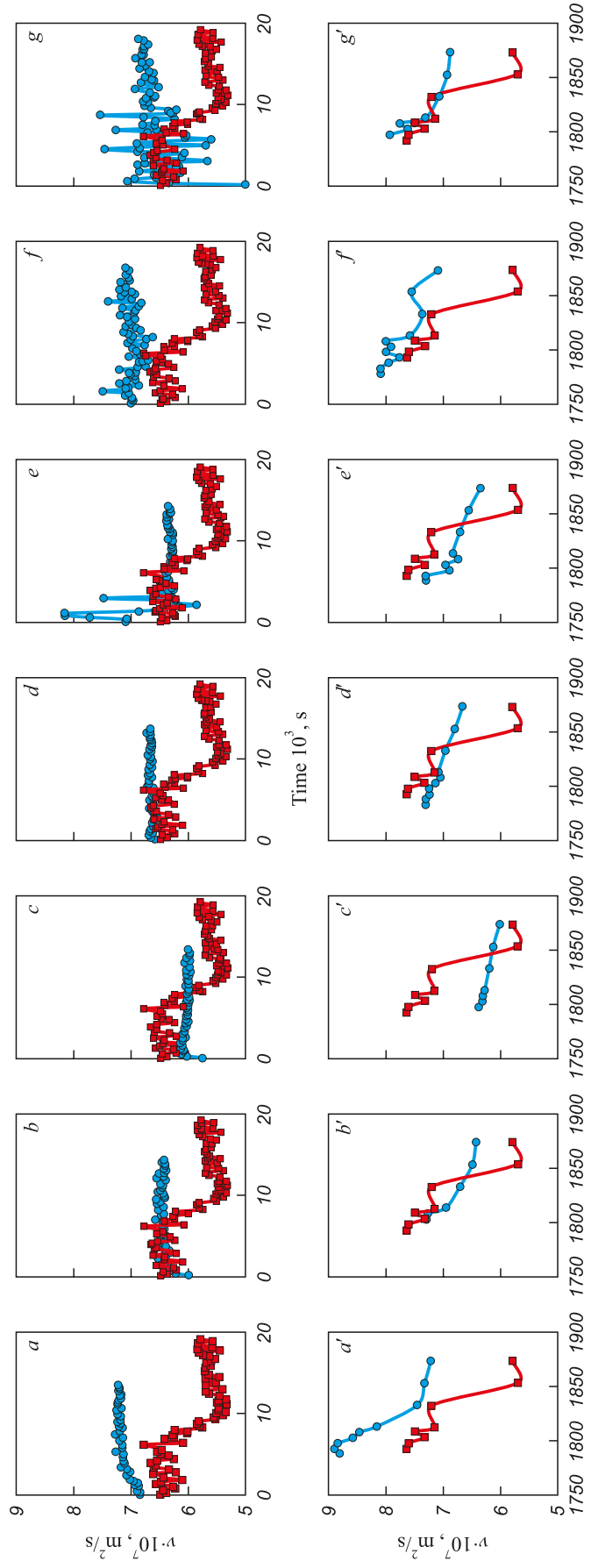

Fig. 3. Results of the viscometric study of dynamics of the Fe – 0.1 % C melt formation during isothermal holding at 1873 K and changes during subsequent cooling to crystallization in comparison with the data for the initial iron (red marker) when using different types of carburizers:
a, *a′* – anthracite; *b*, *b′* –graphite of GMZ grade; *c*, *c′* – graphite of GII-A grade; *d*, *d′* – electrode scrap; *e*, *e′* – glassy carbon;
f, *f′* – diamond powder; *g*, *g′* – nanotubes (heating and melting – mode *1*, crucible material – BeO)

Рис. 3. Результаты исследования методом вискозиметрии динамики формирования расплава Fe – 0,1 % C в ходе изотермической выдержки при 1873 K и изменений в ходе последующего охлаждения до кристаллизации в сопоставлении с данными для исходного железа (красный маркер) при использовании разных типов науглероживателей:
a, *a′* – антрацит; *b*, *b′* – графит марки ГМЗ; *c*, *c′* – графит марки ГИИ-А; *d*, *d′* – электродный бой; *e*, *e′* – стеклоуглерод;
f, *f′* – алмазный порошок; *g*, *g′* – нанотрубки (режим нагрева и плавления – *1*, материал тигля – BeO)

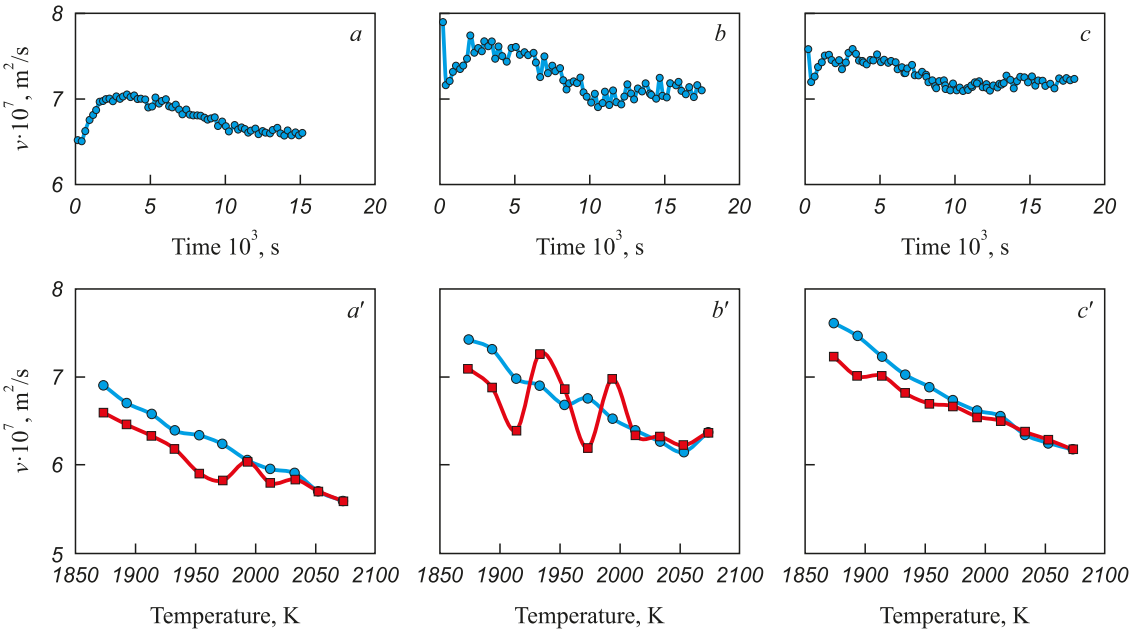

Fig. 4. Results of the viscometric study of dynamics of the melt formation during isothermal holding at 1873 K and changes during subsequent heating to 2023 K (red marker) and cooling to 1873 K (blue marker) during alloying of pure converter iron with carbon (based on obtaining 0.4 % C in the metal) using graphite of GII-A grade from different manufacturers: *a*, *a′*– manufacturer *1*; *б*, *б′* – manufacturer *2*; *в*, *в′* – manufacturer *3* (crucible material – ZrO_2)

Рис. 4. Результаты исследования методом вискозиметрии динамики формирования расплава в ходе изотермической выдержки при 1873 К и изменений в процессе последующего нагрева до 2023 К (красный маркер) и охлаждения до 1873 К (голубой маркер) при легировании углеродом ЖЧК (из расчета получения в металле 0,4% С) при использовании графита марки ГИИ-А разных производителей: *а*, *а′* – производитель *1*; *б*, *б′* – производитель *2*; *в*, *в′* – производитель *3* (материал тигля – ZrO_2)

Accordingly, in addition to crystallite defectiveness and the character and degree of ordering of the carbon hexagonal layers, another significant factor is the type of bonding between the hexagonal networks and their stacks. For different graphites, researchers agree that the interlayer bonds – whether van der Waals, metallic, or weakened covalent [11] – are relatively weak yet stable. The low strength of the bonds between carbon hexagons

Table 2. **Results of *X*-ray structural analysis of graphite of GII-A grade from different manufacturers**

Таблица 2. **Результаты рентгеноструктурного исследования графита марки ГИИ-А разных производителей**

Manufacturer No.	Phase No.	Compound (mineralogical name)	Space group	Quantity, %	Coherent scattering region, nm	Lattice parameters, nm	Degree of graphitization
1	*1*	Graphite-2H	$P6_3/mmc$	64.92	10	$a = 0.2456$; $c = 0.6719$	0.91
	2	Graphite-3R	$R\text{-}3m$	4.07	25	$a = 0.2522$; $c = 3.0889$	0.09
	3	Amorphous phase	–	31.01	–	–	–
2	*1*	Graphite-2H	$P6_3/mmc$	69.63	700	$a = 0.2456$; $c = 0.6721$	0.90
	2	Graphite-3R	$R\text{-}3m$	3.92	25	$a = 0.2522$; $c = 3.0889$	0.09
	3	Amorphous phase	–	26.45	–	–	–
3	*1*	Graphite-2H	$P6_3/mmc$	80.01	1000	$a = 0.2456$; $c = 0.6716$	0.93
	2	Graphite-3R	$R\text{-}3m$	4.05	25	$a = 0.2522$; $c = 3.0889$	0.09
	3	Amorphous phase	–	15.94	–	–	–

(in the form of short hydrocarbon chains [12]) and their partial rupture upon heating facilitate the dissolution of carbon into pure iron when using anthracite, thereby promoting the formation of the most equilibrium structural state, as indicated by the highest kinematic viscosity values. In contrast, when glassy carbon is used, the strong and diverse bonds between hexagonal stacks – including oxygen bridges and triple conjugated (–C≡C–) or double cumulated (=C=C=) C–C bonds [9] – significantly hinder melt formation, increasing the micro-inhomogeneity and instability of its structural state. The even stronger bonding of carbon hexagons in carbon nanotubes may account for the greatest difficulty in melt formation when this material is used as a carburizer.

The use of another allotropic form of carbon – diamond – for carburization of pure iron promotes the formation of a melt structural state with relatively high kinematic viscosity. The noticeable oscillatory component of viscosity variation during melt formation also indicates its micro-inhomogeneity. This behavior may be explained by two factors. First, the spatial configuration of carbon atoms in diamond is similar to that in austenite, allowing carbon to enter the iron lattice as a complete diamond cluster, forming a hybrid of interstitial and substitutional solid solutions [13], which likely facilitates the formation of an fcc-like structural state of the melt. Second, when heated above 1273 K, diamond tends to transform spontaneously into graphite, forming at 1873 K an intermediate carbon structure – a crystalline hybrid of cubic (diamond) and hexagonal (graphite) lattices [14]. Therefore, the observed melt-formation behavior may result from the superposition of graphite dissolution and partial diamond-to-graphite transformation, which undoubtedly enhances the micro-inhomogeneity of the melt's structural state.

Simultaneous carburization and deoxidation of metal

Previously, experiments demonstrated that dissolved oxygen prolongs the time required for the melt to reach structural equilibrium during iron carburization, providing the rationale for treating deoxidation and carburization as concurrent operations [15]. Accordingly, experiments were conducted on simultaneous deoxidation and carburization of iron (Fig. 5). Carbonyl iron with an oxidation level of 870 ppm was used as the base metal. Deoxidation was performed with aluminum to obtain a residual concentration of 0.03 %.

Analysis of the data shows that the previously described influence of the structural parameters of graphitized carbon materials on the degree of structural nonequilibrium of the melt generally persists under these conditions. In particular, using graphite of GMZ grade yields a more equilibrium structural state of the melt than using graphite of GII-A grade. At the same time, melt-formation behavior changes fundamentally when anthracite is used for carburization: the relaxation time becomes the longest, while the kinematic viscosity is the lowest. According to A.A. Vertman [16], dissolved oxygen increases the stability of carbon layer stacks by forming C_xO_y-type oxide films on their surfaces. Under the present conditions, this process is likely most pronounced for natural carbon materials such as anthracite. By contrast, with graphitized materials, oxygen-induced surface deactivation is mitigated because graphitization lowers reactivity and reduces crystal-structure defectiveness [14].

It should be noted separately that the established regularities are consistent with previously obtained experimental data under industrial conditions [3 – 5].

Type of deoxidizer

Under simultaneous deoxidation and carburization, the choice of deoxidizer – in addition to the carbon material – also affects melt-formation behavior. As shown in Fig. 6, deoxidizing carbonyl iron with aluminum and with calcium produces fundamentally different structural states of the melt. With aluminum, the melt shifts to a state with significantly lower kinematic viscosity than that of the starting carbonyl iron. In contrast, calcium deoxidation drives structural changes that increase kinematic viscosity. This response is consistent with a calcium-induced perturbation of the melt's structural state that drives it toward a higher degree of structural equilibrium [17].

Experimental results presented in Fig. 7 show that this deoxidizer-specific effect on the melt's structural state persists under simultaneous deoxidation and carburization. Calcium yields a structural state with substantially higher kinematic viscosity than aluminum, indicating a more nearly equilibrium structure. Moreover, when anthracite is used for carburization, the relaxation time of the introduced non-equilibrium is considerably shorter. The established difference, apart from the distinct effects of the deoxidizers on the structural state of the iron melt, may also be related to the fact that calcium, as a stronger deoxidizer, more effectively neutralizes the influence of oxygen on the deactivation process of the carburizer particle surface.

Overall, the findings show that, during simultaneous deoxidation and carburization, calcium favors the formation of an optimal melt structural state. Therefore, in choosing a deoxidizer, partial or full replacement of aluminum with calcium-containing agents (e.g., calcium carbide) should be considered, particularly for carbide treatment operations.

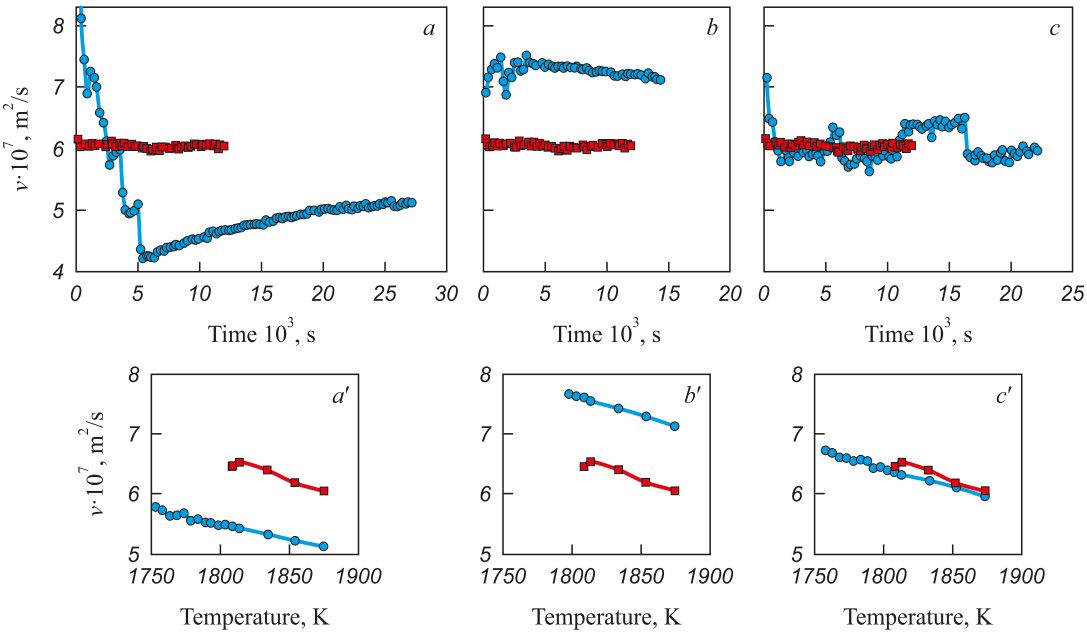

Fig. 5. Results of the viscometric study of dynamics of the Fe – 0.1 % C melt formation with simultaneous deoxidation with aluminum (residual concentration 0.03 %) and carburization during isothermal holding at 1873 K and changes during subsequent cooling to crystallization in comparison with the data for the initial carbonyl iron (red marker) using different types of carburizers: *a*, *a′* – anthracite; *b*, *b′* – graphite of GMZ grade; *c*, *c′* – graphite of GII-A grade (crucible material – BeO)

Рис. 5. Результаты исследования методом вискозиметрии динамики формирования расплава Fe – 0,1 % C при одновременном раскислении алюминием (остаточная концентрация 0,03 %) и науглероживании в ходе изотермической выдержки при 1873 K и изменений в ходе последующего охлаждения до кристаллизации в сопоставлении с данными для исходного карбонильного железа (красный маркер) при использовании разных типов науглероживателей: *a*, *a′* – антрацит; *b*, *b′* – графит марки ГМЗ; *c*, *c′* – графит марки ГИИ-А (материал тигля – BeO)

Conclusions

When forming an iron–carbon melt, the optimal route is carburization of liquid iron with a predominantly FCC-like short-range order. This can be achieved by introducing carbon into the charge, applying forced heating, and melting with substantial superheating above the liquidus.

The structural state of the melt during iron carburization is strongly governed by the structure of the carbon material. With graphitized carbons, it is advisable to reduce the amorphous-phase fraction, increase crystallite size and degree of graphitization, and improve structural homogeneity. Other significant factors include the type of bonding between hexagonal layers and their stacks and the allotropic form of carbon.

The choice of carburizer depends critically on the thermodynamic conditions of melt formation: for pure iron, anthracite gives the most favorable result, whereas for highly oxidized metal, graphitized materials are more effective.

Under simultaneous deoxidation and carburization, an optimal structural state of the iron–carbon melt is promoted by partially or fully substituting aluminum with calcium-containing agents, such as calcium carbide.

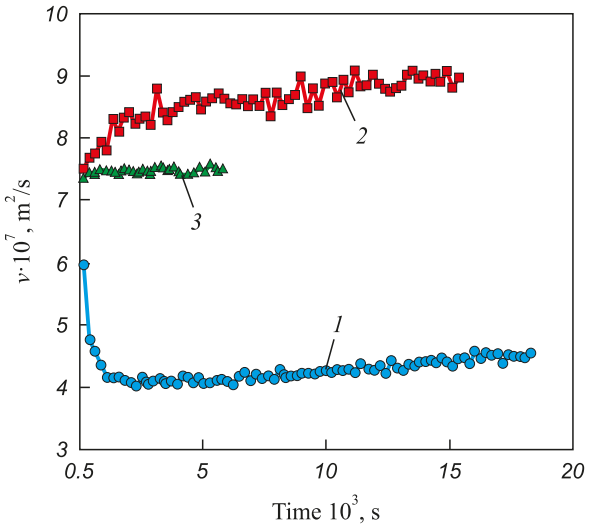

Fig. 6. Results of the viscometric study of dynamics of the melt formation during deoxidation of carbonyl iron by aluminum (*1*) based on a residual concentration of 0.03 % and calcium (*2*) based on a residual concentration of 0.01 % in comparison with the melt formation dynamics of the initial carbonyl iron (*3*) (crucible material – ZrO_2)

Рис. 6. Результаты исследования методом вискозиметрии динамики формирования расплава при раскислении карбонильного железа алюминием (*1*) из расчета остаточной концентрации 0,03 % и кальцием (*2*) из расчета остаточной концентрации 0,01 % в сравнении с динамикой формирования расплава исходного карбонильного железа (*3*) (материал тигля – ZrO_2)

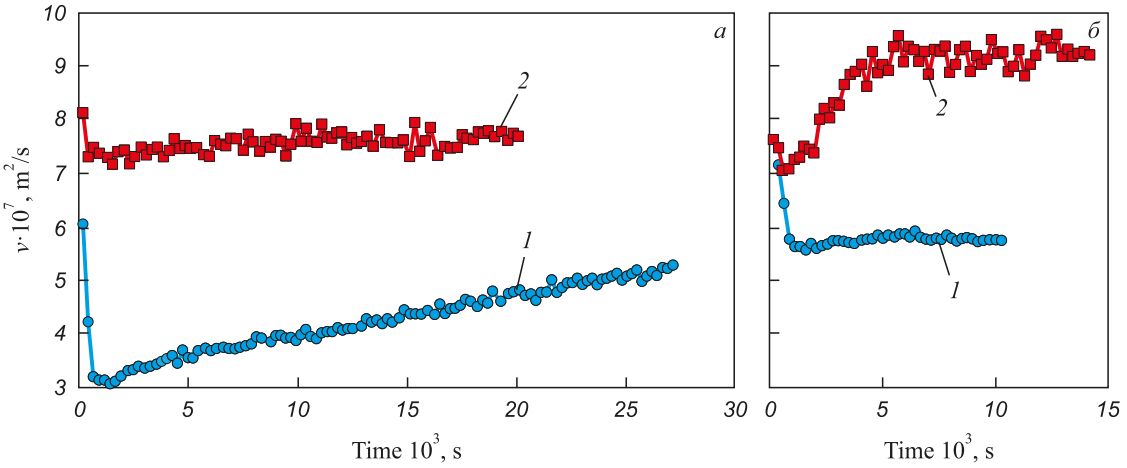

Fig. 7. Results of the viscometric study of dynamics of the melt formation with simultaneous carburization (0.1 % C) and deoxidation of carbonyl iron with aluminum (*1*) based on a residual concentration of 0.03 % and calcium (*2*) based on a residual concentration of 0.01 % using different types of carbon materials: *a* – anthracite; *b* – diamond powder (crucible material – ZrO_2)

Рис. 7. Результаты исследования методом вискозиметрии динамики формирования расплава при одновременном науглероживании (0,1 % С) и раскислении карбонильного железа алюминием (*1*) из расчета остаточной концентрации 0,03 % и кальцием (*2*) из расчета остаточной концентрации 0,01 % при использовании различных типов углеродных материалов: *a* – антрацит; *b* – алмазный порошок (материал тигля – ZrO_2)

References / Список литературы

1. Baum B.A., Khasin G.A., Tyagunov G.V., etc. Liquid Steel. Moscow: Metallurgiya; 1984:208. (In Russ.).

   Баум Б.А., Хасин Г.А., Тягунов Г.В. и др. Жидкая сталь. Москва: Металлургия; 1984:208.
2. Baum B.A., Tyagunov G.V., Baryshev E.E., Tsepelev V.S. Equilibrium and nonequilibrium states of metallic melts. In: *Fundamental Research of Physical Chemistry of Metallic Melts: Proceedings*. Moscow: IKTs Akademkniga; 2002:214–228. (In Russ.).

   Баум Б.А., Тягунов Г.В., Барышев Е.Е., Цепелев В.С. Равновесные и неравновесные состояния металлических расплавов. В кн.: *Фундаментальные исследования физикохимии металлических расплавов: Сборник трудов*. Москва: ИКЦ «Академкнига»; 2002:214–228.
3. Burmasov S.P., Gudov A.G., Degai A.S., Stepanov A.I., Smirnov L.A. Formation of iron-based melts and scope for improvement in steel properties. *Steel in Translation*. 2010;40(8):741–745. https://doi.org/10.3103/S0967091210080127

   Бурмасов С.П., Гудов А.Г., Дегай А.С., Степанов А.И., Смирнов Л.А. Закономерности формирования расплавов на основе железа и металлургические резервы улучшения эксплуатационных свойств сталей. *Сталь*. 2010;(8):42–46.
4. Zuev M.V., Burmasov S.P., Stepanov A.I., Gudov A.G., Murzin A.V., Zhitlukhin E.G. Improvement in steel smelting by studying melt behavior. *Steel in Translation*. 2013;43(2):106–109. https://doi.org/10.3103/S0967091213020204

   Зуев М.В., Бурмасов С.П., Степанов А.И., Гудов А.Г., Мурзин А.В., Житлухин Е.Г. Совершенствование технологии современного сталеплавильного производства на основе закономерностей формирования металлических расплавов. *Сталь*. 2013;(2):27–29.
5. Gudov A.G., Burmasov S.P., Toporov V.A., Murzin A.V. Development of electric steelmaking technology based on the study of non-equilibrium of metal melts. In: *Modern Problems of Steel Electrometallurgy. Proceedings of the XVIII Int. Conf., September 24-27, 2019, Yekaterinburg, Pervouralsk: in 2 parts*. Part 1. Roshchin V.E. ed. Chelyabinsk: SUSU; 2019:3–25. (In Russ.).

   Гудов А.Г., Бурмасов С.П., Топоров В.А., Мурзин А.В. Развитие технологии электросталеплавильного производства на основе исследования неравновесности металлических расплавов. В кн.: *Современные проблемы электрометаллургии стали. Материалы XVIII Международной конференции 24–27 сентября 2019 г., Екатеринбург, Первоуральск: В 2-х частях*. Ч. 1. Под ред. В.Е. Рощина. Челябинск: Издательский центр ЮУрГУ; 2019:3–25.
6. Burmasov S.P., Gudov A.G., Zhitlukhin E.G., Parkhomenko I.P., Stolbov N.S. Directions for reducing chemical heterogeneity of continually cast pipe blank. *Steel in Translation*. 2023;53(9):785–791. https://doi.org/10.3103/s0967091223090048

   Бурмасов С.П., Гудов А.Г., Житлухин Е.Г., Пархоменко И.П., Столбов Н.С. Направления снижения химической неоднородности непрерывнолитой трубной заготовки. *Сталь*. 2023;(8):23–28.
7. Filip'ev S.N., Burmasov S.P., Gudov A.G., etc. Influence of semi-finished product production technology on the quality of liquid metal and the performance properties of spring steel. In: *Proceedings of the XIII Int. Congress of Steelmakers, October 12–18, 2014, Polevskoi*. Yekaterinburg: Ezaprint; 2014:82–87. (In Russ.).

   Филипьев С.Н., Бурмасов С.П., Гудов А.Г. и др. Влияние технологии производства полупродукта на ка-

чество жидкого металла и эксплуатационные свойства рессорной стали. В кн.: *Сборник трудов XIII Международного конгресса сталеплавильщиков 12–18 октября 2014 г., Полевской*. Екатеринбург: ООО «Экспринт»; 2014:82–87.

8. Burmasov S.P., Gudov A.G., Smirnov L.A. Structural states of iron melt and its solutions with vanadium, silicon and carbon. *Teoriya i tekhnologiya metallurgicheskogo proizvodstva*. 2018;(1(24)):21–27. (In Russ.).

   Бурмасов С.П., Гудов А.Г., Смирнов Л.А. Структурные состояния расплава железа и его растворов с ванадием, кремнием и углеродом. *Теория и технология металлургического производства*. 2018;(1(24)):21–27.

9. Fialkov A.S. Carbon-Graphite Materials. Moscow: Energiya; 1979:320. (In Russ.).

   Фиалков А.С. Углеграфитовые материалы. Москва: Энергия; 1979:320.

10. Vertman A.A., Samarin A.M. On the kinetics of carbon dissolution in liquid iron. *Izvestiya AN SSSR. Metally*. 1965;(1):46–54. (In Russ.).

    Вертман А.А., Самарин А.М. О кинетике растворения углерода в жидком железе. *Известия АН СССР. Металлы*. 1965;(1):46–54.

11. Shulepov S.V. Physics of Carbon-Graphite Materials. Moscow: Metallurgiya; 1972:256. (In Russ.).

    Шулепов С.В. Физика углеграфитовых материалов. Москва: Металлургия; 1972:256.

12. Kurakov Yu.I. Development of views on the structure of highly metamorphosed coals. *Izvestiya vuzov. Severo-kavkazskii region. Estestvennye nauki. Prilozhenie*. 2005;(6):100–107. (In Russ.).

    Кураков Ю.И. Развитие взглядов на структуру высокометаморфизованных углей. *Известия вузов. Северокавказский регион. Естественные науки. Приложение*. 2005;(6):100–107.

13. Kraposhin V.S. New mechanism of carbon dissolution in the austenite lattice during steel carburization and its behavior during martensitic and pearlitic transformations of austenite. In: *Nauka i obrazovanie: Scientific Publication of Bauman Moscow State Technical University*. 2011;(11):1–15. (In Russ.).

    Крапошин В.С. Новый механизм растворения углерода в решетке аустенита при цементации стали и его поведение при мартенситном и перлитном превращениях аустенита. В кн.: *Наука и образование: Научное издание МГТУ им. Н.Э. Баумана*. 2011;(11):1–15.

14. Ubbelohde A.R., Lewis F.A. Graphite and Its Crystal Compounds. London: Oxford University Press; 1960:217.

    Убеллоде А.Р., Льюис Ф.А. Графит и его кристаллические соединения. Москва: Мир; 1965:265.

15. Zuev M.V., Burmasov S.P., Gudov A.G., Murzin A.V., Kuzyakin V.G. Carburization of crude steel from a superpowerful arc furnace. *Steel in Translation*. 2014;44(6):433–438. https://doi.org/10.3103/S0967091214060187

    Зуев М.В., Бурмасов С.П., Гудов А.Г., Мурзин А.В., Кузякин В.Г. Исследование и оптимизация технологии науглероживания металла при выплавке стали с использованием полупродукта ДСП. *Сталь*. 2014;(6):25–30.

16. Vertman A.A. Microheterogeneity of metal melts and the problem of regulating the properties of castings. *Fizika i khimiya obrabotki materialov*. 1967;(3):132–141. (In Russ.).

    Вертман А.А. Микрогетерогенность металлических расплавов и проблема регулирования свойств отливок. *Физика и химия обработки материалов*. 1967;(3):132–141.

17. Burmasov S.P., Gudov A.G., Smirnov L.A. On the possibility of increasing the operational properties of steel by technological influences on structural state of iron melts. In: *Influence of the Properties of the Metal Matrix on the Operational Durability of Rails: Proceedings*. Yekaterinburg: JSC UIM; 2006:9–17. (In Russ.).

    Бурмасов С.П., Гудов А.Г., Смирнов Л.А. О возможности повышения эксплуатационных свойств стали путем технологических воздействий на структурное состояние расплавов железа. В кн.: *Влияние свойств металлической матрицы на эксплуатационную стойкость рельсов: Сборник научных трудов*. Екатеринбург: ОАО «УИМ»; 2006:9–17.

Information about the Authors / Сведения об авторах

Aleksandr G. Gudov, *Cand. Sci. (Eng.), Assist. Prof. of the Chair "Metallurgy of Iron and Alloys"*, Ural Federal University named after the first President of Russia B.N. Yeltsin
E-mail: a.g.gudov@urfu.ru

Sergei P. Burmasov, *Cand. Sci. (Eng.), Assist. Prof.*, Ural Federal University named after the first President of Russia B.N. Yeltsin
E-mail: s.p.burmasov@urfu.ru

Leonid A. Smirnov, *Academician, Dr. Sci. (Eng.), Prof., Scientific Director*, JSC "Ural Institute of Metals"
ORCID: 0000-0002-6324-4032
E-mail: secretary@uim-stavan.ru

Александр Геннадьевич Гудов, *к.т.н., доцент кафедры «Металлургия железа и сплавов»*, Уральский федеральный университет имени первого Президента России Б.Н. Ельцина
E-mail: a.g.gudov@urfu.ru

Сергей Петрович Бурмасов, *к.т.н., доцент*, Уральский федеральный университет имени первого Президента России Б.Н. Ельцина
E-mail: s.p.burmasov@urfu.ru

Леонид Андреевич Смирнов, *академик РАН, д.т.н., профессор, научный руководитель*, АО «Уральский институт металлов»
ORCID: 0000-0002-6324-4032
E-mail: secretary@uim-stavan.ru

Contribution of the Authors

A. G. Gudov – planning and conducting experiments, generalization and analysis of results, writing the text.

S. P. Burmasov – highly professional consulting and active participation in setting tasks and discussing research results, choosing approaches to interpreting experimental data and assessing the validity of conclusions.

L. A. Smirnov – highly professional consulting and active participation in setting tasks and discussing research results, choosing approaches to interpreting experimental data and assessing the validity of conclusions.

Вклад авторов

А. Г. Гудов – планирование и проведение экспериментальных исследований, обобщение и анализ результатов, написание статьи.

С. П. Бурмасов – высокопрофессиональное консультирование и активное участие в постановке задач и обсуждении результатов исследования, выборе подходов к трактовке экспериментальных данных и оценке обоснованности выводов.

Л. А. Смирнов – высокопрофессиональное консультирование и активное участие в постановке задач и обсуждении результатов исследования, выборе подходов к трактовке экспериментальных данных и оценке обоснованности выводов.

Received 22.04.2025
Revised 27.04.2025
Accepted 06.06.2025

Поступила в редакцию 22.04.2025
После доработки 27.04.2025
Принята к публикации 06.06.2025

PHYSICO-CHEMICAL BASICS OF METALLURGICAL PROCESSES / ФИЗИКО-ХИМИЧЕСКИЕ ОСНОВЫ МЕТАЛЛУРГИЧЕСКИХ ПРОЦЕССОВ

UDC 532.13+546.73'27+546.73'28
DOI 10.17073/0368-0797-2025-5-517-525

Original article
Оригинальная статья

Viscosity of liquid alloys of cobalt with silicon and boron: Experiment and calculation

N. V. Olyanina, A. L. Beltyukov, V. I. Ladyanov

Udmurt Federal Research Center of the Ural Branch of the Russian Academy of Sciences (34 Tatyana Baramzina Str., Izhevsk, Udmurtian Republic 426067, Russian Federation)

oljanina@mail.ru

Abstract. The temperature (up to 1700 °C) and concentration dependences of the viscosity of liquid binary alloys of cobalt with silicon and boron were studied using an oscillating-cup method. The viscosity polytherms of liquid cobalt and its melts with silicon and boron (up to 54 at. % of the metalloid) are monotonous character without any anomalies and are well described by the Arrhenius equation. Coincidence of the viscosity polytherms obtained in the heating and cooling modes and linear dependence of the viscosity logarithm on the inverse absolute temperature in the supercooled region indicate the preservation of the liquid alloy structure. Microheterogeneous structure of Co–Si and Co–B melts (up to 54 at. % metalloid), associated with the formation of microgroups based on silicides and borides of cobalt with stronger internal bonds, leads to a complex form of concentration dependences of their viscosity and activation energy of viscous flow. The prognostic capabilities of the Kozlov-Romanov-Petrov and Kaptay equations for describing the concentration dependences of the viscosity of liquid metal-metalloid alloys are discussed. Features associated with the application of these equations to the systems in which one of the alloy components (in this case, boron in the Co–B system) is in the solid state at the calculation temperatures are considered. It is shown that the correct way to solve the problem is to use the viscosity value of liquid boron at its melting point as an input parameter for calculating the viscosity isotherms of the Co–B melts. The Kozlov-Romanov-Petrov and Kaptay equations differ only in the coefficients before the melt mixing enthalpy, the physical meaning of which is discussed in the paper. The Kozlov-Romanov-Petrov equation can be recommended for predicting the concentration dependences of the viscosity of liquid alloys of cobalt with silicon and boron.

Keywords: melt, Co–B system, Co–Si system, viscosity, temperature dependence of viscosity, concentration dependence of viscosity, Arrhenius equation, Kozlov-Romanov-Petrov equation, Kaptay equation

For citation: Olyanina N.V., Beltyukov A.L., Ladyanov V.I. Viscosity of liquid alloys of cobalt with silicon and boron: Experiment and calculation. *Izvestiya. Ferrous Metallurgy*. 2025;68(5):517–525. https://doi.org/10.17073/0368-0797-2025-5-517-525

Вязкость жидких сплавов кобальта с кремнием и бором: эксперимент и расчет

Н. В. Олянина, А. Л. Бельтюков, В. И. Ладьянов

Удмуртский федеральный исследовательский центр Уральского отделения РАН (Россия, 426067, Удмуртская Республика, Ижевск, ул. им. Татьяны Барамзиной, 34)

oljanina@mail.ru

Аннотация. Методом крутильных колебаний проведены исследования температурных (до 1700 °С) и концентрационных зависимостей вязкости жидких бинарных сплавов кобальта с кремнием и бором. Температурные зависимости вязкости жидкого кобальта и его расплавов с кремнием и бором (до 54 ат. % металлоида) имеют монотонный характер без каких-либо особенностей и хорошо описываются уравнением Аррениуса. Совпадение политерм вязкости, полученных в режиме нагрева и охлаждения, а также линейная зависимость логарифма вязкости от обратной абсолютной температуры в переохлажденной области свидетельствуют о сохранении структуры жидкого сплава. Микронеоднородное строение расплавов Co–Si и Co–B (до 54 ат. % металлоида), связанное с образованием микрогруппировок на основе силицидов и боридов кобальта с более прочными внутренними связями, приводит к сложному виду концентрационных зависимостей их вязкости и энергии активации вязкого течения. В статье авторы обсуждают прогностические возможности уравнений Козлова-Романова-Петрова и Kaptay для описания концентрационных зависимостей вязкости жидких сплавов типа металл–металлоид. Рассмотрены особенности, связанные с применением этих уравнений к системам, в которых один из компонентов сплава (в данном случае бор в системе Co–B) при температурах расчета находится в твердом состоянии. Показано, что корректным способом решения проблемы является использование значения вязкости жидкого бора при его температуре плавления в качестве входного параметра для расчета изотерм вязкости расплавов системы Co–B. Уравнения Козлова-Романова-Петрова и Kaptay отличаются только коэффициентами перед

энтальпией смешения расплава, физический смысл которых обсуждается в работе. Уравнение Козлова-Романова-Петрова может быть рекомендовано для прогнозирования концентрационных зависимостей вязкости жидких сплавов кобальта с кремнием и бором.

Ключевые слова: расплав, система Co – B, система Co – Si, вязкость, температурная зависимость вязкости, концентрационная зависимость вязкости, уравнение Аррениуса, уравнение Козлова-Романова-Петрова, уравнение Kaptay

Для цитирования: Олянина Н.В., Бельтюков А.Л., Ладьянов В.И. Вязкость жидких сплавов кобальта с кремнием и бором: эксперимент и расчет. *Известия вузов. Черная металлургия*. 2025;68(5):517–525. https://doi.org/10.17073/0368-0797-2025-5-517-525

Introduction

Viscosity is an important physical property of a liquid, governed by interparticle interactions and linked to its structure. It is therefore widely used to probe the structure of high-temperature metallic melts. This is especially relevant for metal-metalloid systems, for which direct diffraction studies have been performed only for individual alloys [1] or at small superheatings above the liquidus line [2]; moreover, the coexistence of metallic and covalent bonding makes the use of modeling methods for these systems a persistent challenge [3; 4].

Accurate viscosity values are needed for many metallurgical processes involving the liquid state [5 – 7]. To predict the viscosity of multicomponent liquid alloys, thermodynamic-based equations are used, in particular the Kozlov–Romanov–Petrov equation [8] and the Kaptay equation [9]. The required input data for these equations are the viscosities of the pure liquid components that form the melt and the melt mixing enthalpy. According to [10], these equations predict the concentration dependences of viscosity well across systems with different phase diagrams. However, validation has mostly been carried out for metal–metal systems. Many advanced materials, by contrast, contain metalloids as well as high-melting elements such as boron, tantalum, and niobium. The presence of refractory elements complicates the application of these equations, because calculations are performed at temperatures at which these elements are in the solid state.

In the present work, experimental measurements of the viscosity of liquid alloys in the Co – Si and Co – B systems are reported, and the applicability of the Kozlov–Romanov–Petrov and Kaptay equations for predicting their concentration dependence is analyzed.

Materials and methods

Co – Si and Co – B master alloys (54 at. % metalloid) were produced in a vacuum resistance furnace by alloying cobalt powder grade PK-1u per GOST 9721–79 (cobalt content ≥99.35 wt. %; principal impurities, wt. %: <0.2 Fe; 0.4 Ni; 0.02 Si and C; 0.04 Cu) with single-crystal silicon (99.9999 wt. % Si) or amorphous boron per TU 113–12–132–83 (94 wt. % B; principal impurities, wt. %: 0.23 Fe; 0.1 Si) in a corundum crucible at a pressure of 10^{-2} Pa, a temperature of 1550 °C, and a 20-min hold. Samples of the required composition were then obtained by alloying cobalt grade K0 per GOST 123–2008 (cobalt content ≥99.98 wt. %; principal impurities, wt. %: <0.003 Fe; <0.005 Ni and C; up to 0.001 Si, Cu, Mg, Zn, and Al) with the Co – Si or Co – B master alloys in the viscometer furnace immediately prior to viscosity measurements.

The kinematic viscosity (ν) of the liquid alloys was measured on an automated setup [11] using the oscillating-cup method in the Shvidkovsky modification [12]. Experiments were carried out in a protective helium atmosphere (grade A) after evacuating the chamber to a pressure of 10^{-2} Pa. Viscosity was measured on heating and subsequent cooling, with stepwise temperature increments of 20 – 30 °C following 10-min isothermal holds at each temperature step. Measurements were carried out in cylindrical Al_2O_3 crucibles with two opposing end-face friction surfaces (the crucible bottom and a lid resting on the melt surface). To create the second end-face surface, a lid with an outer diameter 0.5 – 0.8 mm smaller than the crucible's inner diameter was placed on the sample. The lid design [13; 14] allows free translation along the crucible's vertical axis and co-oscillation with the crucible during torsional oscillations of the suspension system. Using two end-face friction surfaces helps account for uncertainties in viscosity calculations arising from potential oxide-film formation on the melt surface [13; 15] and from wetting of the crucible walls by the liquid metal (meniscus effects) [16; 17]. Prior to viscosity measurements, the samples were remelted at 1680 °C for 10 min to eliminate irreversible processes associated with alloying of the initial charge materials. The total error of viscosity determination at the 0.95 confidence level does not exceed 4 %, with a single-measurement error of 1.5 %; error analysis followed the procedure in [11].

Dynamic viscosity (η) was obtained using literature density data [18 – 20].

Equations for calculating viscosity

The Kozlov–Romanov–Petrov equation [8] was derived within the framework of the theory of oscillatory liquids by relating atomic vibrational motions to the free energy of the solution using the Einstein approximation, and has the following form:

$$\ln \eta = x_1 \ln \eta_1 + x_2 \ln \eta_2 - \frac{\Delta H}{3RT}, \qquad (1)$$

where η and η_i are the dynamic viscosity of the melt and of its pure components ($i = 1, 2$), respectively; x_i is the mole fraction of component i in the alloy; ΔH is the integral mixing enthalpy of the melt; R is the universal gas constant; T is the absolute temperature.

The Kaptay equation [9] is a modification of Eyring's equation [21] for multicomponent alloys and has the following form:

$$\eta = \frac{hN_A}{\sum_{i=1}^{2}\left(x_i V_i\right) + V^E} \exp\left(\frac{\sum_{i=1}^{2}\left(x_i \Delta G_i^*\right) - \alpha \Delta H}{RT}\right), \qquad (2)$$

where V_i is the molar volume of pure component i in the liquid state ($V_i = M_i/\rho_i$, where ρ_i is the density of pure component i in the liquid state, M_i is the molar mass of component i in the alloy); V^E is the excess molar volume upon alloy formation, which is neglected for simplicity; $\alpha = 0.155 \pm 0.015$ is a parameter obtained from the ratio of the activation energy of viscous flow of pure liquid metals to their cohesive energy at the melting temperature; ΔG_i^* is the free energy of activation of viscous flow of pure component i in the liquid state, which is calculated from the measured viscosity of the pure component at a given temperature by the following expression:

$$\Delta G_i^* = RT \ln\left(\frac{\eta_i V_i}{hN_A}\right).$$

Results and discussion

The kinematic viscosity of melts in the Co–B (37 compositions) and Co–Si (24 compositions) systems was investigated over the range from 0 to 54 at. % metalloid. Typical viscosity polytherms are shown in Figs. 1 and 2. The viscosity polytherms exhibit no anomalies and are well approximated by the Arrhenius equation:

$$\nu = A \exp\left(\frac{E_a}{RT}\right), \qquad (3)$$

where A is a constant; E_a is the activation energy of viscous flow. In repeated experiments, the measured data are reproduced within the measurement error (Fig. 2). The absence of differences between viscosities obtained on heating and on cooling, together with the linear dependence of lnν on the inverse absolute temperature in the supercooled region, indicates preservation of the liquid alloy structure over the temperature range studied.

Based on the obtained viscosity polytherms, the concentration dependences for the liquid alloys of the Co–Si and Co–B systems were calculated (Figs. 3, 4). The isotherms of viscosity and of the activation energy of viscous flow for cobalt–silicon and cobalt–boron melts are nonmonotonic and dome-shaped, providing indirect evidence of structural rearrangements in the melt as the metalloid content varies. The maximum in the viscosity–composition curve is attributed to the formation of atomic microgroups composed of unlike atoms, presumably ordered in the manner of intermetallic compounds [22].

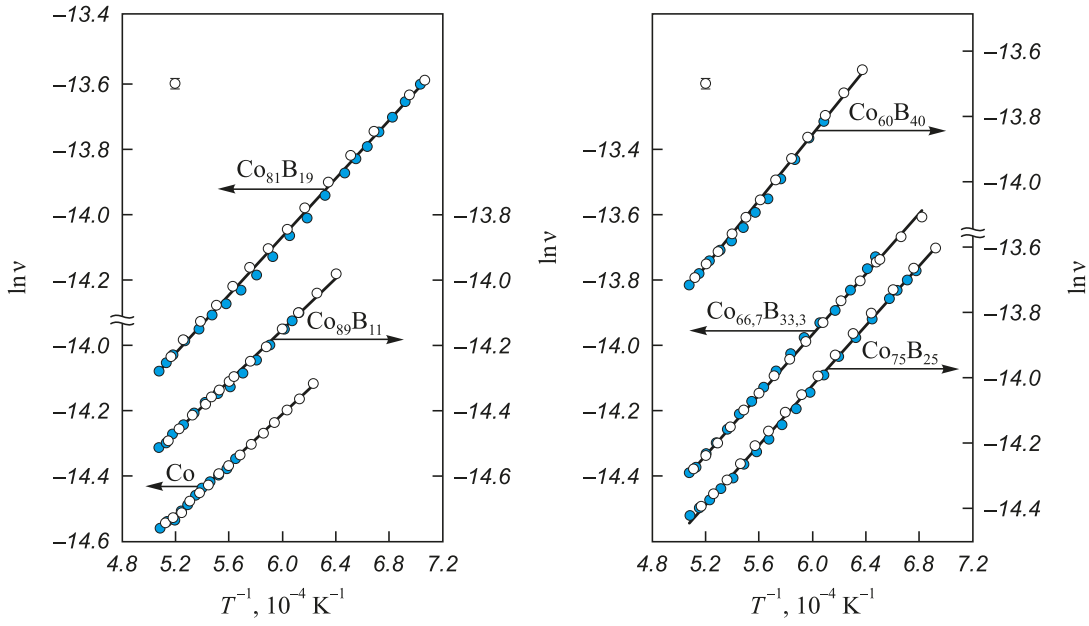

Fig. 1. Viscosity polytherms in lnν – T^{-1} coordinates of the Co–B (at. %) melts in heating (●) and subsequent cooling (○) mode. The graph shows the error of a single experiment of 1.5 %

Рис. 1. Политермы вязкости в координатах lnν – T^{-1} расплавов системы Co–B (ат. %) в режиме нагрева (●) и последующего охлаждения (○). На графике приведена погрешность единичного эксперимента 1,5 %

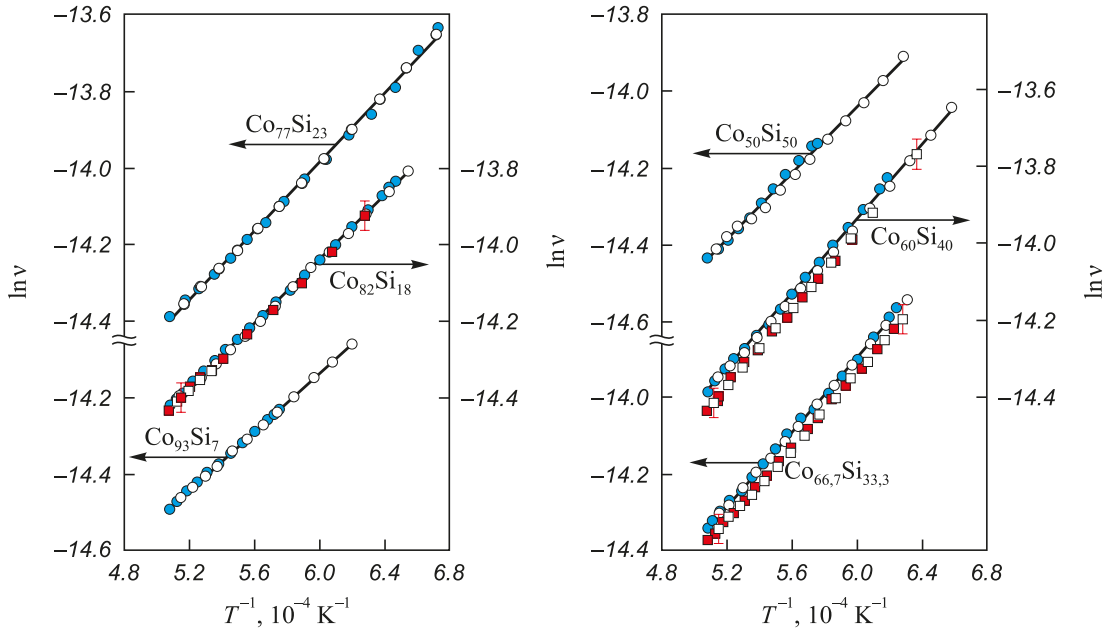

Fig. 2. Viscosity polytherms in lnν – T^{-1} coordinates of the Co–Si (at. %) melts in heating (●, ■) and subsequent cooling (○, □) mode, where ●, ○ is the first sample, and ■, □ is the second sample. The graph shows a total error of 4 %

Рис. 2. Политермы вязкости в координатах lnν – T^{-1} расплавов системы Co–Si (ат. %) в режиме нагрева (●, ■) и последующего охлаждения (○, □), где ●, ○ – первый образец; ■, □ – второй образец. На графике приведена общая погрешность 4 %

Because the maximum on the viscosity isotherm of the Co – Si system coincides with the presence of Co_2Si on the phase diagram, melts containing 30 – 35 at. % Si are likely to exhibit Co_2Si-type ordering. At silicon contents below 30 at. % and above 35 at. %, the melts are microheterogeneous: below 30 at. % Si they contain, in addition to Co_2Si-type microgroups, regions dominated by cobalt atoms, whereas above 35 at. % Si they contain silicon-richer microgroups, for example of the CoSi type.

In the Co – B system, the viscosity changes little over 0 – 20 at. % B, which likely reflects short-range order consistent with a solid-solution–like arrangement in the melt. At boron contents above 20 at. %, both ν and E_a increase, attributable to the formation of atomic microgroups of unlike atoms, presumably ordered in the manner of a compound. However, in this system no correlation is observed between the maxima of the viscosity isotherms and the stoichiometries of compounds on the phase diagram.

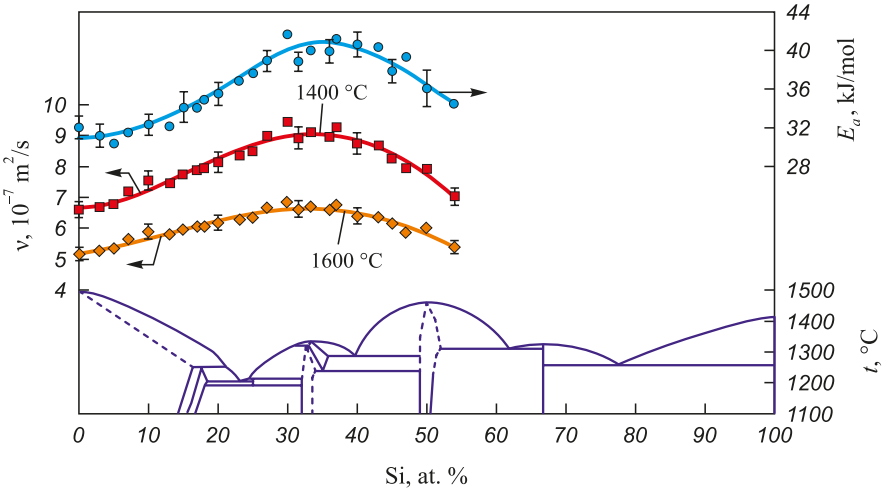

Fig. 3. Concentration dependences of kinematic viscosity and activation energy of viscous flow of the Co–Si melts. A part of the phase diagram of the Co–Si system is given according to the data from [23]

Рис. 3. Концентрационные зависимости кинематической вязкости и энергии активации вязкого течения расплавов системы Co–Si. Приведен фрагмент диаграммы состояния системы Co–Si по данным работы [23]

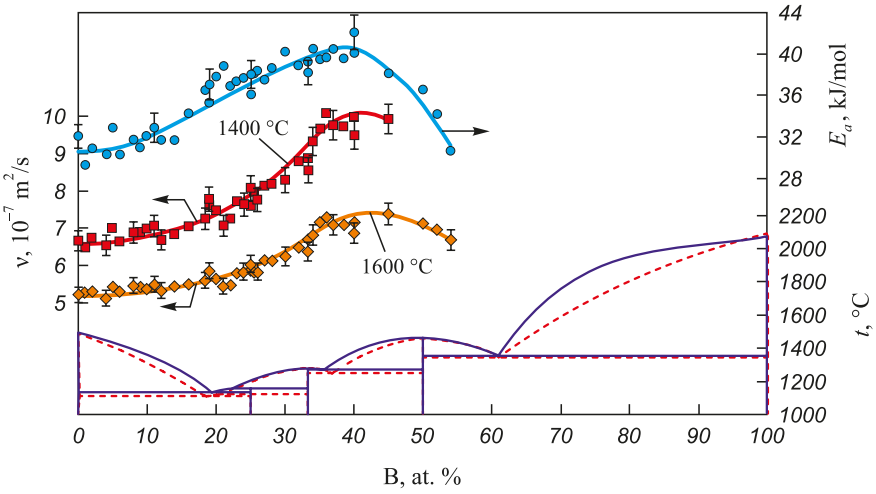

Fig. 4. Concentration dependences of a kinematic viscosity and activation energy of viscous flow of the Co–B melts. The parts of the phase diagram of the Co–B system is given according to the data from [24] (——) and [25] (– – –)

Рис. 4. Концентрационные зависимости кинематической вязкости и энергии активации вязкого течения расплавов системы Co–B. Приведены фрагменты диаграммы состояния системы Co–B по данным работ [24] (——) и [25] (– – –)

The monotonic, exponential character of the viscosity polytherms without hysteresis, together with retention of the viscosity-isotherm shape on heating, indicates that no substantial structural changes occur during heating. This suggests that microgroups of cobalt silicides and borides persist throughout the temperature range investigated.

Fig. 5 presents the results of calculating the concentration dependence of viscosity for Co–Si melts. The required data on the mixing enthalpy of the melt and the viscosity of liquid silicon were taken from [26; 27]. As seen in Fig. 5, the Kozlov–Romanov–Petrov equation predicts not only viscosity values close to the experimental data but also the observed dome-shaped concentration behavior. The maximum deviation of the calculated from the experimental values is +11 %.

Equation (2) was recast into the following form by using the expansion $\ln V_i = V_i - 1$ and setting $V^E = 0$.

$$\ln \eta = x_1 \ln \eta_1 + x_2 \ln \eta_2 - \frac{(0.155 \pm 0.015)\Delta H}{3RT}. \qquad (4)$$

Neglect of the excess molar volume upon alloy formation was also employed in [8] when deriving the Kozlov–Romanov–Petrov equation. Thus, the Kozlov–Romanov–Petrov and Kaptay equations have similar forms and differ only in the coefficient before ΔH. In deriving Equation (1), it was assumed, to first approximation, that atomic motion in a metallic melt is dominated by simple three-dimensional vibrations; hence the coefficient in front of ΔH equals 1/3. In the Kaptay equation the coefficient is 1/6.5, which follows if, in addition to three vibrational degrees of freedom, three rotational degrees of freedom of a nonlinear molecule are considered. In the derivation of Equation (2), only a small fraction of the cohesive energy (enthalpy) was assumed to be expended during viscous flow; therefore, $\alpha = \Delta Z/Z$, where ΔZ is the number of broken bonds during viscous flow and Z is the average coordination number of the melt. Accordingly, $\Delta Z/Z = 1/3$ for the Kozlov–Romanov–Petrov model and $\Delta Z/Z = 1/6.5$ for the Kaptay model. Reference [28] concluded that in a close-packed liquid ($Z = 12$) three bonds are broken during flow, i.e., $\Delta Z/Z = 3/12 = 1/4$. This coef-

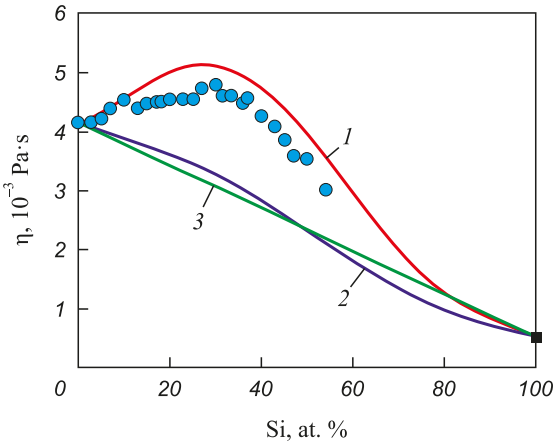

Fig. 5. Calculation results for concentration dependence of dynamic viscosity (η) of the Co–Si melts at 1600 °C obtained using equations:
1 – Kozlov-Romanov-Petrov (eq. 1);
2 – Kaptay (eq. 4);
3 – additive dependence of viscosity ($\eta_{add} = x_1\eta_1 + x_2\eta_2$);
● – our experimental data; ■ – experimental data for pure silicon [27]

Рис. 5. Результаты расчета концентрационной зависимости динамической вязкости (η) расплавов системы Co–Si при 1600 °C по уравнениям:
1 – Козлова-Романова-Петрова (уравнение (1));
2 – Kaptay (уравнение (4));
3 – аддитивная зависимость вязкости ($\eta_{add} = x_1\eta_1 + x_2\eta_2$);
● – экспериментальные данные; ■ – экспериментальные данные для чистого кремния по данным работы [27]

ficient is close to that implied by the Kozlov–Romanov–Petrov equation, which indeed provides the best prediction of the concentration dependence of viscosity for Co – Si melts (Fig. 5). These findings are also consistent with diffraction data [2] indicating that liquid cobalt and Co – Si melts (up to 40 at. % Si) possess a close-packed atomic structure.

When calculating the concentration dependence of viscosity for the Co – B system, two issues arise due to the very high melting temperature ($t_m \approx 2075$ °C) of the second pure component, boron, relative to the calculation temperature. The first concerns the choice of the dynamic viscosity (η_B) and density (ρ_B) of pure boron required to compute the molar volume of the melt. Two approaches are possible: assign to η_B and ρ_B the values for liquid boron at its melting point, namely $\eta_B = (2.6 \pm 0.3)\cdot10^{-3}$ Pa·s [29] and $\rho_B = 2170 \pm 43$ kg/m^3 [30]; or extrapolate the viscosity polytherm of liquid boron using Equation (3) [29] and extrapolate the density polytherm linearly [30] to 1627 °C, the temperature at which the binary isotherm is calculated (supercooled liquid boron), yielding $\eta_B = (10 \pm 1)\cdot10^{-3}$ Pa·s and $\rho_B = 2285 \pm 46$ kg/m^3. The second issue is the choice of the concentration dependence of the mixing enthalpy (ΔH) for Co – B melts with the standard states taken as either "crystalline boron – liquid cobalt" [31] or "liquid supercooled boron – liquid cobalt" [32].

The effects of varying the dynamic viscosity of boron and the mixing enthalpy on the predictive capability of the equations are shown in Fig. 6. Using properties of supercooled liquid boron at 1627 °C in the viscosity-isotherm calculations yields an incorrect additive (ideal solution) trend for the viscosity of the Co – B system (Fig. 6, *c*, *d*). Because Co – B melts exhibit strong unlike-atom interactions [33], a positive deviation of the viscosity isotherm from the additive dependence expected for an ideal solution is anticipated. In contrast, using the viscosity of liquid boron at its melting point as an input yields an additive trend consistent with the experimentally determined isotherm (Fig. 6, *a*, *b*). This approach should also be useful for systems whose components have markedly different melting temperatures.

As seen in Fig. 6, the closest agreement between calculated and experimental viscosity isotherms is obtained when the viscosity of liquid boron at its melting point is combined with the mixing enthalpy referenced to the standard states "crystalline boron – liquid cobalt" [31] (Fig. 6, *a*). Under these conditions, the Kaptay equation reproduces the data up to 20 at. % B, whereas the Kozlov–Romanov–Petrov equation performs better in the 40 – 54 at. % B range. The deviations from experiment are –16 % for the Kaptay equation and +17 % for the Kozlov–Romanov–Petrov equation.

Despite the difficulties in choosing parameter values for calculating the concentration dependences of viscosity in the Co – B system, both the Kozlov–Romanov–Petrov and Kaptay equations predict physically reasonable viscosity values. Given their simple form and the availability of the required parameters in standard data sources, these equations are recommended for predicting viscosity isotherms of liquid systems.

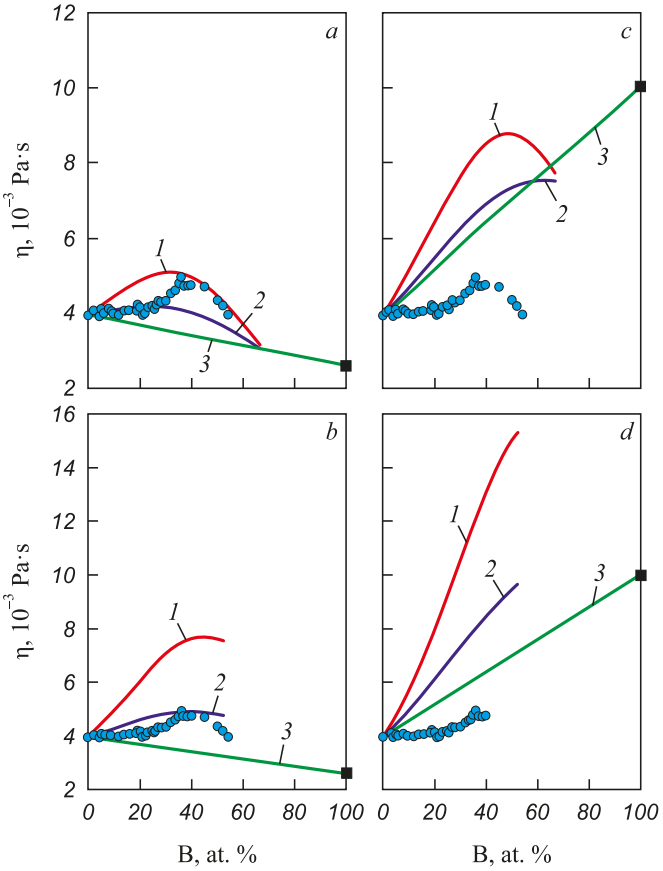

Fig. 6. Calculation results for concentration dependence of dynamic viscosity (η) of the Co – B melts at 1627 °C obtained using equations:
1 – Kozlov-Romanov-Petrov (eq. 1);
2 – Kaptay (eq. 4);
3 – additive dependence of viscosity ($\eta_{add} = x_1\eta_1 + x_2\eta_2$);
● – our experimental data;
■ – experimental data for pure boron.
The following input data were used for calculation:
a – ΔH from [31] and $\eta_B = (2.6 \pm 0.3)\cdot10^{-3}$ Pa·s;
b – ΔH from [32] and $\eta_B = (2.6 \pm 0.3)\cdot10^{-3}$ Pa·s;
c – ΔH from [31] and $\eta_B = (10 \pm 1)\cdot10^{-3}$ Pa·s;
d – ΔH from [32] and $\eta_B = (10 \pm 1)\cdot10^{-3}$ Pa·s

Рис. 6. Результаты расчета концентрационной зависимости динамической вязкости расплавов системы Co – B при 1627 °C по уравнениям:
1 – Козлова-Романова-Петрова (уравнение (1));
2 – Kaptay (уравнение (4));
3 – аддитивная зависимость вязкости ($\eta_{add} = x_1\eta_1 + x_2\eta_2$);
● – экспериментальные данные;
■ – экспериментальные данные для чистого бора.
Для расчета использовались следующие входные данные:
a – ΔH из [31] и $\eta_B = (2{,}6 \pm 0{,}3)\cdot10^{-3}$ Па·с;
b – ΔH из [32] и $\eta_B = (2{,}6 \pm 0{,}3)\cdot10^{-3}$ Па·с;
c – ΔH из [31] и $\eta_B = (10 \pm 1)\cdot10^{-3}$ Па·с;
d – ΔH из [32] и $\eta_B = (10 \pm 1)\cdot10^{-3}$ Па·с

Conclusions

The kinematic viscosity of liquid cobalt and its binary melts with silicon and boron was measured by the oscillating-cup method over wide temperature (up to 1700 °C) and composition (0 – 54 at. % metalloid) ranges.

The resulting viscosity polytherms, obtained on heating and on cooling, coincide (no hysteresis), are monotonic, and are well described by the Arrhenius equation. Their exponential character indicates preservation of the liquid alloy structure in both liquid and supercooled states.

The concentration dependences of viscosity and of the activation energy of viscous flow for Co – Si and Co – B melts are nonmonotonic and dome-shaped, with maxima at 35 at. % Si and 40 at. % B, respectively – signatures of composition-driven structural changes in the melt.

For the first time, concentration dependences of viscosity of high-temperature metal–metalloid melts were calculated using thermodynamic-based equations. The Kozlov–Romanov–Petrov equation provides the best overall prediction for the Co – Si and Co – B systems, with maximum deviations from experiment of 11 and 17 %, respectively. A practical procedure is proposed for predicting viscosity isotherms in liquid systems whose components have substantially different melting temperatures.

References / Список литературы

1. Gruner S., Marczinke J., Hennet L., Hoyer W., Cuello G.J. On the atomic structure of liquid Ni–Si alloys: A neutron diffraction study. *Journal of Physics: Condensed Matter*. 2009;21(38):385403. http://doi.org/10.1088/0953-8984/21/38/385403
2. Roik A.S., Sokol'skii V.E., Kazimirov V.P. *X*-ray differaction investigation moltem Co-Si system. *Rasplavy*. 2003;(6): 69–69. (In Russ.).

   Роик А.С., Сокольский В.Э., Казимиров В.П. Рентгенодифракционное исследование структуры расплавов системы Co-Si. *Расплавы*. 2003;(6):69–69.
3. Wang H.P., Wei B. Thermophysical property of undercooled liquid binary alloy composed of metallic and semiconductor elements. *Journal of Physics D: Applied Physics*. 2008;42(3):035414. http://doi.org/10.1088/0022-3727/42/3/035414
4. Sun H., Zhang C., Tang L., Wang R., Xia W., Wang C.Z. Molecular dynamics simulation of Fe-Si alloys using a neural network machine learning potential. *Physical Review B*. 2023;107(22):224301. https://doi.org/10.1103/PhysRevB.107.224301
5. Ravi K.R., Pillai R.M., Amaranathan K.R., Pai B.C., Chakraborty M. Fluidity of aluminum alloys and composites: A review. *Journal of Alloys and Compounds*. 2008;456(1-2): 201–210. https://doi.org/10.1016/j.jallcom.2007.02.038
6. Parthiban R., Stoica M., Kaban I., Kumar R., Eckert J. Viscosity and fragility of the supercooled liquids and melts from the Fe–Co–B–Si–Nb and Fe–Mo–P–C–B–Si glass-forming alloy systems. *Intermetallics*. 2015;66:48–55. https://doi.org/10.1016/j.intermet.2015.06.016
7. Shi R., Luo A.A. Applications of CALPHAD modeling and databases in advanced lightweight metallic materials. *Calphad*. 2018;62:1–17. https://doi.org/10.1016/j.calphad.2018.04.009
8. Kozlov L.Ya., Romanov L.M., Petrov N.N. Prediction of viscosity of multicomponent metallic melts. *Izvestiya. Ferrous Metallurgy*. 1983;26(3):7–11. (In Russ.).

   Козлов Л.Я., Романов Л.М., Петров Н.Н. Прогнозирование вязкости многокомпонентных металлических расплавов. *Известия вузов. Черная металлургия*. 1983;26(3):7–11.
9. Kaptay G. A new equation to estimate the concentration dependence of the viscosity of liquid metallic alloys from the heat of mixing data. In: *Proceedings of microCAD 2003 conference, Section C: Metallurgy, March 6–7, 2003, Miskolc*. Miskolc: University of Miskolc; 2003:23–28.
10. Gąsior W. Viscosity modeling of binary alloys: Comparative studies. *Calphad*. 2014;44:119–128. https://doi.org/10.1016/j.calphad.2013.10.007
11. Bel'tyukov A.L., Lad'yanov V.I. An automated setup for determining the kinematic viscosity of metal melts. *Instruments and Experimental Techniques*. 2008;51:304–310. https://doi.org/10.1134/S0020441208020279

    Бельтюков А.Л., Ладьянов В.И. Автоматизированная установка для определения кинематической вязкости металлических расплавов. *Приборы и техника эксперимента*. 2008;(20):155–161.
12. Shvidkovsky E.G. Certain Problems of Molten Metals Viscosity. Moscow: Gostekhizdat; 1955:208. (In Russ.).

    Швидковский Е.Г. Некоторые вопросы вязкости расплавленных металлов. Москва: Гостехиздат; 1955:208.
13. Olyanina N.V., Bel'tyukov A.L., Goncharov O.Yu., Lad'yanov V.I. Influence of surface film on results of measuring the viscosity of $Co_{83}B_{17}$ melt by method of torsional vibrations. *Rasplavy*. 2012;(2):83–90. (In Russ.).

    Олянина Н.В., Бельтюков А.Л., Гончаров О.Ю., Ладьянов В.И. Влияние поверхностной пленки на результаты измерения вязкости расплава $Co_{83}B_{17}$ методом крутильных колебаний. *Расплавы*. 2012;(2):83–90.
14. Beltyukov A., Olyanina N., Ladyanov V. The viscosity of liquid Co-Si-B alloys. *Journal of Molecular Liquids*. 2019;281:204–215. https://doi.org/10.1016/j.molliq.2019.02.064
15. Bel'tyukov A.L., Lad'yanov V.I., Olyanina N.V. About of characteristic properties of measurement of stickiness metallic melts by method of torsional vibration. *Rasplavy*. 2009;(6):19–27. (In Russ.).

    Бельтюков А.Л., Ладьянов В.И., Олянина Н.В. Об особенностях измерения вязкости металлических расплавов методом крутильных колебаний. *Расплавы*. 2009;(6): 19–27.
16. Olyanina N.V., Beltyukov A.L., Ladyanov V.I. Viscosity of liquid alloys of cobalt with boron and silicon. *Chemical Physics and Mesoscopy*. 2019;21(1):55–64. (In Russ.). https://doi.org/10.15350/17270529.2019.1.8

    Олянина Н.В., Бельтюков А.Л., Ладьянов В.И. О вязкости жидких сплавов кобальта с бором и кремнием. *Химическая физика и мезоскопия*. 2019;21(1):55–64. https://doi.org/10.15350/17270529.2019.1.8

17. Bel'tyukov A.L., Olyanina N.V., Lad'yanov V.I. Torsional vibration measurement of the viscosity of a metallic melt. *Russian Metallurgy (Metally)*. 2016;2016:156–161. https://doi.org/10.1134/S0036029516020026

Бельтюков А.Л., Олянина Н.В., Ладьянов В.И. Особенности измерения вязкости металлических расплавов методом крутильных колебаний. *Расплавы*. 2016;(2):176–184.

18. Shterner S.R., Dovgopol S.P. Density, electric resistance and short-range order of Co-B and Ni-B melts. *Ukrainskii fizicheskii zhurnal*. 1983;28(6):858–861. (In Russ.).

Штернер С.Р., Довгопол С.П. Плотность, электросопротивление и ближний порядок расплавов Co-B и Ni-B. *Украинский физический журнал*. 1983;28(6):858–861.

19. Tavadze F.N., Bairamashvili I.A., Khantadze D.V. Surface tension and structure of molten borides of iron, cobalt and nickel. *Soviet Physics Doklady*. 1965;162(1):67–69. (In Russ.).

Тавадзе Ф.Н., Байрамашвили И.А., Хантадзе Д.В. Поверхностное натяжение и строение расплавленных боридов железа, кобальта и никеля. *ДАН СССР*. 1965;162(1):67–69.

20. Geld P.V., Gertman Yu.M. Densities of liquid alloys of silicon with cobalt and nickel. *Physics of Metals and Metallography*. 1961;12(1):47–50. (In Russ.).

Гельд П.В., Гертман Ю.М. Плотности жидких сплавов кремния с кобальтом и никелем. *Физика металлов и металловедение*. 1961;12(1):47–50.

21. Glasstone S., Laidler K. L., Eyring H. The Theory of Rate Processes: The Kinetics of Chemical Reactions, Viscosity, Diffusion and Electrochemical Phenomena. New York; London: McGraw-Hill; 1941:611.

Глесстон С., Лейдлер К., Эйринг Г. Теория абсолютных скоростей реакций: кинетика химических реакций, вязкость, диффузия и электрохимические явления. Пер. с англ. Москва: Иностранная литература; 1948:583.

22. Wilson J.R. The structure of liquid metals and alloys. *Metallurgical Reviews*. 1965;10(1):381–590. http://dx.doi.org/10.1179/mtlr.1965.10.1.381

Вилсон Д.Р. Структура жидких металлов и сплавов. Пер. с англ. Москва: Металлургия; 1972:247

23. Ishida K., Nishizawa T., Schlesinger M.E. The Co-Si (cobalt-silicon) system. *Journal of Phase Equilibria*. 1991;12(5):578–586. https://doi.org/10.1007/BF02645074

24. Du Y., Schuster J., Chang Y.A., Jin Z., Huang B.Y. A thermodynamic description of the B-Co system: Modeling and experiment. *International Journal of Materials Research*. 2002;93(11):1157–1163. https://doi.org/10.1515/ijmr-2002-0198

25. Liao P.K., Spear K.E. The B-Co (boron-cobalt) system. *Bulletin of Alloy Phase Diagrams*. 1988;9(4):452–457. https://doi.org/10.1007/BF02881866

26. Chart T.G. Thermochemical data for transition metal-silicon systems. *High Temperatures-High Pressures*. 1973;5(3):241–252.

27. Sato Y., Kameda Y., Nagasawa T., Sakamoto T., Moriguchi S., Yamamura T., Waseda Y. Viscosity of molten silicon and the factors affecting measurement. *Journal of Crystal Growth*. 2003;249(3–4):404–415. https://doi.org/10.1016/S0022-0248(02)02153-X

28. Takahira N. Influence of enthalpy changes on the temperature dependency of the viscosity of pure liquid metals. *ISIJ International*. 2015;55(10):2247–2251. https://doi.org/10.2355/isijinternational.ISIJINT-2015-214

29. Okada J.T., Ishikawa T., Watanabe Yu., Paradis P.F., Watanabe Ya., Kimura K. Viscosity of liquid boron. *Physical Review B*. 2010;81(14):140201(R). https://doi.org/10.1103/PhysRevB.81.140201

30. Paradis P.F., Ishikawa T., Yoda S. Noncontact density measurements of liquid, undercooled, and high temperature solid boron. *Applied Physics Letters*. 2005;86(15):151901. https://doi.org/10.1063/1.1900954

31. Franke P., Neuschütz D. B-Co (boron-cobalt). In: *Thermodynamic Properties of Inorganic Materials. Binary systems. Part 2: Elements and Binary Systems from B-C to Cr-Zr*. Berlin: Springer Materials; 2004;19B2:1-3. https://doi.org/10.1007/10757405_3

32. Witusiewicz V.T. Thermodynamic properties of liquid alloys of 3d transition metals with metalloids (silicon, carbon and boron). *Journal of Alloys and Compounds*. 1994;203:103–116. https://doi.org/10.1016/0925-8388(94)90720-X

33. Mudryi S.I. Structure of Co-B melts. *Inorganic Materials*. 1998;34(1):43–44. (In Russ.).

Мудрый С.И. Структура расплавов системы Co-B. *Неорганические материалы*. 1998;34(1):43–44.

Information about the Authors / Сведения об авторах

Natalia V. Olyanina, *Cand. Sci. (Phys.–Math.), Research Associate,* Udmurt Federal Research Center of the Ural Branch of the Russian Academy of Sciences
ORCID: 0000-0002-5344-4815
E-mail: oljanina@mail.ru

Anatoly L. Beltyukov, *Cand. Sci. (Phys.–Math.), Leading Researcher,* Udmurt Federal Research Center of the Ural Branch of the Russian Academy of Sciences
ORCID: 0000-0002-5764-454X
E-mail: albeltyukov@udman.ru

Vladimir I. Ladyanov, *Dr. Sci. (Phys.–Math.), Chief Researcher, Head of Scientific Center for Metallurgical Physics and Materials Science,* Udmurt Federal Research Center of the Ural Branch of the Russian Academy of Sciences
ORCID: 0000-0002-7751-1007
E-mail: vilad@udman.ru

Наталья Владимировна Олянина, *к.ф.-м.н., научный сотрудник,* Удмуртский федеральный исследовательский центр Уральского отделения РАН
ORCID: 0000-0002-5344-4815
E-mail: oljanina@mail.ru

Анатолий Леонидович Бельтюков, *к.ф.-м.н., ведущий научный сотрудник,* Удмуртский федеральный исследовательский центр Уральского отделения РАН
ORCID: 0000-0002-5764-454X
E-mail: albeltyukov@udman.ru

Владимир Иванович Ладьянов, *д.ф.-м.н., главный научный сотрудник, руководитель научного центра металлургической физики и материаловедения,* Удмуртский федеральный исследовательский центр Уральского отделения РАН
ORCID: 0000-0002-7751-1007
E-mail: vilad@udman.ru

Contribution of the Authors

N. V. Olyanina – conducting experimental research and calculations, literary review, writing the draft.
A. L. Beltyukov – conducting experimental research, follow-on revision of the text, formation of the final conclusions.
V. I. Ladyanov – setting the research task, correcting and editing the article.

Вклад авторов

Н. В. Олянина – проведение экспериментальных исследований и расчетов, литературный обзор, написание исходного текста.
А. Л. Бельтюков – проведение экспериментальных исследований, доработка текста, формирование итоговых выводов.
В. И. Ладьянов – постановка задачи исследований, корректировка и редактирование статьи.

Received 24.04.2025
Revised 19.05.2025
Accepted 06.06.2025

Поступила в редакцию 24.04.2025
После доработки 19.05.2025
Принята к публикации 06.06.2025

PHYSICO-CHEMICAL BASICS OF METALLURGICAL PROCESSES / ФИЗИКО-ХИМИЧЕСКИЕ ОСНОВЫ МЕТАЛЛУРГИЧЕСКИХ ПРОЦЕССОВ

UDC 669.187.28
DOI 10.17073/0368-0797-2025-5-526-533

Original article
Оригинальная статья

Influence of amphoteric oxides content on valve effect characteristics of electric arc

A. V. Sivtsov[1], O. Yu. Sheshukov[1, 2], D. K. Egiazaryan[1, 2] ✉, M. M. Tsymbalist[1], P. P. Orlov[2]

[1] **Vatolin Institute of Metallurgy of the Ural Branch of the Russian Academy of Sciences** (101 Amundsena Str., Yekaterinburg 620016, Russian Federation)
[2] **Ural Federal University named after the first President of Russia B.N. Yeltsin** (19 Mira Str., Yekaterinburg 620002, Russian Federation)

✉ avari@mail.ru

Abstract. The paper presents the experimental data on the effect of amphoteric oxides content (Al_2O_3 and Fe_2O_3) in slags on the metallurgical slags properties. It is noted that the parameters of the electric arc valve effect, such as the constant component of the arc voltage or the constant component of the electrode current, can act as a criterion for assessing the slag basicity. Up to a slag content of 18 wt. %, aluminum oxide exhibits mainly basic properties, and above that, acidic properties. For Fe_2O_3, the threshold value is the content of 20 wt. %. The data obtained make it possible to more reasonably adjust the smelting slag mode. In particular, for the current trend on metallurgical enterprises to replace fluorspar in the out-of-furnace steel processing with other slag liquefiers, these data allow to determine the limit of aluminum oxide content at which the conditions of metal refining from sulfur will not be degraded. For arc steelmaking furnaces, this technique is one of the options for non-contact operational assessment of the metal bath state, the foaming slag quality to cover the arcs, and the metal oxidation degree at the melting end and its readiness for tapping. The use of constant components of the arc voltage and current in the electrode for operational control of the tendency of amphoteric oxides to basic or acidic properties during melting in industrial conditions is not possible due to a large number and multidirectional influence of the slag components. Nevertheless, this technique will be useful in control of steelmaking technological process with digital twin models and their accompanying databases.

Keywords: steel, slag, oxidation, basicity, amphotericity, electric arc, component of constant voltage, electric arc furnace, slag mode

Acknowledgements: The work was performed within the framework of the budget assignment of the Institute of Metallurgy, Ural Branch of the Russian Academy of Sciences.

For citation: Sivtsov A.V., Sheshukov O.Yu., Egiazaryan D.K., Tsymbalist M.M., Orlov P.P. Influence of amphoteric oxides content on valve effect characteristics of electric arc. *Izvestiya. Ferrous Metallurgy*. 2025;68(5):526–533. https://doi.org/10.17073/0368-0797-2025-5-526-533

Влияние содержания амфотерных оксидов в шлаке на характеристики вентильного эффекта электрической дуги

А. В. Сивцов[1], О. Ю. Шешуков[1, 2], Д. К. Егиазарьян[1, 2] ✉, М. М. Цымбалист[1], П. П. Орлов[2]

[1] **Институт металлургии имени академика Н.А. Ватолина Уральского отделения РАН** (Россия, 620016, Екатеринбург, ул. Амундсена, 101)
[2] **Уральский Федеральный университет имени первого Президента России Б. Н. Ельцина** (Россия, 620002, Екатеринбург, ул. Мира, 19)

✉ avari@mail.ru

Аннотация. Приведены экспериментальные данные по влиянию содержания амфотерных оксидов Al_2O_3 и Fe_2O_3 в металлургических шлаках на их свойства. Отмечено, что в роли критерия оценки основности шлака могут выступать параметры вентильного эффекта электрической дуги – постоянная составляющая напряжения дуги или постоянная составляющая тока электрода. Показано, что до содержания в шлаке 18 мас. % оксид алюминия проявляет преимущественно основные свойства, а свыше – кислотные. Для Fe_2O_3 таким пороговым значением служит содержание 20 мас. %. Полученные данные позволяют более обоснованно проводить корректировку шлакового режима плавок. В частности, для имеющейся на металлургичеких предприятиях тенденции по замене плавикового шпата при внепечной обработке стали на иные разжижители шлака эти данные позволяют определить предел содержания оксида алюминия, при котором не будут ухудшаться условия рафинирования металла от серы. Для дуговых сталеплавильных печей данная методика выступает одним из вариантов неконтактной оперативной оценки состояния ванны металла, качества вспенивания шлака для укрытия дуг и степени окисленности металла в конце плавки и готовности его к выпуску. Применение постоянных составляющих напряжения дуги и тока в электроде для оперативного контроля склонности амфотерных оксидов к основным или кислотным свойствам по ходу плавки в промышленных условиях не представляется возможным из-за большого количества и разнонаправленного влияния составляющих шлак компонентов. Тем не менее данная методика будет полезна при ее использовании в целях управления технологическим процессом выплавки стали в моделях цифровых двойников и сопутствующим им базам данных.

Ключевые слова: сталь, шлак, окисленность, основность, амфотерность, электрическая дуга, постоянная составляющая напряжения, дуговая электропечь, шлаковый режим

Благодарности: Работа выполнена в рамках бюджетного задания Института металлургии УРО РАН.

Для цитирования: Сивцов А.В., Шешуков О.Ю., Егиазарьян Д.К., Цымбалист М.М., Орлов П.П. Влияние содержания амфотерных оксидов в шлаке на характеристики вентильного эффекта электрической дуги. *Известия вузов. Черная металлургия*. 2025;68(5):526–533. https://doi.org/10.17073/0368-0797-2025-5-526-533

Introduction

Improving steel quality is one of the key objectives of electric steelmaking. The parameters of the slag mode – composition, viscosity, quantity, and rate of slag formation – have a significant effect on metal quality, process yield, refractory lining durability, and other technological factors. This issue becomes particularly relevant given the continuous decline in scrap quality and the corresponding increase in harmful impurities, most of which are sulfur and phosphorus. Low-quality charge materials lead to higher energy and material losses and cause a considerable decrease in the technical and economic performance indicators of the smelt. In particular, melting time, energy consumption, and the use of ferroalloys and slag-forming materials increase, while furnace productivity decreases.

Modern steelmaking technologies involve the use of electric arc furnaces (EAFs) and basic oxygen converters (BOFs) as the main units for producing unalloyed, non-deoxidized iron–carbon melts using scrap, pig iron, and metallized feedstock as charge materials [1 – 3]. The iron–carbon melt is transferred in ladles to secondary metallurgy units – ladle furnaces (LF) and vacuum treatment units – where the melt composition is adjusted to meet the requirements of specific steel grades and operations are carried out to improve steel quality by removing oxygen, sulfur, and nonmetallic inclusions[1] [4; 5]. Without secondary metallurgy units, a resource- and energy-efficient technology for liquid steel production is not feasible.

Steel production in EAFs accounts for a significant share of global output, second only to the BOF process. This process is associated with high energy consumption, which makes energy and technological optimization of great importance. However, optimization efforts often focus not on technological aspects but on the cost

[1] Dyudkin DA, Kisilenko VV. New technological solutions for out-of-furnace steel treatment using cored wires [Internet]. Available from: https://uas.su/conferences/2010/may/03/00003.php (accessed 2025 May 12).

of the main resource – electric power [6] – or on auxiliary operations that are not directly related to melting [7].

Unlike BOF, EAF is a unit with a large number of adjustable parameters and process control tools that can operate directly within the working zone – even during arcing operation. However, due to the presence of molten metal and slag, burning arcs, and high currents, the working zone is highly aggressive and difficult to access for direct measurements and process control. Therefore, mathematical modeling plays a major role in effective process control [8 – 10], both in general-purpose studies and when accounting for the specific features of a particular unit – for example, when using hot-briquetted iron or various off-gas post-combustion modes [11; 12]. On the other hand, the measurement of EAF electrical characteristics, which eliminates the difficulties associated with the aggressive working environment, faces problems of signal filtering and processing of the recorded signals under circuit-break events, short circuits, short-arc and long-arc operation, and changes in the chemical composition of the arc plasma [13].

Steelmaking slags are mainly composed of calcium and silicon oxides, which together typically account for 85 – 90 wt. % of the total oxide content. Their ratio (CaO/SiO_2) is used as a proxy measure of an important technological parameter – the slag basicity. A more accurate assessment accounts for the contents of other acidic and basic oxides, such as those of iron, magnesium, and manganese.

At the same time, the oxides of many metals – particularly aluminum, titanium, vanadium, iron, and chromium – are amphoteric, meaning that at certain contents they can exhibit either acidic or basic behavior. These oxides have been extensively studied in blast furnace ironmaking [14]. In blast furnaces, any adjustments to ironmaking process or charging process are associated with significant process dead time, i.e., a delayed process response to control interventions. Therefore, researchers model blast furnace slags and investigate the effects of individual components – including aluminum and titanium oxides – on slag viscosity, structure, and refining properties [15]. These oxides can have highly diverse effects: formation of nitrides and refractory spinels in high-temperature zones can extend campaign life, whereas their formation in other zones can decrease the effective working volume and disrupt furnace operation. At the same time, increasingly comprehensive theories are being developed to describe the behavior of amphoteric oxides based on slag structure data [16 – 18].

Interest in amphoteric oxides is driven by the fact that many metallurgical plants, seeking substitutes for fluorspar – a traditional slag liquefier – have begun to use alumina-containing materials composed primarily of aluminum oxides. Consequently, in out-of-furnace slags, the content of this oxide can reach 40 wt. %. It serves not only as a slag liquefier but also stabilizes the solidified slag, preventing its self-disintegration during cooling. However, the primary goal of out-of-furnace metal processing is sulfur removal, the rate and extent of which are determined by the refining ability of the slag.

To absorb substantial amounts of sulfur, the slag must be highly basic. Because basic oxides donate free oxygen anions that mediate sulfur transfer from metal to slag, their content must exceed that of acidic oxides. Yet, the behavior of amphoteric oxides – able to act as either donors or acceptors of these anions – remains difficult to predict. Accordingly, determining the range of aluminum oxide contents in refining slags that does not impede desulfurization – where Al_2O_3 acts predominantly as a donor of free oxygen anions – represents the second reason for the interest in amphoteric oxides.

The third reason concerns assessing the applicability of this approach to the smelting of alloyed steel grades, in which components forming amphoteric oxides may be present in considerable amounts in both the slag and the metal. During arcing, partial evaporation of components from the metal–slag melt surface occurs; these components enter the ionized gaseous phase forming the arc column, which may affect the electrical conductivity of the arc gap in different ways. This aspect is a subject of further research and is not considered in the present study.

Methods

Numerous studies in the scientific literature are based on experimental investigations of the influence of slag composition on the magnitude of the constant component of arc voltage (CCAV) [19 – 21]. In AC circuits with an electric arc this component most often arises due to the difference in electron work function between materials of different nature. Thus, in EAF, the work function of electrons from graphite exceeds that from iron, and as a result, a positively directed constant component of arc voltage appears across the arc gap. This phenomenon is known as the electric arc valve effect.

The current density of thermionic emission is described by the Richardson–Dushman equation

$$j = AT^2 \exp\left(-\frac{\varphi_e}{kT}\right), \quad (1)$$

where A is the Richardson constant; T is the temperature; φ_e is the electron work function; k is the Boltzmann constant.

The current emission density is strongly affected by both temperature and the chemical factor – the electron work function. While the current emission density from the graphite electrode remains nearly constant, for the second electrode – the molten material – this parame-

ter depends significantly on the chemical composition of the melt. Therefore, the difference between the emission currents, which determines the CCAV magnitude, is governed by this composition.

There are data indicating a close relationship between CCAV and the oxygen content in the metal melt of an EAF during the refining stage [22]. In many respects, this relationship resembles the dependence of the electrode potential in an electrolytic cell on oxygen activity (ionic concentration), as described by the Nernst equation (2). This relationship underlies the operation principle of Celox sensors used in industrial practice to measure the oxidation potential of metal and slag:

$$E = E_0 + \frac{RT}{nF} \ln\left(\frac{a_{ox}}{a_{red}}\right), \quad (2)$$

where E is the electrode potential; E_0 is the standard electrode potential; R is the universal gas constant; T is the absolute temperature; n is the number of electrons involved in the process; F is the Faraday constant; a_{ox} and a_{red} are the activities of the oxidizing and reducing agents, respectively.

To process the initial electrical signals, Fourier series decomposition was used, and the CCAV was determined as the zero term of the series. However, for the analysis of experimental data, not the CCAV but the constant component of electrode current (CCEC) was used, since its determination does not require any additional transformation of the initial voltage signal. For correct determination of the CCAV, the voltage drop across the electrode itself and the current leads must be subtracted from the constant component (CC) of the measured voltage signal. The authors have previously developed a procedure for calculating this voltage drop; however, a simpler approach involves determining the constant component of current from the derivative of the electrode current signal, obtained using a Rogowski coil [23].

The key technological parameters of steelmaking in the electric arc furnace – the slag basicity and the metal oxidation degree – are closely related to the CCAV. An increase in slag basicity (i.e., the predominance of basic oxides over acidic oxides) causes a decrease in the CCAV, whereas a rise in oxygen activity (its content) in the metal melt leads to its increase. These relationships were previously observed by the authors in laboratory EAF experiments.

The experimental setup was a single-phase arc furnace lined with magnesia and equipped with an observation window at the level of the arc gap. Electric power was supplied from a welding transformer through two graphite electrodes 30 mm in diameter. The transformer's input voltage was 380 V, and the open-circuit voltage on the secondary side was 80 V.

A graphite crucible containing the material to be melted was placed on the lower electrode. The arc length was controlled by micrometer screws. Three electrical signals were recorded during the process: voltage across the electrodes $u(t)$, arc current $i(t)$, and the current derivative di/dt. The voltage was scaled to a level suitable for analog-to-digital conversion using a voltage divider. The current signal was measured as the voltage drop across a calibrated 0.3 Ω resistor installed in the secondary circuit of the transformer. The voltage proportional to the current derivative was taken from the output of the Rogowski coil. These analog signals were digitized at a sampling frequency of 100 kHz using a 12-bit Advantech PCI-1713 analog-to-digital converter (ADC).

Results and discussion

As an example, previously obtained results are presented for experiments investigating the influence of slag basicity (CaO/SiO_2) on the parameters of the electric arc valve effect, particularly on the constant component of electrode current (Fig. 1). The experiments were performed as follows: the metallic sample was melted, and a solidified binary fused slag containing CaO and SiO_2 at the specified ratio was added to the surface of the molten metal. After each addition, sufficient time was allowed for the slag to melt, dissolve, and reach equilibrium. The experiments were conducted separately for slags with basicity ratios of 0.25, 0.33, 1, 2, 3, and 4. The results confirmed that an increase in slag basicity leads to a decrease in the constant component of electrode current.

Considering this finding, an additional experiment was performed to evaluate the effect of the acidic oxide content in slag on its basicity and on the characteristics of the arc valve effect. A steel sample weighing 161 g

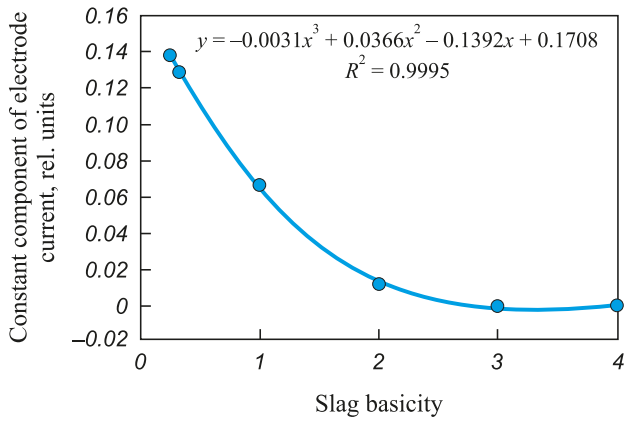

Fig. 1. Constant components of the electrode current at variations in slag basicity

Рис. 1. Постоянные составляющие тока электрода при вариации основности шлака

was melted, and a slag consisting of dicalcium silicate with a 5 wt. % FeO addition was introduced onto the melt surface. After melting the metal, three successive portions of slag were charged into the furnace, totaling 51 g. Following the addition and dissolution of the slag, further FeO portions were added in amounts of 6.5, 8, and 10 g, respectively. The experimental results are shown in Fig. 2. It is evident that additions of an acidic oxide decrease slag basicity and, accordingly, increase its oxidizing capacity and the CCEC.

In general, the amphoteric properties of metal oxides are determined by their ability to accept or donate valence electrons [24]. It is therefore reasonable to assume that additions of Al_2O_3 and Fe_2O_3 to the slag affect its chemical properties and the parameters of the electric arc valve effect depending on their content in the slag. Consequently, one may expect nonmonotonic behavior in the dependence of the CCEC.

Experiments to assess the effect of Fe_2O_3 content on slag properties were carried out using a similar procedure. As shown in Fig. 3, a minimum in the CCEC was observed at an Fe_2O_3 concentration of about 20 wt. %. Thus, up to 20 wt. %, Fe_2O_3 behaves as a basic oxide, promoting an increase in slag basicity, whereas at contents above 20 wt. %, it exhibits acidic properties, reducing basicity. In practice, it is not possible to determine the individual contents of iron oxides (FeO, Fe_2O_3, or Fe_3O_4) in slag. It is also unlikely that the proposed method of assessing them via the constant component of voltage or current would provide sufficient accuracy. Nevertheless, experimental studies in this direction can be extremely useful for addressing general tasks in the control and optimization of steelmaking technological processes in electric arc furnaces.

Among metal oxides, aluminum oxide most clearly exhibits amphoteric behavior. Experiments similar to those described above were conducted using the laboratory arc furnace. According to the data presented in Fig. 4, additions of Al_2O_3 up to about 18 wt. % lead to a decrease in the CCEC, whereas at contents above 20 wt. %, it increases, indicating the predominance of acidic properties of this oxide. The approximate Al_2O_3 content at which a sharp transition from basic to acidic behavior occurs is about 30 wt. %. Therefore, increasing the Al_2O_3 content in refining slags up to 18 wt. % has a beneficial effect on arc stability and on refining properties such as viscosity, interfacial tension, and desulfurizing ability.

From a practical standpoint, it should be noted that Al_2O_3 additions below 20 wt. % do not provide mechanical stability to refining slags without the use of additional stabilizing components, making them prone to spontaneous disintegration into fine powder. Increasing the Al_2O_3 content from 18 to 30 wt. % has only a minor adverse effect on arc operation but allows the stabilization of refining slags without additional methods. However, introducing larger amounts of Al_2O_3 deteriorates not only the refining characteristics of the slag but also its electrical parameters, adversely affecting both the arc stability and the electrical characteristics of the melting process.

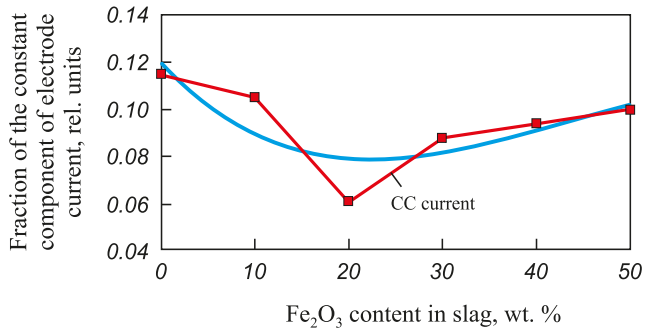

Fig. 3. Dependence of the electrode current constant component on Fe_2O_3 content

Рис. 3. Зависимость постоянной составляющей тока электрода от содержания Fe_2O_3

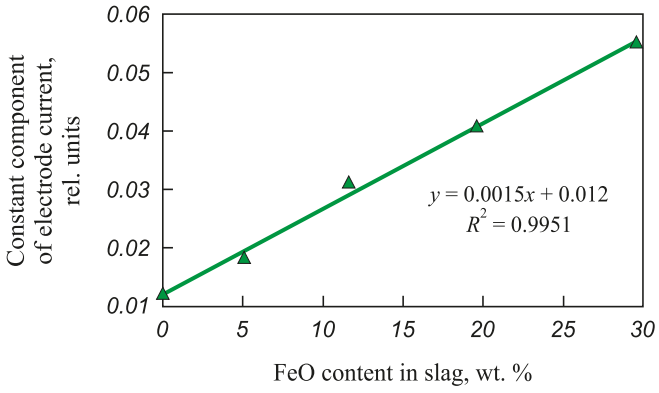

Fig. 2. Dependence of the electrode current constant component on FeO content

Рис. 2. Зависимость постоянной составляющей тока электрода от содержания FeO

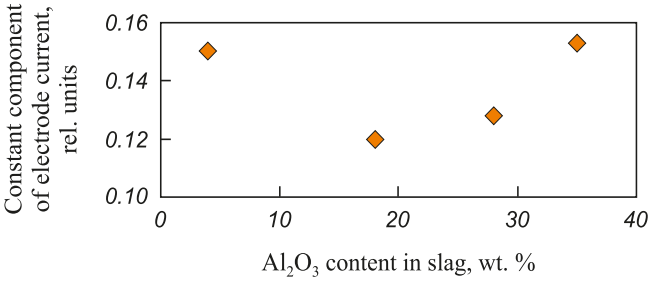

Fig. 4. Dependence of the electrode current constant component on Al_2O_3 content in the slag

Рис. 4. Зависимость постоянной составляющей тока электрода от содержания Al_2O_3 в шлаке

Conclusions

Laboratory studies of the effects of Fe_2O_3 and Al_2O_3 contents in slag on the CCEC showed that these oxides exhibit basic behavior at contents below 20 and 18 wt. %, respectively, and acidic behavior at higher contents. This provides a stronger basis for defining the limiting aluminum oxide content in refining slags, considering both refining performance and slag stabilization.

Further investigation of other amphoteric oxides and their impact on arc characteristics (CCEC and CCAV) using the proposed approach may face several challenges. Metals forming these oxides tend to undergo reduction (chromium, vanadium), carbide formation (chromium, titanium), or nitride formation (chromium, vanadium, titanium). In addition, the laboratory tests used graphite crucibles, which, for other oxides, can substantially affect the slag phase composition, the accuracy of recorded signals, and the reliability of their interpretation.

Using the CCAV and CCEC for real-time control of an oxide's tendency toward basic or acidic behavior during industrial heats is not feasible because of the large number of slag constituents and their complex, often opposing effects. Even so, the method is well suited for process control in digital twin models [25 – 27] and in associated databases. In particular, given the current trend at metallurgical plants to replace fluorspar with other slag liquefiers during out-of-furnace steel processing, these data help define the upper aluminum oxide content that does not impair sulfur removal from metal. For electric arc furnaces, the method also offers a non-contact, real-time means of assessing the metal bath condition, the quality of slag foaming for arc shielding, and the metal oxidation degree at the end of melting and the heat's readiness for tapping.

References / Список литературы

1. Bigeev A.M., Bigeev V.A. Metallurgy of Steel. Magnitogorsk: MSTU; 2000:544. (In Russ.).

   Бигеев А.М., Бигеев В.А. Металлургия стали. Магнитогорск: МГТУ; 2000:544.
2. Gladkikh V.A., Gasik M.I., Ovcharuk A.N., Prokhodak Yu.S. Design and Equipment of Electric Steelmaking and Ferroalloy Workshops: Textbook. Dnepropetrovsk: Sistemnye tekhnologii; 2004:736. (In Russ.).

   Гладких В.А., Гасик М.И., Овчарук А.Н., Пройдак Ю.С. Проектирование и оборудование электросталеплавильных и ферросплавных цехов: Учебник. Днепропетровск: Системные технологии; 2004:736.
3. Bornatskii I.I., Mikhnevich V.F., Yargin S.A. Steelmaking. Moscow: Metallurgiya; 1991:400. (In Russ.).

   Борнацкий И.И., Михневич В.Ф., Яргин С.А. Производство стали. Москва: Металлургия; 1991:400.
4. Dyudkin D.A., Bat' S.Yu., Grinberg S.E., Marintsev S.N. Steel Production on a Ladle-Furnace Unit. Donetsk: Yugo-Vostok, LTD; 2003:300. (In Russ.).

   Дюдкин Д.А., Бать С.Ю., Гринберг С.Е., Маринцев С.Н. Производство стали на агрегате ковш-печь. Донецк: ООО «Юго-Восток, ЛТД»; 2003:300.
5. Povolotskii D.Ya., Gudim Yu.A., Zinurov I.Yu. Design and Operation of Heavy-Duty Arc Steelmaking Furnaces. Moscow: Metallurgiya; 1990:176. (In Russ.).

   Поволоцкий Д.Я., Гудим Ю.А., Зинуров И.Ю. Устройство и работа сверхмощных дуговых сталеплавильных печей. Москва: Металлургия; 1990:176.
6. Shyamal S., Swartz C.L.E. Real-time energy management for electric arc furnace operation. *Journal of Process Control*. 2019;74: 50–62. https://doi.org/10.1016/j.jprocont.2018.03.002
7. Logunova O.S., Oshurkov V.A., Pavlov V.V. The method of efficiency definition of new functional task in electric arc furnace control system. *IOP Conference Series: Materials Science and Engineering*. 2020;718:012011. https://doi.org/10.1088/1757-899X/718/1/012011
8. Abadi M.M., Tang H., Rashidi M.M. A review of simulation and numerical modeling of electric arc furnace (EAF) and its processes. *Heliyon*. 2024;10(11):e32157. https://doi.org/10.1016/j.heliyon.2024.e32157
9. Kozyra J., Lozynskyy A., Łukasik Z., Kuśmińska-Fijałkowska A., Kutsyk A., Kasha L. Increasing the level of autonomy of control of the electric arc furnace by weakening interphase interactions. *Energies*. 2023;16(24):8114. https://doi.org/10.3390/en16248114
10. Saboohi Y., Fathi A., Škrjanc I., Logar V. Comprehensive electric arc furnace model for simulation purposes and model-based control. *Steel Research International*. 2017;88(3): 1600083. https://doi.org/10.1002/srin.201600083
11. Irawan A., Kurniawan T., Alwan H., Muslim Z.A., Akhmal H., Firdaus M.A., Bindar Y. An energy optimization study of the electric arc furnace from the steelmaking process with hot metal charging. *Heliyon*. 2022;8(11):e11448. https://doi.org/10.1016/j.heliyon.2022.e11448
12. Ugarte O., Li J., Haeberle J., Frasz T., Okosun T., Zhou C.Q. CFD modeling of HBI/scrap melting in industrial EAF and the impact of charge layering on melting performance. *Materials*. 2024;17(21):5139. https://doi.org/10.3390/ma17215139
13. Wang B., Mao Z. Detecting outliers in electric arc furnace under the condition of unlabeled, imbalanced, non-stationary and noisy data. *Measurement and Control*. 2018;51(3-4): 83–93. https://doi.org/10.1177/0020294018771097
14. Dmitriev A.N., Chen' K., Zolotykh M.O., Vit'kina G.Yu. Mathematical Modeling of Blast-Furnace Process. Yekaterinburg: Publishing House AMB; 2023:232. (In Russ.).

   Дмитриев А.Н., Чэнь К., Золотых М.О., Витькина Г.Ю. Математическое моделирование доменного процесса. Екатеринбург: ООО «Издательство АМБ»; 2023:232.
15. Zhou W., Li T., Lan D., Sun C., Yang S. Influence of TiO_2, Al_2O_3, and basicity on viscosity and structure of high titanium-bearing blast furnace slag. *Materials*. 2023;16(7):2575. https://doi.org/10.3390/ma16072575
16. Bi Z., Li K., Jiang C., Zhang J., Ma S., Alberto C., Sun M., Bu Y., Barati M., Ren S. New insights into the traditional charge compensation theory: Amphoteric behavior of TiO_2 under the guidance of supply-demand relationship. *ACS Omega*. 2022;7(24):21225–21232. https://doi.org/10.1021/acsomega.2c02252

17. Zhou C., Li J., Wang S., Zhao J., Ai L., Chen Q., Chen Q., Zhao D. Development of molecular dynamics and research progress in the study of slag. *Materials*. 2023;16(15):5373. https://doi.org/10.3390/ma16155373

18. Jiang C., Li K., Bi Z., Ma S., Zhang J., Liu B., Li J. Developments in atomistic and nano structure evolution mechanisms of molten slag using atomistic simulation methods. *Nanomaterials*. 2024;14(5):464. https://doi.org/10.3390/nano14050464

19. Pedro A.A., Arlievskii M.P., Kurtenkov R.V. The constant component of the phase voltage during melting of zirconium electrocorundum. *Elektrometallurgiya*. 2011;(7):37–39. (In Russ.).

Педро А.А., Арлиевский М.П., Куртенков Р.В. Постоянная составляющая фазного напряжения при плавке циркониевого электрокорунда. *Электрометаллургия*. 2011;(7):37–39.

20. Педро А.А., Суслов А.П. Вентильный эффект в электродной печи. *Цветные металлы*. 2012;(12):91–95.

Pedro A.A., Suslov A.P. Valve effect in an electrode furnace. *Tsvetnye Metally*. 2012;(12):91–95. (In Russ.).

21. Sivtsov A.V., Sheshukov O.Yu., Tsymbalist M.M., Nekrasov I.V., Egiazar'yan D.K. The valve effect of an electric arc and problems in controlling electric-arc furnaces. *Metallurgist*. 2015;59(5-6):380–385. https://doi.org/10.1007/s11015-015-0113-6

Сивцов А.В., Шешуков О.Ю., Цымбалист М.М., Некрасов И.В., Егиазарьян Д.К. Вентильный эффект электрической дуги и проблемы управления дуговыми печами. *Металлург*. 2015;58(5):36–40.

22. Sivtsov A.V., Sheshukov O.Yu., Nekrasov I.V., Tsymbalist M.M., Egiazaryan D.K., Orlov P.P. On some features of use of constant arc voltage component for control of metal oxidation at stage of steel refinement. *Elektrometallurgiya*. 2020;(1):2–8. (In Russ.).

Сивцов А.В., Шешуков О.Ю., Некрасов И.В., Цымбалист М.М., Егиазарьян Д.К., Орлов П.П. О некоторых особенностях применения постоянной составляющей напряжения дуги для контроля окисленности металла на стадии рафинирования стали. *Электрометаллургия*. 2020;(1):2–8.

23. Sivtsov A.V., Tsymbalist M.M., Sheshukov O.Yu., Nekrasov I.V., Egiazar'yan D.K. Dynamic volt-ampere characteristics of electric arc circuits as a means of monitoring and controlling technological modes of arc steelmaking furnaces. In: *Modern Problems of Electrometallurgy of Steel. Proceedings of the XVI Int. Conf.: in 2 Parts*. 2015:144–149. (In Russ.).

Сивцов А.В., Цымбалист М.М., Шешуков О.Ю., Некрасов И.В., Егиазарьян Д.К. Динамические вольт-амперные характеристики цепей с электрической дугой как средство контроля и управления технологическими режимами дуговых сталеплавильных печей. В сб.: *Современные проблемы электрометаллургии стали. Материалы XVI Международной конференции: В 2-х частях*. 2015:144–149.

24. Povolotskii D.Ya. Physico-Chemical Fundamentals of Steelmaking Processes. 2nd ed. Chelyabinsk: SUSU; 2007:183. (In Russ.).

Поволоцкий Д.Я. Физико-химические основы процессов производства стали. 2-е изд. Челябинск: ЮУрГУ; 2007:183.

25. Reuter M.A., Kaußen F., Geimer S., Borowski N., Degel R., Lux T. Metallurgical slags enable the circular economy – digital twins of metallurgical systems. *World of Metallurgy – ERZMETALL*. 2021;74(4):192–202.

26. Rauch L., Pietrzyk M. Digital twins as a modern approach to design of industrial processes. *Journal of Machine Engineering*. 2019;19(1):86–97. https://doi.org/10.5604/01.3001.0013.0456

27. Xiang F., Zhi Z., Jiang G. Digital twins technology and its data fusion in iron and steel product life cycle. In: *2018 IEEE 15th Int. Conf. on Networking, Sensing and Control (ICNSC)*. Zhuhai, China. 2018. https://doi.org/10.1109/ICNSC.2018.8361293

Сведения об авторах / Information about the Authors

Andrei V. Sivtsov, *Dr. Sci. (Eng.), Leading Researcher of the Laboratory of Technogenic Formations Problems*, Vatolin Institute of Metallurgy of the Ural Branch of the Russian Academy of Sciences
ORCID: 0000-0002-7840-1088
E-mail: aws2004@mail.ru

Oleg Yu. Sheshukov, *Chief Researcher of the Laboratory of Powder, Composite and Nano-Materials*, Vatolin Institute of Metallurgy of the Ural Branch of the Russian Academy of Sciences; *Dr. Sci. (Eng.), Prof., Director of the Institute of New Materials and Technologies*, Ural Federal University named after the first President of Russia B.N. Yeltsin
ORCID: 0000-0002-2452-826X
E-mail: o.j.sheshukov@urfu.ru

Denis K. Egiazaryan, *Cand. Sci. (Eng.), Senior Researcher, Head of the Laboratory of Technogenic Formations Problems*, Vatolin Institute of Metallurgy of the Ural Branch of the Russian Academy of Sciences; *Assist. Prof. of the Chair of Metallurgy of Iron and Alloys*, Ural Federal University named after the first President of Russia B.N. Yeltsin
ORCID: 0000-0002-9833-7191
E-mail: avari@mail.ru

Сивцов Андрей Владиславович, *д.т.н., ведущий научный сотрудник лаборатории проблем техногенных образований*, Институт металлургии имени академика Н.А. Ватолина Уральского отделения РАН
ORCID: 0000-0002-7840-1088
E-mail: aws2004@mail.ru

Олег Юрьевич Шешуков, *главный научный сотрудник лаборатории порошковых, композиционных и нано-материалов*, Институт металлургии имени академика Н.А. Ватолина Уральского отделения РАН; *д.т.н., профессор, директор Института новых материалов и технологий*, Уральский федеральный университет имени первого Президента России Б.Н. Ельцина
ORCID: 0000-0002-2452-826X
E-mail: o.j.sheshukov@urfu.ru

Денис Константинович Егиазарьян, *к.т.н., старший научный сотрудник, заведующий лабораторией проблем техногенных образований*, Институт металлургии имени академика Н.А. Ватолина Уральского отделения РАН; *доцент кафедры металлургии железа и сплавов*, Уральский федеральный университет им. Первого Президента Б.Н. Ельцина
ORCID: 0000-0002-9833-7191
E-mail: avari@mail.ru

Mikhail M. Tsymbalist, *Cand. Sci. (Eng.), Senior Researcher of the Laboratory of Pyrometallurgy of Reduction Processes*, Vatolin Institute of Metallurgy of the Ural Branch of the Russian Academy of Sciences
ORCID: 0000-0002-9570-040X
E-mail: cherknimne@yandex.ru

Pavel P. Orlov, *Cand. Sci. (Eng.), Engineer, Senior Lecturer of the Chair of Metallurgy of Iron and Alloys of the Institute of New Materials and Technologies*, Ural Federal University named after the first President of Russia B.N. Yeltsin
ORCID: 0000-0003-4616-306X
E-mail: p.p.orlov@urfu.ru

Цымбалист Михаил Михайлович, *к.т.н., старший научный сотрудник лаборатории пирометаллургии восстановительных процессов*, Институт металлургии имени академика Н.А. Ватолина Уральского отделения РАН
ORCID: 0000-0002-9570-040X
E-mail: cherknimne@yandex.ru

Орлов Павел Петрович, *к.т.н., инженер, старший преподаватель кафедры металлургии железа и сплавов института новых материалов и технологий*, Уральский Федеральный Университет им. Первого Президента России Б.Н. Ельцина
ORCID: 0000-0003-4616-306X
E-mail: p.p.orlov@urfu.ru

Contribution of the Authors / Вклад авторов

A. V. Sivtsov – scientific guidance, conducting theoretical research, experimental planning, conducting industrial tests, writing the text.

O. Yu. Sheshukov – setting the research task, planning industrial tests, correcting and editing the article.

D. K. Egiazaryan – conducting laboratory research, discussion of results.
M. M. Tsymbalist – software for experimental research, conducting industrial tests.
P. P. Orlov – conducting laboratory research.

А. В. Сивцов – общее руководство исследованием, теоретические изыскания, планирование эксперимента, проведение промышленных испытаний, написание статьи.
О. Ю. Шешуков – постановка задачи исследований, планирование промышленных испытаний, корректировка и редактирование статьи.
Д. К. Егиазарьян – проведение лабораторных исследований, обсуждение получившихся результатов.
М. М. Цымбалист – программное обеспечение экспериментальных исследований, проведение промышленных испытаний.
П. П. Орлов – проведение лабораторных исследований.

Received 13.05.2025
Revised 03.06.2025
Accepted 10.06.2025

Поступила в редакцию 13.05.2025
После доработки 03.06.2025
Принята к публикации 10.06.2025

PHYSICO-CHEMICAL BASICS OF METALLURGICAL PROCESSES / **ФИЗИКО-ХИМИЧЕСКИЕ ОСНОВЫ МЕТАЛЛУРГИЧЕСКИХ ПРОЦЕССОВ**

UDC 669.018.8
DOI 10.17073/0368-0797-2025-5-534-542

Original article
Оригинальная статья

PHYSICO-CHEMICAL ANALYSIS OF 12KH18N9TL STEEL MELTS FOR QUALITY CONTROL OF CAST PRODUCTS

D. P. Shvetsov[1, 2], O. A. Chikova[1], V. S. Tsepelev[1], N. I. Sinitsin[1] ✉, V. V. V'yukhin[1]

[1] **Ural Federal University named after the first President of Russia B.N. Yeltsin** (19 Mira Str., Yekaterinburg 620002, Russian Federation)
[2] **LLC "Precision Casting Center"** (18, bld. 4 Frontovykh Brigad Str., Yekaterinburg 620078, Russian Federation)

✉ n.i.sinitsin@urfu.ru

Abstract. The authors studied the behavior of slag inclusions in four samples taken during casting of austenitic corrosion-resistant steel grade 12Kh18N9TL. The samples for the study were taken under production conditions after melting the charge (*1*), introducing Ti and FeMn, slag induction and additional loading (*2*), re-introducing Ti, slag induction (*3*), slag induction (*4*). The elemental composition and temperature of the melt were determined under production conditions. The physicochemical properties of the melts obtained from the selected samples were measured under laboratory conditions: surface tension and kinematic viscosity. The measurements were carried out in the temperature range from 1370 to 1760 °C in the mode of heating and subsequent cooling of the sample. When observing the sample during the measurement of surface tension, the release of slag inclusions from the volume of the drop occurs in the heating mode. During subsequent cooling of the formed drop of liquid steel, slag particles flow from the slag bath under the action of the Marangoni force. Analysis of the dependence of the slag particle ascent rate on its size showed that only particles up to 10 μm in size can remain in the melt volume, while larger particles have time to float to the surface of the liquid bath. It was found that slag particles up to 4 mm in size can flow onto the surface of the sample under the action of the Marangoni force. The volume fraction of slag inclusions was determined, and a correlation was established between it and the element composition of the sample. The authors made a conclusion about the effect of Ti additives in the melt as the cause of increase in the volume fraction of slag inclusions in the casting.

Keywords: corrosion-resistant steel, slag inclusions, volume fraction, kinematic viscosity, surface tension, melt preparation, Marangoni effect

Acknowledgements: The work was carried out within the framework of the state work FEUZ-2023-0015.

For citation: Shvetsov D.P., Chikova O.A., Tsepelev V.S., Sinitsin N.I., V'yukhin V.V. Physico-chemical analysis of 12Kh18N9TL steel melts for quality control of cast products. *Izvestiya. Ferrous Metallurgy*. 2025;68(5):534–542. https://doi.org/10.17073/0368-0797-2025-5-534-542

ФИЗИКО-ХИМИЧЕСКИЕ ИССЛЕДОВАНИЯ РАСПЛАВОВ СТАЛИ 12Х18Н9ТЛ ДЛЯ УПРАВЛЕНИЯ КАЧЕСТВОМ ЛИТЫХ ИЗДЕЛИЙ

Д. П. Швецов[1, 2], О. А. Чикова[1], В. С. Цепелев[1], Н. И. Синицин[1] ✉, В. В. Вьюхин[1]

[1] **Уральский федеральный университет имени первого Президента России Б.Н. Ельцина** (Россия, 620002, Екатеринбург, ул. Мира, 19)
[2] **ООО «Центр Точного Литья»** (Россия, 620078, Екатеринбург, улица Фронтовых бригад, 18, корп. 4)

✉ n.i.sinitsin@urfu.ru

Аннотация. Авторы изучили поведение шлаковых включений в четырех образцах, отобранных в процессе разливки аустенитной коррозионностойкой стали марки 12Х18Н9ТЛ. Образцы для исследования отбирали в производственных условиях после расплавления шихты (*1*), введения Ti и FeMn, наведения шлака и дозагрузки (*2*), повторного введения Ti, наведения шлака (*3*), наведения шлака (*4*). Элементный состав и температура расплава были определены в производственных условиях. Физико-химические свойства расплавов, полученных из отобранных образцов, такие как поверхностное натяжение и кинематическая вязкость были измерены в лабораторных условиях. Изме-

рения проводились в диапазоне температур от 1370 до 1760 °С в режиме нагрева и последующего охлаждения образца. При наблюдении за образцом во время измерения поверхностного натяжения в режиме нагрева обнаружено выделение шлаковых включений из объема капли. При последующем охлаждении сформированной капли жидкой стали шлаковые частицы натекают из шлаковой ванны под действием силы Марангони. Анализ зависимости скорости всплывания шлаковой частицы от ее размера показал, что в объеме расплава могут остаться только частицы размером до 10 мкм, более крупные частицы успевают всплыть на поверхность жидкой ванны. Обнаружено, что под действием силы Марангони на поверхность образца могут натекать частицы шлака размером до 4 мм. Была определена объемная доля шлаковых включений и установлена корреляция между объемной долей шлаковых включений и элементном составе образца. Авторы сделали вывод о влиянии добавки титана в расплав как причине увеличения объемной доли шлаковых включений в отливке.

Ключевые слова: коррозионностойкая сталь, шлаковые включения, объемная доля, кинематическая вязкость, поверхностное натяжение, подготовка расплава, эффект Марангони

Благодарности: Статья выполнена в рамках государственной работы FEUZ-2023-0015.

Для цитирования: Швецов Д.П., Чикова О.А., Цепелев В.С., Синицин Н.И., Вьюхин В.В. Физико-химические исследования расплавов стали 12Х18Н9ТЛ для управления качеством литых изделий. *Известия вузов. Черная металлургия*. 2025;68(5):534–542. https://doi.org/10.17073/0368-0797-2025-5-534-542

Introduction

Austenitic corrosion-resistant steel grade 12Kh18N9TL exhibits high mechanical properties combined with resistance to organic acid solutions [1]. The production of castings from 12Kh18N9TL steel is complicated by its low casting properties. The castings are often characterized by microstructural heterogeneity, susceptibility to intergranular corrosion, and low resistance to cracking. During foundry production, increased formation of films, ingot porosity, shrinkage cavities, and a high content of nonmetallic inclusions in the ingot structure are observed [2].

Modern quality requirements for cast products made of corrosion-resistant and heat-resistant steels such as 12Kh18N9TL are driven by their wide application in the power industry, chemical engineering, and aircraft manufacturing. Experimental and exploratory studies are carried out to improve the mechanical properties of cast products by stabilizing the austenitic structure through alloying and thermomechanical treatment [3 – 5]. In [6], the authors suggest that alloying with copper, silicon, titanium, and niobium favors achieving a combination of high corrosion-electrochemical and mechanical properties in steel. In [7], it was shown that laser pulse surface modification of stainless steel 12Kh18N10T produces iron oxide (Fe_3O_4) and chromium oxide (Cr_2O_3), with titanium dioxide (TiO_2) also present [7]. The absence of undesirable surface contaminants, a decrease in their size and quantity, as well as an increase in the amount of retained austenite, enhance the corrosion resistance of austenitic steels [8]. It was established that in samples of austenitic stainless steels grades 03Kh18N10 and 08Kh18N10T, clusters of titanium nitrides and oxides of various dispersity are located around globular nonmetallic inclusions containing a secondary phase [9]. On the surface of cold-rolled sheet made of 08Kh18N10T steel, coarse defects in the form of delaminations were detected, consisting of titanium nitrides and a slag-forming mixture. Nonmetallic inclusions were noted to play a decisive role in degrading the mechanical properties of castings [10].

The casting properties of steel have a direct effect on obtaining castings and ingots with specified technological parameters. The most relevant physicochemical properties of the melt for foundry production are viscosity and surface tension. Slag induction during melting reduces the oxidation loss of volatile components and prevents the formation of oxide compounds. However, during melt tapping from the furnace, the slag becomes entrained in the melt, and slag inclusions may be present in steel ingots. In tests measuring the surface tension of liquid 12Kh18N9TL steel, the authors observed the release of slag during sample heating. Conducting systematic studies of the behavior of slag inclusions in steel is the objective of this work.

At “Precision Casting Center” (LLC, Ekaterinburg), castings of 12Kh18N9TL steel are produced as part of the import substitution program, highlighting the need to improve product quality at the melt preparation stage. Defects in finished products have been linked to the presence of slag inclusions in the casting. The objective of this study is to characterize the regularities of slag inclusion behavior in castings to improve control over the quality of 12Kh18N9TL cast products.

Materials and methods

Samples of 12Kh18N9TL steel were taken from an induction crucible furnace under production conditions at “Precision Casting Center” (LLC, Ekaterinburg) according to the technological scheme shown in Fig. 1.

The production process of cast products made of 12Kh18N9TL steel has the following specific features. As the metal charge, returns of the same grade from in-house production and B26-grade scrap are used. The melting of the metal charge lasts about 3.5 h, with heating of the melt to 1580 °C, at which point a sample is taken for elemental composition analysis. The elemental composition is determined using an MSA emission spect-

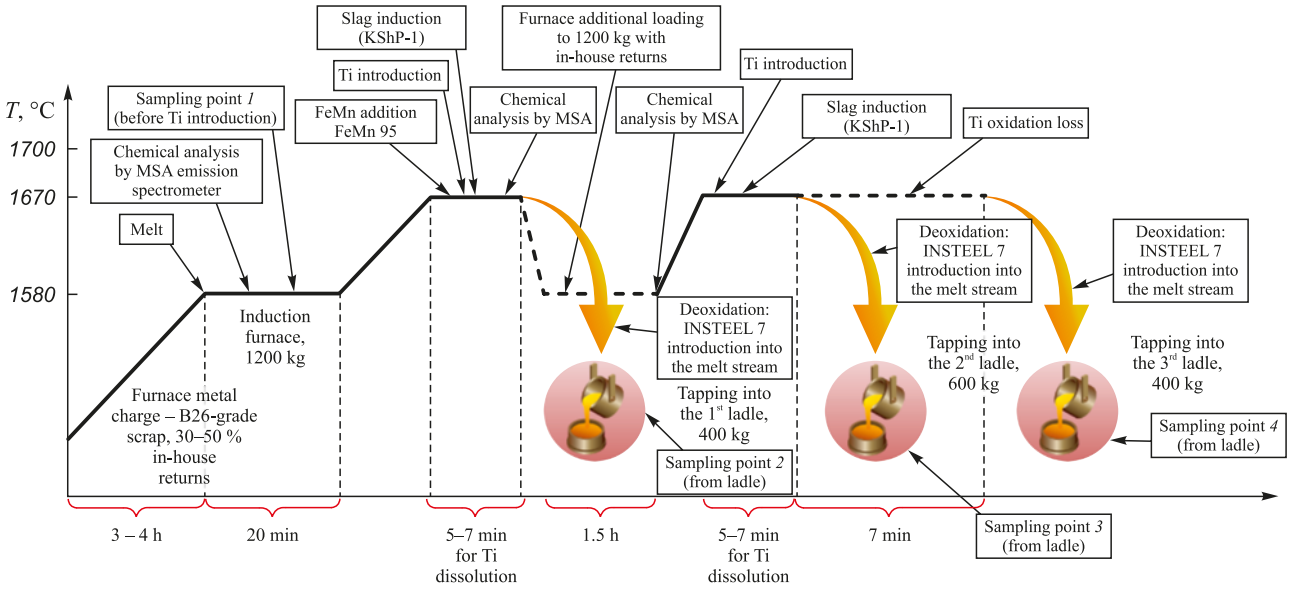

Fig. 1. Technological scheme of 12Kh18N9TL steel smelting with indication of sampling points for research

Рис. 1. Технологическая схема выплавки стали 12Х18Н9ТЛ с указанием отбора образцов для исследования

rometer (model MSA II v5). After titanium introduction, the melt surface was covered with the perlite-based slag coagulator KShP-1. The holding time for titanium dissolution in the melt is 5 – 7 min, and the melt tapping temperature into the ladle is 1650 – 1670 °C. Before melt tapping, a 200 g portion of aluminum is placed at the bottom of the ladle. The modifier INSTEEL 7 is introduced into the melt stream at a rate of 500 g per 400 kg of metal. After tapping the first portion of the melt into the ladle, the residual melt in the furnace is additionally loaded with 12Kh18N9TL steel and then heated to 1580 °C for 1.5 h, after which another sample is taken for elemental analysis. An 8 kg portion of titanium is added based on the elemental analysis results to achieve the required elemental composition. Before tapping the melt into the second and third ladles, slag induction on the melt surface is repeated, followed by heating to 1650 – 1670 °C. A 300 g portion of aluminum is also placed at the bottom of each ladle. During melt tapping, the modifier INSTEEL 7 is again introduced into the melt stream at a rate of 750 g per 600 kg of metal.

Thus, samples for the present study were taken under production conditions in accordance with the technological scheme shown in Fig. 1. Sample *1* was taken from the furnace before titanium introduction at a melt temperature of 1580 °C. Sample *2* was taken from the ladle after titanium introduction. Samples *3* and *4* were taken from the second and third ladles, respectively. The results of the chemical analysis of 12Kh18N9TL steel samples are presented in Table 1.

The kinematic viscosity (ν) and surface tension (σ) of liquid 12Kh18N9TL steel were measured using the equipment of the Research Center of Physics of Metallic Liquids, Institute of Physics of Metals (UrFU, Russia). The kinematic viscosity was measured by the oscillating-cup method [11; 12]. The tests were carried out in an atmosphere of high-purity helium under a pressure of 10^5 Pa. The temperature was measured with a BP-5/20 thermocouple, the readings of which were transmitted to a Termodat-14E2 controller. Kinematic viscosity was measured in 30 – 40 °C increments during heating and subsequent cooling. At each temperature, at least ten consecutive readings were acquired. Values were considered stabilized when the root-mean-square (RMS) deviation did not exceed the random measurement error. The oscillation parameters were recorded optically throughout the tests. The systematic error of the viscosity measurement was 3 %, and the random error governing within-test scatter did not exceed 1.5 % at the 95 % confidence level ($p = 0.95$).

The surface tension of liquid 12Kh18N9TL steel was measured by the sessile-drop method during heating to 1750 °C, followed by sample cooling. The working

Table 1. **Chemical composition of 12Kh18N9TL steel samples, wt. %**

Таблица 1. **Химический состав проб стали 12Х18Н9ТЛ, мас. %**

Sample No.	C	Si	Mn	Ni	Cr	Ti	Fe
1	0.059	0.423	1.174	9.373	17.49	0.022	70.31
2	0.060	0.563	1.196	9.298	17.41	0.503	69.80
3	0.065	0.558	1.113	9.549	17.50	0.595	69.48
4	0.064	0.655	1.044	9.430	17.43	0.401	70.31

chamber was evacuated to 0.001 Pa and then backfilled with helium to approximately 10^5 Pa. Samples were held in the inert-gas chamber for 5 – 8 min at the melting temperature, then heated to 1750 °C in 30 – 40 °C increments. The isothermal hold at each setpoint was at least 15 min. The drop profile was recorded with a digital camera, and the images were processed on a computer. The geometric parameters of the drop profile were determined using SIAMS 700 image-analysis software with an accuracy of 0.3 – 0.6°. No melt evaporation or drop volume loss was observed. The measurement error for density and surface tension did not exceed 7 %, and the random error governing within-test scatter did not exceed 1.5 % at the 95 % confidence level (p = 0.95) [13 – 16]. The method and apparatus for determining the density and surface tension of metallic melts are described in [17 – 19].

Results and discussion

During observation of the sample with a digital camera in the course of surface tension measurements, slag release was detected during sample heating (Fig. 2, *a*), which made it impossible to perform measurements in the heating mode. When the maximum temperature was reached, the contour of the liquid drop was formed as the slag drained from the drop surface into the slag bath (Fig. 2, *b*). Upon subsequent cooling, slag flowed from the formed slag bath onto the sample surface (Fig. 2, *c*).

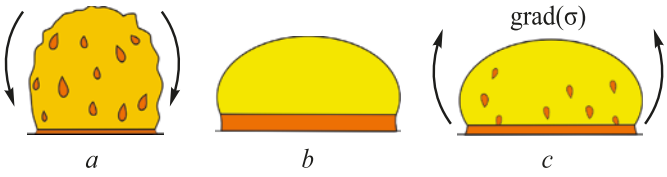

Fig. 2. Formation and evolution of slag inclusions on the sample surface during experiments on measuring the surface tension of liquid steel 12Kh18N9TL using the sessile-drop method

Рис. 2. Формирование и эволюция шлаковых включений на поверхности образца в опытах по измерению поверхностного натяжения жидкой стали 12Х18Н9ТЛ методом сидящей капли

These observations confirmed the presence of slag inclusions within the sample volume.

The volume fraction of slag in the sample was determined according to the procedure described in [20]. Fig. 3 shows the temperature dependence of the volume fraction of slag inclusions m (%) in the 12Kh18N9TL steel samples. A progressive increase in the volume fraction of slag inclusions from sample *1* to sample *3* is observed, whereas the lowest value was recorded for sample *4*. The volume fractions of slag inclusions at the melting temperature of 12Kh18N9TL steel are given in Table 2.

The volume fraction of slag inclusions increases from the first sample taken from the melt before titanium introduction to the third sample taken from the second ladle after furnace replenishment. In the fourth sample,

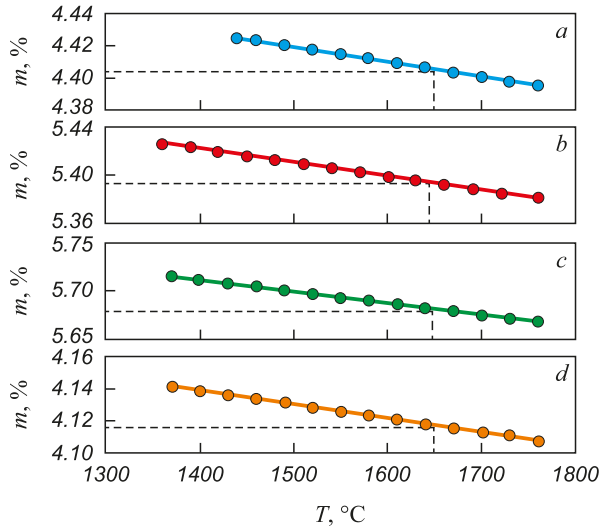

Fig. 3. Temperature dependences of volume fraction of slag inclusions in the samples of liquid steel12Kh18N9TL:
a – sample *1*; *b* – sample *2*; *c* – sample *3*; *d* – sample *4*
The dotted line shows the value of volume fraction of slag inclusions at smelting temperature

Рис. 3. Температурные зависимости объемной доли шлаковых включений в образцах жидкой стали 12Х18Н9ТЛ:
a – образец *1*; *b* – образец *2*; *c* – образец *3*; *d* – образец *4*
Пунктирной линей показано значение объемной доли шлаковых включений при температуре плавки

Table 2. **Volume fraction of slag inclusions, surface tension and kinematic viscosity of 12Kh18N9TL steel at smelting temperature (1670 °C)**

Таблица 2. **Объемная доля шлаковых включений, поверхностное натяжение и кинематическая вязкость стали 12Х18Н9ТЛ при температуре плавки 1670 °С**

Sample No.	Volume fraction of slag inclusions m, %	Surface tension σ, mJ/m^2	Kinematic viscosity $\nu \cdot 10^{-7}$, m^2/s
1	4.41	1930	6.20
2	5.39	1650	5.85
3	5.68	1850	5.67
4	4.12	1980	6.07

taken from the third ladle according to the technological scheme (Fig. 1), the volume fraction of slag inclusions was minimal.

A slag particle of radius r_{sl} and density d_{sl} located in the melt of density d_m and dynamic viscosity μ, is affected by buoyancy force $F_A = \frac{4}{3}\pi r^3 d_m g$, gravity $F_T = \frac{4}{3}\pi r^3 d_{sl} g$ and the Stokes force $F_s = 6\pi r\mu u$. Under the combined action of these forces, slag particles rise to the surface of the melt because of the density difference between the slag and the liquid metal (Fig. 4). When all three forces are balanced, a slag particle moves through the melt volume at a constant velocity u.

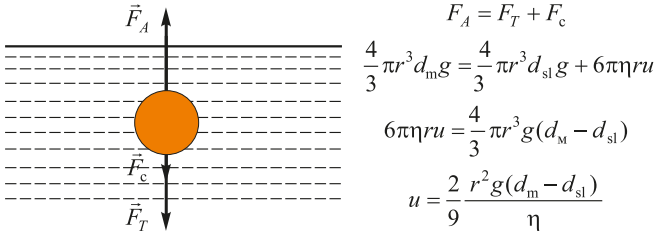

Fig. 4. Illustration of slag particles floating in the melt volume

Рис. 4. Иллюстрация процесса всплытия шлаковых частиц в объеме расплава

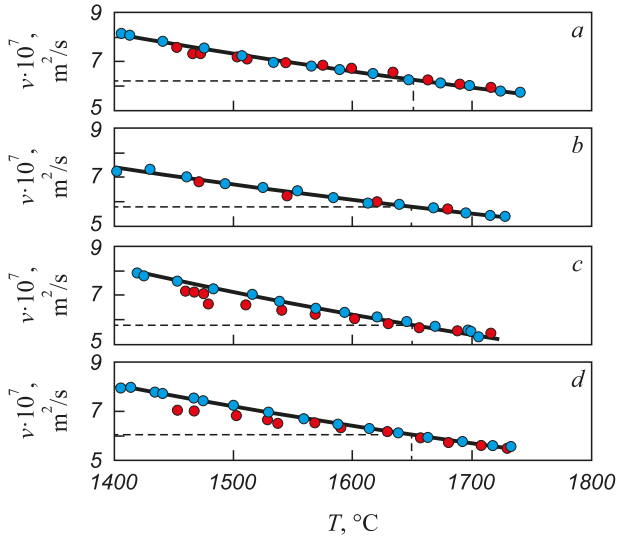

Fig. 5. Temperature dependences of kinematic viscosity of liquid steel 12Kh18N9TL obtained in heating mode with subsequent cooling:
a – sample *1*; *b* – sample *2*; *c* – sample *3*; *d* – sample *4*
● – heating, ● – cooling
The dotted line shows the value of kinematic viscosity at smelting temperature

Рис. 5. Температурные зависимости кинематической вязкости жидкой стали 12Х18Н9ТЛ, полученные в режиме нагрева с последующим охлаждением:
a – образец *1*; *b* – образец *2*; *c* – образец *3*; *d* – образец *4*
● – нагрев; ● – охлаждение
Пунктирной линей показано значение кинематической вязкости при температуре плавки

The ascent rate u of a slag particle depends on its size and can be expressed as

$$u = \frac{2r^2 g(d_m - d_{sl})}{9\nu d_m}, \quad (1)$$

where r is the particle radius; g is the acceleration due to gravity; d_m is the density of the liquid metal; d_{sl} is the slag density; ν is the kinematic viscosity of the liquid metal.

Fig. 5 presents the temperature dependence of kinematic viscosity obtained during heating and subsequent cooling. The absence of hysteresis between the heating and cooling branches indicates the lack of irreversible structural transformations in the melt, and consequently, the stability of slag particles within the melt volume up to 1740 °C. Therefore, slag particle removal from the melt is possible only due to their ascent to the surface.

Fig. 6 shows the dependence of slag particle velocity in liquid 12Kh18N9TL steel on particle size, as calculated from Equation (1). It follows from Fig. 6 that large particles rise rapidly to the surface, while particles smaller than 10 μm fail to reach the surface during the smelting process and remain within the melt volume.

Fig. 7 displays the results of surface tension measurements for liquid 12Kh18N9TL steel samples. In the temperature dependences for samples 3 and 4, anomalies were detected near 1600 °C, associated with the formation of a slag film on the sample surface due to slag flow from the slag bath. Slag particles and liquid metal possess different surface tension values. The surface tension determines the force that pulls the drop toward an ellipsoidal shape. A surface tension gradient ($d\sigma/dr$) in

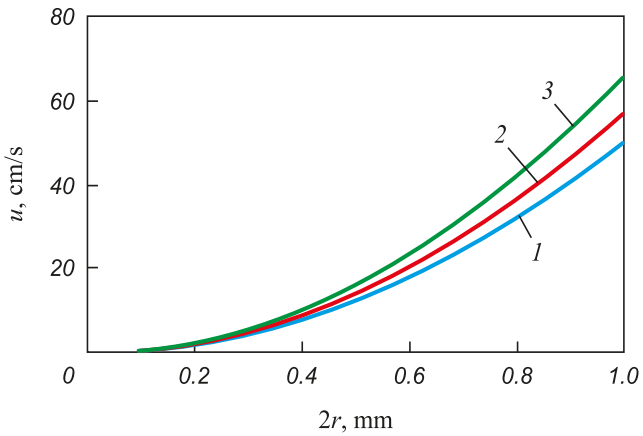

Fig. 6. Dependence of floating rate of slag particles in liquid steel 12Kh18N9TL on particle size, °C:
1 – 1500; *2* – 1600; *3* – 1700

Рис. 6. Зависимость скорости всплытия шлаковых частиц в жидкой стали 12Х18Н9ТЛ от размера при температуре, °С:
1 – 1500; *2* – 1600; *3* – 1700

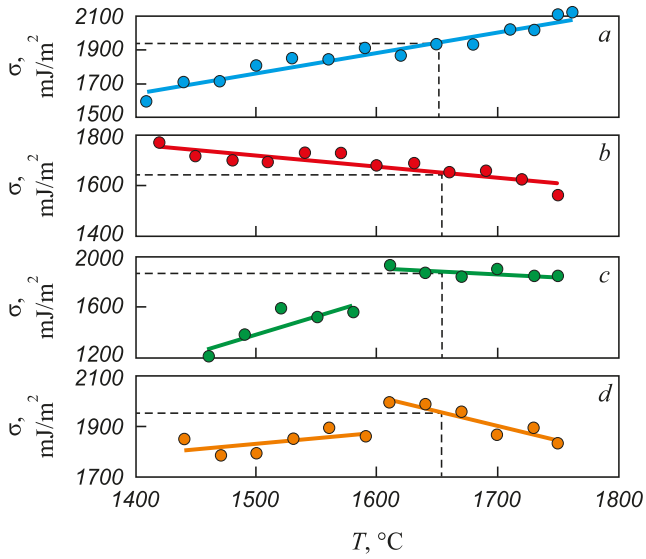

Fig. 7. Temperature dependences of surface tension of liquid steel 12Kh18N9TL samples obtained in cooling mode:
a – sample *1*; *b* – sample *2*; *c* – sample *3*; *d* – sample *4*
The dotted line shows the value of surface tension of slag inclusions at smelting temperature

Рис. 7. Температурные зависимости поверхностного натяжения образцов жидкой стали 12Х18Н9ТЛ, полученные в режиме охлаждения:
a – образец *1*; *b* – образец *2*; *c* – образец *3*; *d* – образец *4*
Пунктирной линией показано значение поверхностного натяжения при температуре плавки

the vertical direction induces the Marangoni force, which drives slag particles from the base of the drop toward its apex; this force is counterbalanced by gravity (Fig. 8). The Marangoni force was estimated from the surface tension gradient ($d\sigma/dr$) using expression [21]

$$F_m = 4\pi r^2 \frac{d\sigma}{dT}\frac{\partial T}{\partial r} \Rightarrow F_m = 4\pi r^2 \frac{d\sigma}{dr}. \quad (2)$$

Thus, a slag particle located on the surface of a liquid 12Kh18N9TL steel drop is subject to both gravity $F_f = \rho_{sl} g V_p$ and the Marangoni force (2) (Fig. 8). The equilibrium condition of these forces can be written as:

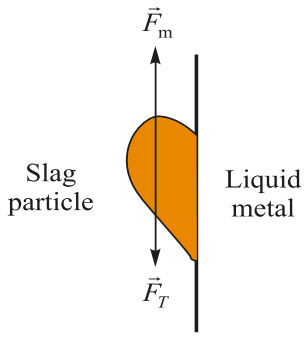

Fig. 8. The Marangoni effect

Рис. 8. Эффект Марангони

$$\frac{4}{3}\pi r^3 \rho_{sl} g = 4\pi r^2 \frac{d\sigma}{dr},$$

$$\frac{d\sigma}{dr} = \rho_{sl} g r.$$

From this, the expression for $\Delta\sigma$ can be obtained $\int d\sigma = \int \rho_{sl} g r dr$,

$$\Delta\sigma = \frac{\rho_{sl} g r^2}{2}. \quad (3)$$

In equation (3), $\Delta\sigma$ represents the difference between the surface tension values of slag and metal, at which the slag particle remains in equilibrium under the opposing actions of gravity and the Marangoni force. Fig. 9 shows the dependence of $\Delta\sigma$ on the slag particle radius on the drop surface. When $\Delta\sigma = 200$ mJ/m^2, slag particles larger than 4 mm can move upward from the base toward the apex of the drop surface. The observed slag flow phenomenon indicates that during slag bath formation at the base of the drop, the surface tension changes to a value at which the Marangoni forces become dominant.

Table 3 presents the chemical composition of the samples and the corresponding volume fraction of slag inclusions. Analysis of the data shows that the volume fraction of slag inclusions increases with increasing titanium content, suggesting a decisive role of titanium additions in the formation of slag inclusions.

Conclusions

The behavior of slag inclusions was studied in samples taken during the casting of austenitic corrosion-resistant steel 12Kh18N9TL. In surface tension tests of liquid steel performed by the sessile-drop method using a digital camera, slag release from the sample was observed upon heating to 1760 °C. Slag drops flowed from the sample surface, forming a slag bath at the base of the drop. Dur-

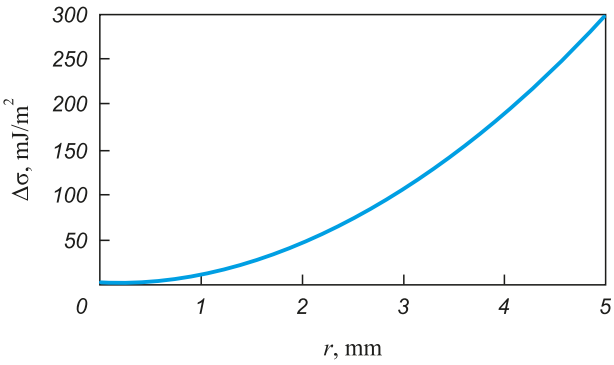

Fig. 9. Dependence of $\Delta\sigma$ on the radius r of a slag particle on the surface of liquid steel 12Kh18N9TL

Рис. 9. Зависимость $\Delta\sigma$ от радиуса r шлаковой частицы на поверхности жидкой стали 12Х18Н9ТЛ

Table 3. **Chemical composition of the samples, wt. % and volume fraction of inclusions**

Таблица 3. **Химический состав образцов, мас. % и объемная доля включений**

Sample No.	C	Si	Mn	Ni	Cr	Ti	Fe	Volume fraction of slag inclusions *m*, %
1	0.059	0.423	1.174	9.373	17.49	0.022	70.31	4.41
2	0.060	0.563	1.196	9.298	17.41	0.503	69.80	5.39
3	0.065	0.558	1.113	9.549	17.50	0.595	69.48	5.68
4	0.064	0.655	1.044	9.430	17.43	0.401	70.31	4.12

ing subsequent cooling of the liquid-steel drop, slag particles were found to flow from the slag bath onto the sample surface under the action of the Marangoni force. The size dependence of the slag inclusion ascent rate and the Marangoni force magnitude was evaluated. Analysis of the relationship between slag particle ascent rate and particle size showed that only particles smaller than 10 μm can remain in the melt volume, while larger particles rise to the surface of the liquid bath. It was established that slag particles up to 4 mm in size can flow onto the sample surface under the action of the Marangoni force.

The physicochemical properties of liquid 12Kh18N9TL steel relevant to foundry practice, namely surface tension and kinematic viscosity, were measured over a temperature range of 1370 – 1760 °C. No hysteresis between the heating and cooling branches of the kinematic-viscosity curves was observed, indicating the absence of irreversible structural transformations in the melt. This suggests that slag particles remain stable in the melt up to 1760 °C. In the temperature dependences of surface tension for samples taken from the third and fourth ladles during 12Kh18N9TL steel casting, anomalies were detected near 1600 °C, corresponding to a sharp decrease in surface tension. Such anomalous behavior is attributed to slag particle flow from the formed slag bath onto the drop surface under the influence of the Marangoni force. The volume fraction of slag inclusions in the melt was also evaluated. The lowest volume fractions were recorded in the sample taken before titanium addition and in the sample taken from the fourth ladle.

The volume fraction of slag inclusions in the melt was also evaluated. The lowest volume fractions were recorded in the sample taken before titanium addition and in the sample taken from the fourth ladle. The reduction in slag inclusion volume fraction in the latter sample, taken from the final ladle into which the residual liquid metal was tapped from the furnace, is associated with slag particle flotation to the liquid-metal surface during steel smelting. A correlation was established between the volume fraction of slag inclusions and the titanium content in the samples. An increase in titanium concentration was accompanied by a rise in the volume fraction of slag inclusions, indicating that titanium plays a decisive role in the formation of slag inclusions. It was concluded that titanium additions to the melt lead to an increase in the volume fraction of slag inclusions in the casting.

References / Список литературы

1. Ul`yanin E.A. Corrosion-Resistant Steels and Alloys: Reference Book. Moscow: Metallurgiya; 1991:256. (In Russ.).

   Ульянин Е.А. Коррозионностойкие стали и сплавы: Справочник. Москва: Металлургия; 1991:256.
2. Ramazanov A.K., Ganeev A.A. Features of casting pipeline valve body parts made of corrosion-resistant steel 12Kh18N9TL. *Vestnik of Nosov Magnitogorsk State Technical University*. 2018;18(2):22–29. (In Russ.).
   https://doi.org/10.18503/1995-2732-2020-18-2-22-29

   Рамазанов А.К., Ганеев А.А. Особенности литья корпусных деталей трубопроводной арматуры из коррозионностойкой стали марки 12Х18Н9ТЛ. *Вестник Магнитогорского государственного технического университета им. Г.И. Носова*. 2018;18(2):22–29.
   https://doi.org/10.18503/1995-2732-2020-18-2-22-29
3. Makarov A.V., Skorynina P.A., Osintseva A.L., Yurovskikh A.S., Savrai R.A. Improving the tribological properties of austenitic 12Kh18N10T steel by nanostructuring frictional treatment. *Metal Working and Material Science*. 2015;69(4):80–92. (In Russ.).
   http://dx.doi.org/10.17212/1994-6309-2015-4-80-92

   Макаров А.В., Скорынина П.А., Осинцева А.Л., Юровских А.С., Саврай Р.А. Повышение трибологических свойств аустенитной стали 12Х18Н10Т наноструктурирующей фрикционной обработкой. *Обработка металлов (технология, оборудование, инструменты)*. 2015;69(4):80–92.
   http://dx.doi.org/10.17212/1994-6309-2015-4-80-92
4. Voronenko B.I. Modern corrosion-resistant austenitic-ferritic steels (Review). *Metal Science and Heat Treatment*. 1997;(10):20–28. (In Russ.).

   Вороненко Б.И. Современные коррозионно-стойкие аустенитно-ферритные стали (Обзор). *Металловедение и термическая обработка металлов*. 1997;(10):20–28.
5. Tsukanov V.V., Tsyganko L.K., Shandyba G.A., Ziza A.I. Alloying and heat treatment effects on the properties of cast corrosion-resistant nitrogenous austenitic steel. *Voprosy materialivedeniya*. 2015;81(1):7–11. (In Russ.).

Цуканов В.В., Цыганко Л.К., Шандыба Г.А., Зиза А.И. Влияние легирования и термической обработки на характеристики литейной коррозионно-стойкой азотсодержащей стали аустенитного класса. *Вопросы материаловедения*. 2015;81(1):7–11.

6. Fel'dgandler E.G., Plaskeev A.V. The alloying effect of Si and Cu on the mechanical and corrosive-electrochemical properties of austenite steel. *Metallovedenie i termicheskaya obrabotka metallov*. 2003;(10):12–21. (In Russ.).

   Фельдгандлер Э.Г., Пласкеев А.В. Влияние легирования Si и Cu на коррозионно-электрохимические и механические свойства аустенитной стали. *Металловедение и термическая обработка металлов*. 2003;(10):12–21.

7. Proskuryakov V.I., Rodionov I.V. Formation of the composition and characteristics of the surface of chromonicel steel 12CR18NI10T during laser modification in a layer of experimental alloying coating. *Technical Physics*. 2022;92(1):84–91.
   https://doi.org/10.21883/JTF.2022.01.51856.173-21

   Проскуряков В.И., Родионов И.В. Формирование состава и характеристик поверхности хромоникелевой стали 12Х18Н10Т при лазерном модифицировании в слое экспериментальной легирующей обмазки. *Журнал технической физики*. 2022;92(1):84–91.
   https://doi.org/10.21883/JTF.2022.01.51856.173-21

8. Moradi M., Ghorbani D., Moghadam M.K., Kazazi M., Rouzbahani F., Karazi S. Nd:YAG laser hardening of AISI 410 stainless steel: Microstructural evaluation, mechanical properties, and corrosion behavior. *Journal of Alloys and Compounds*. 2019;795:213–222.
   https://doi.org/10.1016/j.jallcom.2019.05.016

9. Tokovoi O.K., Shaburov D.V. Study of nonmetallic phase in austenitic stainless steel. *Izvestiya. Ferrous Metallurgy*. 2014;57(12):20–24. (In Russ.).
   https://doi.org/10.17073/0368-0797-2014-12-20-24

   Токовой О.К., Шабуров Д.В. Исследование неметаллической фазы в аустенитной нержавеющей стали. *Известия вузов. Черная Металлургия*. 2014;57(12):20–24.
   https://doi.org/10.17073/0368-0797-2014-12-20-24

10. Polonskii Ya.Ya., Bondareva O.P., Gonik I.L. Fractographic studies of metal from experimental melts of ferritic-austenitic steel 08Kh18G8N2T. *Izvestiya Volgogradskogo gosuderstvennogo universiteta*. 2011;5(78):142–144. (In Russ.).

    Полонский Я.Я., Бондарева О.П., Гоник И.Л. Фрактографические исследования металла опытных плавок феррито-аустенитной стали 08Х18Г8Н2Т. *Известия Волгоградского государственного технического университета*. 2011;5(78):142–144.

11. Shvidkovskii E.G. Some Issues of Molten Metals Viscosity. Moscow: Gos. iz-vo tekhniko-teoreticheskoi literatury; 1955:206. (In Russ.).

    Швидковский Е.Г. Некоторые вопросы вязкости расплавленных металлов. Москва: Государственное издательство технико-теоретической литературы; 1955:206.

12. Arsent'ev P.P., Yakovlev V.V., Krasheninnikov M.G., etc. Physicochemical Methods for Studying Metallurgical Processes. Moscow: Metallurgiya; 1988:511. (In Russ.).

    Арсентьев П.П., Яковлев В.В., Крашенинников М.Г. и др. Физико-химические методы исследования металлургических процессов. Москва: Металлургия; 1988:511.

13. Liggieri L., Passerone A. An automatic technique for measuring the surface tension of liquid metals. *High Temperature Technology*. 1989;7(2):82–86.
    https://doi.org/10.1080/02619180.1989.11753417

14. Egry I., Ricci E., Novakovic R., Ozawa S. Surface tension of liquid metals and alloys – Recent developments. *Advances in Colloid and Interface Science*. 2010;159(2):198–212.
    https://doi.org/10.1016/j.cis.2010.06.009

15. Ivashchenko Yu.N., Khilya G.P. Installation for measuring the free surface energy, contact angle and density of melts by the sessile drop method. *Pribory i tekhnika eksperimenta*. 1972;(6):208–211. (In Russ.).

    Иващенко Ю.Н., Хиля Г.П. Установка для измерения свободной поверхностной энергии, контактного угла и плотности расплавов методом лежащей капли. *Приборы и техника эксперимента*. 1972;(6):208–211.

16. Lee J., Kiyose A., Nakatsuka S., Nakamoto M., Tanaka T. Improvements in surface tension measurements of liquid metals having low capillary constants by the constrained drop method. *ISIJ International*. 2004;44(11):1793–1799.
    https://doi.org/10.2355/isijinternational.44.1793

17. Direktor L.B., Zaichenko V.M., Maikov I.L. An improved method of sessile drop for determining the surface tension of liquids. *High Temperature*. 2010;48(2):176–180.
    https://doi.org/10.1134/S0018151X10020069

    Директор Л.Б., Зайченко В.М., Майков И.Л. Усовершенствованный метод лежащей капли для определения поверхностного натяжения жидкостей. *Теплофизика высоких температур*. 2010;48(2):193–197.

18. Prasad L.C., Chatterjee S.K., Jha R.K. Atomic order and interionic pair potentials in Cu-Sn liquid alloys. *Journal of Alloys and Compounds*. 2007;441(1-2):43–51.
    https://doi.org/10.1016/j.jallcom.2006.09.079

19. Ricci E., Giuranno D., Grosso I., Lanata T., Amore S., Novakovic R., Arato E. Surface tension of molten Cu-Sn alloys under different oxygen containing atmospheres. *Journal of Chemical and Engineering Data*. 2009;54(6):1660–1665.
    https://doi.org/10.1021/je800717a

20. Gluzman L.D., E`del`man I.I. Laboratory control of coke production. Xar'kov: Gos. nauchno-tekhn. izd-vo literatury po chernij i tszvetnoi metallurgii; 1957:635. (In Russ.).

    Глузман Л.Д., Эдельман И.И. Лабораторный контроль коксохимического производства. Харьков: Государственное научно-техническое издательствоо литературы по черной и цветной металлургии; 1957:635.

21. Zhao D., Gao J. Liquid phase separation in undercooled Cu–Co alloys under the influence of static magnetic fields. *Philosophical Transactions of the Royal Society A*. 2019;377:20180207.
    http://dx.doi.org/10.1098/rsta.2018.0207

Information about the Authors

Daniil P. Shvetsov, *Engineer of the Research Center of Physics of Metallic Liquids*, Ural Federal University named after the first President of Russia B.N. Yeltsin; *Head of Technical Control Department*, LLC "Precision Casting Center"
ORCID: 0000-0002-1428-4564
E-mail: shwedmail@gmail.com

Ol'ga A. Chikova, *Dr. Sci. (Phys.–Math.), Prof. of the Chair of Physics*, Ural Federal University named after the first President of Russia B.N. Yeltsin
ORCID: 0000-0002-3347-9148
E-mail: chik63@mail.ru

Vladimir S. Tsepelev, *Dr. Sci. (Eng.), Prof., Director of the Research Center of Physics of Metallic Liquids*, Ural Federal University named after the first President of Russia B.N. Yeltsin
ORCID: 0000-0003-4195-9042
E-mail: v.s.tsepelev@urfu.ru

Nikolai I. Sinitsin, *Cand. Sci. (Phys.–Math.), Assist. Prof. of the Chair of Physics, Senior Researcher of the Research Center of Physics of Metallic Liquids*, Ural Federal University named after the first President of Russia B.N. Yeltsin
ORCID: 0000-0002-6264-6523
E-mail: n.i.sinitsin@urfu.ru

Vladimir V. V'yukhin, *Research Associate of the Research Center of Physics of Metallic Liquids*, Ural Federal University named after the first President of Russia B.N. Yeltsin
ORCID: 0000-0002-0772-8155
E-mail: v.v.vyukhin@urfu.ru

Сведения об авторах

Даниил Петрович Швецов, *инженер Исследовательского центра физики металлических жидкостей*, Уральский федеральный университет имени первого Президента России Б.Н. Ельцина; *начальник отдела технического контроля*, ООО «Центр Точного Литья»
ORCID: 0000-0002-1428-4564
E-mail: shwedmail@gmail.com

Ольга Анатольевна Чикова, *д.ф.-м.н., профессор кафедры физики*, Уральский федеральный университет имени первого Президента России Б.Н. Ельцина
ORCID: 0000-0002-3347-9148
E-mail: chik63@mail.ru

Владимир Степанович Цепелев, *д.т.н., профессор, директор Исследовательского центра физики металлических жидкостей*, Уральский федеральный университет имени первого Президента России Б.Н. Ельцина
ORCID: 0000-0003-4195-9042
E-mail: v.s.tsepelev@urfu.ru

Николай Иванович Синицин, *к.ф.-м.н., доцент кафедры физики, старший научный сотрудник Исследовательского центра физики металлических жидкостей*, Уральский федеральный университет имени первого Президента России Б.Н. Ельцина
ORCID: 0000-0002-6264-6523
E-mail: n.i.sinitsin@urfu.ru

Владимир Викторович Вьюхин, *научный сотрудник Исследовательского центра физики металлических жидкостей*, Уральский федеральный университет имени первого Президента России Б.Н. Ельцина
ORCID: 0000-0002-0772-8155
E-mail: v.v.vyukhin@urfu.ru

Contribution of the Authors

D. P. Shvetsov – research initiative, sample preparation, experiment planning, conducting research, writing the text.

O. A. Chikova – writing the text, discussion of results, conceptualization.
V. S. Tsepelev – scientific guidance, discussion of results, conceptualization.
N. I. Sinitsin – writing the text, discussion of results, performing calculations.
V. V. V'yukhin – conducting research, discussion of results, designing visual materials.

Вклад авторов

Д. П. Швецов – инициатива исследования, подготовка образцов, планирование экспериментов, проведение исследования, работа над текстом.
О. А. Чикова – написание текста, обсуждение результатов, формулировка концепции исследования.
В. С. Цепелев – научное руководство, обсуждение результатов, формулировка концепции исследования.
Н. И. Синицин – написание текста, обсуждение результатов, выполнение расчетов.
В. В. Вьюхин – проведение исследования, обсуждение результатов, оформление графических материалов.

Received 02.05.2025
Revised 11.07.2025
Accepted 29.09.2025

Поступила в редакцию 02.05.2025
После доработки 11.07.2025
Принята к публикации 29.09.2025

Ecology and rational use of natural resources / **Экология и рациональное природопользование**

UDC 669.531.5
DOI 10.17073/0368-0797-2025-5-543-549

Original article
Оригинальная статья

Removal of chlorine from electric arc furnace dust by oxidative roasting

E. V. Grigor'ev ✉, Yu. E. Kapelyushin, A. Bil'genov, D. V. Stepanov, A. A. Khalikulov

South Ural State University (76 Lenina Ave., Chelyabinsk 454080, Russian Federation)

✉ grigorevev@susu.ru

Abstract. The growth of steel production and consumption leads to the formation of a large amount of technogenic waste. One of the wastes is electric arc furnace (EAF) dust. In the Russian Federation, about 0.7 million tons of dust are annually generated. The paper studies the dust of one of the metallurgical enterprises, in which zinc is mainly contained in the form of $ZnFe_2O_4$, and also contains harmful compounds of Cl and Pb, which reduce the quality of Waelz oxide during subsequent processing. The studied dust was subjected to high-temperature oxidative roasting in a muffle furnace. The experiments were carried out in the temperature range of 300 – 1100 °C with roasting time of 1 h. In the temperature range of 900 – 1100 °C, the roasting time varied within 3 – 9 h. The composition was determined using XRD phase analysis and micro-*X*-ray spectral method. It was found that at temperature of 900 °C and roasting time of 9 h the degree of Cl removal reaches 78 %. At temperature of 1000 °C and roasting time of 9 h, the degree of Cl removal reaches 99.4 % with Zn losses of 19.8 %. At temperature of 1100 °C and roasting time of 3 h the degree of Cl removal is 91.2 %, and Zn losses reach 37.8 %; thereby, carrying out the oxidative roasting at this temperature is impractical. Experimental studies have shown that it is possible to effectively remove chlorine from EAF dust which predominantly contains zinc in the form of $ZnFe_2O_4$ using high-temperature oxidative roasting with relatively low zinc losses in the temperature range of 900 – 1000 °C.

Keywords: EAF dust, electric arc furnace steelmaking, recycling, chlorine, zinc, dechlorination, Waelz oxide, oxidative roasting

Acknowledgements: The work was supported by the Russian Science Foundation, grant No. 24-79-10120, https://rscf.ru/project/24-79-10120/.

For citation: Grigor'ev E.V., Kapelyushin Yu.E., Bil'genov A., Stepanov D.V., Khalikulov A.A. Removal of chlorine from electric arc furnace dust by oxidative roasting. *Izvestiya. Ferrous Metallurgy*. 2025;68(5):543–549. *https://doi.org/10.17073/0368-0797-2025-5-549-555*

Удаление хлора из пыли дугового сталеплавильного производства окислительным обжигом

Е. В. Григорьев ✉, Ю. Е. Капелюшин, А. Бильгенов, Д. В. Степанов, А. А. Халикулов

Южно-Уральский государственный университет (Россия, 454080, Челябинск, пр. Ленина, 76)

✉ grigorevev@susu.ru

Аннотация. Рост производства и потребления стали приводит к образованию большого количества техногенных отходов. Одним из отходов выступает пыль электродугового сталеплавильного производства. В Российской Федерации ежегодно образуется порядка 0,7 млн т пыли. В работе изучена пыль одного из металлургических предприятий, в которой цинк преимущественно содержится в виде $ZnFe_2O_4$, а также присутствуют вредные соединения хлора и свинца, которые снижают качество вельц-оксида при последующей переработке. Исследуемая пыль подвергалась высокотемпературному окислительному обжигу в муфельной печи. Эксперименты проводились в интервале температур 300 – 1100 °С при времени выдержки 1 ч. В интервале температур 900 – 1100 °С время выдержки варьировалось в пределах 3 – 9 ч. Фазовый состав пыли определяли с помощью рентгенофазового анализа, химический состав – микрорентгеноспектральным методом. Установлено, что при температуре 900 °С и времени выдержки 9 ч степень удаления хлора составляет 78 %. При температуре обжига 1000 °С и времени выдержки 9 ч степень удаления хлора достигает 99,4 % при потерях цинка 19,8 %. При температуре обжига 1100 °С и времени выдержки 3 ч степень удаления хлора составляет 91,2 %, а потери цинка достигают 37,8 %, поэтому проведение окислительного обжига при данной температуре является нецелесообразным. Экспериментальные исследования показали, что из пыли электроду-

говой печи, в которой цинк преимущественно содержится в виде $ZnFe_2O_4$, возможно реализовать эффективное удаление хлора методом высокотемпературного окислительного обжига с относительно низкими потерями цинка в интервале температур 900 – 1000 °С.

Ключевые слова: пыль ЭДП, электросталеплавильное производство, рециклинг, хлор, цинк, дехлорирование, вельц-оксид, окислительный обжиг

Благодарности: Исследование выполнено за счет гранта Российского научного фонда № 24-79-10120, https://rscf.ru/project/24-79-10120/.

Для цитирования: Григорьев Е.В., Капелюшин Ю.Е., Бильгенов А., Степанов Д.В., Халикулов А.А. Удаление хлора из пыли дугового сталеплавильного производства окислительным обжигом. *Известия вузов. Черная металлургия*. 2025;68(5):543–549. https://doi.org/10.17073/0368-0797-2025-5-549-555

Introduction

The continuous growth of steel production and consumption inevitably leads to the generation of large amounts of technogenic waste. On average, 25 – 30 kg of electric arc furnace (EAF) dust is produced per ton of steel. In the Russian Federation, approximately 0.7 million tons of this dust are generated every year. It is typically stored in dumps, resulting in the loss of valuable metals such as iron, zinc, and lead[1] [1; 2]. The accumulation of such waste poses a potential hazard to both ecosystems and human health [3]. The chemical composition of EAF dust varies depending on the specific production technology. The zinc content ranges from 2 to 25 %, and in some cases reaches up to 40 %. Understanding the physicochemical behavior of EAF dust components with the aim of extracting zinc, lead, and iron, as well as removing chlorine, is an important objective of modern metallurgical production [4 – 6].

In industrial practice, EAF dust is most often treated using pyrometallurgical methods. The Waelz process remains the predominant technology, accounting for about 80 % of all processed dust [7]. EAF dust is composed mainly (up to 90 %) of oxides, while the remaining portion consists of ferrites, sulfates, and chlorides, including sodium chloride (NaCl), potassium chloride (KCl), and chlorides of zinc and lead [8]. One of the main challenges in EAF dust recycling is its high chloride content. These chlorides originate from chlorine-containing compounds present in the steel scrap, such as polymer materials and paint coatings.

Roasting is one of the approaches used to remove contaminants from EAF dust. In studies [9; 10], oxidative roasting was performed at 950 °C with additional air supply. According to the results, about 98 % Pb and Cl and 1 % Zn volatilized. Other studies [11 – 13] investigated roasting in various gaseous atmospheres – air, CO_2, and SO_2. The dust samples were heated to 200 – 600 °C and held for 1 – 5 h. The authors selected low-temperature conditions to minimize zinc losses that occur at elevated temperatures. The most effective atmospheres were CO_2 and SO_2, whereas roasting in air showed the lowest efficiency. Sulfatizing roasting reduced the chloride content by 83 % (from 70.2 to 12.1 mg/kg), while carbonation roasting achieved an 81 % reduction (from 70.20 to 13.23 mg/kg). In another study [14], EAF dust was roasted with CaO added to convert zinc ferrite into zinc oxide. The experiments were conducted at 1100 °C for 3 h, and it was found that approximately 98 % Cl and Pb were removed from the initial dust. In [15], roasting was carried out in a muffle furnace at temperatures ranging from 300 to 1150 °C. The results showed that heating the dust to 1150 °C completely eliminated sodium and chlorine, while potassium and lead contents decreased by 81 and 83.5 %, respectively. Zinc losses did not exceed 5 %. Chlorine removal results by roasting were also reported in [16]. Crucibles containing dust were heated at a rate of 300 °C/h to 900, 1000, and 1100 °C with a roasting time of 240 min. After roasting, the chlorine content in the sinter decreased from 3.02 to 0.01 – 0.02 %, corresponding to a chlorine removal degree of 99.6 %. However, no data on zinc losses were provided.

Overall, published studies report inconsistent results concerning the efficiency of oxidative roasting in air atmosphere, especially with respect to zinc losses. Therefore, the aim of this study was to further evaluate the effectiveness of oxidative roasting in air atmosphere for chlorine removal from EAF dust at high temperatures.

Initial dust and experimental procedure

The study investigated electric arc furnace (EAF) dust obtained from one of the metallurgical enterprises. A representative sample for chemical and phase composition analysis was prepared by homogenizing the collected dust. The phase composition of the dust was determined by *X*-ray diffraction (XRD) using a Rigaku Ultima IV diffractometer. The data were processed with the Match software package. The main identified phases (%) were as follows: $ZnFe_2O_4$ – 69; ZnO – 6; $CaCO_3$ – 17; SiO_2 – 5; and KCl – 3.

The elemental chemical composition of the researched dust is presented in Tables 1 and 2. The composition was determined by micro-*X*-ray spectral analysis using

[1] World Steel in Figures. https://worldsteel.org/steel-by-topic/statistics/world-steel-in-figures/ (Accessed 19.03.2025).

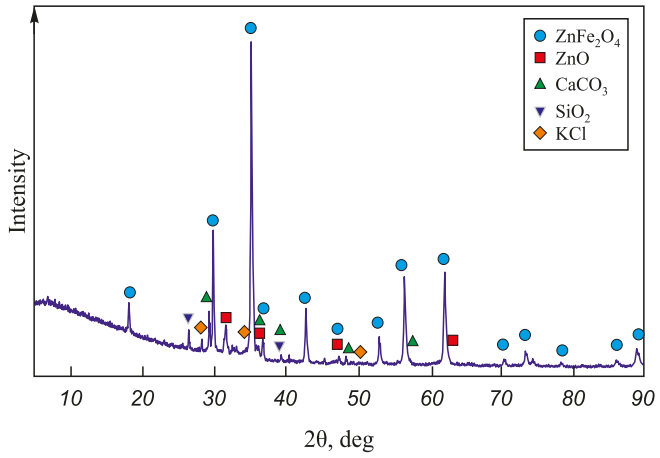

Fig. 1. Phase composition of the researched EAF dust

Рис. 1. Фазовый состав исследуемой пыли

a JEOL JSM-7001F scanning electron microscope. Statistical errors were evaluated using mathematical methods. To obtain statistically reliable data, nine samples (portions of the homogenized EAF dust) were collected from a well-mixed bulk container. For each sample, four spectra were recorded (area analysis at 100× magnification). Mean values of the analyzed elements were calculated from 36 spectra, and the confidence interval radius was determined using the SPSS software. The resulting data are shown in Table 1.

A series of oxidative roasting experiments was carried out in a muffle furnace. Each 18 g dust sample was placed in a corundum crucible and loaded into the furnace preheated to the desired temperature. The experiments were conducted in the temperature range of 300 – 1100 °C with a roasting time of 60 min under an air atmosphere.

Results and discussion

Fig. 2 illustrates the effects of temperature and time on the mass change of EAF dust samples during oxidative roasting.

As seen in Fig. 2, an increase in temperature causes slight mass variations of the samples (within 1 – 3 %), both upward and downward. These fluctuations are likely associated with the decomposition of carbonates and hydroxides, the volatilization of certain elements and compounds, as well as the further oxidation of metals to higher oxides.

After roasting, the dust samples were examined under an electron microscope. The results are presented in Table 3.

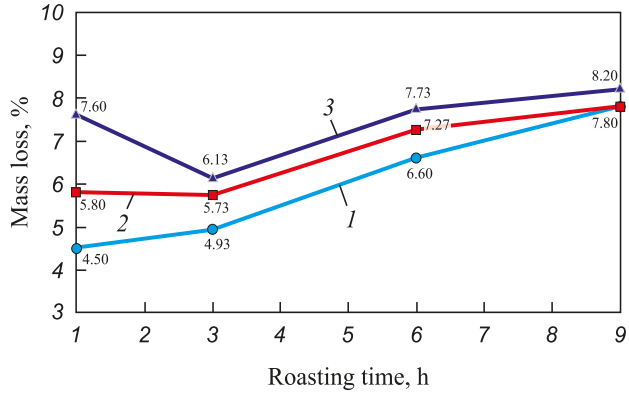

Fig. 2. Effects of time and temperature on mass change of the EAF dust samples:
1 – 900 °C; *2* – 1000 °C; *3* – 1100 °C

Рис. 2. Зависимость изменения массы образцов от времени и температуры:
1 – 900 °C; *2* – 1000 °C; *3* – 1100 °C

Table 1. **Composition of the researched EAF dust (statistical data, wt. %)**

Таблица 1. **Состав исследуемой пыли ЭДП (статистические данные, мас. %)**

Element	O	Na	Mg	Si	S	Cl	K	Ca	Cr	Mn	Fe	Cu	Zn	Pb
Mean value	27.0	2.3	0.8	2.2	0.8	1.8	1.7	3.9	0.5	4.5	40.2	0.5	12.9	1.0
95 % confidence interval radius	0.9	0.5	0.1	0.1	0.1	0.1	0.1	0.2	0.0	0.1	0.7	0.1	0.3	0.1
Upper confidence limit	27.9	2.8	1.0	2.3	0.9	2.0	1.7	4.1	0.6	4.6	40.9	0.5	13.1	1.1
Lower confidence limit	26.2	1.9	0.7	2.1	0.8	1.7	1.6	3.7	0.5	4.4	39.5	0.4	12.6	0.8

Таблица 2. **Средний состав исследуемой пыль ЭДП, мас. %**

Table 2. **Average composition of the researched EAF dust, wt. %**

Element	O	Na	Mg	Si	S	Cl	K	Ca	Cr	Mn	Fe	Cu	Zn	Pb	Total
Mean value	27.0	2.3	0.8	2.2	0.8	1.8	1.7	3.9	0.5	4.5	40.2	0.5	12.9	1.0	100.0

Table 3. **Composition of the EAF dust after oxidative roasting at various temperatures, wt. %**

Таблица 3. **Состав пыли после окислительного обжига при различных температурах, мас. %**

Element	O	Mg	Al	Si	S	Cl	K	Ca	Cr	Mn	Fe	Zn	Total
EAF initial dust	17.7	1.0	0.4	2.8	0.9	1.7	1.8	4.2	0.5	5.6	49.3	14.2	100.0
300 °C	15.8	1.5	0.5	2.4	0.9	1.9	1.8	4.0	0.5	5.3	50.6	14.9	100.0
400 °C	16.5	1.0	0.4	2.6	0.9	1.8	1.9	4.0	0.6	5.3	49.5	15.5	100.0
500 °C	17.6	1.2	0.3	2.7	0.8	1.9	1.7	4.4	0.8	5.3	49.0	14.4	100.0
600 °C	16.3	1.3	0.5	2.6	0.7	2.5	1.8	5.4	0.7	5.0	48.2	15.2	100.0
700 °C	17.3	0.9	0.4	2.5	0.7	2.3	1.8	5.8	0.6	5.6	48.8	13.5	100.0
800 °C	15.8	1.4	0.4	2.5	0.6	2.2	1.7	6.6	0.6	5.3	49.2	13.8	100.0
900 °C	15.8	1.1	0.3	2.4	0.8	1.2	1.2	6.4	0.7	5.5	51.2	13.4	100.0
1000 °C	13.1	0.7	0.4	2.3	0.6	1.6	1.1	6.5	0.8	5.9	55.6	11.4	100.0
1100 °C	16.3	1.5	0.4	3.7	0.7	0.9	0.6	7.1	0.9	5.1	51.4	11.6	100.0

As shown in Table 3, an increase in temperature leads to a decrease in the chlorine content of the EAF dust samples. Based on these findings, additional high-temperature oxidative roasting experiments were carried out with varying roasting times to evaluate the effect of this parameter on dust dechlorination. Dust samples weighing 10 g were placed in corundum crucibles and loaded into a muffle furnace. The experiments were conducted at temperatures ranging from 900 to 1100 °C, with roasting times of 3, 6, and 9 h. After roasting, the samples were analyzed using electron microscopy. The experiments showed that the maximum degree of dechlorination reached approximately 98.9 % at 1100 °C and a roasting time of at least 6 h. At a roasting time of 9 h, a similar dechlorination degree of 96.8 % was obtained. The experimental results are shown in Fig. 3.

Further electron microscopy analysis revealed that oxidative roasting at 1100 °C for more than 6 h is inefficient because of increased zinc losses. At 1000 °C, zinc losses reached approximately 24.8 %, whereas at 1100 °C they increased to 38.5 %. These results are presented in Fig. 4.

The findings indicate that increasing temperature and roasting time during oxidative roasting significantly reduces the chlorine content in EAF dust, from 1.70 to 0.04 – 0.10 %. Temperature is therefore one of the most critical parameters influencing the efficiency of dechlorination. According to the data in Table 3, the maximum chlorine content (2.5 wt. %) was observed at 600 °C, which can be attributed to minimal chlorine removal and to the decomposition of calcium hydroxide $Ca(OH)_2$ and calcium carbonate $CaCO_3$. This temperature range corresponds to the decomposition temperatures of these com-

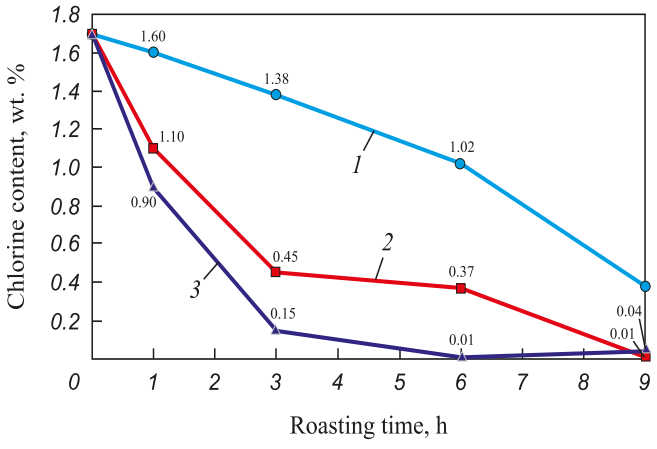

Fig. 3. Effects of time and temperature on Cl content in the EAF dust samples during oxidative roasting in air atmosphere:
1 – 900 °C; *2* – 1000 °C; *3* – 1100 °C

Рис 3. Зависимость содержания хлора в пыли ЭДП от времени и температуры при окислительном обжиге на воздухе:
1 – 900 °C; *2* – 1000 °C; *3* – 1100 °C

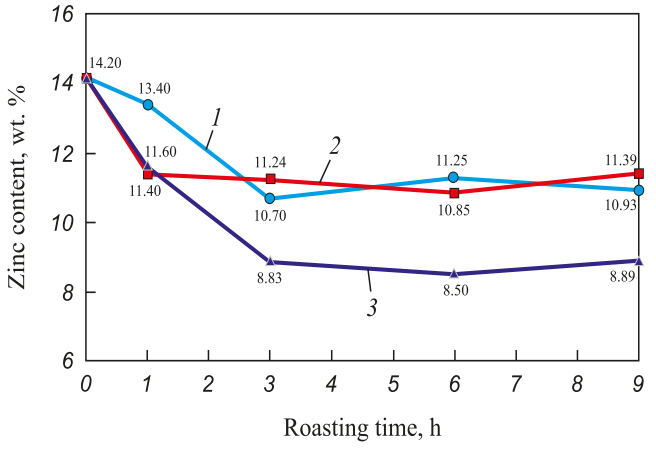

Fig. 4. Effects of time and temperature on Zn content in the EAF dust samples during oxidative roasting in air atmosphere:
1 – 900 °C; *2* – 1000 °C; *3* – 1100 °C

Рис 4. Зависимость содержания цинка в пыли ЭДП от времени и температуры при окислительном обжиге на воздухе:
1 – 900 °C; *2* – 1000 °C; *3* – 1100 °C

Table 4. **Degree of chlorine removal and zinc loss at different temperatures and roasting time, %**

Таблица 4. **Степень удаления хлора и потери цинка при различных температурах и времени выдержки, %**

Roasting time, h	Temperature, °C					
	900		1000		1100	
	Cl removal	Zn loss	Cl removal	Zn loss	Cl removal	Zn loss
1	5.8	5.6	35.3	19.7	47.0	18.3
3	18.8	24.6	73.5	20.8	91.1	37.8
6	40.0	20.7	78.2	23.6	99.4	40.1
9	77.6	23.0	97.6	19.8	99.4	37.4

pounds. A general increase in the concentrations of other elements in the dust was also noted. However, to confirm the relationship between these effects and the decomposition of hydroxides and carbonates, additional studies on phase transformations during heating are required. In the temperature range of 700 – 1100 °C, the chlorine content decreased from 2.5 to 0.9 wt. %, which agrees with the data reported in [15; 17 – 19]. Additional experiments were performed to assess the effect of roasting time at 900 – 1100 °C, varying from 1 to 9 h with 3 h intervals. As seen in Figs. 3 and 4, both chlorine and zinc losses increase with longer roasting time. Table 4 summarizes the obtained dechlorination degrees and zinc losses.

At a roasting temperature of 1000 °C and a roasting time of 3 h, the degree of chlorine removal was 73.5 %, while zinc losses remained within 20.8 %. Extending the roasting time to 9 h resulted in almost complete chlorine removal (97.4 %) with zinc losses of 19.8 %. At a roasting temperature of 1100 °C and a roasting time of 3 h, the degree of chlorine removal reached 91.2 %, but zinc losses increased significantly to 37.8 %. When the roasting time was increased to 6 h, chlorine removal was nearly complete (99.4 %), accompanied by similarly high zinc losses of approximately 40.1 %.

Conclusions

The literature provides conflicting information regarding the practicality of high-temperature oxidative roasting, mainly due to inconsistent data on zinc losses. However, the present experimental study has shown that effective chlorine removal from EAF dust – where zinc is predominantly present in the form of $ZnFe_2O_4$ – can be achieved. The main parameters influencing the efficiency of chlorine removal are the roasting temperature and roasting time. Maximum efficiency is reached at temperatures above 900 °C and roasting times longer than 3 h. At 1000 °C and a roasting time of 9 h, almost complete chlorine removal was achieved, while zinc losses reached about 20 wt. %.

Thus, high-temperature oxidative roasting at an optimal temperature of 900 – 1000 °C (to avoid excessive zinc losses) can be considered an effective method for EAF dust dechlorination and can be integrated into existing metallurgical production processes.

References / Список литературы

1. Leont'ev L.I., Dyubanov V.G. Technogenic wastes of ferrous and non-ferrous metallurgy and environmental problems. *Ekologiya i promyshlennost' Rossii*. 2011;(4):32–35. (In Russ.).

   Леонтьев Л.И. Дюбанов В.Г. Техногенные отходы черной и цветной металлургии и проблемы окружающей среды. *Экология и промышленность России*. 2011;(4):32–35.
2. Adilov G., Kareva N.T., Roshchin V.E. Influence of copper and silicon on phase transformations in the iron – carbon system. *Izvestiya. Ferrous Metallurgy*. 2024;67(1):73–75. (In Russ.). https://doi.org/10.17073/0368-0797-2024-1-73-75

   Адилов Г., Карева Н.Т., Рощин В.Е. Влияние меди и кремния на фазовые превращения в системе железо – углерод. *Известия вузов. Черная металлургия*. 2024;67(1):73–75. https://doi.org/10.17073/0368-0797-2024-1-73-75
3. Konakova A.G., Osipova E.A. Prevalence of zinc compounds in the environment and their role for living organisms. In: *University Complex as a Regional Centre of Education, Science and Culture: Proceedings of the All-Rus. Sci.-Method. Conf. Orenburg*, 2023. 2023:4384–4387. (In Russ.).

   Конакова А.Г., Осипова Е.А. Распространенность соединений цинка в окружающей среде и их роль для живых организмов. *Университетский комплекс как региональный центр образования, науки и культуры: Сборник материалов Всероссийской научно-методической конференции. Оренбург, 2023*. 2023:4384–4387.
4. Adilov G., Povolotskii A.D., Roshchin V.E. Thermodynamic modeling of metal reduction in copper-smelting slags and experimental verification of its results. *Izvestiya. Ferrous Metallurgy*. 2022;65(8):581–589. (In Russ.). https://doi.org/10.17073/0368-0797-2022-8-581-589

   Адилов Г., Поволоцкий А.Д., Рощин В.Е. Термодинамическое моделирование восстановления металлов в медеплавильных шлаках и экспериментальная проверка результатов. *Известия вузов. Черная металлургия*. 2022;65(8):581–589. https://doi.org/10.17073/0368-0797-2022-8-581-589
5. Martins F.M., dos Reis Neto J.M., da Cunha C.J. Mineral phases of weathered and recent electric arc furnace dust.

Journal of Hazardous Materials. 2008;154(1–3):417–425. https://doi.org/10.1016/j.jhazmat.2007.10.041

6. Simonyan L.M., Demidova N.V. Selective extraction of carbon-free zinc and lead from EAF-dust. *Izvestiya. Ferrous Metallurgy*. 2020;63(8):631–638. (In Russ.). https://doi.org/10.17073/0368-0797-2020-8-631-638

   Симонян Л. М., Демидова Н. В. Исследование процесса безуглеродного селективного извлечения цинка и свинца из пыли ДСП. *Известия вузов. Черная металлургия*. 2020;63(8):631–638. https://doi.org/10.17073/0368-0797-2020-8-631-638
7. Ryazanov A.G., Koryagin Yu.D. Influence of heat treatment modes on the phase composition of zinc-containing materials: Final qualifying work. 2017:14–16. (In Russ.).

   Рязанов А.Г., Корягин Ю.Д. Влияние режимов термообработки на фазовый состав цинкосодержащих материалов: выпускная квалификационная работа. 2017:14–16.
8. Grigor'ev E.V., Kapelyushin Yu.E. Manufacturing, curing and mechanical testing of BREX from electric arc furnace dust. *Ferrous Metallurgy. Bulletin of Scientific, Technical and Economic Information*. 2023;79(4):334–339. (In Russ.).

   Григорьев Е.В., Капелюшин Ю.Е. Изготовление, сушка и механические испытания брэксов из пыли электродугового сталеплавильного производства. *Черная металлургия. Бюллетень научно-технической и экономической информации*. 2023;79(4):334–339.
9. Stovpchenko A.P., Kamkina L.V., Proidak Yu.S., Derevyanchenko I.V., Kucherenko O.L., Bondarenko M.Yu. Theoretical and experimental studies of composition and reducibility of dust of arc steelmaking furnaces. *Electrometallurgy*. 2009;(8):29–36. (In Russ.).

   Стовпченко А.П., Камкина Л.В., Пройдак Ю.С., Деревянченко И.В., Кучеренко О.Л., Бондаренко М.Ю. Теоретические и экспериментальные исследования состава и восстановимости пыли дуговых сталеплавильных печей. *Электрометаллургия*. 2009;(8):29–36.
10. Doronin I.E. Industrial methods of steelmaking dust processing. *Metallurg*. 2010;(10):48–53. (In Russ.).

    Доронин И.Е. Промышленные способы переработки сталеплавильной пыли. *Металлург*. 2010;(10):48–53.
11. Yoo J.M., Kim B.S., Lee J.C., Kim M.S., Nam C.W. Kinetics of the volatilization removal of lead in electric arc furnace dust. *Materials Transactions*. 2005;46(2);323–328. https://doi.org/10.2320/matertrans.46.323
12. Zhu F., Takaoka M., Oshita K., Kitajima Y., Inada Y., Morisawa S., Tsuno H. Chlorides behavior in raw fly ash washing experiments. *Journal of Hazardous Materials*. 2010;178(1–3):547–552. https://doi.org/10.1016/j.jhazmat.2010.01.119
13. Chen W.S., Shen Y.H., Tsai M.S., Chang F.C. Removal of chloride from electric arc furnace dust. *Journal of Hazardous Materials*. 2011;190(1–3):639–644. https://doi.org/10.1016/j.jhazmat.2011.03.096
14. Chairaksa-Fujimoto R., Inoue Y., Umeda N., Itoh S., Nagasaka T. New pyrometallurgical process of EAF dust treatment with CaO addition. *International Journal of Minerals, Metallurgy, and Materials*. 2015;22:788–797. https://doi.org/10.1007/s12613-015-1135-6
15. Yakornov S.A. Technology of processing of zinc-containing dusts of arc steelmaking furnaces with obtaining zinc powder: Cand. Tech. Sci. Diss. 2024:81–82,90,93. (In Russ.).

    Якорнов С.А. Технология переработки цинкосодержащих пылей дуговых сталеплавильных печей с получением цинкового порошка: Диссертация … кандидата технических наук. 2024:81–82,90,93.
16. Chen W.S., Chou W.S., Wu C.C., Tsai M.S. Removal of chloride from EAF-dust by reactive roasting at low temperature. *100th Annual Conf. and Exhibition of the Air and Waste Management Association 2007*. ACE 2007, Air and Waste Management Association; 2007.
17. Simonyan L.M., Demidova N.V. Dioxins and furans' behavior in the process of zinc and lead removing from EAF dust. *Izvestiya. Ferrous Metallurgy*. 2019;62(11):840–845. (In Russ.). https://doi.org/10.17073/0368-0797-2019-11-840-845

    Симонян Л.М., Демидова Н.В. Изучение поведения диоксинов и фуранов в процессе удаления цинка и свинца из пыли ДСП. *Известия вузов. Черная металлургия*. 2019;62(11):840–845. https://doi.org/10.17073/0368-0797-2019-11-840-845
18. Demin A.V., Rozhkov A.I., Grudnitskii O.M., Nikolaev V.V., Feklistov A.V. Finding ways of recycling dust of arc steel furnaces at the Belarusian metallurgic plant. *Vestnik KIGIT*. 2014;2(44):40–49. (In Russ.).

    Демин А.В., Рожков А.И., Грудницкий О.М., Николаев В.В., Феклистов А.В. Поиск способов утилизации пыли дуговых сталеплавильных печей на Белорусском металлургическом заводе. *Вестник КИГИТ*. 2014;2(44):40–49.
19. Leclerc N., Meux E., Lecuire J.M. Hydrometallurgical recovery of zinc and lead from electric arc furnace dust using mononitrilotriacetate anion and hexahydrated ferric chloride *Journal of Hazardous Materials*. 2002;91(1–3):257–270. https://doi.org/10.1016/S0304-3894(01)00394-6

Сведения об авторах / Information about the Authors

Евгений Вячеславович Григорьев, *инженер-исследователь научно-исследовательской лаборатории «Водородные технологии в металлургии»,* Южно-Уральский государственный университет
E-mail: grigorevev@susu.ru

Юрий Евгеньевич Капелюшин, *старший научный сотрудник научно-исследовательской лаборатории «Водородные технологии в металлургии»,* Южно-Уральский государственный университет
ORCID: 0000-0002-3352-1780
E-mail: kapelyshnye@susu.ru

Evgenii V. Grigor'ev, *Research Engineer of the Research Laboratory "Hydrogen Technologies in Metallurgy",* South Ural State University
E-mail: grigorevev@susu.ru

Yury E. Kapelyushin, *Senior Researcher of the Research Laboratory "Hydrogen Technologies in Metallurgy",* South Ural State University
ORCID: 0000-0002-3352-1780
E-mail: kapelyshnye@susu.ru

Арман Бильгенов, *старший преподаватель кафедры «Пирометаллургические и литейные технологии»*, Южно-Уральский государственный университет
ORCID: 0009-0001-8592-7870
E-mail: bilgenova@susu.ru

Дмитрий Владимирович Степанов, *инженер-исследователь управления научной и инновационной деятельности*, Южно-Уральский государственный университет
E-mail: aqaseq@gmail.com

Артур Алексеевич Халикулов, *лаборант управления научной и инновационной деятельности*, Южно-Уральский государственный университет
E-mail: artur.dragonil@mail.ru

Arman Bil'genov, *Senior Lecturer of the Chair "Pyrometallurgical and Foundry Technologies"*, South Ural State University
ORCID: 0009-0001-8592-7870
E-mail: bilgenova@susu.ru

Dmitrii V. Stepanov, *Research Engineer of Department of Scientific and Innovation Activities*, South Ural State University
E-mail: aqaseq@gmail.com

Artur A. Khalikulov, *Laboratory Assistant of Department of Scientific and Innovation Activities*, South Ural State University
E-mail: artur.dragonil@mail.ru

Вклад авторов / Contribution of the Authors

Е. В. Григорьев – проведение исследований, обработка данных, написание статьи.
Ю. Е. Капелюшин – научное руководство, написание статьи, редактирование статьи.
А. Бильгенов – редактирование статьи, анализ литературных данных.
Д. В. Степанов – проведение экспериментов, написание статьи, подготовка литературного обзора.
А. А. Халикулов – проведение экспериментов.

E. V. Grigor'ev – conducting the research, data processing, writing the text.
Yu. E. Kapelyushin – scientific guidance, writing and editing the text.
A. Bil'genov – editing the text, analysis of literary data.
D. V. Stepanov – conducting the experiments, writing the text, preparing a literary review.
A. A. Khalikulov – conducting the experiments.

Поступила в редакцию 20.05.2025
После доработки 27.06.2025
Принята к публикации 29.08.2025

Received 20.05.2025
Revised 27.06.2025
Accepted 29.08.2025

Над номером работали:

Л.И. Леонтьев, *главный редактор*

Е.В. Протопопов, *заместитель главного редактора*

Е.А. Ивани, *ответственный секретарь*

Л.П. Бащенко, *заместитель ответственного секретаря*

Е.Ю. Потапова, *заместитель главного редактора по развитию*

О.А. Долицкая, *научный редактор*

В.В. Расенець, *верстка, иллюстрации*

Г.Ю. Острогорская, *менеджер по работе с клиентами*

Подписано в печать 25.10.2025. Формат 60×90 $^{1}/_{8}$. Бум. офсетная № 1.
Печать цифровая. Усл. печ. л. 14,5. Заказ 23327. Цена свободная.

Отпечатано в типографии Издательского Дома МИСИС.
119049, Москва, Ленинский пр-кт, д. 4, стр. 1.
Тел./факс: +7 (499) 236-76-17

Зарегистрирован Федеральной службой по надзору в сфере связи, информационных технологий и массовых коммуникаций. Свидетельство о регистрации ПИ № ФС77-35456.

Подписной индекс 70383.